FRAGMENTATION OF LANTHANIDE (III) CATIONIZED SMALL PEPTIDES: GENERATION OF PEPTIDE RADICAL CATIONS AND DIPOSITIVE a AND b IONS

YATING WANG

A DISSERTATION SUBMITTED TO
THE FACULTY OF GRADUATE STUDIES
IN PARTIAL FULFILLMENT OF THE REQUIREMENTS
FOR THE DEGREE OF
DOCTOR OF PHILOSOPHY

GRADUATE PROGRAM IN CHEMISTRY
YORK UNIVERSITY,
TORONTO, ONTARIO

March 2018

ABSTRACT

This research work examines the dissociation chemistry of tripositive complexes formed by trivalent lanthanide ions and small peptides with tandem mass spectrometry under low-energy collision-induced dissociation (CID). By fragmentation of the tripositive lanthanide (III) cationized small peptide, a new route to generate peptide radical cations has been discovered. The dipositive b ions are also observed and the mechanisms by which they fragment are investigated by MS^n.

Tripositive complexes of lanthanide(III)/peptide have similar fragmentation chemistries in the gas phase when lanthanide = yttrium, lanthanum, cerium, samarium, gadolinium and terbium; $[a_3+H]^{2+}$ ions are formed and there are no peptide radical cations observed. When the lanthanide is europium(III), radical cations of tryptophan-, tyrosine-, phenylalanine-, methionine-containing peptides and of aliphatic peptides have been generated.

Fragmentations of tripositive Ce(III)/peptide and Eu(III)/peptide complexes show very different behaviours. Abundant CO loss is only observed for dissociation of Ce(III)/peptide complexes, whereas CO_2 loss is the predominant channel for Eu(III)/peptide complexes. Similarly, CO loss and CO_2 loss are the predominant channels for the dissociations of $[Ce(peptide\text{-}H)]^{2+}$ and $[Eu(peptide\text{-}H)]^{2+}$, respectively. Peptide radical cations are only generated by the fragmentation of Eu(III)/peptide complexes, while protonated a and b ions are only observed when Ce(III)/peptide complexes dissociate.

The dissociations of aliphatic $[peptide]^{\bullet+}$ ions generate $[b_3\text{-}H]^{\bullet+}$/ $[b_2\text{-}H]^{\bullet+}$ ions for most peptides. In the dissociation of $[a_3+H]^{\bullet+}$ ions, $[b_2\text{-}H]^{\bullet+}$ ions are formed from most peptides.

$[a_3+H]^{2+}$ ions usually cleave at the C-terminal amide bonds, creating two singly charged ions, a $[b_2]^+$ ion and an iminium ion derived from the C-terminal residue. Some $[a_3+H]^{2+}$ ions also lose

small neutral molecules. The composition of the peptides dictates the preferred mode of the fragmentation of $[b_3+H]^{2+}$ ions, either loss of CO to form $[a_3+H]^{2+}$, or loss of CO plus H_2O.

Fragmentations of $[Ce(peptide\text{-}H)]^{2+}$ ions show CO loss, and CO_2 losses are observed for peptides with aromatic side chains or a methionine residue at C-terminus. For $[Ce(peptide\text{-}H)(peptide)]^{2+}$ complexes, neutral losses are also observed but formation of two singly charged ions is dominant. The dissociation behaviour of $[Ce(peptide\text{-}H)(CH_3CN)]^{2+}$ and $[Eu(peptide\text{-}H)(CH_3CN)]^{2+}$ complexes are quite different. The former loses only CH_3CN whereas the latter loses only CO_2.

ACKNOWLEDGEMENTS

I would like to thank my daughter Anni first. She is the light of my life that guides me through the dark journey. I would also like to thank my mother and my brothers for their continuous support, financially and mentally.

To my late father: I will never forget the good characters you taught me: integrity, honest, brave, perseverance. Without these, many things don't make sense.

I would like to thank my supervisor Professor K. W. Michael Siu for his guidance, support, encouragement and opportunities he has given me through my graduate study.

My special appreciation goes to my supervisor Professor Alan C. Hopkinson. Without his exceptional knowledge, patient guidance, numerous lectures and discussions, I would not have been able to reach my goal.

I would like to thank Dr Udo H. Verkerk for his encouragement and help, with his wisdom of life and expertise in organic synthesis.

I would like to thank John Van Nostrand for training me in mass spectrometers from the very beginning of my study here, and thank you for sharing your knowledge and expertise in instrumentation without reservation.

I sincerely thank Dr Justin Kai-Chi Lau for all the contribution in theoretical calculation and in-depth discussion on the mechanism and the dissertation.

To Dr Isaac Lai: thanks for helping me without reservation.

I would also like to thank the Siu group and members of Centre for Research in Mass Spectrometry (CRMS). Thank you, Dr Olena Masui, Dr Irene Saminathan, Backen Wu, Brian Lam, Dr Xiaoyan Mu for your friendship and help.

In memory of my father

TABLE OF CONTENTS

LIST OF TABLES

LIST OF FIGURES

Chapter 1

Introduction

1.1 Metal/peptides complexes

Metal cations play important roles in biological processes. The metal binding site typically plays a number of critical functions, including structural integrity, electron transfer, ligand (e.g. oxygen) binding and catalysis [1-2]. Alzheimer's disease (AD) is a protein misfolding disease. Its physical manifestation in the brain is the deposit of insoluble amyloid-β peptides (Aβ peptides), which are the fragments of the amyloid precursor protein (APP). Understanding the accumulation of Aβ peptides will help to solve the molecular mechanism of AD [3-8]. The interaction of zinc, copper, iron and other metal ions can modify the aggregation pathways of Aβ peptides. Since the levels of metal ions (for example, Zn^{2+} and Cu^{2+}) in patients with AD are 3-7 fold higher than those in healthy people, potential treatment for AD by metal chelator therapy has been proposed [9-10]. Mass spectrometry has been applied to study AD [11-14], and in particular the metal/Aβ complexes, the metal/peptide stoichiometry, and the fragmentation mechanism of Aβ-Metal ion complexes.

Another example where metal ions play an important role in biology is in zinc finger proteins (ZFPs), the large transcription factors in the eukaryotic genome. ZFPs are zinc-binding proteins that regulate protein-protein and protein-nucleic acid interactions. Many ZFPs regulate the normal growth and development of the cell and tissues, while some ZFPs have been reported as key transcriptional regulators involved in adipogenesis [2, 15]; these proteins are potential targets for human obesity treatment [15]. In the binding site, zinc is chelated to the cysteine thiol group and histidine imidazole [2, 16]. ESI-MS was used to examine the binding of Zn^{2+} and Co^{2+}

to cysteinylglycine (CG) and histidylglycine (HG) as small model molecules of ZFPs [17]. The results showed that the $[Zn(CG)(HG)]^{2+}$ complex was able to recognize DNA. Complexes $[M_n(peptide\text{-}2(n\text{-}1)H]^{2+}$, where $M=Pb^{2+}$ or Zn^{2+} and peptide = N-terminal blocked zinc-like 12-residue peptide, were investigated by tandem mass spectrometry [18]. The MS^2 spectra of the complexes showed water and methane loss and revealed the location and coordination of the metal cations. Zinc was found to prefer binding with histidine and then with cysteine, while lead prefers binding with cystine residues.

In addition to zinc, calcium(II) plays a key role in biological processes. Calmodulin (CaM), a calcium-binding protein, is an intracellular calcium sensor. The recognition of Ca^{2+}-CaM to the polypeptide segment in target protein induces conformation changes in CaM and target protein and activates the function of the target protein. CaM can wrap the target protein, and the methionine residues of the hydrophobic patches optimize the contact of the CaM with the target protein [19]. With electrospray ionization mass spectrometry, the stoichiometry of the calcium-binding to calmodulin was determined [20]. A model peptide containing aspartic acid, glutamic acid, and asparagines, which are in the calcium binding site, was synthesized to study the calcium binding sites by fragmentation of the Ca^{2+}/peptide complexes in the gas phase [21]. Under low-energy collision-induced dissociation, the CID spectra indicate that Ca^{2+} prefers binding to deprotonated acidic side chains and carbonyl oxygens.

One more reason why the study of the metal ion/peptide complexes is important is that the fragmentation of a metal-cationized peptide gives information on the primary structure (sequence) of the peptide. Alkaline metal ions bind with small peptides mainly at the carbonyl oxygens of both the C-terminal residue and the adjacent amide group. With fast atom bombardment combined with tandem mass spectrometry, the C-terminal amino acid residue can be determined

quickly by fragmentation of the [Peptide + Li]$^+$ ion [22]. C-terminal peptide sequencing is also proposed for sodium-cationized peptides by the MS^n experiment under low-energy collision-induced dissociation conditions using the quadrupole ion trap and ion cyclotron resonance mass spectrometers [23]. Rearrangment reactions result in the loss of the C-terminal residue and formation of the product ion with one amino acid shorter than the precursor. Sequential cleavage of the C-terminal residue can then happen by repeating the reaction. Two mechanisms have been proposed for this process [24]: 1) The alkali metal cation coordinates to the carbonyl oxygen of the amide bond [25] and stimulates nucleophilic attack by the C-terminal carboxyl group; 2) the peptide has a zwitterionic-type structure in which the alkali metal ion binds to the C-terminal carboxylate anion [26] and the positive charge is carried remotely by a protonated nitrogen or oxygen; nucleophilic attack on the amide is then initiated by the metallated carboxylate. Both mechanisms lead to the formation of five-membered ring oxazolidin-5-one derivative, as shown in Scheme **I** [24].

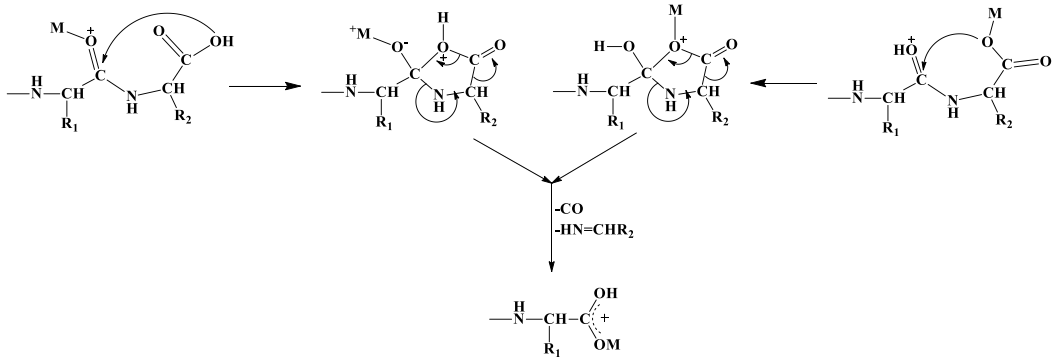

Scheme **I**

Further investigations on the mechanism of C-terminal fragmentations in alkali metal ion complexes of peptides, using mass spectrometry and ab initio calculations (MP2/6-31+G(d)//HF/6-31+G(d)), suggested that the pathways to form the structures in Scheme 1 have

high energy barriers [24]. A mechanism involving a rearrangement to give a symmetrical anhydride of GlyGly intermediate prior to forming the observed products has much lower activation energies. The mechanism starting from a zwitterionic form of diglycine is shown in Scheme **II** [24].

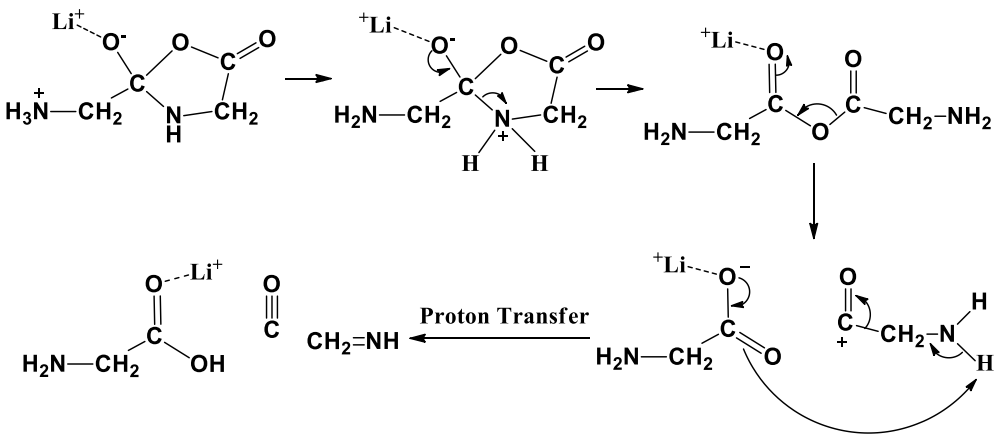

Scheme **II**, adopted from [24]

Compared to Na^+ or K^+, Ag^+ binds to peptides at higher affinity. Under collision-induced dissociation, Ag/peptide complexes can fragment to give improved sequence coverage of peptides [27-28]. $[a_n\text{-H+M}]^+$ and $[b_n\text{+OH+M}]^+$ ions are the dominant products for the fragmentation of metal/peptide complexes (where M=Li or Na) [25]. Instead, for Ag/peptide complexes, $[a_n\text{-H+M}]^+$, $[b_n\text{-H+M}]^+$, $[y_n\text{+H+M}]^+$ and $[b_n\text{+OH+M}]^+$ ions [29] are prevalent. $[b_2\text{-H+Ag}]^+$ ions have been found to be N-argentinated oxazolones, but can further dissociate to form $[a_2\text{-H+Ag}]^+$ions [30].

An analytical application based on the dissociation of the Ag/peptide complex has been proposed [27]: the CID spectra of $[\text{peptide+Ag}]^+$ complexes show a triplet of ions $[b_n\text{+OH+Ag}]^+$, $[b_n\text{-H+Ag}]^+$ and $[a_n\text{-H+Ag}]^+$, which are separated by 18 and 28 *m/z* units, respectively. The difference in *m/z* values of adjacent triplets gives the mass of the amino acid residue that is

cleaved. The complexes of alkali metal ions (Li^+, Na^+, K^+, Rb^+, Cs^+) with peptides that contain only aliphatic residues, for example polyalanines, have been studied with ion-mobility mass spectrometry [31]. By substituting an alkali metal ion for the proton, a polyalanine peptide transforms into a rigid helix from a random globule. The helical conformations of polyalanine peptides can be locked by formation of metal-mediated cross-links due to coordination of the oxyphilic metal ions to the CO groups, and thus facilitate the interactions between the metal ion and the helix dipole [32]. Systematic comparison of the complexes of M^+ (M= Li, Na, K, Rb, Cs), M^{2+} (M=Mg, Ca, Sr, Ba) with polyalanines shows that the abundances of the $[Ala_n+M]^{m+}$ complexes are $M^+>M^{2+}$. $[Ala_n+M]^{2+}$ complexes show helical conformation, with substantial disruption at the C-terminus due to the strong metal coordination [32].

As discussed earlier in this chapter, many divalent metal ions play key roles in biology [5-8, 16, 19]. Gas-phase characterization of metal-peptide interactions discloses the intrinsic properties of such interactions in the absence of solvents and counter ions [21, 32, 33]. Systematic study of the fragmentation of the complexes of alkaline earth metal cationized peptides shows metal ions coordinated at the C-terminus and solvated by neighbouring electron pair donors [34]. Complexes of peptides with transition metal ions (Zn^{2+}, Co^{2+}, Cu^{2+} and Ni^{2+}) generated by ESI were investigated by tandem mass spectrometry [35]. The results show that Zn^{2+}, Co^{2+}, and Ni^{2+} bind at the histidine site for histidine-containing peptides, while Cu^{2+} binds at the C-terminus and gives CO_2 upon dissociation. When the C-terminus is not a carboxylate group, the histidine residue is the Cu^{2+} binding site [35]. One additional unique feature for Cu^{2+} [35] is that fragmentation of Cu(II)/angiotensin I peptide (AngI, Asp^1-Arg^2-Val^3-Tyr^4-Ile^5-His^6-Pro^7-Phe^8-His^9-Leu^{10}) produces a radical ion $[a_{n-1}^{\bullet}+Cu]^{2+}$. Research on the interaction of a series of divalent metal cations (M^{2+}= Ca, Co, Ni, Cu, and Zn) with angiotensin I has been examined by CID and

ion mobility spectrometry–mass spectrometry (IMS–MS) [36]. Results showed that Ca^{2+} prefers binding to oxygen atoms along the peptide backbone and the transition metals prefer binding to the histidine side chain at a site that involves histidine residues.

Among the divalent metal ions studied, copper shows unique characteristics [35]. Copper (II) ions bind nitrogen and oxygen ligands, readily giving ternary complexes [37]. Copper (II) can induce redox and radical type reactions which is useful for structure elucidation of peptides. Under low-energy CID, fragmentation of $[Cu(peptide)(dien)]^{2+}$ (where dien = diethylenetriamine) generated in electrospray mass spectrometry can give the molecular radical cation of the peptide $[peptide]^{+\bullet}$ and $[Cu^{I}(dien)]^{+}$ [38]. The fragmentation of peptide radical cations shows rich radical-induced chemistry, which complements the information obtained by the fragmentation of protonated peptides, and can provide extra peptide sequencing information.

As discussed, investigation of the coordination of metal ions with various peptides and how the attached metal ion affects the dissociation of peptides provides information which is helpful for peptide sequencing and examining the conformation of proteins [20-38]. However, formation of tripositive metal(III)/peptide complexes is challenging in the gas phase, because the trivalent metal ions are readily reduced by protic ligands. This maybe explained by the ionization energy of metal ions and peptide.

The ionization energies of most solvent molecules are 8-12 eV, and for divalent metals, the second ionization energies are between 15 to 22 eV, except Ca^{2+}, Sr^{2+} and Ba^{2+}which are below 12 eV. Third ionization potentials are above 19 eV, and thus metal trications are not usually observed in the gas phase [39-40]. Solvated metal dications can be generated by ESI and then transferred into the gas phase [40-44]. With the presence of aprotic solvents dimethyl sulphoxide

(DMSO) or acetonitrile, complexes $[Y(DMSO)_m]^{3+}$ and $[La(CH_3CN)_m]^{3+}$ were observed in high abundance [45].

While an auxiliary ligand can lower the ionization energies of the metal ions, then make them more stable in the gas phase, the effort to introduce the metal(III)/peptide complexes to the gas phase in the absence of solvent has never been given up. An initial attempt to generate the tripositive of complex of polyalanine (n=14-25) with trivalent metal ions (In^{3+}, Sc^{3+} and Y^{3+}) using ESI-IMS-quadrupole mass spectrometer was not successful [32]. Despite this, a series of trivalent metal ions (La, Al, Ga, Fe, V and Cr) were reported to form the tripositive metal(III)/peptide complex for three peptides with 9-13 residues that contain a basic amino acid (arginine), and one with a highly acidic residue with 21-amino acids [40].

La(III) was found to be stable in the gas phase when CH_3CN was used as a ligand [45], and its coordinations with CH_3CN and peptides have been investigated [46-47]. Under low-energy collision-induced dissociation conditions, ion-molecule reactions of $[La(CH_3CN)_n]^{3+}$ (n=6-9) or $[La(NC(CH_2)_4CN)_n]^{3+}$ (n=3-4) with water showed the preferred coordination number of La^{3+} is eight, since the products $[La(CH_3CN)_p(H_2O)_{8-p}]]^{3+}$ (p=6-8) and $[La(NC(CH_2)_4CN)_q(H_2O)_{8-2q}]^{3+}$ were most abundant under a wide-range of experimental conditions [46]. To generate a stable $[La(peptide)]^{3+}$ complex for an oligopeptide, the presence of a basic amino acid residue is necessary in order to form a zwitterionic peptide. Ln^{3+} is bound to the deprotonated carboxylate group, as well as carbonyl oxygen, while the basic functional group is protonated (see Scheme **III**) [47]. In the presence of an arginine residue, $[La(peptide)]^{3+}$ complexes with peptides (2-4 amino-acid residue) were observed. The sulfur atom in the methionine residue can also contribute to La^{3+} binding. Scheme III shows the coordination of La^{3+} to the peptide GGR and MR, and the plausible resulting structures [47].

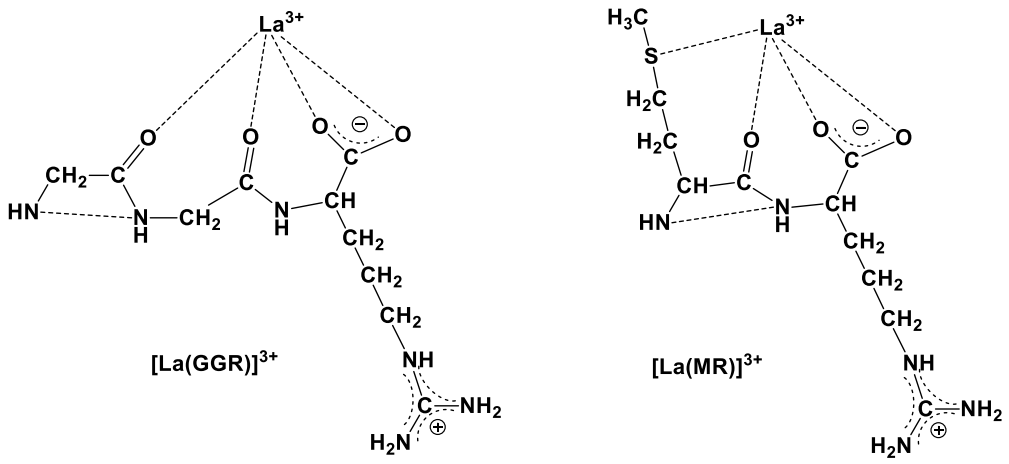

Scheme III $[La(GGR)]^{3+}$ and $[La(MR)]^{3+}$, adopted from [47]

The interaction of the trivalent lanthanide cations with peptides has attracted interest as Ln^{3+} ions were used to mimic Ca^{2+} [48]. The lanthanides have been used as metal-based drugs, for example, lanthanum carbonate for the treatment of hyperphosphatemia and cerium nitrate as a topical cream with silver sulfadiazine for the treatment of burn wounds. The lanthanides have diverse physical properties: Eu^{3+} and Tb^{3+} have long-lived luminescence, while Gd^{3+} has high spin values and long electronic relaxation times [49]. The binding of lanthanides to peptides has systematically examined [50].

The coordination of lanthanide metal cations with peptides has also been investigated with infrared multiple photon dissociation (IRMPD) spectroscopy to obtain structural and binding details [51]. In IRMPD, a mass-selected ion is irradiated with a tunable infrared laser at given frequencies. IRMPD simulates IR absorption spectroscopy but relies on the percent dissociation of the mass selected ion at a given frequency [52]. IRMPD has been proven to be a reliable proxy to IR absorption spectroscopy in many experiments, but largely in relatively simple ions [52]. IRMPD has been used to probe the structures of metal-ion peptide complexes of small peptides. A theoretical computation study together with IRMPD experiments was used to

determine if the metal was bound to the peptide via a charge-solvated (CS) (to amide carbonyl oxygens) or an iminol model (to amide nitrogen) [53-54]. It was suggested that for the singly-charged complexes, the CS model is preferred, whereas for doubly-and triply-charged complexes, the “late” or “transition” metal ions favor iminol, and “early” or “ main-group” metal prefers CS. Mg(II) and Mn(II) show the boundary value across the two models.

The first IRMPD experiment on triply charged metal ion complexes was on lanthanum-tryptophan complexes [55]. Combining density functional theory (DFT) calculations and IRMPD experimental results, the binding sites of La^{3+} proved to be the indole rings of the tryptophan derivatives, and also the carbonyl oxygens. IRMPD was used to study the metal(III)/peptide complexes of trivalent lanthanide cations La^{3+}, Ho^{3+} and Eu^{3+} with deprotonated polyalanine Ala_n (n=2-5) and leucine enkephalin (Leu-enk) (YGGFL), which has a salt bridge structure, that is, metal ions coordinating to the carboxylate group of the peptide [51]. IRMPD spectra show that all of the carbonyl groups of the Ala_n solvate the metal cations in the complexes. When there is an aromatic residue in the peptide, for example W or F, the π-electron system of the aromatic group interacts with the metal cation, including alkali metal ions [56]. Coordination of the metal ion with the aromatic side chain prevents coordination with the backbone carbonyl groups, thus free carbonyl groups can be observed.

As mentioned earlier in this section, CID has been used for the study on the interaction of metal ions with peptides, and it is also used in this work to study the dissociation behaviour of metal(III)/peptide complexes. CID is the most popular dissociation technique for peptide sequencing, while electron transfer dissociation (ETD) and electron capture dissociation (ECD) are two alternative dissociation techniques also used in peptide sequencing [57-58]. ECD [59] utilizes low-energy electrons, typically from an electron gun, to interact with multiply-charged

biomolecules, for example, proteins to cause specific cleavage of the N-Cα bond to form c/z type ions. These ions provide complementary peptide fragmentation information to CID, which primarily cleaves the peptide bind to form b/y type ions. An important characteristic of ECD is that fragmentation of the peptide backbone is preferred over cleavage of post-translation modification (PTM), in contrast to CID, and hence is very useful in PTM analysis [60-61]. Electron capture dissociation was developed on relatively expensive FT-ICR instruments; by contrast, electron transfer dissociation [62] can be practical in relatively inexpensive quadrupole linear ion traps by electron transfer from a singly charged anthracene anion to a multiply protonated peptide. In general, ECD and ETD spectra are similar.

With the ECD technique, divalent alkaline-earth metal ions including Mg^{2+}, Ca^{2+}, Sr^{2+} and Ba^{2+}, have been used as the charge carrier to study the electron capture dissociation of peptides [63]. The complexes of model peptides (RGGGVGGGR or NGGGWGGGN) with the above metal ions all generated very similar ECD spectra. The predominant products were metalated *c*-ions and *z*-ions. Some non-metalated c-ions were observed for $[Mg + RGGGVGGGR]^{2+}$ only. Informed by ab initio calculations, it was postulated that the acidity of the amide hydrogens was activated by the metal ion. The metal/peptide complex can exist in the zwitterionic form by deprotonating an amide group on the peptide backbone and protonating the N-terminal amino group or the side chain of the arginine residue. Further studies have also been carried out on the divalent metal/peptide complexes of transition metal ions, including Mn^{2+}, Fe^{2+}, Co^{2+}, Ni^{2+},Cu^{2+}, and Zn^{2+} [64]. ECD of peptide complexes with Mn^{2+} or Zn^{2+} showed similar spectra as that with alkaline-earth metal ions [64], and with c/z type fragments being abundant. Those with Fe^{2+},Co^{2+} or Ni^{2+} gave abundant metal-containing a/y type fragment ions, whereas those with Cu^{2+} generated abundant Cu^{2+}-containing b/y type product ions. It was suggested that the dissociation

of metal(II)/ peptide complexes under ECD condition is mainly determined by the electronic configuration of the metal ion, and there are two compeptitive channels to capture the electron. With fully-filled metal ion Zn^{2+} and half-filled Mn^{2+}, electron capture is not energetically favourable, and fragmentation after electron-proton recombination is the predominant channel. For other metal(II)/peptide complexes, a/b/y ions generated, energy transfer after electron-metal ion recombination is predominant channel.

Details of dissociation of Cu(II)/peptide complexes have also been examined by ECD and CID [65]. It was found that the amide hydrogen plays a critical role in the formation of metalated b-ions in ECD. Internal electron transfer between the tryptophan residue and metal ion within the complexes can occur in CID [65]. Increasing the peptide length suppressed the dissociation [65]. In contrast to ECD studies, the dissociation of $[Cu(II)(peptide+H)]^{3+}$ in ETD, where the peptide contains strongly coordinating residues, such as aspartic acid (D), histidine (H), methionine (M) and glutamic acid (E), generates abundant c- and z- type product ions [66]. The strong binding sites can lower the recombination energy of Cu(II) and enable electron transfer to a Cu-remote site, which competes with Cu(II) reduction, thus leading to formation of the c/z type product ions. Hence Cu(II) reduction is not involved in the processes despite the fact that Cu has a high second ionization energy.

The dissociation of Ln(III)/peptide complexes was studied with ECD [67], where Ln = La, Tm, Lu, Sm, Ho, Yb, Pm, Tb or Eu. For peptides with molecular weights below ~1000 Da, $[Ln(peptide-H)]^{2+}$ was readily formed. The fragmentation of $[Ln(peptide-H)]^{2+}$ gave extensive fragmentations which potentially could be used for peptide sequencing.

ECD of these doubly charged complexes containing trivalent metal ions displays much higher electron capture efficiency and sequence coverage compared to those of doubly charged divalent

Metal(II)/peptide complexes. For larger peptides, $[Ln(peptide)]^{3+}$ is predominant and its dissociation results in electron capture by the metal-remote protonation site. All metal/peptide complexes gave abundant c/z fragments without direct reduction, except Eu^{3+}. Eu^{3+} reduced to Eu^{2+} in the complex, and b/y type ions and small neutral molecule loss were observed. Dissociation of the complexes of bradykinin-derived peptides with trivalent metal ions (Al^{3+}, Ga^{3+}, In^{3+} or Rh^{3+}) [68] under ECD showed that c/z type ions with or without the metal were observed for Group IIIB metal ions (Al^{3+}, Ga^{3+}, In^{3+}); this suggests that the electron was captured by the proton in the salt-bridge of the complexes. By contrast, metalated a/b type ions and y ions without the metal were observed for Rh^{3+} /peptide complexes, indicating that the electron is captured by the metal ion in a charge-solvated complexes.

Under ETD conditions, sequencing of acidic peptides could be realized with the dissociation of lanthanide/peptide complexes [69]. Trivalent lanthanides generates $[Ln + peptide + H]^{4+}$, $[Ln + peptide]^{3+}$ and $[Ln + peptide\text{-}H]^{2+}$ ions, which undergo ETD fragmentation, and form c/z type ions with or without the metal ion. Abundant sequence–informative product ions and extensive backbone cleavage make the ETD of lanthanide/peptide complexes a potential strategy for peptide sequencing [69]. All lanthanide ions studied show similar fragmentation behaviour, except Eu(III). Among them Pr(III) was proposed to be the best candidate since it produced abundant metal/complex ions, while Sm(III) could be used to assist confirmation of the metallated product ions [69].

1.2 Peptide radical cations

As described in section 1.1, under low-energy CID, fragmentation of Cu/peptide ternary complexes can generate the molecular radical cation of the peptide, $[peptide]^{+\bullet}$ [38]. The

dissociation of $[peptide]^{+\bullet}$ is not only charge-driven, but also radical driven; hence, the CID spectrum of $[peptide]^{+\bullet}$ gives more information about peptide primary structure.

There are a number of methods that have been used to generate cationic peptide radicals [70]. For example: 1) CID of ternary metal complexes with peptide and an auxiliary ligand; 2) UV-photo-excitation of peptide cations, or UV-photo-dissociation of photolabile radical precursor; 3) free radical initiated peptide sequence (FRIPS); and 4) loss of NO from a peptide nitrosylated at a tryptophan or cysteine residue [71]. In the past decade, the most widely used method of the four was 1): generation of peptide radical cations by CID of dipositive Cu(II)-peptide complexes in the gas phase [72-77].

The generation of peptide radical cations can be described by equation 1:

$$[Cu^{II}(peptide)(L)]^{\bullet 2+} \xrightarrow{CID} [Cu^{I}(L)]^{+} + peptide^{\bullet +} \qquad \text{(Equation 1)}$$

where L is the auxiliary ligand and can be diethylenetriamine, a crown ether, 1,4,7-triazacyclononane or terpyridine. Formation of peptide radical cations occurs most readily if the peptide contains a tyrosine, tryptophan, methionine, or a basic residue arginine, lysine or histidine. The redox chemistry is coupled to fragmentation of the $[Cu^{II}(peptide)(L)]^{2+}$ complex. Dissociation of the complex by homolytic bond cleavage produces the molecular peptide radical cations, oxidized by Cu^{2+}, and formation of the reduced copper/ligand complex $[Cu^{I}(L)]^{+}$ as the counter ion. The abundance of the molecular peptide radical cations generated by this method is dependent on four competitive fragmentation channels as follows [73, 78].

$$[Cu^{II}(peptide)(ligand)]^{2+} \longrightarrow [Cu^{I}(ligand)]^{+} + [peptide]^{\bullet +} \qquad \text{(Peptide radical formation)}$$

$$\longrightarrow [Cu^{II}(ligand\text{-}H)]^{+} + [peptide+H]^{+} \qquad \text{(Proton transfer)}$$

$$\longrightarrow [Cu^{II}(peptide\text{-}H)]^{+} + [ligand+H]^{+} \qquad \text{(Proton transfer)}$$

$$\longrightarrow [Cu^{II}(\text{peptide-}b_n)(\text{ligand})]^{\bullet+} + [b_n]^+ \quad \text{(Peptide fragmentation)}$$

In contrast with the multiply-protonated peptides radicals found in ECD and ETD, the molecular radical cations have been described as hydrogen-deficient radical cations [79]. Fragmentation of peptide radical cations can be radical-driven or proton-driven. For this reason, the CID spectra of peptide radical cations normally give richer sequence-informative product ions. Due to the high 3rd ionization potential of trivalent metal ions, it is challenging to transfer the tripositive complexes metal^{III}/peptide to the gas phase. Triply charged metal ion/peptide complexes tend to be more fragile under typical MS sampling conditions. Trivalent metal ion complexes have been succesfully examined by tandem mass spectrometry when the triple charge of the metal ions was partially offset by an anionic ligand, for example, in the monopositive [Metal^{III}(salen-2H)(peptide)]$^+$ complex where metal = Cr, Mn, Fe, or Co [80].

1.3 Lanthanide chemistry

The lanthanides are a series of metallic elements that have stable +3 charged ions and they have similar chemical and physical characteristics. Lanthanum and the other 14 elements with atomic numbers 57 to 71 are called the "Lanthanides, or Lanthanoids" (abbreviated as Ln). Together with scandium and yttrium, they are sometimes referred to as the "Rare Earth Elements", although this name is not recommended by IUPAC. The lowest energy electronic configurations of the lanthanides are typically [Xe]$4f^n6s^2$ or [Xe]$4f^{n-1}5d^16s^2$ [81], where [Xe] describes the electronic configuration of xenon: $1s^22s^22p^63s^23p^63d^{10}4s^24p^64d^{10}5s^25p^6$. The electronic ground state of lanthanum is [Xe] $5d^16s^2$. For the next elements and beginning with Ce, the elements start to fill the 4f orbitals one by one. Lathanum, cerium and gadolinium belong to the [Xe]$4f^{n-1}5d^16s^2$ configuration and all the other lanthanides belong to [Xe]$4f^n6s^2$ as shown in Table 1.

Scandium and yittrium have the $(n-1)d^1ns^2$ configuration for their outer electrons, so they have chemical properties similar to lanthanides and hence sometimes are treated as lanthanides [81].

An unusual characteristic of the lanthanides is the "lanthanide contraction", that is, with increasing atomic number, the atomic radius and ionic radius all decrease steadily as shown in Table 1. The 4f orbitals are rarely involved in binding because they are buried deeply. The lanthanide contraction contributes to the similarity of chemistry within the lanthanide family [81, 83, 88-91]. The lanthanide contraction is a consequence of the relatively poor shielding by the f-electrons as the nuclear charge increases. As the nuclear charge increases, the increase in electrostatic attraction between the nucleus and the electrons is balanced by the increased electrostatic repulsion between the electrons. For the inner electrons, the shielding effect decreases in the order of s>p>d>f. The 4f electrons are diffuse, have poor shielding effect. As a consequence, as the atomic number increases, the electrostatic attraction between the nucleus and the outer electrons increases, resulting in a reduction of the atomic or ionic radius [83].The preferred coordination number of the lanthanides is 8 or 9; by comparison the preferred coordination number of Ca^{2+} is six [48, 81].

Table 1.1 Selected chemical and physical parameters of rare earth elements [81-87]

Element	Atomic Radius (pm) [81-82]	Ionic Radius (M^{3+}) in Å [83]	1st IE [84]	2nd IE [84]	3rd IE [84]	Un-paired electron	Electron Configuration [81]	Naturally occurring Isotopes and abundance [85,86]	Standard atomic weight [87]
^{21}Sc	162	68	6.56	12.80	24.76	1	[Ar] $3d^1\ 4s^2$	^{45}Sc, 100%	45.0
^{39}Y	180	88	6.22	12.23	20.52	1	[Kr] $4d^1\ 5s^2$	^{89}Y, 100%	88.9
^{57}La	187.7	106.1	5.58	11.06	19.17	0	[Xe] $5d^1\ 6s^2$	^{138}La, 0.09%; ^{139}La, 9.91%	138.9
^{58}Ce	182	103.4	5.46	10.85	20.20	1	[Xe] $4f^1\ 5d^1\ 6s^2$	^{136}Ce, 0.19%; ^{138}Ce, 0.25%; ^{140}Ce, 88.4%; ^{142}Ce, 11.11%	140.1
^{59}Pr	182.8	101.3	5.42	10.55	21.62	2	[Xe] $4f^3\ 6s^2$	^{141}Pr, 100%	140.9
^{60}Nd	182.1	99.5	5.49	10.73	22.10	3	[Xe] $4f^4\ 6s^2$	^{142}Nd, 7.2%, ^{143}Nd, 12.2%; ^{144}Nd, 23.8%; ^{145}Nd, 8.3%; ^{146}Nd, 17.2%; ^{148}Nd, 5.8% ^{150}Nd, 5.6%	
^{61}Pm	181	97.9	5.56	10.90	22.30	4	[Xe] $4f^5\ 6s^2$	^{147}Pm, trace	145
^{62}Sm	180.2	96.4	5.63	11.07	23.40	5	[Xe] $4f^6\ 6s^2$	^{144}Sm, 3.1%, ^{147}Sm, 15.0%; ^{148}Sm, 11.3%; ^{149}Sm, 13.8%; ^{150}Sm, 7.4%; ^{152}Sm, 26.7%; ^{154}Sm, 22.7%	150.4
^{63}Eu	204.2	95.0	5.67	11.25	24.92	6	[Xe] $4f^7\ 6s^2$	^{151}Eu, 47.8%, ^{153}Eu, 52.2%	152.0

^{64}Gd	180.2	93.8	6.15	12.08	20.62	7	[Xe] $4f^7 5d^1 6s^2$	^{152}Gd, 0.2%, ^{154}Gd, 2.2%; ^{155}Gd, 14.8%; ^{156}Gd, 15.7%; ^{158}Gd, 24.8%; ^{160}Gd, 21.9%	157.3
^{65}Tb	178.2	92.3	5.86	11.53	21.91	6	[Xe] $4f^9$ $6s^2$	^{159}Tb, 100%;	158.9
^{66}Dy	177.3	90.8	5.93	11.67	22.94	5	[Xe] $4f^{10}$ $6s^2$	^{156}Dy, 0.1%, ^{158}Dy, 0.1%; ^{160}Dy, 2.3%; ^{161}Dy, 18.9%; ^{162}Dy, 25.5%; ^{163}Dy, 24.9%; ^{164}Dy, 28.3%	162.5
^{67}Ho	176.6	89.4	6.02	11.80	22.84	4	[Xe] $4f^{11}$ $6s^2$	^{165}Ho, 100%;	164.9
^{68}Er	175.7	88.1	6.10	11.93	22.74	3	[Xe] $4f^{12}$ $6s^2$	^{162}Er, 0.1%, ^{164}Er, 1.6%; ^{166}Er, 33.5%; ^{167}Er, 22.9%; ^{168}Er, 27.0%; ^{170}Er, 14.9%;	167.3
^{69}Tm	174.6	86.9	6.19	12.05	23.68	2	[Xe] $4f^{13}$ $6s^2$	^{169}Tm, 100%;	168.9
^{70}Yb	194.0	85.8	6.25	12.19	25.03	1	[Xe] $4f^{14}$ $6s^2$	^{168}Yb, 0.1%, ^{170}Yb, 3.0%; ^{171}Yb, 14.2%; ^{172}Yb, 21.8%; ^{173}Yb, 16.1%; ^{174}Yb, 31.9%; ^{176}Yb, 12.9%	173.0
^{71}Lu	173.4	84.8	5.43	13.90	20.96	0	[Xe]$4f^{14}5d^1$ $6s^2$	^{175}Lu, 97.4%; ^{176}Lu , 2.6%	175.0

According to Hund's rule, electrons occupying a degenerate set of atomic orbitals, e.g. 4f, will adopt an electronic configuration with a maximum multiplicity. Consequently, there is extra stability associated with a half-filled set of orbitals, which is $4f^7$. Similarly, a fully filled set of orbitals has a particular stability. For the lanthanides elements, this explains the preference for La^{3+}, Ce^{4+}, Eu^{2+}, Tb^{4+} and Yb^{2+}.

The lanthanides have unique spectroscopic and magnetic properties. Europium (III) chelates can be used in fluoroimmunoassay [92]. Gadolinium (III), has high-spin paramagnetism (a high spin of 7/2) and its complexes are able to enhance the longitudinal relaxation rate of water protons. Gd(III) has become the most important contrasting agents for magnetic resonance imaging [92-93]. For example, $[Gd(dtpa)]^{2-}$ has been used to enhance the contrast of cerebral tumor images.

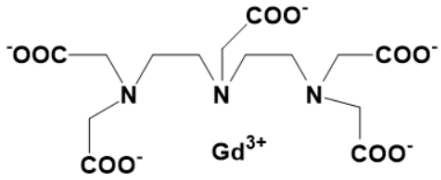

$[Gd(dtpa)]^{2-}$
Magnevist

As described at the beginning of this chapter, the interaction of metal ions with proteins or peptides has drawn interests because of the significance of metalloproteins in electron-transfer in biological systems. The lanthanide elements have similar ionic radii to the calcium ion, Ca^{2+}.

The ionic radius of Ca^{2+} is 99 pm, while the ionic radii of lanthanides are in the range of 84 to 110 pm. Due to a higher charge than Ca^{2+} although having similar ionic radii, Ln^{3+} ions have a higher binding affinity than Ca^{2+}, and hence can act as a Ca^{2+} inhibitor or probe [48]. For example, many Ca^{2+}-dependent enzymes are inhibited by La^{3+} because the higher charge of the

lanthanides tend to result in complexes with enzymes that are more stable than those of Ca^{2+} [94-95].

1.4 $[a_n+H]^{2+}$ ions

It was reported previously [47] that $[La(peptide)]^{3+}$ ion was formed in the gas phase using ESI-triple-quadrupole mass spectrometry for peptides as small as a dipeptide when it contains both methionine and arginine [47]. The dissociation of $[La(peptide)(CH_3CN)_2]^{3+}$ under CID in tandem mass spectrometry has been investigated and dipositive ions, $[a_3+H]^{2+}$ and $[a_2+H]^{2+}$, of the tripeptide GGG were observed [96]. Density functional theory (DFT) calculations showed that the preferred conformation of GGG in the La/GGG complex is zwitterionic. La was attached to GGG by coordinating with O, which causes the cleavage of the carboxylate group and a second positive charge stays on the imino group [96]. The $[a_3+H]^{2+}$ ion is fragile and gives $[H_2N{=}CH_2]^+$ and two types of $[b_2]^+$ ions, protonated oxazolone and amino-protonated ketene, by charge separation. The proposed structure of the $[a_3+H]^{2+}$ ion is linear, which maximmizes charge separation.

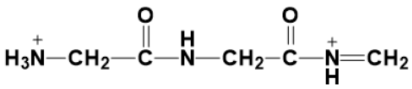

Abundant $[a_3+H]^{2+}$ from the tripeptide PPP, and $[a_2+H]^{2+}$ from the dipeptide PP, were generated, when $[La(PPP)(CH_3CN)]^{3+}$ and $[La(PP)(CH_3CN)_2]^{3+}$ were fragmented under CID, respectively [97]. The pyrrolidine-derived rings delocalize the charges on the backbone, making formation of the $[a_n+H]^{2+}$ ions the major dissociation channels. The peptide composition significantly influences the abundance of the $[a_n+H]^{2+}$ ions generated and has been investigated systematically [98]. The presence of proline, especially in the N-terminal position is crucial to producing abundant $[a_n+H]^{2+}$ ions. PPP gives the most abundant $[a_3+H]^{2+}$ ions of all the peptides examined.

An interesting observation is that although abundant $[a_n+H]^{2+}$ ions were observed in N-terminal proline-containing dipeptides and tripeptide, no $[b_2+H]^{2+}$ or $[b_3+H]^{2+}$ ions were apparent [97-98].

1.5 Thesis research

This thesis examines the chemistries of the formation and dissociation of $[Ln(peptide)(CH_3CN)_n]^{3+}$, where n = 0-6, and their fragmentation products. The focus is on the dissociation of $[Ln(peptide)(CH_3CN)_n]^{3+}$ and the discovery of new routes to generate peptide radical cations.

Chapter 2 describes the experimental methods and the instrumentation.

Chapter 3 describes a detailed study on the formation and dissociation of $[Ln(peptide)(CH_3CN)_n]^{3+}$, where Ln = Y, La, Ce, Sm, Eu, Gd, Tb and Yb. A new route to generate peptide radical cations with peptide-trivalent metal cations in the +3 charge state is described. Comparisons of the fragmentations of tripositive complexes of Ln(III)/peptide of different lanthanide are made.

Chapter 4 presents the fragmentations of tripositive Ce(III)/peptide and Eu(III)/peptide complexes, including unsolvated $[Ce(peptide)]^{3+}$ and $[Eu(peptide)]^{3+}$ ions. CIDs of the product ions of $[Ce(peptide-H)]^{2+}$ and $[Eu(peptide-H)]^{2+}$ are also compared.

Chapter 5 presents a detailed study of the fragmentations of molecular radical cations of aliphatic peptides with or without proline. The $[peptide]^{\bullet+}$ and $[a_3+H]^{\bullet+}$ ions of tripeptides containing only G, A or P, whose formation is very challenging, but viable with CIDs of $[Eu(peptide)(ligand)_n]^{3+}$ or $[Cu(peptide)(ligand)]^{2+}$ are examined.

Chapter 6 describes the formation and fragmentation of $[b_n+H]^{2+}$ and $[a_n+H]^{2+}$, where n=2 or 3. New doubly charged peptide fragments $[b_n+H]^{2+}$ ions are described. The fragmentation patterns

of $[b_n+H]^{2+}$ and $[a_n+H]^{2+}$, where n=2 or 3, are systematically examined with different peptide compositions.

Chapter 7 presents data on the dissociations of $[Ce(peptide\text{-}H)]^{2+}$, $[Ce(peptide\text{-}H)(peptide)]^{2+}$and $[Eu(peptide\text{-}H)]^{2+}$ complexes.

1.6 References

1. Holm, R. H., Kennepohl, P. and Solomon, E. I. Structural and Functional Aspects of Metal Sites in Biology. Chem Rev. 1996; 96(7): 2239–2314.
2. Carlton, D. D. and Schug, K. A. A review on the interrogation of peptide–metal interactions using electrospray ionization-mass spectrometry. Anal Chim Acta. 2011; 686(1): 19–39.
3. Glenner, G. G. Wong C. W. Alzheimer's disease: Initial report of the purification and characterization of a novel cerebrovascular amyloid protein. Biochem Biophys Res Commun. 1984; 120(3): 885–890
4. Wärmländer, S., Tiiman, A., Abelein, A., Luo, J., Jarvet, J., Söderberg, K. L., Jens, D. and Gräslund, A. Biophysical Studies of the Amyloid β-Peptide: Interactions with Metal Ions and Small Molecules. ChemBioChem. 2013; 14(14): 1692–1704.
5. Lin, C.-J., Huang, H.-C., and Jiang, Z.-F. Cu(II) interaction with amyloid-β peptide: A review of neuroactive mechanisms in AD brains. Brain Res Bull. 2010; 82(5): 235–242.
6. Bush, A. I., Pettingell, W. H., Multhaup, G., Paradis, M. d, Vonsattel, J. P., Gusella, J. F., Beyreuther K., Masters C.CL., Tanzi, R. E. Rapid induction of Alzheimer A beta amyloid formation by zinc. Science. 1994. 265(5177), 1464–1467.
7. Cuajungco, M. P. and Fagé, K.Y. Zinc takes the center stage: its paradoxical role in Alzheimer's disease. Brain Res Rev. 2003; 41(1): 44–56.
8. Bush, A. I., Masters, C. L. and Tanzi, R. E. Copper, β-amyloid, and Alzheimer's disease: tapping a sensitive connection. Proc. Natl Acad Sci. 2003; 100(20): 11193–11194.
9. Domingo, J. L. Aluminum and other metals in Alzheimer's disease: A review of potential therapy with chelating agents. J Alzheimers Dis. 2006; 10(2–3): 331–341.

10. Huang, W., Wei, W. and Shen, Z. Drug-like chelating agents: a potential lead for Alzheimer's disease. RSC Advances. 2014; 4(94): 52088–52099.

11. Zirah, S., Rebuffat, S., Kozin, S. A., Debey, P., Fournier, F., Lesage, D. and Tabet, J.-C. Zinc binding properties of the amyloid fragment Aβ (1–16) studied by electrospray-ionization mass spectrometry. Int J Mass spectrom. 2003; 228(2–3): 999–1016.

12. Drochioiu, G. An Electrospray Ionization Mass Spectrometric Study of Iron Binding to Amyloid-β Peptides. Eur J of Mass Spectrom.2009; 15(5): 651–659.

13. Grasso, G. The use of mass spectrometry to study amyloid-β peptides. Mass Spectrom Rev. 2010; 30(3): 347–365.

14. Giuffrida, M. L., Grasso, G., Ruvo, M., Pedone, C., Saporito, A., Marasco, D., Pignataro B., Cascio C., Copani A. and Rizzarelli, E. Aβ (25–35) and its C- and/or N-blocked derivatives: Copper driven structural features and neurotoxicity. J Neurosci Res. 2007; 85(3): 623–633.

15. Wei, S., Zhang, L., Zhou, X., Du, M., Jiang, Z., Hausman, G. J., Bergen W. G., Zan L. and Dodson, M. V. Emerging roles of zinc finger proteins in regulating adipogenesis. Cell Mol Life Sci. 2013; 70(23): 4569–4584.

16. Maret, W. and Li, Y. Coordination Dynamics of Zinc in Proteins. Chem Rev. 2009; 109(10): 4682–4707.

17. Reddy, P. R., Radhika, M. and Rao, K. S. Interaction of zinc and cobalt with dipeptides and their DNA binding studies. J Chem Sci. 2004; 116(4): 221–226.

18. Banu, L., Blagojevic, V. and Bohme, D. K. Locating Pb^{2+} and Zn^{2+} in Zinc Finger-Like Peptides Using Mass Spectrometry. J Am Soc Mass Spectrom. 2013; 24(10): 1534–1542.

19. Crivici, A. and Ikura, M. Molecular and structural basis of target recognition by calmodulin. Annu Rev Biophys Biomol Struct. 1995; 24(1): 85–116.

20. Hu, P., Ye, Q.Z. and Loo, J. A. Calcium Stoichiometry Determination for Calcium Binding Proteins by Electrospray Ionization Mass Spectrometry. Anal Chem. 1994; 66(23): 4190–4194.

21. Nemirovskiy, O. and Gross, M. Determination of calcium binding sites in gas-phase small peptides by tandem mass spectrometry. J Am Soc Mass Spectrom. 1998; 9(10): 1020–1028.

22. Grese, R. P., Cerny, R. L. and Gross, M. L. Metal ion-peptide interactions in the gas phase: a tandem mass spectrometry study of alkali metal cationized peptides. J Am Chem Soc. 1989; 111(8): 2835–2842.

23. Lin, T. and Glish, G. L. C-Terminal Peptide Sequencing via Multistage Mass Spectrometry. Anal Chem. 1998; 70(24): 5162–5165.

24. Feng, W. Y., Gronert, S., Fletcher, K.A., Warres, A. and Lebrilla, C. B. The mechanism of C-terminal fragmentations in alkali metal ion complexes of peptides. Int J Mass Spectrom. 2003; 222(1–3): 117–134.

25. Teesch, L. M. and Adams, J. Fragmentations of gas-phase complexes between alkali metal ions and peptides: metal ion binding to carbonyl oxygens and other neutral functional groups. J Am Chem Soc. 1991; 113(3): 812–820.

26. Grese, R. P. and Gross, M. L. Gas-phase interactions of lithium ions and dipeptides. J Am Chem Soc. 1990; 112(13): 5098–5104.

27. Chu, I. K., Guo, X., Lau, T.-C. and Siu, K. W. M. Sequencing of Argentinated Peptides by Means of Electrospray Tandem Mass Spectrometry. Anal Chem. 1999; 71(13): 2364–2372.

28. Barr, J. M. and Van Stipdonk, M. J. Multi-stage tandem mass spectrometry of metal cationized leucine enkephalin and leucine enkephalin amide. Rapid Commun Mass Spectrom. 2002; 16(6), 566–578.

29. Li, H., Siu, K. M., Guevremont, R. and Le Blanc, J. Y. Complexes of silver (I) with peptides and proteins as produced in electrospray mass spectrometry. J Am Soc Mass Spectrom. 1997; 8(8): 781–792.

30. Lee, V. W.-M., Li, H., Lau, T.-C. and Siu, K. W. M. Structures of b and a Product Ions from the Fragmentation of Argentinated Peptides. J Am Chem Soc. 1998; 120(29): 7302–7309.

31. Kohtani, M., Kinnear, B. S. and Jarrold, M. F. Metal-Ion Enhanced Helicity in the Gas Phase. J Am Chem Soc. 2000; 122(49): 12377–12378.

32. Kohtani, M., Jarrold, M. F., Wee, S. and O'Hair, R. A. J. Metal Ion Interactions with Polyalanine Peptides. J Phys Chem B. 2004; 108(19): 6093–6097.

33. Hu, P. and Gross, M. L. Gas-phase interactions of transition-metal ions and di- and tripeptides: a comparison with alkaline-earth-metal-ion interactions. J Am Chem Soc. 1993; 115(19): 8821–8828.

34. Küjckelmann, U., Müller, D. and Weber, C. Systematic studies of the mass spectrometric properties of alkaline earth metal cationized amino acids and peptides. J Mol Struct. 1997; 412(1): 135–139.

35. Hu, P. and Loo, J. A. Gas-Phase Coordination Properties of Zn^{2+}, Cu^{2+}, Ni^{2+}, and Co^{2+} with Histidine-Containing Peptides. J Am Chem Soc. 1995; 117(45): 11314–11319.

36. Glover, M. S., Dilger, J. M., Zhu, F. and Clemmer, D. E. The binding of Ca^{2+}, Co^{2+}, Ni^{2+}, Cu^{2+}, and Zn^{2+} cations to angiotensin I determined by mass spectrometry based techniques. Int J Mass Spectrom. 2013; 354–355: 318–325.

37. Tureček, F. Copper-biomolecule complexes in the gas phase. The ternary way. Mass Spectrom Rev. 2007; 26(4): 563–582.

38. Chu, I. K., Rodriquez, C. F., Lau, T.-C., Hopkinson, A. C. and Siu, K. W. M. Molecular Radical Cations of Oligopeptides. J Phys Chem B. 2000; 104(15): 3393–3397.

39. Spears, K. G. and Fehsenfeld, F. C. (1972). Termolecular Association Reactions of Mg, Ca, and Ba Ions. J Chem Phys, 56(11), 5698–5705.

40. Shvartsburg, A. A. and Jones, R. C. Attachment of metal trications to peptides. J Am Soc Mass Spectrom. 2004; 15(3): 406–408.

41. Shvartsburg, A. A. Gas-Phase Metal Trications in Protic Solvent Complexes. J Am Chem Soc. 2002; 124(27): 7910–7911.

42. Cheng, Z. L., Siu, K. W. M., Guevremont, R. and Berman, S. S. Electrospray mass spectrometry: a study on some aqueous solutions of metal salts. J Am Soc Mass Spectrom. 1992; 3(4): 281–288.

43. Jockusch, R. A., Lemoff, A. S. and Williams, E. R. Effect of Metal Ion and Water Coordination on the Structure of a Gas-Phase Amino Acid. J Am Chem Soc. 2001; 123(49): 12255–12265.

44. Shvartsburg, A. A., Wilkes, J. G., Lay, J. O. and Siu, K. W. M. Fragmentation and charge transfer in gas-phase complexes of divalent metal ions with acetonitrile. Chem Phys Lett. 2001; 350(3): 216–224.

45. Cheng, Z. L., Siu, K. W. M., Guevremont, R. and Berman, S. S. Solvent-derived metal oxides in electrospray mass spectrometry of metal salt solutions. Org Mass Spectrom. 1992; 27(12): 1370–1376.

46. Shi, T., Hopkinson, A. C. and Siu, K. W. M. Coordination of Triply Charged Lanthanum in the Gas Phase: Theory and Experiment. Chem Euro J. 2007; 13(4), 1142–1151.

47. Shi, T., Siu, K. W. M. and Hopkinson, A. C. Generation of [La(peptide)]$^{3+}$ Complexes in the Gas Phase: Determination of the Number of Binding Sites Provided by Dipeptide, Tripeptide, and Tetrapeptide Ligands. J Phys Chem A. 2007; 111(45), 11562–11571.

48. Fricker, S. P. The therapeutic application of lanthanides. Chem Soc Rev. 2006; 35(6): 524–533.

49. Bünzli, J.-C. G. Benefiting from the Unique Properties of Lanthanide Ions. Accounts of Chem Res. 2006; 39(1): 53–61.

50. Ancel, L., Niedźwiecka, A., Lebrun, C., Gateau, C. and Delangle, P. Rational design of lanthanide binding peptides. C R Chim. 2013; 16(6): 515–523.

51. Prell, J. S., Flick, T. G., Oomens, J., Berden, G. and Williams, E. R. Coordination of Trivalent Metal Cations to Peptides: Results from IRMPD Spectroscopy and Theory. J Phys Chem A. 2010; 114(2): 854–860.

52. Polfer, N. C. Infrared multiple photon dissociation spectroscopy of trapped ions. Chem Soc Rev. 2011; 40(5): 2211–2221.

53. Dunbar, R. C., Polfer, N. C., Berden, G. and Oomens, J. Metal ion binding to peptides: Oxygen or nitrogen sites? Int J Mass Spectrom. 2012; 330–332: 71–77.

54. Dunbar, R. C., Berden, G. and Oomens, J. How does a small peptide choose how to bind a metal ion? IRMPD and computational survey of CS versus Iminol binding preferences. Int J Mass Spectrom. 2013; 354: 356–364.

55. Verkerk, U. H., Zhao, J., Saminathan, I. S., Lau, J. K.-C., Oomens, J., Hopkinson, A. C. and Siu, K. W. M. Infrared Multiple-Photon Dissociation Spectroscopy of Tripositive Ions: Lanthanum–Tryptophan Complexes. Inorg Chem. 2012; 51(8): 4707–4710.

56. Polfer, N. C., Oomens, J. and Dunbar, R. C. Alkali Metal Complexes of the Dipeptides PheAla and AlaPhe: IRMPD Spectroscopy. ChemPhysChem. 2008; 9(4), 579–589.

57. Chen, C.-H. (Winston). Review of a current role of mass spectrometry for proteome research. Anal Chim Acta. 2008; 624(1): 16–36.

58. Guthals, A. and Bandeira, N. Peptide Identification by Tandem Mass Spectrometry with Alternate Fragmentation Modes. MolCell Proteomics : MCP. 2012; 11(9): 550.

59. Zubarev, R. A., Kelleher, N. L. and McLafferty, F. W. Electron capture dissociation of multiply charged protein cations. A nonergodic process. J Am Chem Soc. 1998; 120(13): 3265–3266.

60. Shi, S. D.-H., Hemling, M. E., Carr, S. A., Horn, D. M., Lindh, I. and McLafferty, F. W. Phosphopeptide/Phosphoprotein Mapping by Electron Capture Dissociation Mass Spectrometry. Anal Chem. 2001; 73(1): 19–22.

61. Mirgorodskaya, E., Roepstorff, P. and Zubarev, R. A. Localization of O-Glycosylation Sites in Peptides by Electron Capture Dissociation in a Fourier Transform Mass Spectrometer. Anal Chem. 1999; 71(20): 4431–4436.

62. Syka, J. E., Coon, J. J., Schroeder, M. J., Shabanowitz, J. and Hunt, D. F. Peptide and protein sequence analysis by electron transfer dissociation mass spectrometry. Proc Natl Acad Sci USA. 2004; 101(26): 9528–9533.

63. Fung, Y. M. E., Liu, H. and Chan, T.-W. D. Electron capture dissociation of peptides metalated with alkaline-earth metal ions. J Am Soc Mass Spectrom. 2006; 17(6): 757–771.

64. Chen, X., Fung, Y. M. E., Chan, W. Y. K., Wong, P. S., Yeung, H. S. and Chan, T.-W. D. Transition Metal Ions: Charge Carriers that Mediate the Electron Capture Dissociation Pathways of Peptides. J Am Soc Mass Spectrom. 2011; 22(12): 2232–2245.

65. Chen, X., Wang, Z., Li, W., Wong, Y. L. E. and Chan, T.-W. D. Effect of Structural Parameters on the Electron Capture Dissociation and Collision-Induced Dissociation Pathways of Copper(II)–Peptide Complexes. Euro J Mass Spectrom. 2015; 21(4), 649–657.

66. Dong, J. and Vachet, R. W. Coordination Sphere Tuning of the Electron Transfer Dissociation Behavior of Cu(II)–Peptide Complexes. J Am Soc Mass Spectrom. 2012; 23(2): 321–329.

67. Flick, T. G., Donald, W. A. and Williams, E. R. Electron Capture Dissociation of Trivalent Metal Ion-Peptide Complexes. J Am Soc Mass Spectrom. 2013; 24(2): 193–201.

68. Chen, X., Liu, G., Elaine Wong, Y. L., Deng, L., Wang, Z., Li, W. and Dominic Chan, T.-W. Dissociation of trivalent metal ion (Al^{3+}, Ga^{3+}, In^{3+} and Rh^{3+})–peptide complexes under electron capture dissociation conditions. Rapid Commun Mass Spectrom, 2016; 30(6): 705–710.

69. Commodore, J. J. and Cassady, C. J. The Effects of Trivalent Lanthanide Cationization on the Electron Transfer Dissociation of Acidic Fibrinopeptide B and its Analogs. J Am Soc Mass Spectrom. 2016; 27(9): 1499–1509.

70. Oh, H. B. and Moon, B. Radical-driven peptide backbone dissociation tandem mass spectrometry: Radical –Driven Peptide Backbone dissociation MS/MS. Mass Spectrom Rev. 2015; 34(2): 116–132.

71. Jones, A. W., Winn, P. J. and Cooper, H. J. The Radical Ion Chemistry of S-Nitrosylated Peptides. J Am Soc Mass Spectrom. 2012; 23(12): 2063–2074.

72. Chu, I. K., Rodriquez, C. F., Lau, T.-C., Hopkinson, A. C., and Siu, K. W. M. Molecular Radical Cations of Oligopeptides. J Phys Chem B. 2000; 104(15): 3393–3397.

73. Laskin, J. and Lifshitz, C. Principles of mass spectrometry applied to biomolecules. Hoboken, N.J: Wiley-Interscience. 2006

74. Chu, I. K., Rodriquez, C.F., Hopkinson, A.C., Siu., K.W.C. Formation of molecular radical cations of enkephalin derivatives via collision-induced dissociation of electrospray-generated copper (II) complex ions of amines and peptides. J Am Soc Mass Spectrom, 2001, 12(10): 1114–1119.

75. Bagheri-Majdi, E., Ke, Y., Orlova, G., Chu, I. K., Hopkinson, A. C. and Siu, K. W. M. Copper-Mediated Peptide Radical Ions in the Gas Phase. J Phys Chem B, 2004; 108(30): 11170–11181.

76. Chaparro, A. L., and Vachet, R. W. Tandem mass spectrometry of Cu(II) complexes: the effects of ligand donor group on dissociation. J Mass Spectrom, 2003; 38(3): 333–342.

77. Tureček, F. Copper-biomolecule complexes in the gas phase. The ternary way. Mass Spectrom Rev, 2007; 26(4): 563–582.

78. Chu, I. K. and Laskin, J. Review: Formation of peptide radical ions through dissociative electron transfer in ternary metal–ligand–peptide complexes. Euro J Mass Spectrom. 2011; 17(6), 543.

79. Tureček, F. and Julian, R. R. Peptide Radicals and Cation Radicals in the Gas Phase. Chem Rev. 2013; 113(8): 6691–6733.

80. Barlow, C. K., McFadyen, W. D. and O'Hair, R. A. J. Formation of Cationic Peptide Radicals by Gas-Phase Redox Reactions with Trivalent Chromium, Manganese, Iron, and Cobalt Complexes. J Am Chem Soc. 2005; 127(16): 6109–6115.

81. Huang, C.-H. Rare earth coordination chemistry: fundamentals and applications. Singapore: John Wiley & Sons. 2010.

82. Chemical Rubber Company, Cleveland. CRC handbook of chemistry and physics. CRC Press. 1978

83. Gschneidner, K. A. and Eyring, L. Handbook on the physics and chemistry of rare earths. Amsterdam: North-Holland Pub. Co. 1978. Volume 3.

84. Mingos, D. M. P. Essential trends in inorganic chemistry. New York: Oxford University Press.1998.

85. Böhlke, J. K., de Laeter, J. R., De Bièvre, P., Hidaka, H., Peiser, H. S., Rosman, K. J. R. and Taylor, P. D. P. Atomic Weights of the Elements Review 2000 (IUPAC Technical Report).

86. Böhlke, J. K., de Laeter, J. R., De Bièvre, P., Hidaka, H., Peiser, H. S., Rosman, K. J. R. and Taylor, P. D. P. Isotopic Compositions of the Elements, 2001. J Phys Chem Ref Data. 2005, 34(1): 57–67.

87. Meija, J., Coplen, T. B., Berglund, M., Brand, W. A., De Bièvre, P., Gröning, M. Holden, N.E., Irrgeher, J., Loss, R. D., Walczyk T. and Prohaska, T. Atomic weights of the elements 2013 (IUPAC Technical Report). Pure Appl Chem. 2016, 88(3): 265-291

88. Moeller, T. The chemistry of the lanthanides. Oxford: Pergamon Press. 1975.

89. Aspinall, H. C. Chemistry of the f-block elements. Australia: Gordon & Breach. 2001.

90. Bünzli, J.-C. G. Review: Lanthanide coordination chemistry: from old concepts to coordination polymers. J Coord Chem. 2014; 67(23–24): 3706–3733.

91. Pode, J.S.F. The periodic Table: experiment and theory. Halsted Press, New York. 1973.

92. Kremer, C., Torres, J., Dominguez, S. and Mederos, A. Structure and thermodynamic stability of lanthanide complexes with amino acids and peptides. Coord Chem Rev. 2005; 249(5–6): 567–590.

93. Bünzli, J.-C. G., André, N., Elhabiri, M., Muller, G. and Piguet, C. Trivalent lanthanide ions: versatile coordination centers with unique spectroscopic and magnetic properties. J Alloys and Compd. 2000; 303: 66–74.

94. Polya, G. M., Klucis, E., and Haritou, M. Resolution and characterization of two soluble calcium-dependent protein kinases from silver beet leaves. Biochim Biophys Acta (BBA)-Mol Cell Res, 1987; 931(1): 68–77.

95. Gschneidner, K. A., Eyring, L. Handbook on the physics and chemistry of rare earths. Amsterdam: North-Holland Pub. Co. 1978; Volume 13.

96. Shi, T., Siu, C.-K., Siu, K. W. M. and Hopkinson, A. C. Dipositively Charged Protonated a_3 and a_2 Ions: Generation by Fragmentation of $[La(GGG)(CH_3CN)_2]^{3+}$. Angew Chem Intl Ed, 47(43), 8288–8291.

97. Zhao, J., Siu, C.-K., Shi, T., Hopkinson, A. C. and Siu, K. W. M. Abundant Dipositively Charged Protonated a_2 and a_3 Ions from Diproline and Triproline. J Phys Chem B. 2009; 113(14): 4963–4969.

98. Saminathan, I. S., Zhao, J., Siu, K. W. M. and Hopkinson, A. C. Doubly charged protonated a ions derived from small peptides. Phys Chem Chem Phys. 2011; 13(41): 18307.

Chapter 2

Instrumentation and Experiments

2.1 Introduction to the mass spectrometer

The major components of a mass spectrometer include the ion source, the mass analyzer and the detector, in addition to a vacuum system which is used to acquire and maintain the low-pressure environment, and a computer system for data acquisition and system control [1-2].

2.1.1 Ion sources

In the mass spectrometer, the ion source is used to create gas-phase ions. Depending on the application, different ion sources are used. For example, electron ionization and chemical ionization are suitable for volatile and thermally stable analytes. By contrast, for non-volatile or thermally labile analytes, ion sources such as matrix assisted laser desorption/ionization (MALDI) and electrospray ionization (ESI) are appropriate [2]. MALDI is a desorption/ionization technique that transfers ions in a solid matrix to the gas phase via a laser irradiation. It is especially powerful for the analysis of some polymers, proteins and DNAs. Electrospray ionization is a technique that has revolutionalized the analysis of proteins and other biomolecules. ESI and MALDI are two soft ionization techniques widely used in protein identification and characterization [3-6]. ESI can generate multiply protonated ions, which enables protein analysis on quadrupole and time-of-flight analysers of limited *m/z* range [7]. It is also very gentle source that generates little fragmentation provided that the ion sampling process is also gentle [1]. The two major mechanisms for ESI are the ion evaporation model and the charge residue model [8-11]. The electrospray process comprises the following steps that are illustrated in Figure 2.1: 1) Formation of charged droplets at the electrically biased (1-5KV) capillary tip; 2) Ejection of the droplets from the Taylor cone. 3) Evaporation of solvent from the droplets and increase of

surface charge density until the Rayleigh stability limit is reached; 4) Explosion of the droplets due to Coulombic repulsion; 5) Production of single solvated ions by repeated Rayleigh explosions and/or ion evaporation. Some of these ions are then sampled by the downstream ion elements into the mass analyzer for measurements and further manipulations [1, 8-12].

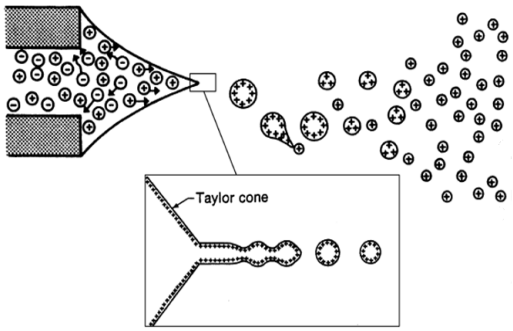

.

Figure 2.1 Schematic presentation of electrospray process (Adopted from [8])

2.1.2 Fragmentation techniques

Collision-induced dissociation (CID) [13] is a common fragmentation technique used for peptide sequencing in mass spectrometry-based proteomics [14-15]. Fragmentation of a peptide by CID tends to generate $[b_n]^+$ and $[y_n+2H]^+$ ions [16-19]. The peptide precursor ions are accelerated before colliding with gas molecules, and the collision converts some of the kinetic energy of the ion into internal energy. The excited ion then fragments breaking the weakest bonds. Electron capture dissociation (ECD) and electron transfer dissociation (ETD) are generally preferred in post-translational modification (PTM) analyses because they facilitate backbone cleavage while retaining the PTM. ECD and ETD are electron-mediated radical-driven techniques, which tend to give better results for large, highly charged peptides, while CID is better for doubly charged peptides formed by protein trypsinization [20-28].

2.1.3 Mass analyzers

Common mass analyzers used for peptide analysis include the quadrupole (Q), ion trap, Orbitrap, Fourier transform ion cyclotron resonance (FT-ICR), and time-of-flight (TOF) [29, 30-33]. Typically FT-ICR and the Orbitrap offer the highest resolution, but tend to be the most costly [30-31].

The linear quadrupole analyzer comprises four parallel hyperbolic rods where opposite rods have the same applied potentials but different from the other pair in the direction [31, 34].

The quadrupole field has a direct current (DC) and a radio frequency (RF) component that transmit ions within a given *m/z* window whose width is dependent on the ratio of DC to RF amplitudes. Mass scanning is achieved by sweeping both DC and RF while keeping their ratio constant. A special case exists when only the RF is applied (DC=0), in which case ions of *m/z* values are passed and the quadrupole function as an ion guide**.**

Three quadrupoles can be arranged in tandem to perform MS/MS. In the MS/MS mode, Q1 obtains full scan MS1, and the RF-only q_2 works as the collision cell for CID and Q3 is used to mass-analyze the fragmentation products coming out of q_2. The quadrupoles can be operated differently to give full scan, product ion scan, precursor ion scan and neutral loss scan [32].

The triple quadrupole achives MS/MS by a linear combination of three quadrupole analyzers - a tandem in space arrangement. By contrast, the quadrupole ion trap (QIT) performs tandem MS by tandem in time. The QIT consists of two hyperbolic cap electrodes and one ring electrode, which can create a three-dimensional quadrupole field to store and scan ions [29, 31, 33, 36]. For linear ion trap, ions are confined radially by a two-dimensional quadrupole frequency and axially

by higher potentials applied to the end electrodes (i.e. the front and back sections, Figure 2.2) [37-38].

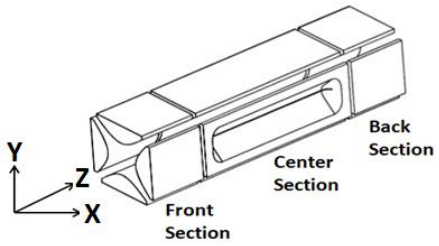

Figure 2.2 Schematic presentation of two-dimensional linear ion trap. Adopted from [38].

2.1.4 Tandem mass spectrometry

To perform MS/MS analysis, two or more beam transmitting mass analyzers (TOF and quadrupole analyzer) can be arranged in series, for example, TOF/TOF, QTOF and QqQ [39]. This is called Tandem-in-Space [29]. MS/MS analysis can also be operated in a tandem-in-time mass spectrometer, which combines ion selection, ion activation and fragments analysis in the same place for example QIT, LIT and FT-ICR. Higher stages of MS^n can be more easily obtained in a tandem-in-time instrument, while a tandem-in-space mass spectrometer is typically limited to MS/MS [29].

2.2 Instruments and experimental conditions

2.2.1 2000 QTRAP® and 4000 QTRAP®

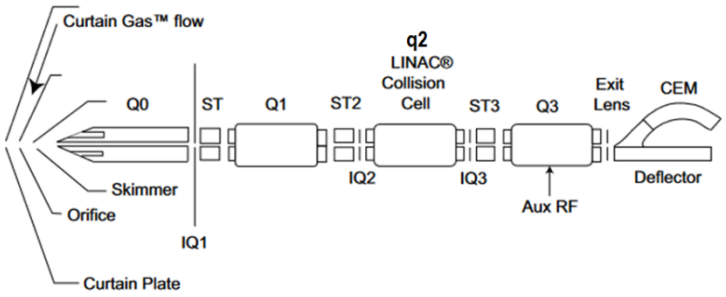

Figure 2.3 Schematic presentation of 4000 QTRAP® system ion optics [40]

The SCIEX 2000 QTRAP® prototype linear ion trap and the 4000 QTRAP® were two of the three mass spectrometers used in this thesis studies. The 2000 QTRAP®and 4000 QTRAP® are tandem mass spectrometers of QqLIT, which can offer higher trapping and fragmentation efficiency. The ion optics of the 4000 QTRAP® is shown in Figure 2.3 [40].

MS/MS scan is acquired in the quadrupole mode by fixing the Q1 to transmit the precursor ion and sweeping the Q3 to mass analyze the product ions. The third stage of the MS/MS/MS scan is performed in the Q3 in LIT mode. Ions from Q1 are transmitted to q_2 and fragmented in q_2 by colliding with the collision gas in q_2. The product ions are then transmitted and collected in Q3. The target ion is isolated in Q3 by removing all other ions through applying normal mode RF-DC voltages. A second auxiliary AC frequency is applied to Q3 and the ion of interest is resonantly excited and then collided with the residual nitrogen gas in Q3 to fragment to obtain the MS/MS/MS spectrum of the ion of interest [40].

2.2.2 Obitrap Elite Mass Spectrometer

The Orbitrap Elite mass spectrometer is a hybrid mass spectrometer combining the Velos Pro™ dual cell linear trap and the high-field Orbitrap™ analyzer.

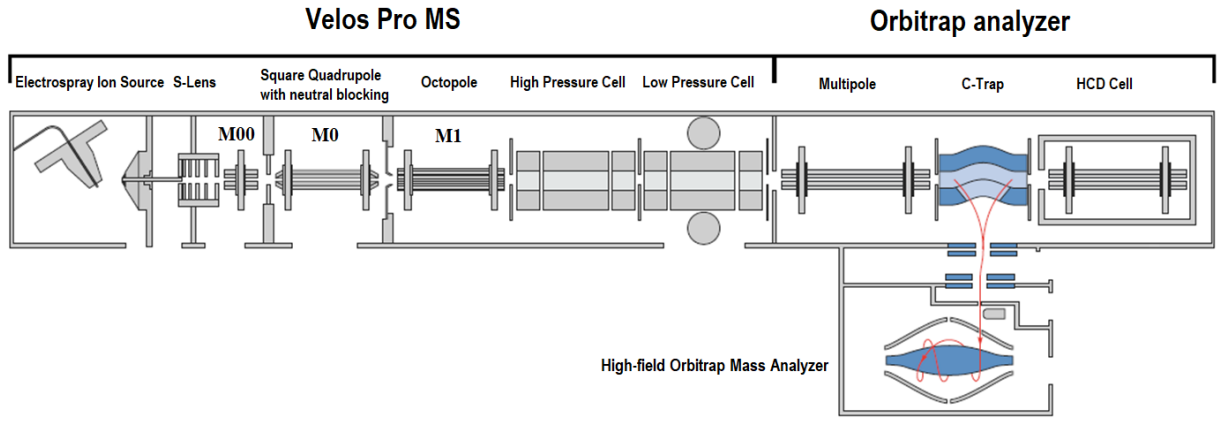

Figure 2.4 LTQ Orbitrap Elite mass spectrometer configuration. Adopted from [41]

The Orbitrap analyzer can be operated with resolving power > 240,000 FWHM.

It consists of the four main components [41-42]: 1) Dual cell linear ion trap (Thermo Scientific Velos Pro) for sample ionization, precursor ion selection, fragmentation, Auto Gain Control™ (AGC) for setting the ion injection time to maintain the optimum quantity of ions for each scan. 2) Intermediate storage device (curved linear trap) that is required in pulse injection. 3) High-field Orbitrap analyzer for Fourier transformation-based analysis; 4) Collision cell for performing higher energy CID experiments. In this dissertation work, only the Velos Pro Mass spectrometer (i.e., the dual cell linear ion trap) was used for acquiring MS^n spectra.

Electrosprayed ions are transferred from the ion transfer tube and pass through the S-Lens and Exit lens, and then the three ion guides M00, M0 (square rod quadrupole) and M1 (octopole round rods assembly) that are RF only. Each ion guide includes a lens with voltage applied on it to facilitate ion transfer.

The dual-LIT has two identical LITs in tandem operated at high pressure (HPC) and low pressure (LPC), respectively. These two LITs are connected to the same RF and auxiliary AC power supplies, with DC offset for trapping delivered separately [29]. In a higher pressure, the trapping efficiency and fragmentation effectiveness can be improved, while in a lower pressure, higher scan rate and better resolving power can be obtained. While the second LIT is analyzing the mass of the fragment ions, the first LIT can start to trap the ions for the next cycle [42].

The dual linear ion trap stores, isolates and fragments ions and then sends them to the Orbitrap or SEM detector. In our studies, the fragmented ions are sent to the off-axis SEM detector, which includes a conversion dynode and channel electron multiplier for MS, MS/MS and MS^n analysis [42].

The typical ESI source operation conditions for metal complexes studies were 3 µL/min flow rate, ion transfer tube temperature ~ 200°C, and sheath gas ~ 5 psi. All other parameters were optimized for maximum sensitivity.

2.3 9-fluorenylmethoxycarbonyl (Fmoc)-based solid-phase peptide synthesis (SPPS)

PGW, P(^{18}O)GG, PG(^{18}O)G, PYG, PGGG were synthesized according to standard Fmoc-based solid-phase peptide synthesis methods [43-45]. ^{18}O labelled Fmoc-amino acids were synthesized by the reaction of Fmoc-amino acid with acetyl chloride and dioxane [46].

SPPS starts from the C-terminal and the procedure to synthesize a peptide with the sequence of $AA_nAA_{n-1}\ldots AA_2AA_1$ (AA= amino acid) is described briefly here. This scheme uses the Wang resin bead which is a polystyrene polymer linked to the Fmoc-protected amino acid via 1% divinylbenzene cross linking [47].

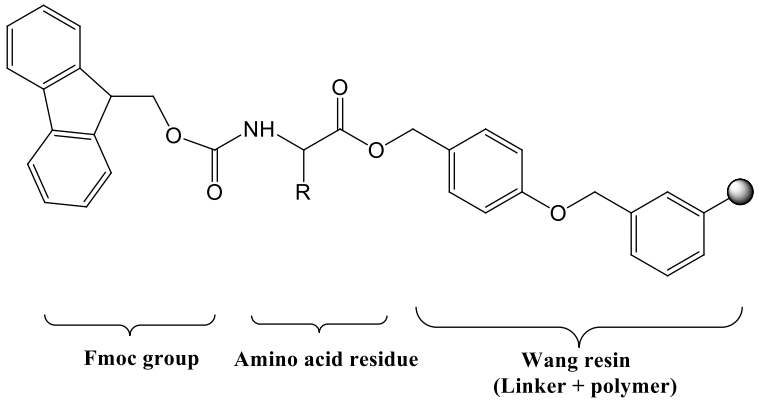

Scheme 2.1 Fmoc-AA-Wang resin (Fmoc-Ala-4-alkoxybenzyl alcohol resin). Adopted from [47]

(1) Deprotection of N-terminal Fmoc group. Fmoc-AA_1-Wang resin was added to a solid-phase peptide synthesis glass vessel (Figure 2.5) and 20% 4-methyl piperidine in dimethylformamide (DMF) was added to remove the Fmoc group with bubbling of N_2 for 20 min.

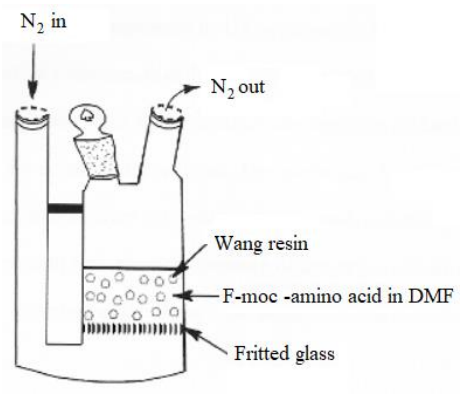

Figure 2.5 Schematic of the solid-phase peptide synthesis apparatus. Adopted from [45]

(2) Coupling of amino acid on the C-terminus. The remaining solution was removed, and the N-terminal de-protected AA_1-Wang resin was washed three times with DMF and dichloromethane (DCM) before adding Fmoc-AA_2-OH and coupling reagents 1-hydroxybenzotriazole (HOBT) and diisopropylcarbodiimide (DIC). The mixture of reactants was agitated by bubbling with N_2 for two hours for complete coupling.

(3) Deprotection. The resin was filtered and washed with DMF for 3 times and DCM for 3 times before adding deprotection reagents 20% (v/v) 4-methyl-piperidine in DMF. The mixture was then agitated with bubbling N_2 gas for 20 min.

(4) Repeating step 2 and 3 to couple AA3, AA4…..AAn-1 and AA_n.

(5) Cleavage of C-terminal Resin. The liquid in the mixture was removed, and the resin was washed with DMF for 3 times and DCM for 3 times, then the cleavage reagent containing trifluoroacetic acid (TFA), DCM, triisopropylsilane (TIS) and water at the ratio of 14:4:1:1 (v/v/v/v) was added. The reaction was stopped after two hours with bubbling N_2 gas.

(6) Concentration and purification of synthesized peptides $AA_nAA_{n-1}\ldots AA_2AA_1$. The reactant mixture was filtered and the filtrate was collected. The resin bead was washed with TFA for 3 times and the filtrate was collected and combined with the initial filtrate. The filtrate was then dried under N_2 and water was added to re-dissolve the crude peptides. The re-suspended

peptide solution was then dried with Speedvac under vacuum to remove TFA residue in the solution. Diethyl ether was added to the solution after the drying. The precipitate was collected after centrifuging at 12000 rpm for 2 min. The purification step was repeated for 2 to 3 times, depending on the experiment requirement of peptide purity.

2.4 Chemicals

Most peptides were commercially available from Bachem BioSciences Inc (Torrance, California, USA); and proline-containing peptides were available from Pepnome limited (Zhuhai, Guangdong, China). Some peptides were synthesized by following the Fmoc-based solid phasepeptide synthesis (SPPS) procedure described in Section 2.3.

Deuterated acetonitrile (CD_3CN) was available from C/D/N Isotopes (Pointe-Claire, Quebec, Canada). All solvents (acetonitrile, methanol, water) were Optima® LC-MS grade from Fisher Scientific (USA). Trivalent metal salts of chloride or nitrate were purchased from Sigma-Aldrich (St. Louis, MO). All materials were used as received.

5 mM Stock solutions of Sc, Y, La, Ce, Sm, Eu, Gd, Tb and Yb were prepared from the salts of chloride or nitrate in water. Stock solutions of peptides (Bachem) were prepared in water or water/methanol depending on their solubility in water. The appropriate volumes of stock solutions of peptides and trivalent metal ions were mixed with 1:1 (v/v) water/acetonitrile for the experiments.

2.5 References

1. Ekman, R. Mass spectrometry: instrumentation, interpretation, and applications. Hoboken, N.J: John Wiley & Sons. 2009.
2. Hoffmann, E. de and Stroobant, V. Mass spectrometry: principles and applications (3rd ed./). Chichester, England: J. Wiley. 2007.
3. El-Aneed, A., Cohen, A. and Banoub, J. Mass Spectrometry, Review of the Basics: Electrospray, MALDI, and Commonly Used Mass Analyzers. Appl Spectrosc Rev. 2009; 44(3):210–230.
4. Yates, J. R. Mass spectrometry and the age of the proteome. Journal of Mass Spectrometry. 1998; 33(1): 1–19.
5. Fenn, J. B., Mann, M., Meng, C. K., Wong, S. F. and Whitehouse, C. M. Electrospray ionization for mass spectrometry of large biomolecules. Science. 1989; 246(4926): 64–71.
6. Hillenkamp, F., Karas, M., Beavis, R. C. and Chait, B. T. Matrix-Assisted Laser Desorption/Ionization Mass Spectrometry of Biopolymers. Analytical Chemistry. 1991; 63(24): 1193A–1203A.
7. Ho, C., Lam, C., Chan, M., Cheung, R., Law, L., Lit, L., Ng, K., Suen, N. and Tai, H. Electrospray Ionisation Mass Spectrometry: Principles and Clinical Applications. Clin Biochem Rev. 2003; 24(1): 3–12.
8. Kebarle, P., and Tang, L. From ions in solution to ions in the gas phase - the mechanism of electrospray mass spectrometry. Anal Chem. 1993; 65(22): 972A–986A.
9. Rohner, T. C., Lion, N. and Girault, H. H. Electrochemical and theoretical aspects of electrospray ionisation. Phys Chem Chem Phys. 2004; 6(12): 3056.

10. Kebarle, P. A brief overview of the present status of the mechanisms involved in electrospray mass spectrometry. J Mass Spectrom. 2000;, 35(7): 804–817.

11. Kebarle, P. and Peschke, M. On the mechanisms by which the charged droplets produced by electrospray lead to gas phase ions. Anal Chim Acta. 2000; 406(1): 11–35.

12. Cole, R. B. Electrospray and MALDI mass spectrometry: fundamentals, instrumentation, practicalities, and biological applications (2nd ed.). Hoboken, N.J: John Wiley. 2010.

13. Cooks, R. G. Collision-induced dissociation: Readings and commentary. J Mass Spectrom. 1995; 30(9):1215–1221.

14. Mitchell Wells, J., and McLuckey, S. A. Collision-Induced Dissociation (CID) of Peptides and Proteins. In Methods in Enzymology.(Vol. 402, pp. 148–185). Elsevier. 2005

15. Aebersold, R., and Goodlett, D. R. Mass Spectrometry in Proteomics. Chemical Reviews. 2001; 101(2): 269–296.

16. Hunt, D. F., Yates, J. R., Shabanowitz, J., Winston, S. and Hauer, C. R. Protein sequencing by tandem mass spectrometry. Proc Natl Acad Sci USA. 1986; 83(17): 6233–6237.

17. Biemann, K. Contributions of mass spectrometry to peptide and protein structure. Biol Mass Spectrom. 1988; 16(1–12): 99–111.

18. Papayannopoulos, I. A. The interpretation of collision-induced dissociation tandem mass spectra of peptides. Mass Spectrom Rev. 1995; 14(1): 49–73.

19. Paizs, B. and Suhai, S. Fragmentation pathways of protonated peptides. Mass Spectrom Rev. 2005; 24(4), 508–548.

20. Wiesner, J., Premsler, T. and Sickmann, A. Application of electron transfer dissociation (ETD) for the analysis of posttranslational modifications. PROTEOMICS. 2008; 8(21): 4466–4483.

21. Zubarev, R. A., Kelleher, N. L. and McLafferty, F. W. Electron capture dissociation of multiply charged protein cations. A nonergodic process. J Am Chem Soc. 1998; 120(13): 3265–3266.

22. Sweet, S. M. and Cooper, H. J. Electron capture dissociation in the analysis of protein phosphorylation. Expert Rev of Proteomics. 2007; 4(2):149–159.

23. Sarbu, M., Ghiulai, R. M. and Zamfir, A. D. Recent developments and applications of electron transfer dissociation mass spectrometry in proteomics. Amino Acids. 2014; 46(7): 1625–1634.

24. Syka, J. E., Coon, J. J., Schroeder, M. J., Shabanowitz, J. and Hunt, D. F. Peptide and protein sequence analysis by electron transfer dissociation mass spectrometry. Proc Natl Acad Sci USA. 2004; 101(26): 9528–9533.

25. Kim, M.-S. and Pandey, A. Electron transfer dissociation mass spectrometry in proteomics. Proteomics. 2012: 12(4–5), 530–542.

26. Wysocki, V. H., Resing, K. A., Zhang, Q. and Cheng, G. Mass spectrometry of peptides and proteins. Methods. 2005; 35(3), 211–222.

27. Zhurov, K. O., Fornelli, L., Wodrich, M. D., Laskay, Ü. A. and Tsybin, Y. O. Principles of electron capture and transfer dissociation mass spectrometry applied to peptide and protein structure analysis. Chem Soc Rev. 2013; 42(12): 5014.

28. Guthals, A. and Bandeira, N. Peptide Identification by Tandem Mass Spectrometry with Alternate Fragmentation Modes. Mol Cell Proteomics : MCP. 2012; 11(9): 550.

29. Gross, J. H., Springer E-books - York University, & SpringerLink (Online service). Mass spectrometry: a textbook (2nd ed.). Berlin: Springer. 2010

30. Domon, B. and Aebersold, R. Mass Spectrometry and Protein Analysis. Science. 2006; 312(5771): 212–217.

31. Ahmed, F. E. Utility of mass spectrometry for proteome analysis: part I. Conceptual and experimental approaches. Expert Rev Proteomics. 2008; 5(6): 841–864.

32. Himmelsbach, M. 10 years of MS instrumental developments – Impact on LC–MS/MS in clinical chemistry. J Chromatogr B. 2012; 883–884: 3–17.

33. Kollipara, S., Agarwal, N., Varshney, B. and Paliwal, J. Technological Advancements in Mass Spectrometry and Its Impact on Proteomics. Anal Lett. 2011; 44(8): 1498–1520.

34. Paul, W. Steinwedel H. A. Z. Naturforsch. 1953; 8(7): 448–450.

35. March, R. E. Quadrupole ion trap mass spectrometry: theory, simulation, recent developments and applications. Rapid Commun Mass Spectrom. 1998; 12(20): 1543–1554.

36. Mayya, V. Systematic Comparison of a Two-dimensional Ion Trap and a Three-dimensional Ion Trap Mass Spectrometer in Proteomics. Mol Cell Proteomics. 2004; 4(2): 214–223.

37. Schwartz, J. C., Senko, M. W. and Syka, J. E. P. A two-dimensional quadrupole ion trap mass spectrometer. J Am Soc Mass Spectrom. 2002; 13(6): 659–669.

38. Douglas, D. J., Frank, A. J. and Mao, D. Linear ion traps in mass spectrometry. Mass Spectrom Rev, 24(1), 1–29.

39. Gillet, L. C., Leitner, A. and Aebersold, R. Mass Spectrometry Applied to Bottom-Up Proteomics: Entering the High-Throughput Era for Hypothesis Testing. Annu Rev Anal Chem. 2016; 9(1), 449–472.

40. AB Applied Biosystems/MDS SCIEX: 4000 Q TRAP™ LC/MS/MS system Operators Manual. June 2003.

41. Thermo Scientific: Orbitrap Elite Hardware Manual. 2011

42. LTQ Orbitrap Operations Course, Thermo Scientifc Training Institute

43. Chan, W. C. and White, P. D. Fmoc solid phase peptide synthesis: a practical approach. New York: Oxford University Press. 2000.

44. Howl, J. Peptide synthesis and applications. Humana Press. New Jersey. 2005.

45. Saminathan, I. S. Fragmentations of cationized small peptides; formation of dipositive $(a_n+H)^{2+}$ ions from lanthanum complexes. York University, PhD thesis, 2013.

46. Murphy, R. C. and Clay, K. L. Synthesis and back exchange of ^{18}O labeled amino acids for use as internal standards with mass spectrometry. Biol Mass Spectrom, 1979; 6(7): 309–314.

47. Wang, S.-S. p-Alkoxybenzyl alcohol resin and p-alkoxybenzyloxycarbonylhydrazide resin for solid phase synthesis of protected peptide fragments. J Am Chem Soc. 1973; 95(4): 1328–1333

CHAPTER 3

Fragmentation of $[Ln(III)(peptide)(CH_3CN)_n]^{3+}$ Complexes

3.1 Introduction

Due to the higher charge density of the smaller sized trivalent metal ions, formation of tripositive complexes of trivalent metal ion in the gas phase using ESI is always a challenge. O'Hair and co-workers' effort to form the ternary peptide complexes in +3 charge state to generate peptide radical cations was not successful; they circumvented this challenge by utilizing salen N,N'-ethylenebis(salicylideneaminato)] to form compounds with trivalent metal ions Cr(III), Mn(III), Fe(III) and Co(III), and then by homolytic cleavage of the metal peptide bond, produced corresponding peptide radical cations for the first time other than from copper(II) [1]. The reaction can be described in equation 1.

$$[Metal^{III}(salenX\text{-}2H)(peptide)]^{\bullet+} \longrightarrow [Metal^{II}(salenX\text{-}2H)] + peptide^{\bullet+} \quad \text{(Equation 1)}$$

In the dissociation pathway showed above, a single-electron transfer from peptide to metal occurs, and the peptide radical cation is produced along with the neutral metal/salen radical complex.

There are other competitive fragmentation channels depending on the metal ions, ligand and peptides. Among them is the generation of neutral peptide (equation 2).

$$[Metal^{III}(salenX\text{-}2H)(peptide)]^{\bullet+} \longrightarrow [Metal^{III}(salenX\text{-}2H)]^{\bullet+} + peptide \quad \text{(Equation 2)}$$

The competition between the equation 1 and 2 can be modulated by substitution at the 5, 5′-positions of salen, which is located far from the metal center and supposedly not affecting the geometry surrounding the metal (Structure **I**).

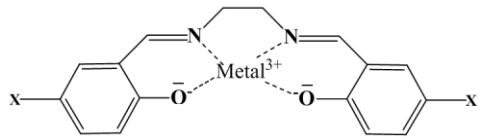

Structure I The structure of Metal/salen, where X=NO_2, Cl, H or OMe respectively

The research result shows that for electron-withdrawing functional group X, homolytic cleavage of the metal peptide bond is favoured and therefore the peptide radical cations are generated. The dissociation favours the generation of neutral peptide by cleavage of metal-peptide bond if the X functional group is electron-donating, as evident by the more and more abundant $[Metal^{III}(salenX\text{-}2H)]^+$ observed in the CID spectra of $[Metal^{III}(salenX\text{-}2H)(peptide)]^+$ in the order of X= $NO_2 \rightarrow Cl \rightarrow H \rightarrow OMe$ when Metal =Mn and Fe.

Although the potential to tune the generation of peptide radical cations by the substitution in the ligand, these complexes in the gas phase are still singly charged, even with the trivalent metal ion. The higher charged complexes in gas phase always draw interests, especially for using the ETD and ECD techniques.

Under low-energy collision-induced dissociation, La(III) has a preferred coordination number of eight [2], and $[La(III)(peptide)]^{3+}$ ions were generated for arginine-containing di-, tri- and tetra-peptides [3]. To generate the complex in the absence of solvent, a dipeptide containing not only arginine, but also methionine, was required in order to provide the minimum four coordination sites to La(III).

A novel highly charged protonated ion $[a_3+H]^{2+}$ was observed in the fragmentation products of CID of $[La(III)(GGG)(CH_3CN)_2]^{3+}$[4]. Further investigation on the impact of protein composition on the CID of $[La(III)(peptide)(CH_3CN)_n]^{3+}$ suggests the N-terminal proline-

containing peptide is the key factor to stabilize the small dipositive a ions [5,6]. No molecular peptide radical cations were observed in the dissociation of the tripositive metal/peptide complex.

In addition to dissociation under CID conditions, infrared multiple photon dissociation (IRMPD) spectra have also been reported for the investigation of tripositive lanthanum^{III}/tryptophan complexes[7], and the results showed that La^{3+} binds with the indole ring by π-interaction in addition to coordination with the carbonyl oxygen. A study on the coordination of trivalent metal ions to peptides by IRMPD was carried on the dipositive complexes $[Ln(III)(Ala_n\text{-}H)]^{2+}$ where Ln=La, Ho and Eu) and n=2-5, considering the advantage of the limited conformation space due to the formation of salt-bridge structure of metal ion with the deprotonated peptides [8].

Due to the high charge of trivalent metal ions, the sequencing-informative fragmentation of M(III)/peptide complexes has also stimulated the study on the dissociation of $[M(III)(peptide)]^{3+}$ by other new dissociation techniques such as ECD and ETD [9-11].

Our aim here is to further explore the possibility of formation of peptide molecular radical cations from tripositive trivalent metal/peptide complexes under CID conditions, where the trivalent metal elements are rare earth metals. We report here the discovery of a new route to produce peptide radical cations by the fragmentation of trivalent/peptide complexes in the +3 charge state.

3.2 Results and Discussion

$[Ln(III)(Peptide)(CH_3CN)_n]^{3+}$**,** where Ln = Sc, Y, La, Ce, Sm, Eu, Gd, Tb, Yb, have been investigated. Complexes containing Sc(III) showed different behaviour compared to those of the other eight metal ions because of its strong tendency to react with water. It only formed dipositive ions $[Sc(OH)(CH_3CN)_n]^{2+}$ with a maximum of five acetonitrile molecules, because its ionic radius is much smaller than that of Y(III), La(III) and Ce(III), as shown in Table 1.1 in

Chapter 1. The other eight metal ions can form stable $[Ln(III)(CH_3CN)_n]^{3+}$ complexes and $[Ln(III)(peptide)(CH_3CN)_n]^{3+}$, where n = 4, 5, 6 or 7 in the gas phase.

3.2.1 Fragmentation of $[Ln(III)(GWG)(CH_3CN)_n]^{3+}$ where Ln=La, Ce, Eu, and the generation of radical cations

As the molecular peptide radical cations $[peptide]^{\bullet+}$ are easily produced by CID of $[Cu(peptide)(Ligand)]^{2+}$ for oligopeptides that contain either tryptophan or tyrosine residue [12-18], in this work, Gly-Trp-Gly (GWG) and Gly-Tyr-Gly (GYG) were selected as the model peptides to check the feasibility of the new route to generate peptide radical cations by CID of tripositive Ln(III)/peptide complexes. Instead of amine, the aprotic solvent CH_3CN was used as the auxiliary ligand for lanthanide coordination, since previous work [19-20] showed that Ln(III)/peptide complexes can be introduced to the gas phase stabilized by using CH_3CN as the ligand, and the preferred coordination number of CH_3CN to lanthanum(III) is eight.

In the front end of the mass spectrometer, complexes $[Ln(III)(peptide)(CH_3CN)_n]^{3+}$ were formed, and the solvent molecules were removed one by one under low-energy collision-induced dissociation, as the example shown in Figure 3.1a. After removing two CH_3CN molecules from the complex, a water molecule is attached and this is the major fragmentation product when the collision energy is very low. Formation of dipositive $[Ln(III)/(GWG\text{-}H)(Solvent)_n]^{2+}$ complexes are also a major pathway. In summary, the fragmentations of $[Ln(III)(peptide)(CH_3CN)_n]^{3+}$, where Ln=La and Ce, show two major fragmentation pathways: 1) Formation of tripositive fragments cluster $[Ln(III)(GWG)(CH_3CN)_n(H_2O)_m]^{3+}$ ions, where m=0-2 and n=2-4, by peeling off CH_3CN or replacing CH_3CN with H_2O; 2) Formation of dipositive fragments cluster $[Ln(III)(GWG\text{-}H)(CH_3CN)_n(H_2O)_m]^{2+}$ ions, where m, n=0-2.

To assign the fragments in the CID spectra correctly, deuterated acetonitrile was used as solvent to help in interpreting the spectra based on corresponding mass shifts if there were CH_3CN molecules in the fragments (Figure 3.1b). For example, the $[Ce(III)(GWG)(CH_3CN)_3]^{3+}$, *m/z* =193.8, corresponds to $[Ce(III)(GWG)(CD_3CN)_3]^{3+}$ at *m/z* =196.8. Comparison between the CID spectra of $[Ce(III)(GWG)(CH_3CN)_5]^{3+}$ and $[La(III)(GWG)(CH_3CN)_5]^{3+}$ also assist in the interpretation of the CID spectra, because the mass difference between Ce and La is 1. For example the $[Ce(III)(GWG)(CH_3CN)_4]^{3+}$, *m/z* 207.5 ion corresponds to the $[La(III)(GWG)(CH_3CN)_4]^{3+}$, *m/z* 207.2 ion, and $[Ce(III)(GWG\text{-}H)(CH_3CN)_2]^{2+}$, *m/z* 269.7 to $[La(III)(GWG\text{-}H)(CH_3CN)_2]^{2+}$ at *m/z* 269.2.

Figure 3.2 shows that further increasing the collision energy can peel off all the solvent molecules, and the study of the fragmentation of $[Ln(III)(peptide)]^{3+}$ complexes will give direct information regarding the interaction of tripositive metal ion with small peptide molecules.

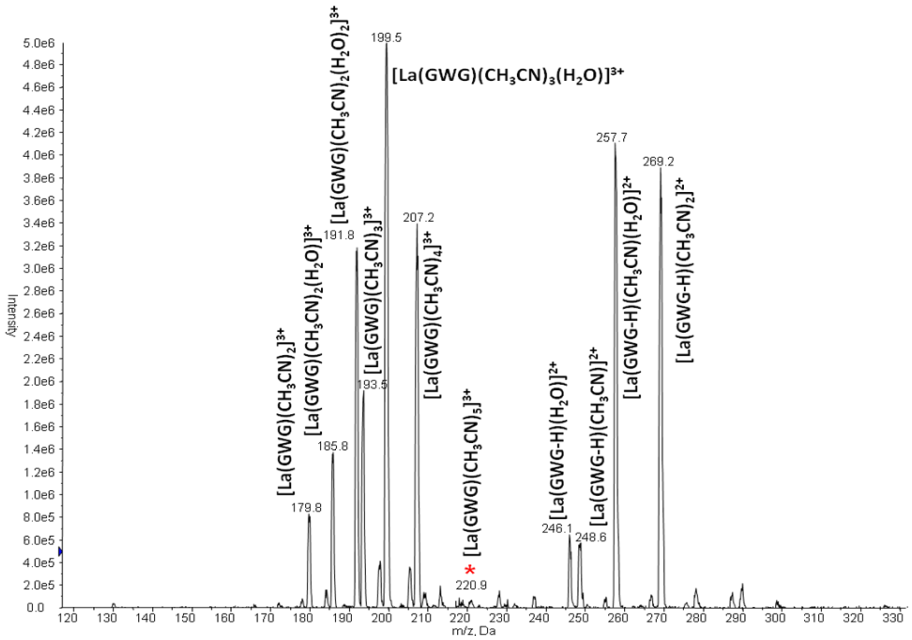

Figure 3.1(a) CID spectrum of $[La(GWG)(CH_3CN)_5]^{3+}$ at *m/z* 220.9, E_{lab}=15 eV. The precursor ion is labelled with an asterisk (*)

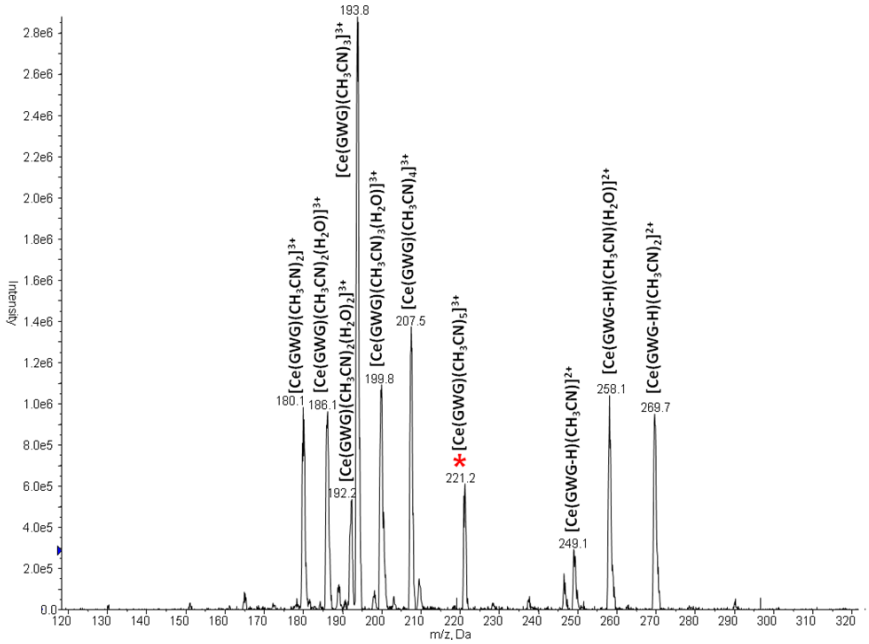

Figure 3.1(b) CID spectrum of $[Ce(GWG)(CH_3CN)_5]^{3+}$ at *m/z* 221.2, E_{lab}=15 eV. The precursor ion is labelled with an asterisk (*)

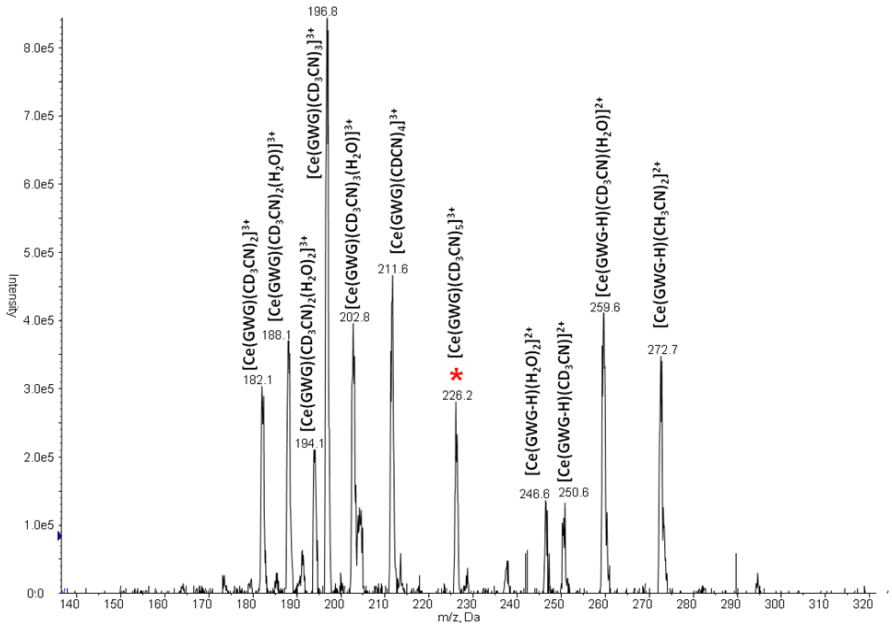

Figure 3.1(c) CID spectrum of $[Ce(GWG)(CD_3CN)_5]^{3+}$ at *m/z* 226.2, E_{lab}=15 eV. The precursor ion is labelled with an asterisk (*)

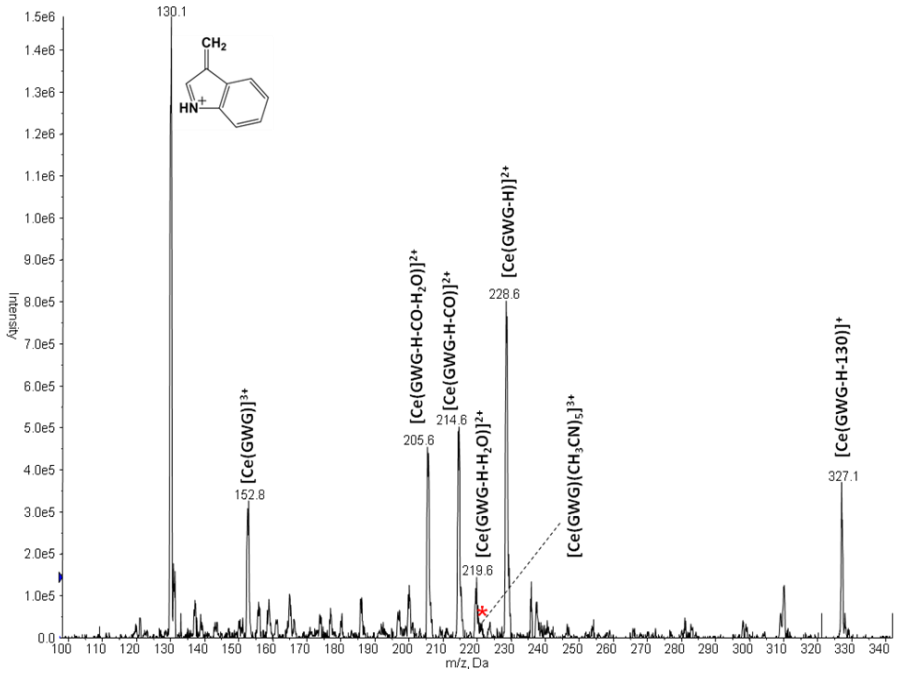

Figure 3.2 CID spectrum of $[Ce(GWG)(CH_3CN)_5]^{3+}$ at *m/z* 221.2, E_{lab}=60 eV. The precursor ion is labelled with an asterisk (*)

The breakdown curves of $[Ce(GWG)(CH_3CN)_5]^{3+}$ in Figure 3.3 shows that it breaks down to $[Ce(GWG)(CH_3CN)_4]^{3+}$ and $[Ce(GWG)(CH_3CN)_3]^{3+}$ by losing one or two CH_3CN molecules; these two ions break down to $[Ce(GWG)(CH_3CN)_2]^{3+}$. Then, $[Ce(GWG)(CH_3CN)_2]^{3+}$ breaks down further to $[Ce(GWG)(CH_3CN)]^{3+}$ and $[Ce(GWG\text{-}H)]^{2+}$. $[Ce(GWG)(CH_3CN)]^{3+}$ loses the remaining CH_3CN and become $[Ce(GWG)]^{3+}$; meanwhile, $[Ce(GWG\text{-}H)]^{2+}$ gives side chain loss. When all the cerium-containing complex breaks down, $[CeO]^{+}$ ion appears.

From the CID spectra of $[Ce(GWG)(CH_3CN)_5]^{3+}$ and $[La(GWG)(CH_3CN)_5]^{3+}$ at different collision energies, no radical cation $[GWG]^{\bullet+}$ was observed. However, when $[Eu(III)(GWG)(CH_3CN)_5]^{3+}$ dissociated, $[GWG]^{\bullet+}$ was generated, as shown in Figure 3.4, and the complementary ion $[Eu(CH_3CN)_5]^{2+}$ was observed at *m/z* 179.1.

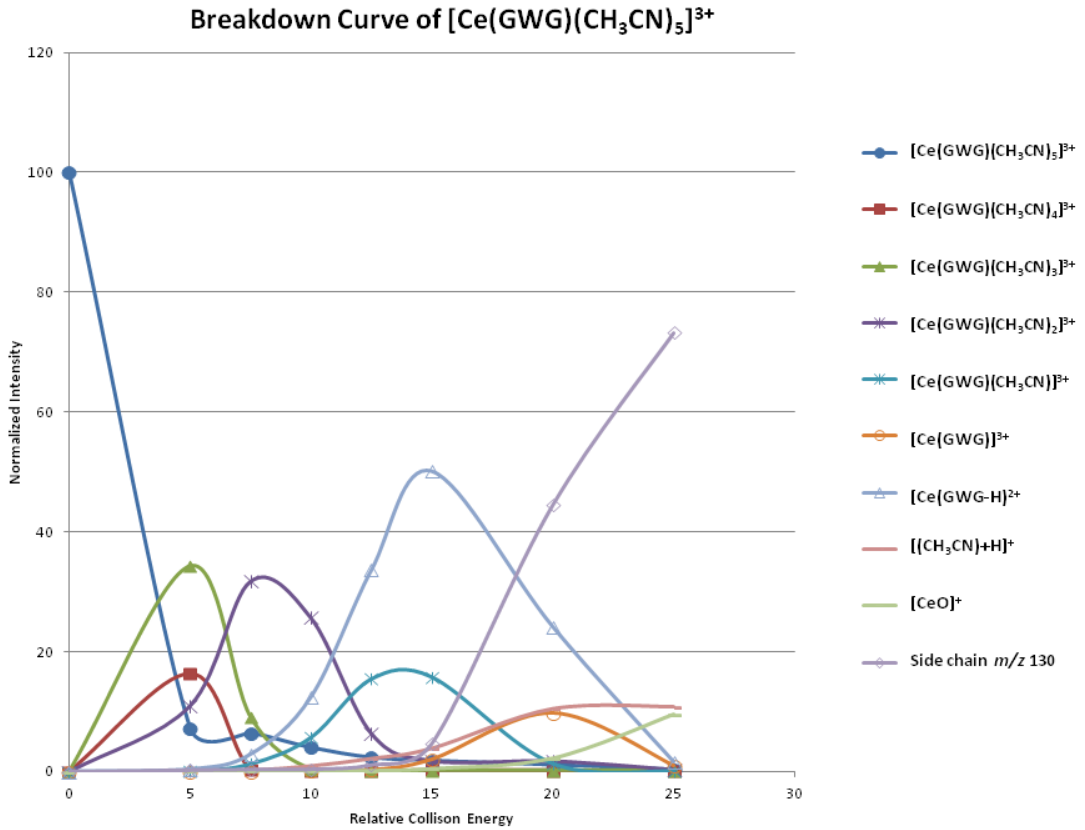

Figure 3.3 Breakdown Curve of $[Ce(GWG)(CH_3CN)_5]^{3+}$

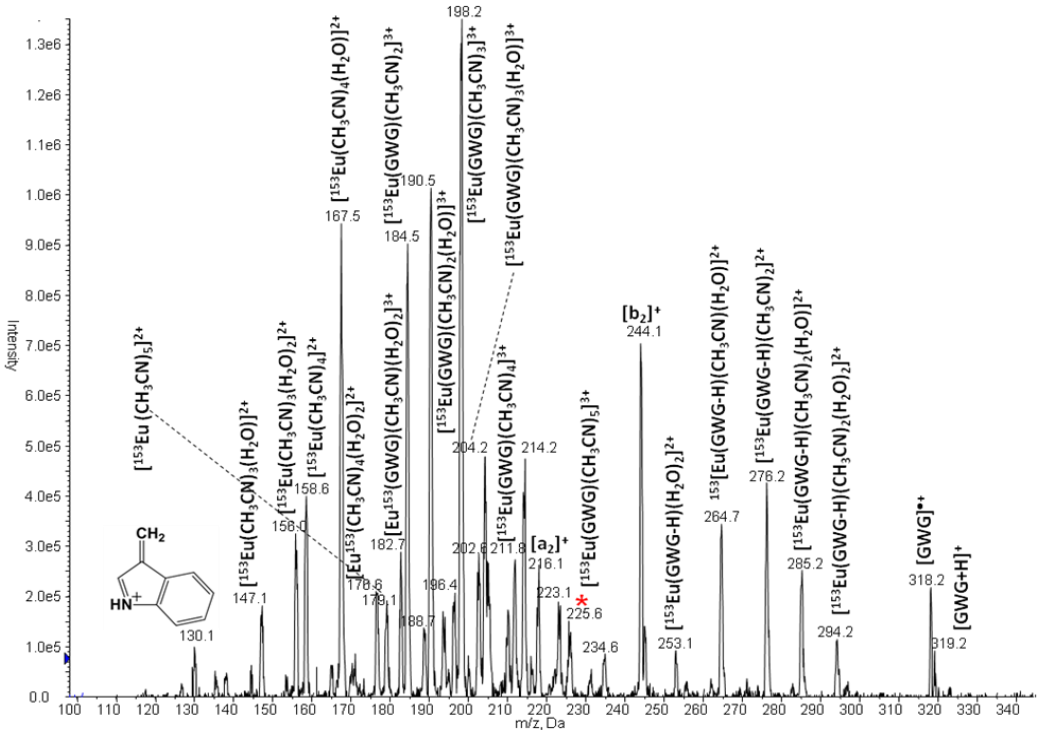

Figure 3.4 CID spectrum of $[Eu(GWG)(CH_3CN)_5]^{3+}$ at *m/z* 225.6, E_{lab}=15 eV. The precursor ion is labelled with an asterisk (*)

Compared to the fragmentations of $[Ce(GWG)(CH_3CN)_5]^{3+}$ and $[La(GWG)(CH_3CN)_5]^{3+}$, which have two major fragmentation pathways, the fragmentation of $[Eu(GWG)(CH_3CN)_5]^{3+}$ has three additional pathways. The first two are the same as observed for Ce and La, the last three are different pathways. 1) Formation of tripositive fragments cluster $[Eu(III)(GWG)(CH_3CN)_n(H_2O)_m]^{3+}$ ions, where m=0-2 and n=2-3, by peeling off CH_3CN or replacing CH_3CN with H_2O; 2) Formation of dipositive fragment $[Eu(III)(GWG\text{-}H)(CH_3CN)_n(H_2O)_m]^{2+}$ ions, where m, n=0-2; 3) Formation of dipositive fragments $[Eu(II)(CH_3CN)_n(H_2O)_m]^{2+}$ ions, where m=0-2, and m=3-4; and the complementary radical cations $[GWG]^{\bullet+}$ formed by reduction of the europium (as in Figure 3.4) ; 4) Formation of

protonated GWG and its CID products, $[b_2]^+$ and $[a_2]^+$ ions; and 5) Loss of the side chain of W as the 3-methylene-3H- indolium ion.

3.2.2 Radical cations of GYG, GF, and AF generated from complexes $[Eu(peptide)(CH_3CN)_n]^{3+}$, where n=5 or 6

By isolating and dissociating $[Eu(peptide)(CH_3CN)_n]^{3+}$, where n=5-7, cationic peptide radicals have also been generated for GYG, GGM, WGG, GGF.

Earlier research on copper-peptide-ligand complexes showed that generation of peptide radical cations was not only ligand-dependent, but also sequence-dependent [13, 15, 21, 22]. The fragmentation of $[Cu(terpy)(GGX)]^{2+}$ or $[Cu(9\text{-}aneN3)(GGX)]^{2+}$ complexes [16, 23] only generated $[peptide]^{\bullet+}$ when X=lysine, arginine, histidine, tyrosine or tryptophan. This was ascribed to the peptide locating in close proximity to the metal ion. With a sterically encumbered macrocyclic ligand 12-crown-4, the $[GGX]^{\bullet+}$ was observed when X= seventeen different amino acids [16]. 39% to 100% abundance of the intact peptide radical cations were observed for X=K(39%), Y(44%), P (54%), R(74%), W(99%), H(100%); 10% to 16% abundance of the peptide radical cations were observed for X=L(10%), G(11%), F(11%), M(11%), Q(16%), and 5% to 9% abundance of the molecular peptide radical cations were observed for X=A(5%), V(5%), E(5%),D(5%), N(6%), I(9%). Here, surprisingly, by fragmentation of $[Eu(peptide)(CH_3CN)_n]^{2+}$, 50% $[GGM]^{\bullet+}$ and 20% $[GGF]^{\bullet+}$ were observed in the CID spectra, again showing that the generation of molecular peptide radical is metal ion dependent.

Figure 3.5a shows that under low-energy collision-induced dissociation, $[GYG]^{\bullet+}$ is generated in high abundance. Tripositive fragments $[Eu(III)(GYG)(CH_3CN)_n(H_2O)_m]^{3+}$ and dipositive fragments $[Eu(III)(GYG\text{-}H)(CH_3CN)_n(H_2O)_m]^{2+}$ are present too. The dipositive fragments cluster

$[^{153}Eu(II)(CH_3CN)_n(H_2O)_m]^{2+}$ and $[^{153}Eu(III)(OH)(CH_3CN)_n(H_2O)m]^{2+}$ are also abundant products.

Dipeptide radical cations have also been formed for GF, AF, FM, PF, FM and GM. Deuterated acetonitrile was used as solvent to assist in assigning the fragments in the CID spectra to confirm the presence of peptide radical cations.

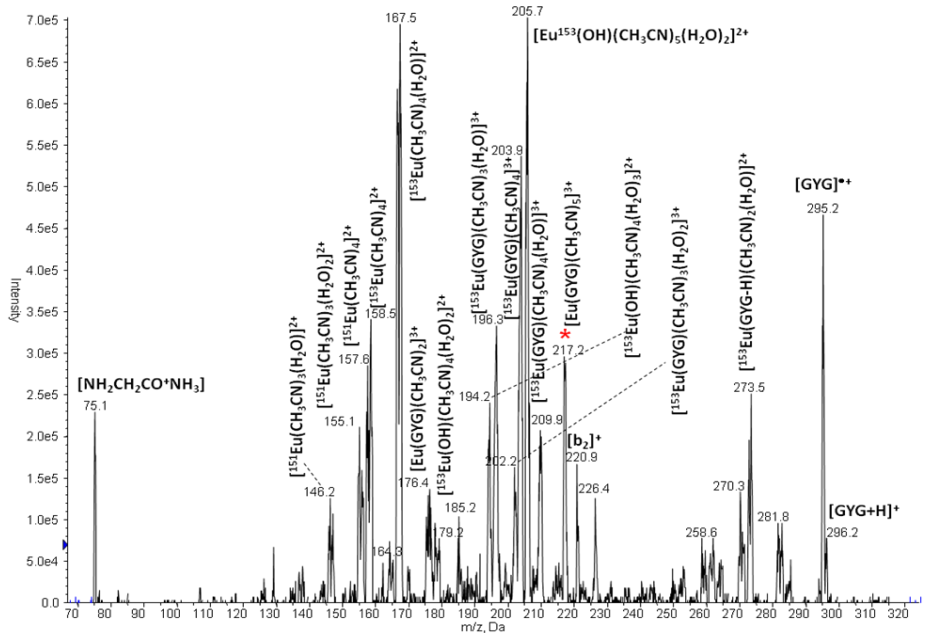

Figure 3.**5 (a)** CID spectrum of $[Eu(GYG)(CH_3CN)_5]^{3+}$ at *m/z* 217.4 , E_{lab}=15 eV. The precursor ion is labelled with an asterisk (*)

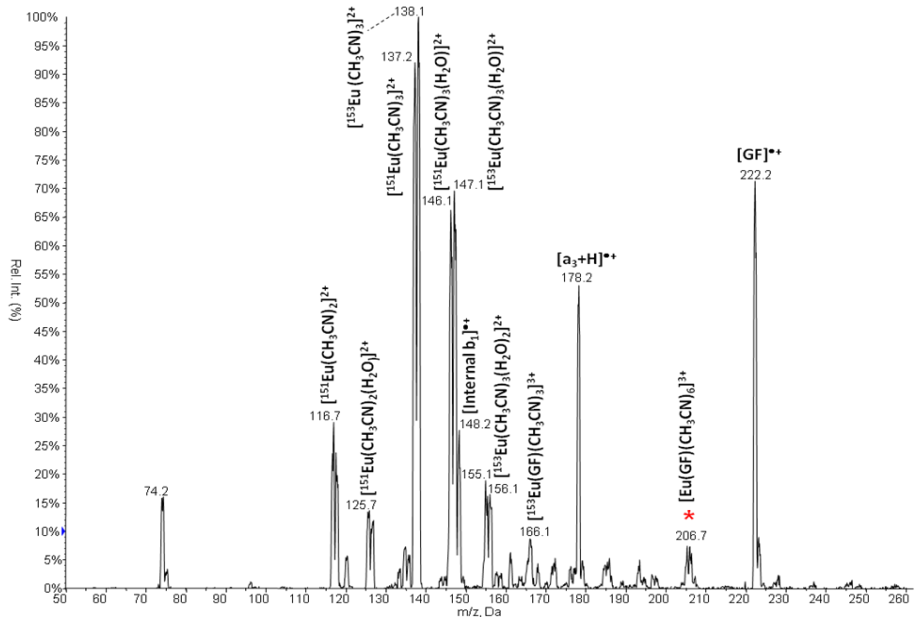

Figure 3.5 **(b)** CID spectrum of $[Eu(GF)(CH_3CN)_6]^{3+}$ at *m/z* 206.7 , E_{lab}=30 eV. The precursor ion is labelled with an asterisk (*)

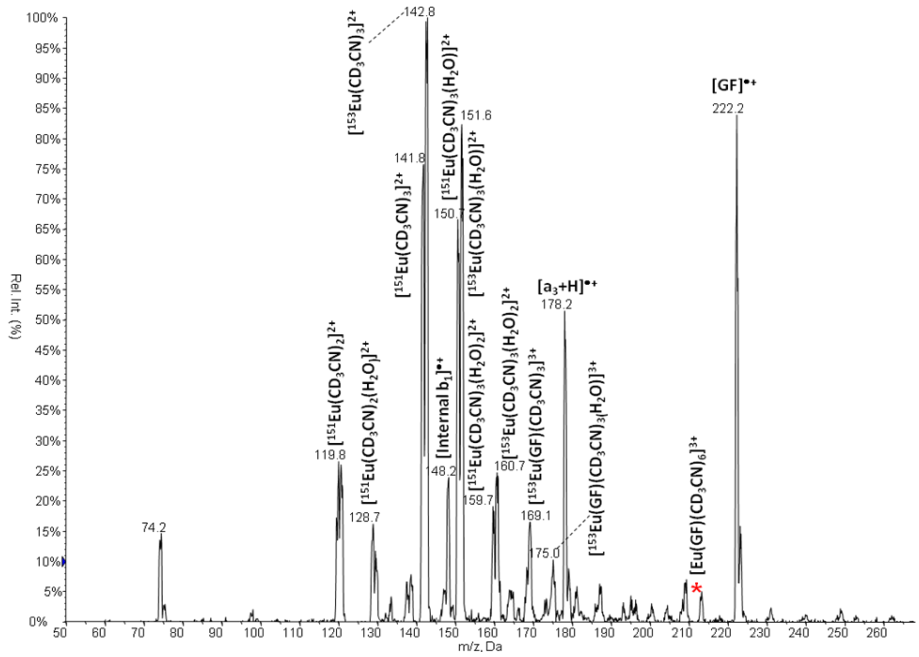

Figure 3.5 **(c)** CID spectrum of $[Eu(GF)(CD_3CN)_6]^{3+}$ at *m/z* 212.8 , E_{lab}=30 eV. The precursor ion is labelled with an asterisk (*)

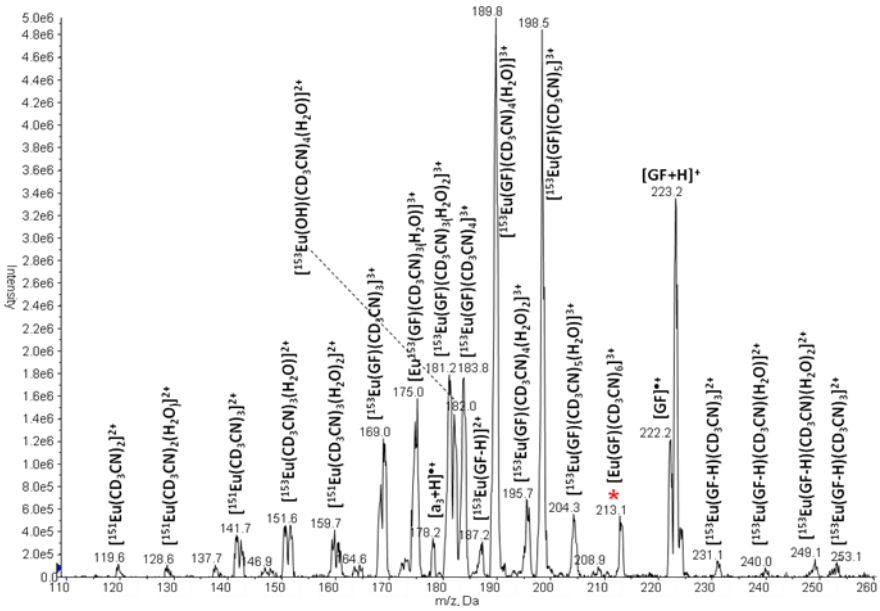

Figure 3.5 (d) CID spectrum of $[Eu(GF)(CD_3CN)_6]^{3+}$ at *m/z* 212.8 , E_{lab}=15 eV. The precursor ion is labelled with an asterisk (*)

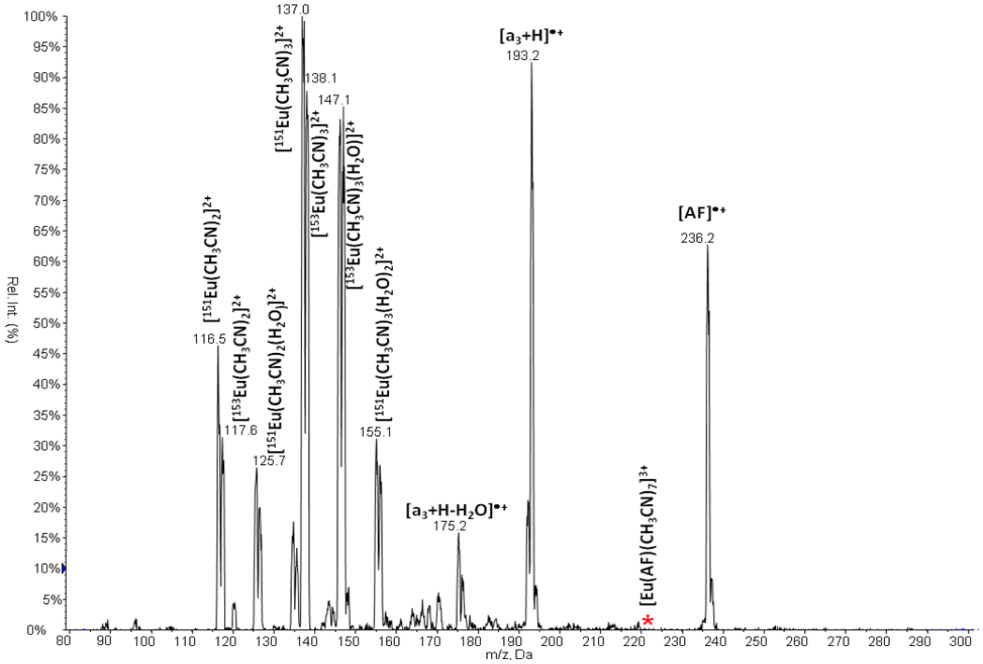

Figure 3.5 (e) CID spectrum of $[Eu(AF)(CH_3CN)_7]^{3+}$ at *m/z* 224.9 , E_{lab}=37.5 eV. The precursor ion is labelled with an asterisk (*)

Under higher collision energy (E_{lab}=30 eV) for $[Eu(GF)(CH_3CN)_6]^{3+}$ at *m/z* 206.7, $[Eu(GF)(CD_3CN)_6]^{3+}$ at *m/z* 212.8 and $[Eu(AF)(CH_3CN)_7]^{3+}$ at *m/z* 224.9 at E_{lab}=37.5 eV , the major fragmentation pathways have changed to the following: 1) $[Eu(II)(CH_3CN)_n(H_2O)_m]^{2+}$ where m=0-2 and n=2-3; 2) $[GF]^{\bullet+}$ or $[AF]^{\bullet+}$, and 3) $[a_3+H]^{\bullet+}$ ions; the latter are peptide radical cations minus CO_2, i.e., $[GF-CO_2]^{\bullet+}$ Low abundance of $[Eu(GF)(CH_3CN)_3(H_2O)_n]^{3+}$ or $[Eu(GF)(CD_3CN)_3(H_2O)_n]^{3+}$, where n=0 or 1, are present but $[Eu(AF)(CH_3CN)_3(H_2O)_n]^{3+}$ is not observed, probably due to the higher collision energy. At lower collision energy (Elab=15 eV), $[Eu(GF)(CH_3CN)_3(H_2O)_n]^{3+}$ ions are observed as major fragmentation products again, together with abundant protonated peptide. Peptide radical cation $[GF]^{\bullet+}$ is also present but, only in 40% abundance.

3.2.3 Fragmentations of $[Ln(PGG)(CH_3CN)_5]^{3+}$ ions, where Ln=Y, La, Ce, Eu, Gd and Tb

As previously reported [6], the fragmentation of $[La(PGG)(CH_3CN)_6]^{3+}$ generated protonated $[a_3+H]^{2+}$ ions and no $[PGG]^{\bullet+}$ was observed. Here we report the formation of aliphatic tripeptide radical cations $[PGG]^{\bullet+}$ from the dissociation of the tripositive Eu/PGG complex, although it is well known that only peptides containing aromatic amino acid residues can readily generate radical cations. As was observed, in the CID spectrum of $[Eu(GF)(CH_3CN)_6]^{3+}$ (Figure 3.5b), the major products in the spectrum of $[Eu(PGG)(CH_3CN)_6]^{3+}$ as displayed in Figure 3.6a are: 1) Formation of $[Eu(II)(CH_3CN)_n(H_2O)_m]^{2+}$, where m=0-3 and n=2-3, and the complementary ions of $[PGG]^{\bullet+}$ and $[a_3+H]^{\bullet+}$ ions. 2) Formation of $[b_2-H]^{\bullet+}$ ions, formally $[PGG]^{\bullet+}$ minus glycine (75 Da). Moderate abundance of $[Eu(PGG)(CH_3CN)_3(H_2O)_n]^{3+}$, where n=2 or 3 was also present.

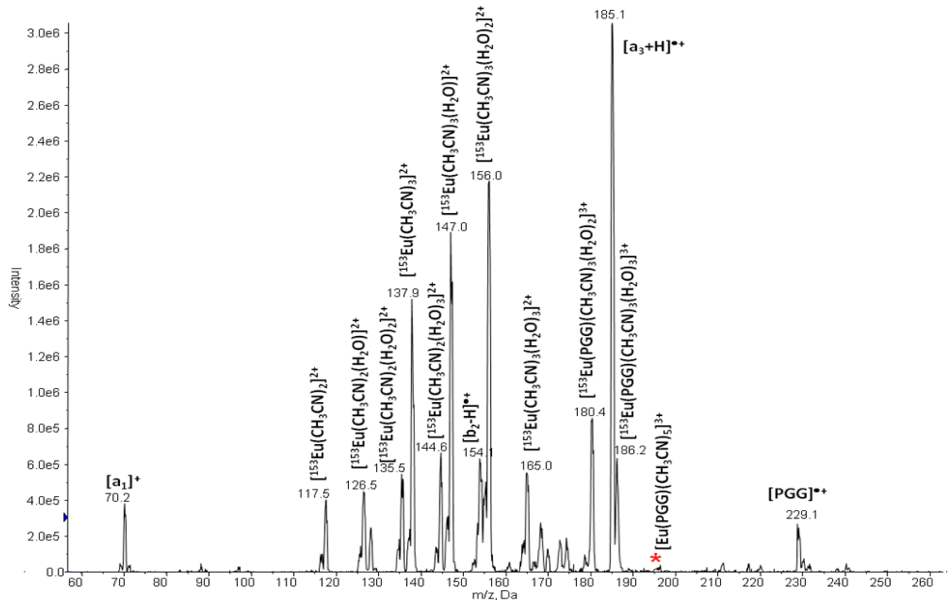

Figure 3.6 (a) CID spectrum of $[Eu(PGG)(CH_3CN)_6]^{3+}$ at *m/z* 195.6 , E_{lab}=30 eV. The precursor ion is labelled with an asterisk (*)

A further look at the fragmentations of $[La(PGG)(CH_3CN)_6]^{3+}$ and $[Ce(PGG)(CH_3CN)_6]^{3+}$ revealed almost identical fragmentation behaviour for these two metal-peptide complexes. Figures 3.6b and 3.6c show that $[PGG+H]^+$ is present in both spectra. A group of tripositive $[Ln(III)(PGG)(CH_3CN)_m(H_2O)_n]^{3+}$ ions, in which CH_3CN has been displaced by water, are the most abundant. A group of dipositive $[Ln(III)(PGG\text{-}H)(CH_3CN)_m(H_2O)_n]^{3+}$ ions where m, n=0~4, are products in lower abundance. No peptide radical cations were observed, i.e., they gave similar spectra to those in Figures 3.1a and 3.1b.

Tripositive complexes of $[Ln(III)PGG)(CH_3CN)_n]^{3+}$ were investigated, where Ln= Y, Gd, Tb, Yb. The CID spectra also have very similar fragmentation patterns, except for that of $[Yb(III)(PGG)(CH_3CN)_n]^{3+}$ shown in Figure 3.6d, where there is more similarity to that of $[Eu(III)(PGG)(CH_3CN)_n]^{3+}$.

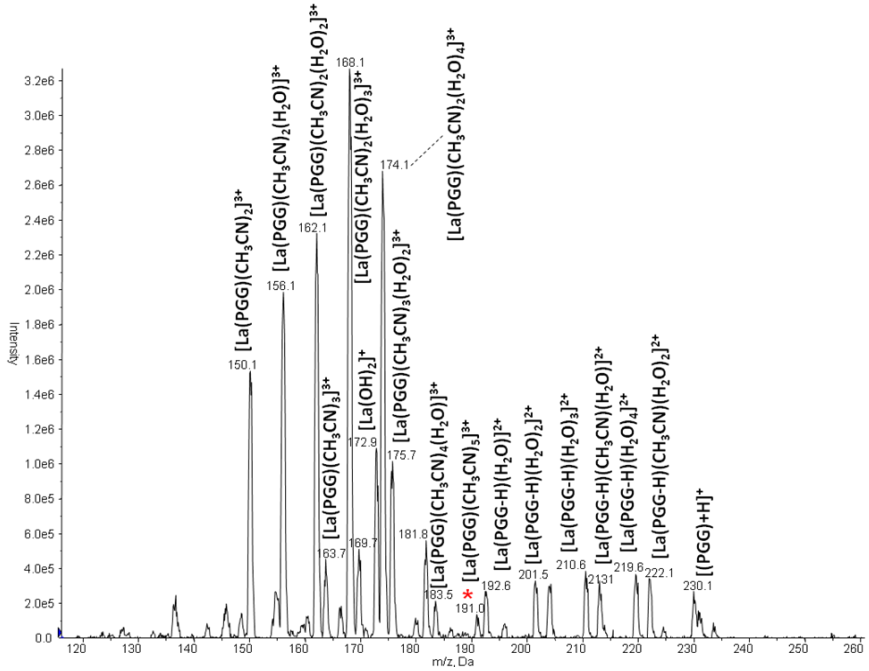

Figure 3.6 (b) CID spectrum of $[La(PGG)(CH_3CN)_6]^{3+}$ at *m/z* 191.2 , E_{lab}=30 eV. The precursor ion is labelled with an asterisk (*)

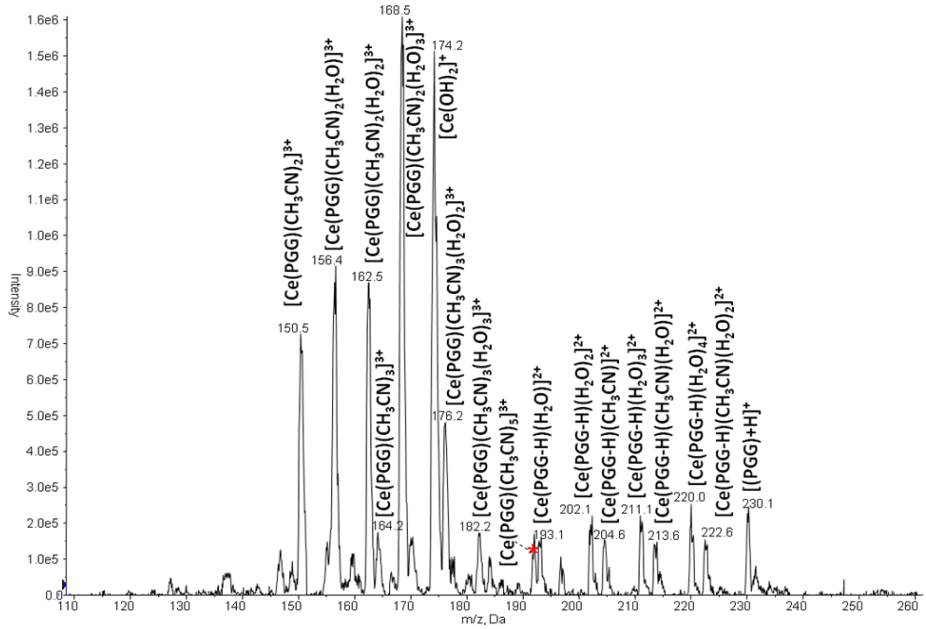

Figure 3.6 (c) CID spectrum of $[Ce(PGG)(CH_3CN)_6]^{3+}$ at *m/z* 191.7 , E_{lab}=30 eV. The precursor ion is labelled with an asterisk (*)

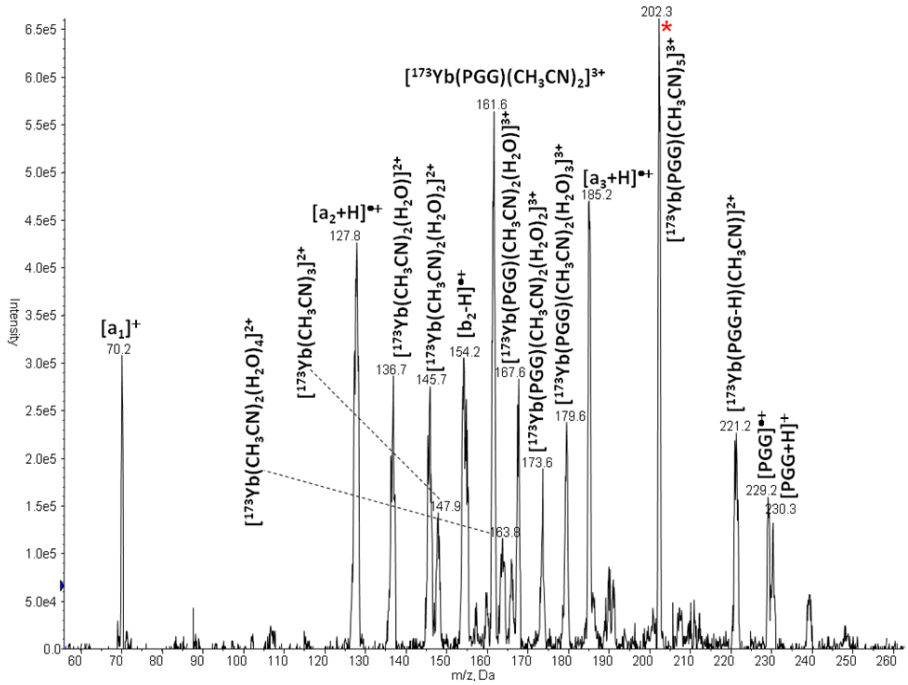

Figure 3.6 (d) CID spectrum of $[Yb(PGG)(CH_3CN)_6]^{3+}$ at *m/z* 202.5 , E_{lab}=45 eV. The precursor ion is labelled with an asterisk (*)

Peptide radical cations $[PGG]^{\bullet+}$, $[a_3+H]^{\bullet+}$ and $[b_2-H]^{\bullet+}$ are present in Figure 3.6d as major fragmentation products, a reflection of the ease with which Yb is reduced. In addition, there are three other reduced products common to the $[Eu(PGG)(CH_3CN)_6]^{3+}$ complexes: 1) $[^{173}Yb(II)(PGG)(CH_3CN)_n(H_2O)_m]^{3+}$; 2) $[^{173}Yb(II)(CH_3CN)_n(H_2O)_m]^{2+}$; and 3) $[^{173}Yb(II)\ (PGG\text{-}H)(CH_3CN)_n]^{3+}$, where n, m =0-3.

3.2.4 Fragmentations of $[Ln(GYG)(CH_3CN)_5]^{3+}$, where Ln=Y, Sm, Gd, Tb, Yb

Since the fragmentation of the copper(II)/peptide/amine ternary complexes generated peptide radical cations [16-17, 21], and the initial research showed that CID of $[Eu(GWG)(CH_3CN)_5]^{3+}$ (Figure 3.4) and $[Eu(GYG)(CH_3CN)_5]^{3+}$ (Figure 3.5a) produced radical cations $[GWG]^{\bullet+}$ and $[GYG]^{\bullet+}$ in abundances of 18% and 65% respectively, GYG was selected as a model peptide to

investigate the fragmentation of the $[Ln(III)(peptide)(CH_3CN)_n]^{3+}$ complexes containing different metals.

$[La(III)(GYG)(CH_3CN)_5]^{3+}$ and $[Ce(III)(GYG)(CH_3CN)_5]^{3+}$ have almost identical spectra, except that the mass shifts due to the 1 unit mass difference between La and Ce. The CID spectra in Figure 3.7 shows the fragmentation of the tripositive complex $[Y(III)(GYG)(CH_3CN)_5]^{3+}$, $[Gd(III)(GYG)(CH_3CN)_5]^{3+}$ and $[Tb(III)(GYG)(CH_3CN)_5]^{3+}$, which are very similar to those of $[La(III)(GYG)(CH_3CN)_5]^{3+}$ and $[Ce(III)(GYG)(CH_3CN)_5]^{3+}$, and there is no $[GYG]^{\bullet+}$ present. $[Sm(III)(GYG)(CH_3CN)_5]^{3+}$ and $[Yb(III)(GYG)(CH_3CN)_5]^{3+}$ have been investigated (not shown here) and there are no peptide radical cations formed. Also the spectra of $[Yb(III)(GWG)(CH_3CN)_5]^{3+}$ and $[Yb(III)(GGM)(CH_3CN)_5]^{3+}$ showed no presence of $[GWG]^{\bullet+}$ and $[GGM]^{\bullet+}$, although they can be formed by the fragmentation of the tripositive Eu(III)/peptide complexes. This contrasts with the spectrum of $[Yb(III)(PGG)(CH_3CN)_6]^{3+}$, where $[PGG]^{\bullet+}$ was observed (Figure 3.6d).

Yitterbium and Europium have the largest 3rd ionization energies (see Table 1.1 in Chapter 1), i.e, 25.03 eV and 24.92 eV, respectively. Apart from the high ionization energy, half-filled electronic shells have extra stable electronic configurations; so reduction from Eu^{3+} to Eu^{2+} which makes it become $4f^7$, strongly stabilize the products containing Eu^{2+}. Similarly conversion of Yb^{3+} to Yb^{2+}, makes it become $4f^{14}$, a fully-filled shell which again is energetically favored; hence, the peptide radical cations $[PGG]^{\bullet+}$ can be generated by the fragmentation of Ln(III)/PGG complex where Ln = Eu and Yb.

The reason why ytterbium-containing complexes generate $[PGG]^{\bullet+}$ by CID of $[Yb(III)(PGG)(CH_3CN)_6]^{3+}$, but do not give radical cations from peptides containing aromatic

amino acid residue, is not understood yet. The ETD experiment on the lanthanide cationized Fibrinopeptide B and two peptide analogs showed the similar trend [24]. The ETD fragmentation patterns of the Ln(III)/peptide complexes were different where Ln = Eu and Yb. It was explained as the different E^0 in aqueous [24-25] for Ln(III) to Ln(II), that is, -0.36 V for Eu and -1.05 V for Yb, respectively. Fibrinopeptide B has 14 amino acid residues, which provides the aqueous-like environment for Ln(III). In this case, Eu(III) is reduced more easily than Yb(III); as a consequence the peptide radical cations are generated due to electron transfer under low-energy collision-induced dissociation, although the tripeptide offers the less aqueous-like environment.

As Yb has seven naturally occurring isotopes in abundances of 0.1% to 31.9%, it is not considered a good candidate for further research on the fragmentation of Ln(III)/peptide complexes.

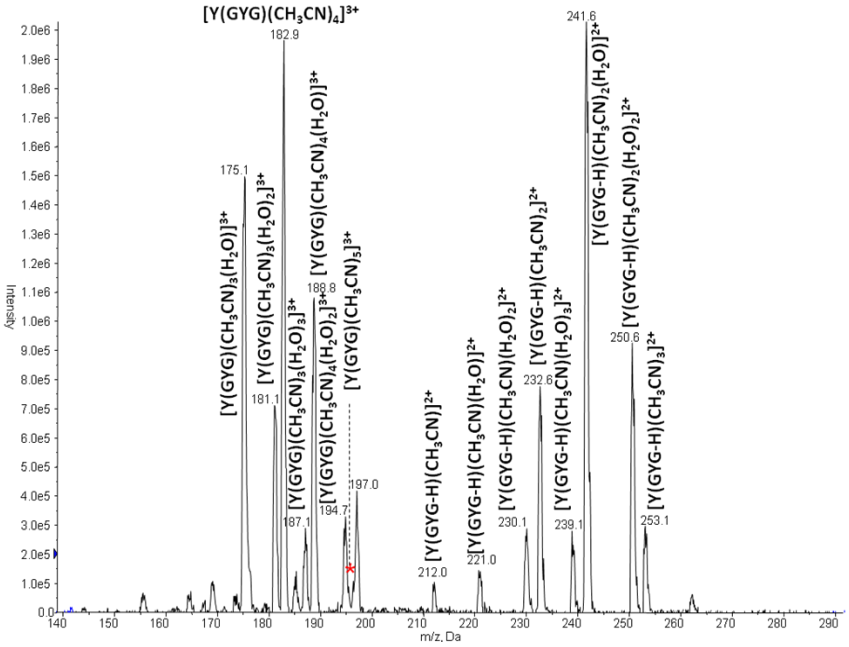

Figure 3.7 (a) CID spectrum of $[Y(III)(GYG)(CH_3CN)_5]^{3+}$ at *m/z* 196.7 , E_{lab}=15 eV. The precursor ion is labelled with an asterisk (*)

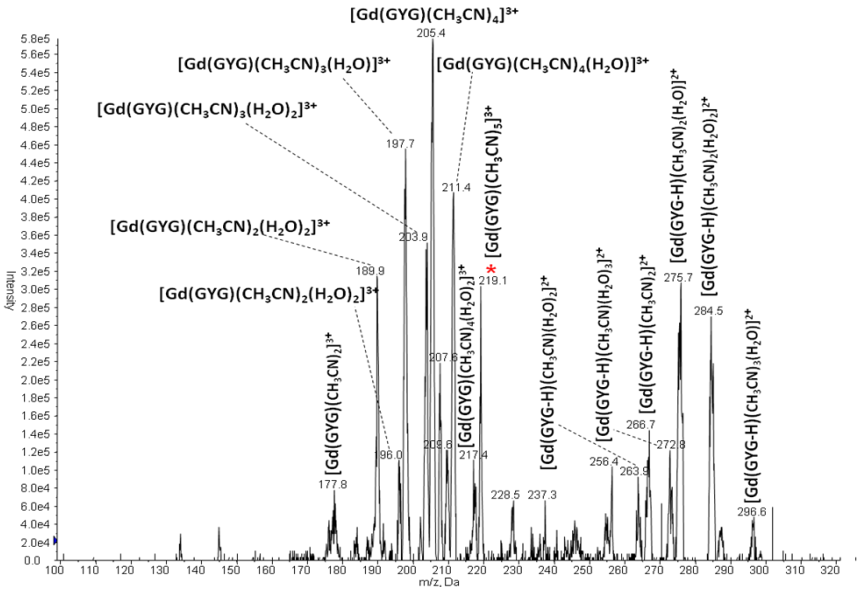

Figure 3.7 (b) CID spectrum of $[Gd(III)(GYG)(CH_3CN)_5]^{3+}$ at *m/z* 219.1 , E_{lab}=15 eV. The precursor ion is labelled with an asterisk (*)

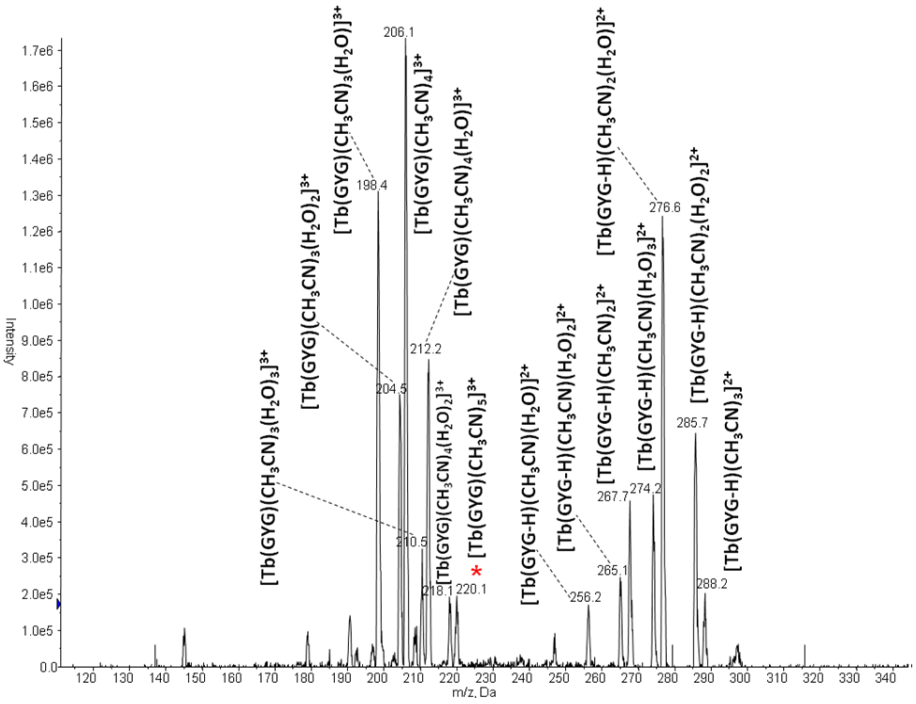

Figure 3.7 (c) CID spectrum of $[Tb(III)(GYG)(CH_3CN)_5]^{3+}$ at *m/z* 219.9 , E_{lab}=15 eV. The precursor ion is labelled with an asterisk (*)

3.3 Conclusion

Sc(III) did not form stable $[Sc(peptide)(CH_3CN)_m]^{3+}$ complexes in the gas phase; hence ths metal was not investigated further. Among the rare earth element studied, the tripositive complexes of Ln(III)/peptide, where Ln = Y, La, Ce, Sm, Gd, Tb, show very similar fragmentation patterns in the gas phase under low energy collision-induced dissociation. That is: 1) Formation of tripositive fragments $[Ln(III)(Peptide)(CH_3CN)_n(H_2O)_m]^{3+}$, where m, n = 0 - 4, by peeling off CH_3CN or replacing CH_3CN with H_2O; 2) Formation of dipositive fragments cluster $[Ln(III)(Peptide\text{-}H)(CH_3CN)_n(H_2O)_m]^{2+}$, where m, n = 0 - 2.

Europium (III) shows different characteristics and generates peptide radical cations for W-, Y-, F-, M-containing peptides and also for the aliphatic peptide PGG. It is reduced to Eu(II), by accepting an electron from the peptide to form radical cations or $[a_3+H]^{\bullet+}$ ions. The major fragmentation channels for $[Eu(III)(peptide)(CH_3CN)_n]^{3+}$ complexes are 1) formation of $[Eu(II)(CH_3CN)_n(H_2O)_m]^{2+}$, where m, n = 0 - 3; and 2) formation of $[peptide]^{\bullet+}$, $[a_3+H]^{\bullet+}$ and $[b_2\text{-}H]^{\bullet+}$. Moderate abundance of $[Eu(peptide)(CH_3CN)_n(H_2O)_m]^{3+}$ complexes, where n = 0 - 4, depending on the precursors are also present under low energy collision-induced dissociation conditions.

Eu(II) has a half-filled electronic shells which is a stable electronic configuration, and Yb(II) has fully-filled f-shells which also is a stable electronic configuration. Consequently, Eu(II) and Yb(II) have the two highest 3rd ionization energies. This may explain why CID of $[Yb(III)(PGG)(CH_3CN)_6]^{3+}$ and $[Yb(III)(PGG)(CH_3CN)_6]^{3+}$ complexes both give $[PGG]^{\bullet+}$. However, only CID of $[Eu(III)(GYG)(CH_3CN)_5]^{3+}$ gives $[GYG]^{\bullet+}$; CID of $[Yb(III)(GYG)(CH_3CN)_5]^{3+}$ does not. These may be due to the fact that Eu(III) is more easily

reduced to Eu(II) compared to the reduction of Yb(III) to Yb(II). The lower ionization energy of GYG compared to that of PGG may also be important.

3.4 References

1. Barlow, C. K., McFadyen, W. D., and O'Hair, R. A. J. Formation of Cationic Peptide Radicals by Gas-Phase Redox Reactions with Trivalent Chromium, Manganese, Iron, and Cobalt Complexes. J Am Chem Soc, 2005; 127(16): 6109–6115.
2. Shi, T., Hopkinson, A. C., and Siu, K. W. M. Coordination of Triply Charged Lanthanum in the Gas Phase: Theory and Experiment. Chem Eur J, 2007; 13(4): 1142–1151.
3. Shi, T., Siu, K. W. M., and Hopkinson, A. C. Generation of $[La(peptide)]^{3+}$ Complexes in the Gas Phase: Determination of the Number of Binding Sites Provided by Dipeptide, Tripeptide, and Tetrapeptide Ligands. J Phys Chem A, 2007; 111(45): 11562–11571.
4. Shi, T., Siu, C.-K., Siu, K. W. M., and Hopkinson, A. C. Dipositively Charged Protonated a_3 and a_2 Ions: Generation by Fragmentation of $[La(GGG)(CH_3CN)_2]^{3+}$. Angew Chem Int Ed, 2008; 47(43): 8288–8291.
5. Zhao, J., Siu, C.-K., Shi, T., Hopkinson, A. C. and Siu, K. W. M. Abundant Dipositively Charged Protonated a_2 and a_3 Ions from Diproline and Triproline. J Phys Chem B. 2009; 113(14): 4963–4969.
6. Saminathan, I. S., Zhao, J., Siu, K. W. M., and Hopkinson, A. C. Doubly charged protonated a ions derived from small peptides. Phys Chem Chem Phys. 2011; 13(41): 18307.
7. Verkerk, U. H., Zhao, J., Saminathan, I. S., Lau, J. K.-C., Oomens, J., Hopkinson, A. C. and Siu, K. W. M. Infrared Multiple-Photon Dissociation Spectroscopy of Tripositive Ions: Lanthanum–Tryptophan Complexes. Inorg Chem. 2012; 51(8): 4707–4710.
8. Prell, J. S., Flick, T. G., Oomens, J., Berden, G., and Williams, E. R. Coordination of Trivalent Metal Cations to Peptides: Results from IRMPD Spectroscopy and Theory. J Phys Chem A. 2010; 114(2): 854–860.

9. Flick, T. G., Donald, W. A. and Williams, E. R. Electron Capture Dissociation of Trivalent Metal Ion-Peptide Complexes. J Am Soc Mass Spectrom. 2013; 24(2): 193–201.

10. Chen, X., Liu, G., Elaine Wong, Y. L., Deng, L., Wang, Z., Li, W. and Dominic Chan, T.-W. Dissociation of trivalent metal ion (Al^{3+}, Ga^{3+}, In^{3+} and Rh^{3+})–peptide complexes under electron capture dissociation conditions. Rapid Commun Mass Spectrom, 2016; 30(6), 705–710.

11. Commodore, J. J. and Cassady, C. J. The Effects of Trivalent Lanthanide Cationization on the Electron Transfer Dissociation of Acidic Fibrinopeptide B and its Analogs. J Am Soc Mass Spectrom. 2016; 27(9): 1499–1509.

12. Chu, I. K., Rodriquez, C. F., Lau, T.-C., Hopkinson, A. C., and Siu, K. W. M. Molecular Radical Cations of Oligopeptides. J Phys Chem B. 2000; 104(15): 3393–3397.

13. Chu, I. K., Rodriquez, C.F., Hopkinson, A.C., Siu., K.W.C. Formation of molecular radical cations of enkephalin derivatives via collision-induced dissociation of electrospray-generated copper (II) complex ions of amines and peptides. J Am Soc Mass Spectrom, 2001, 12(10): 1114–1119.

14. Laskin, J. and Lifshitz, C. Principles of mass spectrometry applied to biomolecules. Hoboken, N.J: Wiley-Interscience. 2006

15. Chu, I. K., Siu, S. O., Lam, C. N. W., Chan, J. C. Y. and Rodriquez, C. F. Formation of molecular radical cations of aliphatic tripeptides from their complexes with CuII(12-crown-4). Rapid Commun Mass Spectrom. 2004; 18(16): 1798–1802.

16. Lam, C. N. W., Siu, S. O., Orlova, G. and Chu, I. K. Macrocyclic effect of auxiliary ligand on the gas-phase dissociation of ternary copper(II)–GGX complexes. Rapid Commun Mass Spectrom. 2006; 20(5): 790–796.

17. Hopkinson, A. C. Radical cations of amino acids and peptides: Structures and stabilities. Mass Spectrom Rev. 2009; 28(4): 655–671.

18. Siu, C.-K., Ke, Y., Guo, Y., Hopkinson, A. C. and Siu, K. W. M. Dissociations of copper(II)-containing complexes of aromatic amino acids: radical cations of tryptophan, tyrosine, and phenylalanine. Phys Chem Chem Phys. 2008; 10(38), 5908–5918.

19. Shvartsburg, A. A. and Jones, R. C. Attachment of metal trications to peptides. J Am Soc Mass Spectrom. 2004; 15(3): 406–408.

20. Shi, T., Hopkinson, A. C. and Siu, K. W. M. Coordination of Triply Charged Lanthanum in the Gas Phase: Theory and Experiment. Chem Euro J. 2007; 13(4), 1142–1151.

21. Bagheri-Majdi, E., Ke, Y., Orlova, G., Chu, I. K., Hopkinson, A. C. and Siu, K. W. M. Copper-Mediated Peptide Radical Ions in the Gas Phase. J Phys Chem B, 2004; 108(30): 11170–11181

22. Chu, I. K. and Laskin, J. Review: Formation of peptide radical ions through dissociative electron transfer in ternary metal–ligand–peptide complexes. Eur J Mass Spectrom. 2011; 17(6), 543.

23. Chu, I. K., Lam, C. N. W. and Siu, S. O. Facile generation of tripeptide radical cations in vacuo via intramolecular electron transfer in Cu^{II} tripeptide complexes containing sterically encumbered terpyridine ligands. J Am Soc Mass Spectrom. 2005; 16(5): 763–771.

24. Commodore, J. J. and Cassady, C. J. The Effects of Trivalent Lanthanide Cationization on the Electron Transfer Dissociation of Acidic Fibrinopeptide B and its Analogs. J Am Soc Mass Spectrom. 2016; 27(9), 1499-1509

25. Lide, D. R. (ed.) CRC handbook of chemistry and physics, 73rd ed.; CRC press, Cleveland, OH (1992-1993)

CHAPTER 4

Fragmentations of $[Ln^{III}(peptide)(CH_3CN)_n]^{3+}$ Complexes---Further Investigation

4.1 Introduction

Electrospray ionization (ESI) coupled with tandem mass spectrometry is a crucial tool in peptide and protein sequencing [1-3]. Protonated peptides and proteins can be fragmented by collision-induced dissociation (CID) into $[b]^+$ and $[y+2H]^+$ ions [3]. Fragmentation along the backbone does not always happen, and non-specific cleavage and miscleavage can make peptide sequencing ambiguous [4]. Metal/peptide complexes draw interest because of the potential to increase backbone fragmentation and obtain more sequence information to complement that obtained from protonated peptide fragmentation [5]. Various other dissociation techniques, for example, electron transfer dissociation (ETD) [6-7], electron capture dissociation (ECD) [8-10] and infrared multiphoton dissociation (IRMPD) are extensively utilized to investigate the interaction of metal ions with amino acids, peptides and proteins [11-12], in addition to the collision-induced dissociation technique [6,13-14]. The complexes of monovalent metal ions and divalent metal ions have been studied extensively in the past few decades [15-20], and it is believed that amide carbonyl oxygens and carboxylate oxygen atoms normally interact strongly with metal ions to form the salt bridge structure in the metal/tripeptide complexes [11]. Metal ions prefer to coordinate the most basic sites of peptides, carbonyl oxygens, aromatic groups, or the C-terminus carboxyl group [7, 11, 19-23]. C-terminal sequencing is proposed for alkali cationized peptides due to the tendency for peptides cationized by a metal ion to dissociate from the C-terminus [24-25]. A study on the CID of polyalanines [6] showed that Cu(II) is a promising cationizing reagent for sequencing, since $[Cu(Peptide\text{-}H)]^+$ and $[Cu(peptide)]^{2+}$ show

complementary spectra for full sequencing of the peptide studied, and provide more information than the CID spectra of protonated peptide.

The trivalent metal ion/peptide complexes are difficult to observe in the gas phase, since the metal trications are easily reduced by protic ligands [13, 26] due to the big difference between the 3rd ionization energy of trivalent metal ions and that of a typical organic ligands. However, with ESI, the trivalent metal cations can be introduced to the gas phase inside a solvent shell that prevents them from being reduced [27]. Tripositive metal trication/peptide complexes in the absence of solvent were first observed for peptides with 9 to 13 residues that contain at least one arginine residue with metal trications La^{3+}, Al^{3+}, V^{3+}, Ga^{3+}, Fe^{3+} or Cr^{3+}. Fragmentation pathways followed by these metal/peptide complexes were not investigated [13]. The shortest peptide reported to form an unsolvated tripositive metal(III)/peptide complex had nine residues, bradykinin.

Unsolvated metal ion/peptide complexes provide more information on the intrinsic interaction between a metal ion and a peptide and are useful in modeling metal ion function in biological systems. Silver(I)/peptide complexes, in the absence of solvent, have been studied under CID conditions for peptides with two to eleven residues containing methionine residues or just with neutral side-chain groups [28]. The results showed silver/peptide complex rearrangement due to the absence of solvent, which results in silver coordinating to nitrogen and oxygen on the peptide backbone in addition to the methionine sulfur. Fragmentations of $[Ca(Peptide)]^{2+}$ and $[Ca(Peptide\text{-}H)]^{+}$ were investigated for small peptides with five to seven amino acid residues. These peptides are models for calcium binding site III of rabbit skeleton troponin C; and experiment results indicated that Ca^{2+} binds specific oxygen ligands including the acidic side chain [29]. The study of $[AngI+M+H]^{3+}$ ions of the interaction of angiotensin I (AngI, Asp^{1}-

Arg^2-Val^3-Tyr^4-Ile^5-His^6-Pro^7-Phe^8-His^9-Leu^{10}) with a series of doubly charged cations including Ca, Co, Ni, Cu, and Zn in the absence of solvent indicates that the transition metals bind near the His^6 residue while Ca^{2+} does not favor this site; Ca^{2+} favors association with oxygen atoms spanning the peptide backbone [30]. Previous research[15, 31] with ESI and ion mobility measurements shows that monovalent metal ions (Li^+, Na^+, K^+, Cs^+ and Rb^+) form complexes with polyalanine, Ala_n, where n=6-20. In the absence of solvent, the metal ion changed the polyalanine conformation of random globule in the protonated form to a rigid helix because the metal ions coordinate to the CO group at the C-terminus. For divalent metal ions (Mg^{2+}, Ca^{2+}, Sr^{2+}, Ba^{2+}), the conformation of the Ala_n, where n=14-25, in the unsolvated divalent metalleted complexes have α-helical conformations that are stabilized by the metal ion at the C-terminus, which hence deformed the helix conformation in the C-terminus due to strong metal coordination at this binding site. However, the unsolvated complexes of Ala_n with trivalent metal ion (In^{3+}, Sc^{3+}, Y^{3+}) have not been observed.

For arginine-containing peptides, $[La(peptide)]^{3+}$ complexes have been observed for tetrapeptides and tripeptides. The smallest peptide that has been reported to form an unsolvated tripositive metal trication/peptide complex is Met-Arg [32]. The arginine residue immobilizes the proton on its guanidine group of the basic side chain, and forms a zwitterionic form with COO^- group which binds with La^{3+}. However, the $[La(Gly\text{-}Arg)]^{3+}$ complex was not observed, showing that interaction with the methionine is required. The introduction of an additional binding site on the sulfur atom in the methionine side chain stabilized the tripositive complexes.

When there is no arginine in the peptide, the only peptide that has been reported to form the tripositive metal cation/peptide complex in the absence of solvent has twenty one residues [13]. The dissociation of trivalent metal ion/peptide complexes has also been investigated with ECD

for lanthanide metal ions La^{3+}, Tm^{3+}, Lu^{3+}, Sm^{3+}, Ho^{3+}, Yb^{3+}, Pm^{3+}, or Eu^{3+} for peptides with minimum length of eight residues that contain arginine [10]. For peptides with molecular weights below ~1000 Da, mainly $[Ln(peptide\text{-}H)]^{2+}$ ions are formed, and where the peptide has a molecular weight above 1000, $[Ln(peptide)]^{3+}$ ions are predominant. For larger peptides ECD does not give the reduction of trivalent metal ions except with Eu^{3+}. Eu^{3+} is directly reduced and b/y ions are formed instead of the c/z ions that are formed by other lanthanide metal ions studied, where reduction is driven by the protonated site located remotely from metal ion. It is proposed that the larger peptide provides similar environments as in water. Lanthanide elements, except radioactive promethium, have also been investigated for the unsolvated metal ion/peptide complexes under ETD for Fibrinopeptide B and its analogs (all containing arginine) [33]. All the peptides contain at least two acidic sites that will coordinate with lanthanide metal ions and generate abundant sequence-informative product ions and peptide backbone cleavage. It is reported that all lanthanide metal peptide complexes show similar behaviour except for Europium (Eu).

It ws suggested [32] that in the $[La(peptide)]^{3+}$ complexes, the indole group of the tryptophan residue in Leu-Trp-Met-Arg also coordinates with La^{3+}, in addition to the five oxygen atoms and the sulfur. Previous research [34] also showed that aromatic rings take part in the metal coordination. Here we report the formation and fragmentation of tripositive metal cation/small peptide complexes in the absence of solvent, where the peptide has no basic residue or methionine residues; instead, a tryptophan residue is in the second position of the tripeptides. Based on our research result in Chapter 3 and the work from other researchers [10, 33], Ce^{3+} and Eu^{3+} are selected as the model metal ions in that only Eu^{3+} shows very different behaviour from Y^{3+} and other lanthanide metal ions.

4.2 Results and Discussion

4.2.1 Formation and Fragmentation of [Ln(III)(peptide)]$^{3+}$, where Ln=Ce or Eu

As only the dissociation of Eu(III)/peptide complexes generates radical cations, a comparison of the fragmentation behaviour of Eu(III)/peptide complex with other Ln(III)/peptide complexes is of interest. Ce(III)/peptide complexes show fragmentation behaviour typical of other Ln(III)/peptide complexes (Ln= La, Sm, Gd, Tb) and Y(III)/peptide complexes other than Eu(III)/peptide complexes, so the investigation is focused on the comparison between Eu(III)/peptide and Ce(III)/peptide complexes.

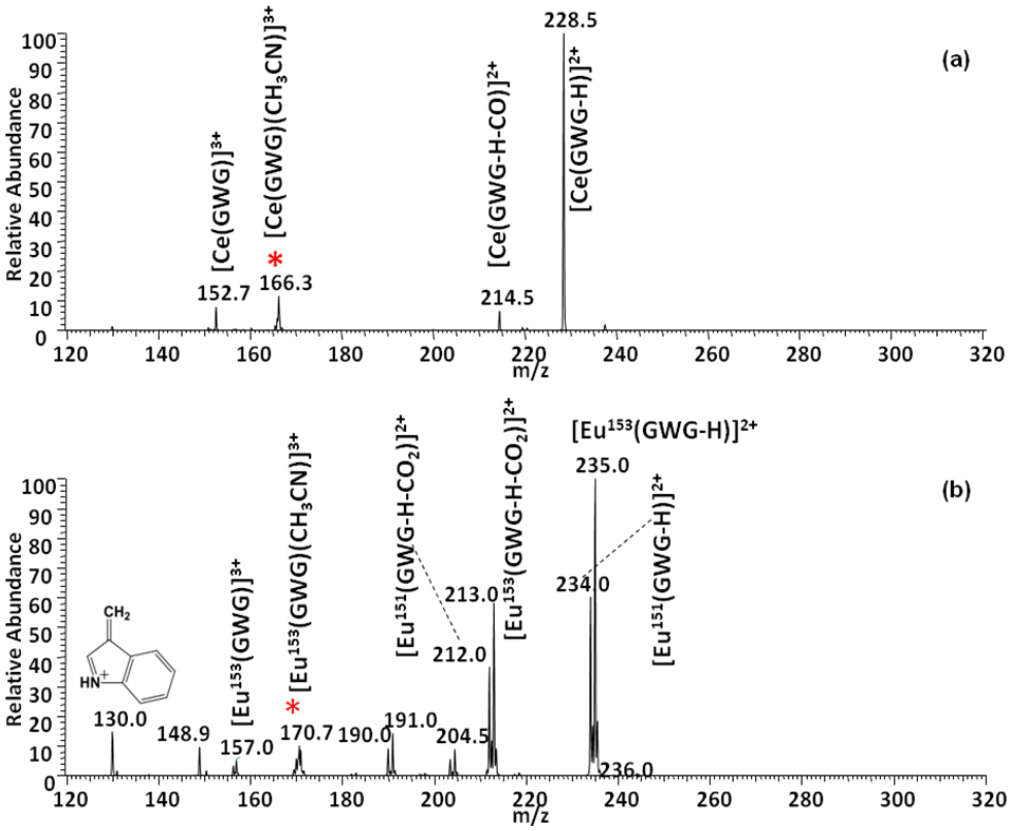

Figure 4.1 CID spectra of (a) [Ce(III)(GWG)(CH_3CN)]$^{3+}$, *m/z* 166.3, CE=11 and (b) [Eu(III)(GWG)(CH_3CN)]$^{3+}$ *m/z* 170.7, CE=10. The precursor ions are labelled with asterisks (*)

Figure 4.1 shows the major products in the fragmentations of $[Ce(III)(GWG)(CH_3CN)]^{3+}$ and $[Eu(III)(GWG)(CH_3CN)]^{3+}$ are similar, namely the dipositive complexes $[Ce(III)(GWG\text{-}H)]^{2+}$ and $[Eu(III)(GWG\text{-}H)]^{2+}$ respectively after solvent CH_3CN loss. The tripositive complexes without any solvent molecules are present in both spectra, although in a small amount (10% abundance at *m/z* 152.7 for Ce and 6% at *m/z* 157.0 for Eu). Further comparison of the two CID spectra shows that the CID spectrum of $[Eu(III)(GWG)(CH_3CN)]^{3+}$ is more complicated compared to that of $[Ce(III)(GWG)(CH_3CN)]^{3+}$. Only $[Eu(III)(GWG)(CH_3CN)]^{3+}$ shows the side chain loss of tryptophan as the 3-methylene-3H-indolium ion accompanied by its complementary ion at *m/z* 191. In addition, CO_2 loss from the $[Eu(III)(GWG\text{-}H)]^{2+}$ and CO loss from $[Ce(III)(GWG\text{-}H)]^{2+}$ are observed, respectively (See Chapter 7).

Further fragmentations of $[Ce(III)(GWG)]^{3+}$and $Eu(III)(GWG)]^{3+}$ are shown in Figure 4.2. The tripositive ions are normally not stable due to the high charge density, especially when there are no solvent molecules coordinated to the metal ion. By contrast with the CID spectra of $[Ce(III)(GWG)(CH_3CN)]^{3+}$ and $[Eu(III)(GWG)(CH_3CN)]^{3+}$, $[Ce(III)(GWG)]^{3+}$ has a more complicated fragmentation pattern than $[Eu(III)(GWG)]^{3+}$. Fragmentation of $[Eu(III)(GWG)]^{3+}$ gives only two abundant products: the side chain of tryptophan residue (*m/z* =130) and its counterpart $Eu(III)(GWG\text{-}130)]^{2+}$ (*m/z* 169.4, 170.4 for ^{151}Eu, ^{153}Eu).

Density functional theory calculations on $[Eu(GGG)]^{3+}$ shows that the lowest energy structure has the GGG ligand present as a zwitterion with the Eu^{3+} ion coordinated by the three carbonyl oxygens. An unusual feature of this ion is that the high Lewis acidity of the Eu^{3+} ion has induced deprotonatation of the nitrogen of the first amide nitrogen while the more acidic carboxylic acid group is not deprotonated. If the $[Eu(GWG)]^{3+}$ ion has the same structure as found for

$[Eu(GGG)]^{3+}$, then loss of the side chain of the tryptophan residue formally converts the oxygen of the second amide group into an anion (see Scheme 4.1)

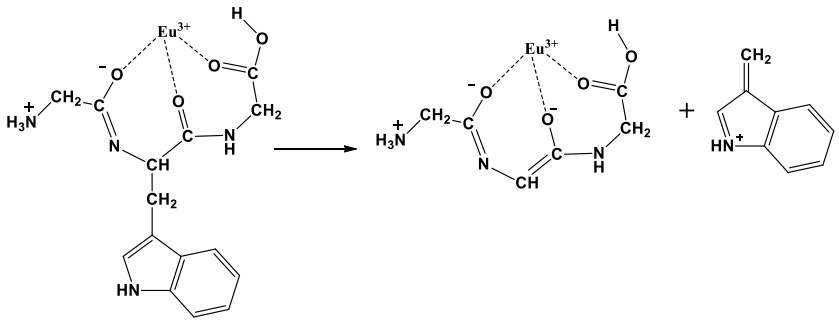

Scheme 4.1

However, for $[Ce(III)(GWG)]^{3+}$, in addition to the side chain loss of tryptophan (*m/z* 130) and its counterpart $[Ce(III)(GWG\text{-}130)]^{2+}$ (*m/z* 164), neutral losses of CO, H_2O or $(CO+H_2O)$ are observed for $[Ce(III)(GWG)]^{3+}$ with the most abundant product formed by CO loss giving $[Ce(III)(GWG\text{-}CO)]^{3+}$. Cleavage at the first amide bond gives an $[a_1]^+$ ion (too low a mass to be observed), CO and the abundant $[Ce(WG\text{-}H)]^{2+}$ ion at *m/z* 200. The $[a_3+H]^{2+}$ ion of GWG is also observed in the spectrum at *m/z* 137.0. To differentiate between the fragments at *m/z* 137.0 and *m/z* 137.3, the CID spectrum of the latter, $[Ce(GWG\text{-}CO\text{-}H_2O)]^{3+}$, is shown in Figure 4.3(a); here side chain loss is the main fragmentation pathway, to give ions at *m/z* 130 and 140.9. The CID spectrum of $[a_3+H]^{2+}$ of GWG can be found in Chapter 6; it has no products similar to those of $[Ce(GWG\text{-}CO\text{-}H_2O)]^{3+}$. Figure 4.3(b) shows that $[Ce(GWG\text{-}CO)]^{3+}$ dissociates mainly into the $[a_3+H]^+$ ion and $[CeO]^+$.

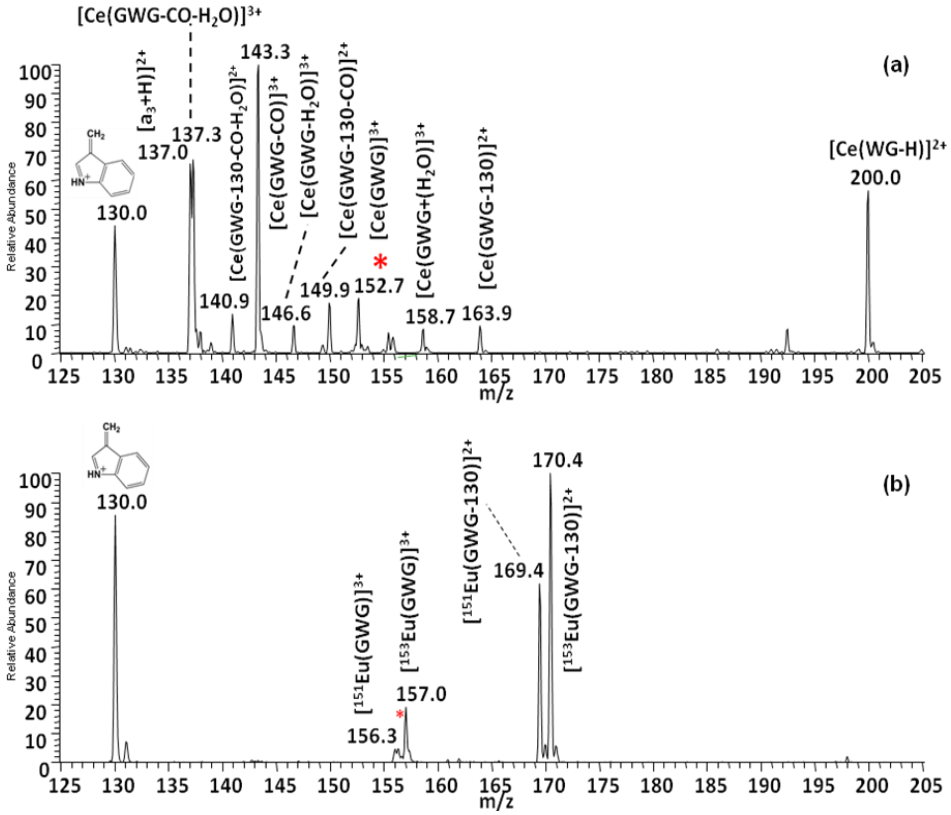

Figure 4.2 CID spectra of $[Ce(GWG)]^{3+}$ (*m/z* 152.7) CE=12 and $[Eu(GWG)]^{3+}$ (*m/z* 156.6) CE=10. The precursor ions are labelled with an asterisk (*)

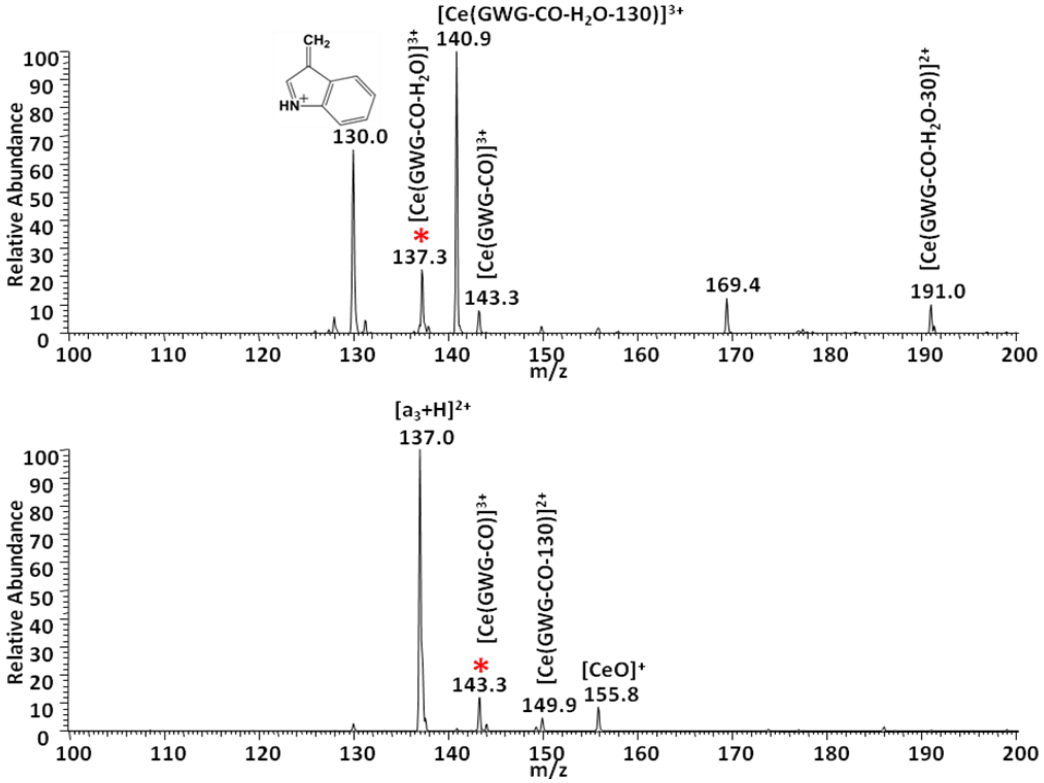

Figure 4.3 CID spectra of (a) $[Ce(GWG\text{-}CO\text{-}H_2O)]^{3+}$, (*m/z* 137.6) CE=8 and (b)$[Ce(GWG\text{-}CO)]^{3+}$, (*m/z* 143.3) CE=10. The precursor ions are labelled with asterisks (*)

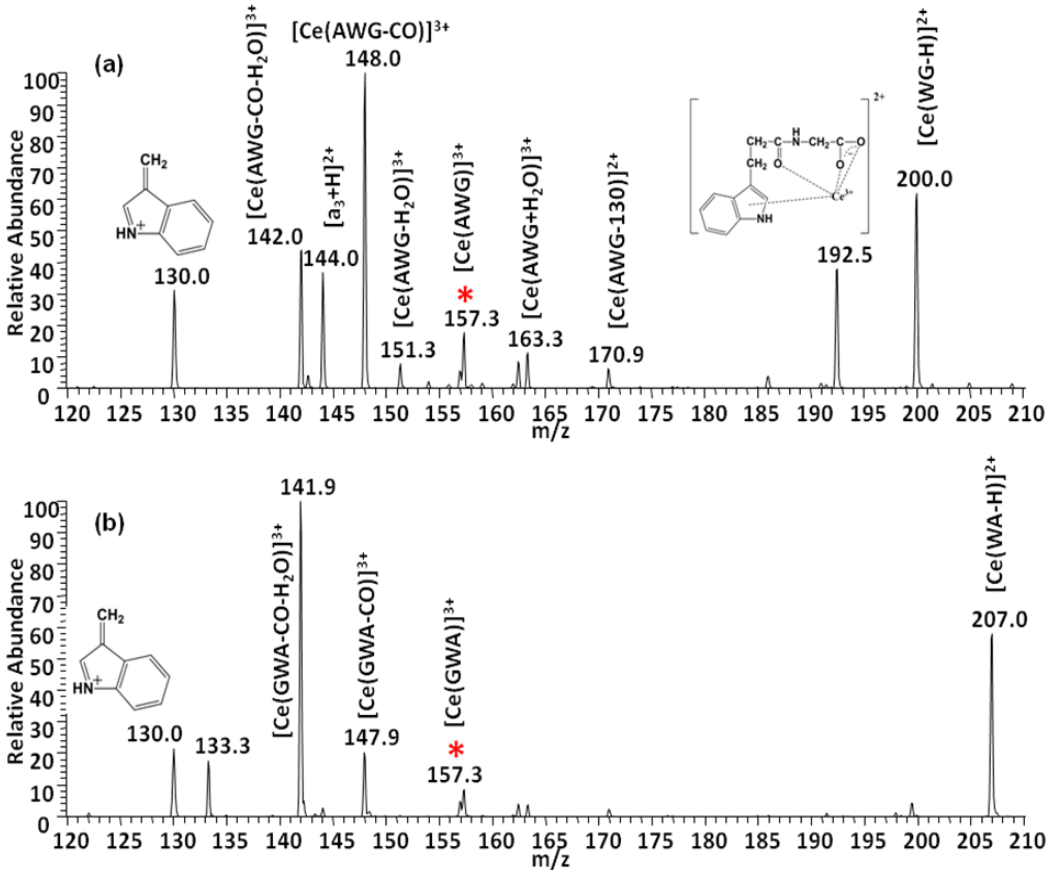

Figure 4.4 CID spectra of (a) $[Ce(AWG)]^{3+}$ (*m/z* 157.3) CE=12 and (b) $[Ce(GWA)]^{3+}$ (*m/z* 157.3) CE=12. The precursor ions are labelled with asterisks (*)

Figure 4.4 shows the CID spectra of $[Ce(AWG)]^{3+}$ and $[Ce(GWA)]^{3+}$, which are very similar to that of $[Ce(GWG)]^{3+}$. The comparison of the three CID spectra helps to interpret the fragments in the spectra. For example, abundant fragments at *m/z* 200.0 only appear in the CID spectra of $[Ce(GWG)]^{3+}$ and $[Ce(AWG)]^{3+}$, corresponding to losses of the N-terminal residue. For $[Ce(III)(GWA)]^{3+}$, the corresponding fragment at *m/z* 207.0 is observed, which suggests the fragment at *m/z* 200.0 is the $[Ce(WG\text{-}H)]^{2+}$, while the fragment at *m/z* 207.0 is the $[Ce(WA)\text{-}H]^{2+}$ ion.

The fragmentation pattern of $[Ce(AWG)]^{3+}$ is very similar to that of **[**$Ce(GWG)]^{3+}$. Features are:

1) CO losses at *m/z* 148.0 and 143.3 provide the most abundant product in both CID spectra;

2) ($CO+H_2O$) losses are observed at *m/z* 142 and 137.3 respectively;

3) side chain losses from tryptophan at *m/z* 130.0 and its counterpart at *m/z* 170.9 and 163.9 for $[Ce(AWG)]^{3+}$ and $[Ce(GWG)]^{3+}$;

4) the products of cleavage at the first amide bond, $[Ce(WG-H)]^{2+}$ at *m/z* 200.0 are observed in both CID spectra;

5) the products of cleavage at C_α-N bond of tryptophan residue at *m/z* 192.5 (the complementary $H_2N^+=C(CH_3)CONH_2$ ion is not observed);

6) $[a_3+H]^{2+}$ of AWG (*m/z* 144.0) and GWG (*m/z* 137.0) are observed.

Based on the above experimental result, we assumed the fragmentation pattern of $[Ce(GWA)]^{3+}$ would be very similar to those of $[Ce(GWG)]^{3+}$ and $[Ce(AWG)]^{3+}$. However, as shown in the right of Figure 4.4, the major pathway is not CO loss; instead, it is ($CO+H_2O$) loss. Although losses of CO, H_2O and the side chain of tryptophan residue at *m/z* 130.0 and $[Ce(WA-H)]^{2+}$ were observed, $[a_3+H]^{2+}$ was not observed, and the corresponding product of the cleavage at C_α-N bond of tryptophan for GWA at *m/z* 199.5 was not seen. In addition to these, the 20% abundance of the *m/z* 133.3 ion is difficult to explain.

According to the above CID spectra, four possible fragmentation pathways and overall pathways by which $[Ce(GWG)]^{3+}$ fragments are proposed as in Scheme 4.2. The density functional calculations showed that the structure at the global minimum for $[La(GGG)]^{3+}$ also has GGG bound as a zwitterion, but with a carboxylate anion bound to the metal ion (Scheme 4.3). For this reason a different structure is the starting point used for the dissociation pathways in Scheme 4.2.

Overall

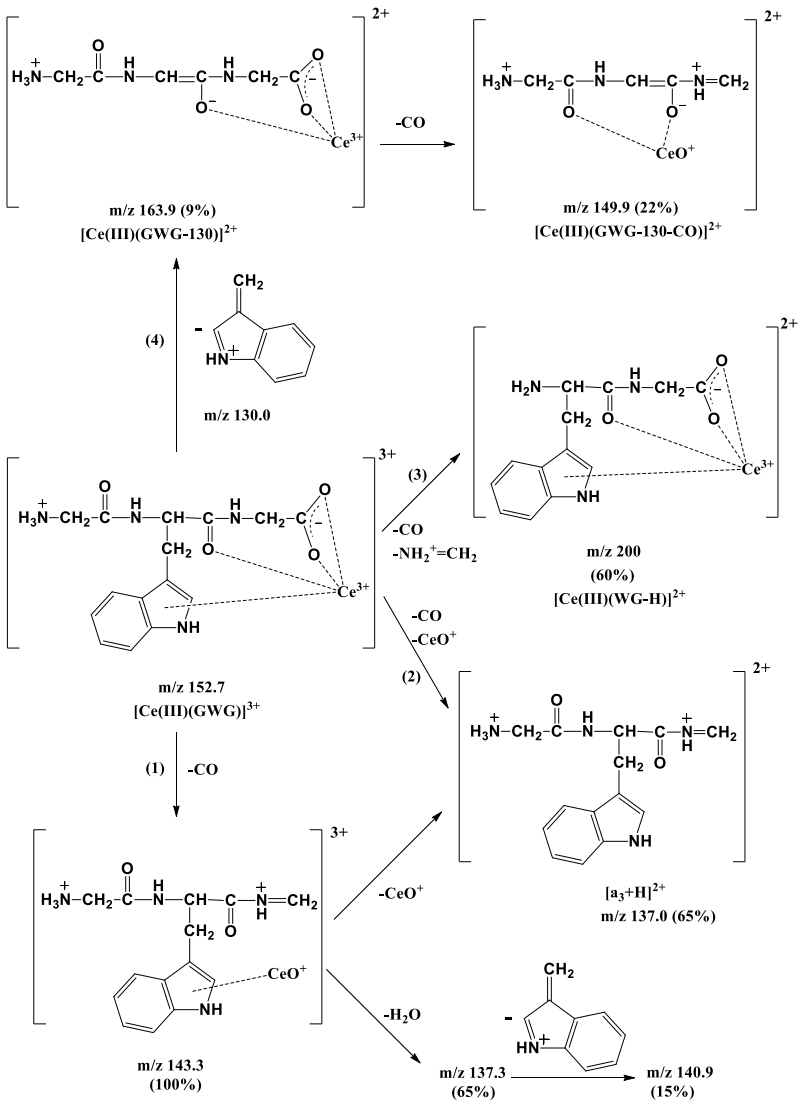

Scheme 4.2 Possible fragmentation pathways of $[Ce(GWG)]^{3+}$

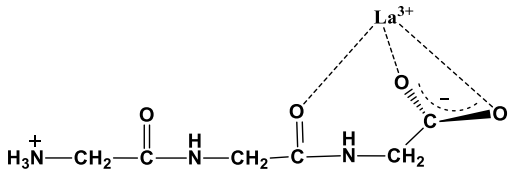

Scheme 4.3

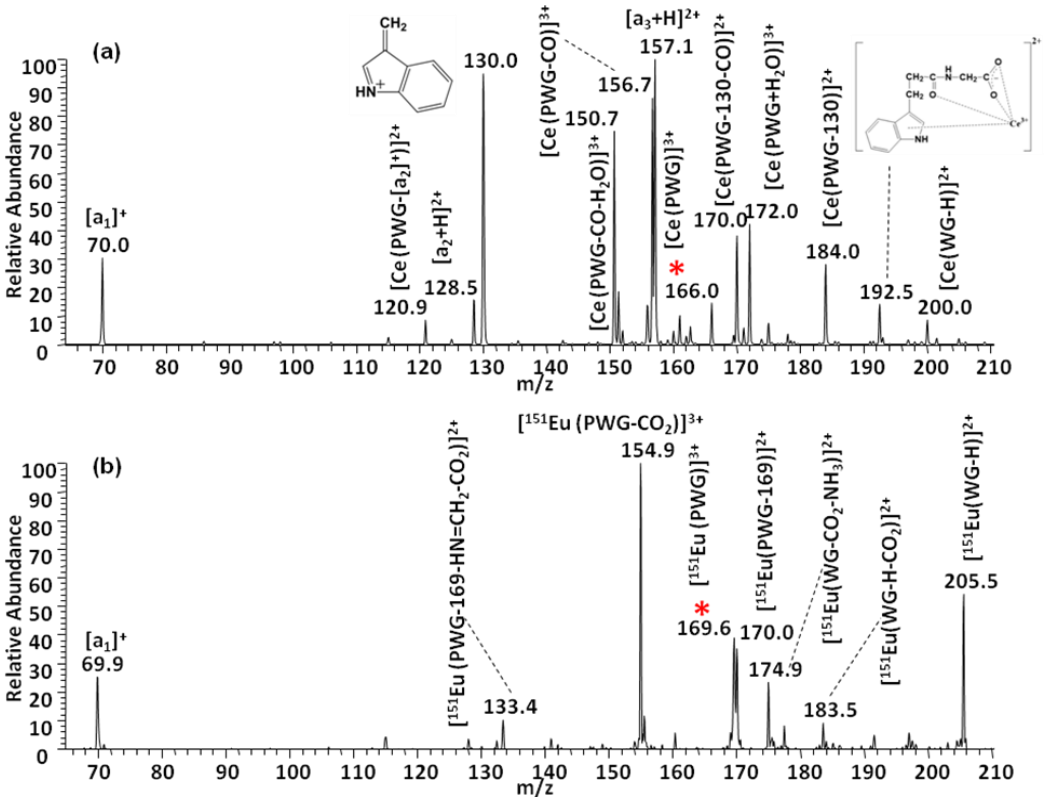

Figure 4.5 CID spectra of (a) $[Ce(PWG)]^{3+}$ (*m/z* 166.0) CE=13 and (b) $[Eu(PWG)]^{3+}$ (*m/z* 169.7) CE=14. The precursor ions are labelled with asterisks (*)

Figure 4.5 shows the CID spectra of $[Ce(PWG)]^{3+}$ (*m/z* 166.0) and $[Eu(PWG)]^{3+}$ (*m/z* 169.7). N-terminal proline helps solvate the high density charge. The major fragmentation pathway of $[Ce(PWG)]^{3+}$ is the formation of $[a_3+H]^{2+}$, the 3-methylene-3H-indolium ion and the product of CO loss (*m/z* 156.7). For $[Eu(PWG)]^{3+}$, CO_2 loss is the predominant fragmentation pathway, although the abundance of the product formed by the cleavage at the first amide bond at *m/z* 205.5 is also significant.

The dissociations of $[Ce(peptide)]^{3+}$ and $[Eu(peptide)]^{3+}$ are peptide and metal-dependent. For the tripeptide with a tryptophan residue in the middle position, the side chain loss is significant.

When proline is at the N-terminus, the side chain loss is barely observed in the CID spectrum of $[Eu(PWG)]^{3+}$. In contrast, the side chain loss from tryptophan (giving the *m/z* 130 ion) is in 93% abundance in the CID spectrum of $[Ce(PWG)]^{3+}$; 45% abundance in the CID spectrum of $[Ce(GWG)]^{3+}$ and 89% abundance in that of $[Eu(GWG)]^{3+}$. The $[a_3+H]^{2+}$ ion is observed in the CID spectra of $[Ce(PWG)]^{3+}$(100%), $[Ce(GWG)]^{3+}$(66%) and $[Ce(AWG)]^{3+}$(37%), but not observed in the CID spectrum of $[Ce(GWA)]^{3+}$ and $[Eu(GWG)]^{3+}$ or $[Eu(PWG)]^{3+}$. Coincidently, $(CO+H_2O)$ loss is present in the CID spectra of $[Ce(GWA)]^{3+}$ as the predominant product and CO loss is only 34%, while in the CID spectra of $[Ce(GWG)]^{3+}$, $[Ce(AWG)]^{3+}$, $[Ce(PWG)]^{3+}$, $(CO+H_2O)$ loss is 67%, 44% and 72% respectively, which is less abundant than that of CO loss ($[Ce(GWG)]^{3+}$(100%), $[Ce(AWG)]^{3+}$(100%) and $[Ce(PWG)]^{3+}$(85%) respectively). CO loss is not observed in the spectra of $[Eu(GWG)]^{3+}$ or $[Eu(PWG)]^{3+}$, just as $[a_3+H]^{2+}$ is not observed. CO_2 loss is only observed for $[Eu(PWG)]^{3+}$ as the predominant fragment.

4.2.2 Formation of $[Ln(peptide\text{-}H)]^{2+}$

The dipositive ion $[Ce(GWG\text{-}H)]^{2+}$ is the main dissociation for $[Ce(GWG)(CH_3CN)]^{3+}$, and $[Eu(GWG\text{-}H)]^{2+}$ is the main product in the fragmentation of $[Eu(GWG)(CH_3CN)]^{3+}$. The fragmentations of $[Ce(GWG\text{-}H)]^{2+}$ and $[Eu(GWG\text{-}H)]^{2+}$ were investigated and compared.

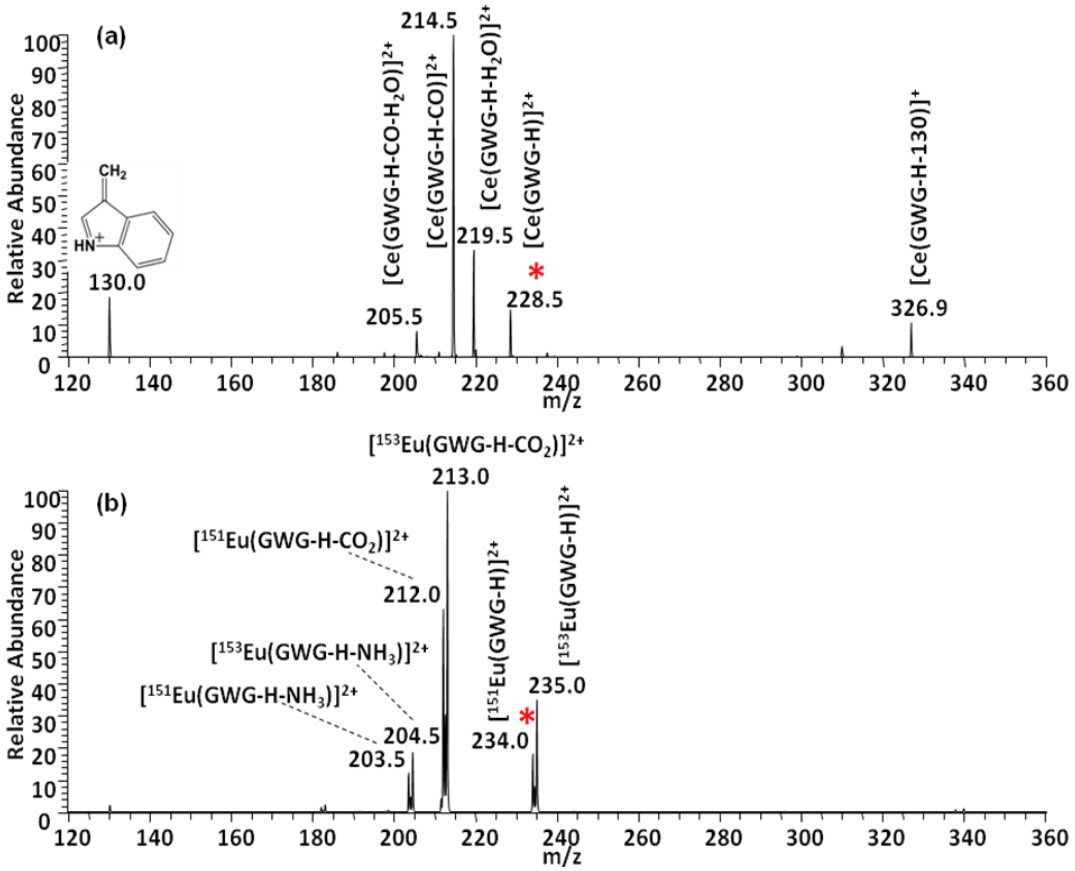

Figure 4.6 CID spectra of (a) $[Ce(III)(GWG\text{-}H)]^{2+}$ (*m/z* 228.5) CE=13 and (b) $[Eu(III)(GWG\text{-}H)]^{2+}$ (*m/z* 234.5) CE=9.5. The precursor ions are labelled with asterisks (*)

The CID spectra in Figure 4.6 show that for $[Ce(peptide\text{-}H)]^{2+}$, CO loss is the major fragmentation pathway, while for $[Eu(peptide\text{-}H)]^{2+}$, CO_2 loss is the major pathway. Figure 4.7 shows the high similarity between the dissociation of $[Ce(AAA\text{-}H)]^{2+}$ and $[La(AAA\text{-}H)]^{2+}$. The fragmentations of $[Ce(peptide\text{-}H)]^{2+}$ complexes are compared with those of $[Eu(peptide\text{-}H)]^{2+}$ complexes in Chapter 7.

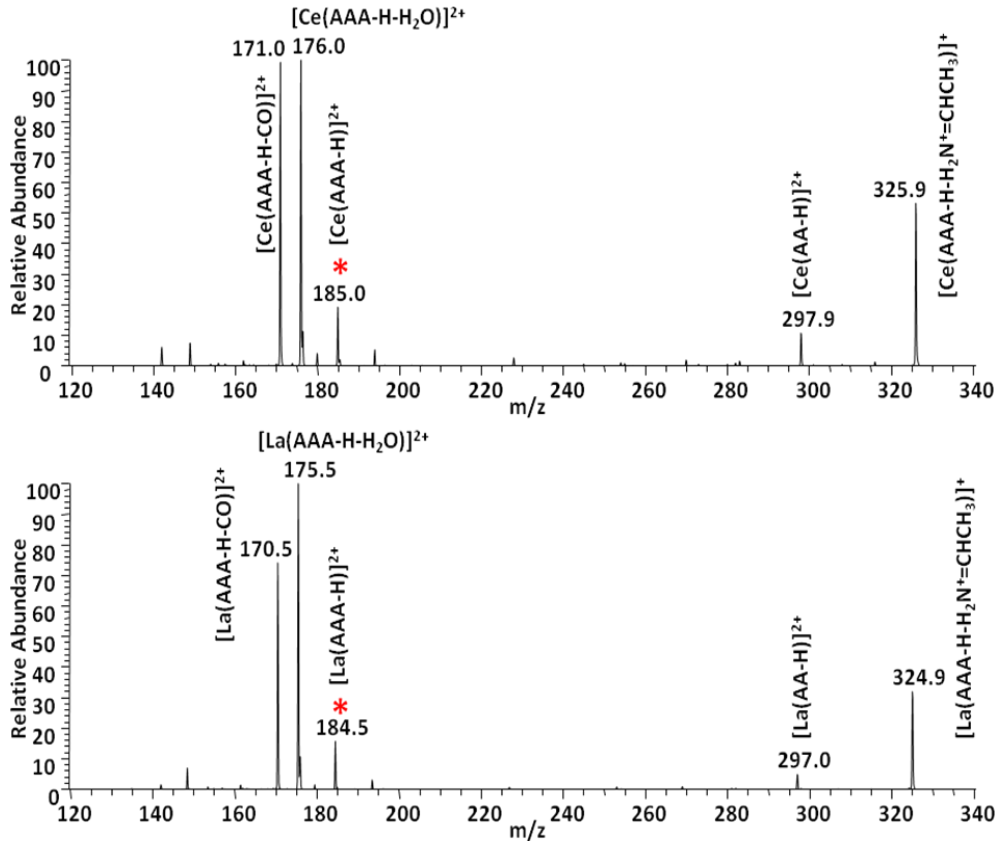

Figure 4.7 CID spectra of (a) $[Ce(III)(AAA\text{-}H)]^{2+}$ (*m/z* 185) CE= 20 and (b) $[La(III)(AAA\text{-}H)]^{2+}$ (*m/z* 184.5) CE=13. The precursor ions are labelled with asterisks (*)

4.2.3 Formation of Peptide Radical Cations and $[b_3+H]^{2+}$

$[b_3+H]^{2+}$ ions are generated when $[Ce(peptide)(CH_3CN)_n]^{3+}$ or $[La(peptide)(CH_3CN)_n]^{3+}$ complexes fragment. $[a_3+H]^{2+}$ can also be formed in CID of $[Ce(peptide)(CH_3CN)_n]^{3+}$ or $[La(peptide)(CH_3CN)_n]^{3+}$ too. These products are not found in the CID of $[Eu(peptide)(CH_3CN)_n]^{3+}$. Details can be found in Chapter 6, where the possible fragmentation mechanisms leading to $[b_3+H]^{2+}$ and $[a_3+H]^{2+}$ under low energy collision-induced dissociation are also investigated.

4.3 Conclusion

Fragmentations of tripositive Ce(III)/peptide and Eu(III)/peptide complexes show very different behaviour which is possibly due to different types of coordination between the metal and the peptide. Abundant CO loss is only observed for Ce(III)/peptide complexes and not from Eu(III)/peptide complexes, and CO_2 loss is the predominant dissociation pathway for Eu/ peptide complexes. Although the aromatic side chain loss can be the major pathway, the major trend for the dissociation of $[Ce(peptide)]^{3+}$ is CO loss, while for $[Eu(peptide)]^{3+}$, it is CO_2 loss. This is also true for dissociations of $[Ce(peptide\text{-}H)]^{2+}$ and $[Eu(peptide\text{-}H)]^{2+}$, where CO loss and CO_2 loss are again the predominant fragmentation pathways. Two other major differences for the tripositive Ce/peptide and Eu/peptide complexes are that peptide radical cations can only be generated by the fragmentation of Eu(III)/peptide; conversely, $[b_3+H]^{2+}$ and $[a_3+H]^{2+}$ ions are only observed when Ce(III)/peptide complexes are fragmented.

This is the first example of formation and fragmentation of lanthanide/peptide complexes under CID where the peptide length is as short as three residues, and there are no basic amino acid residues or methionine. It suggests again that the aromatic side chain of tryptophan can coordinate with lanthanide metal ions and stabilize the $[Ln(peptide)]^{3+}$ in the absence of solvent.

4.4 References

1. Biemann, K. and Martin, S. A. Mass spectrometric determination of the amino acid sequence of peptides and proteins. Mass Spectrom Rev. 1987; *6*(1): 1–75.

2. Yefremova, Y., Al-Majdoub, M., Opuni, K. F. M., Koy, C., Cui, W., Yan, Y., Gross M. L., Glocker, M. O. "De-novo" amino acid sequence elucidation of protein G′e by combined "Top-Down" and "Bottom-Up" mass spectrometry. J Am Soc Mass Spectrom. 2015; 26(3): 482–492.

3. Paizs, B. and Suhai, S. Fragmentation pathways of protonated peptides. Mass Spectrom Rev. 2005; 24(4): 508–548.

4. Lubec, G. and Afjehi-Sadat, L. Limitations and Pitfalls in Protein Identification by Mass Spectrometry. Chem Rev. 2007; 107(8): 3568–3584.

5. Morishetti, K. K., Russell, S. C., Zhao, X., Robinson, D. B. and Ren, J. Tandem mass spectrometry studies of protonated and alkali metalated peptoids: Enhanced sequence coverage by metal cation addition. Int J Mass Spectrom. 2011; 308(1): 98–108.

6. Watson, H. M., Vincent, J. B. and Cassady, C. J. Effects of transition metal ion coordination on the collision-induced dissociation of polyalanines. J Mass Spectrom. 2011; 46(11): 1099–1107.

7. Commodore, J. J. and Cassady, C. J. The Effects of Trivalent Lanthanide Cationization on the Electron Transfer Dissociation of Acidic Fibrinopeptide B and its Analogs. J Am Soc Mass Spectrom. 2016; 27(9): 1499–1509.

8. Mosely, J. A., Murray, B. S. and Parker, D. Electron-Capture Dissociation and Collision-Induced Dissociation of Lanthanide Metal–Ligand Complexes and Lanthanide Metal–Ligand Complexes Bound to Phosphopeptides. Eur J Mass Spectrom. 2009; 15(2): 145–155.

9. Chen, X., Liu, G., Elaine Wong, Y. L., Deng, L., Wang, Z., Li, W. and Dominic Chan, T.-W. Dissociation of trivalent metal ion (Al^{3+}, Ga^{3+}, In^{3+} and Rh^{3+})–peptide complexes under electron capture dissociation conditions. Rapid Commun Mass Spectrom. 2016; 30(6): 705–710.

10. Flick, T. G., Donald, W. A. and Williams, E. R. Electron Capture Dissociation of Trivalent Metal Ion-Peptide Complexes. J Am Soc Mass Spectrom. 2013; 24(2): 193–201.

11. Prell, J. S., Flick, T. G., Oomens, J., Berden, G. and Williams, E. R. Coordination of Trivalent Metal Cations to Peptides: Results from IRMPD Spectroscopy and Theory. J Phys Chem A. 2010; 114(2): 854–860.

12. Verkerk, U. H., Zhao, J., Saminathan, I. S., Lau, J. K.-C., Oomens, J., Hopkinson, A. C., & Siu, K. W. M. Infrared Multiple-Photon Dissociation Spectroscopy of Tripositive Ions: Lanthanum–Tryptophan Complexes. Inorg Chem. 2012; 51(8): 4707–4710.

13. Shvartsburg, A. A. and Jones, R. C. Attachment of metal trications to peptides. J Am Soc Mass Spectrom. 2004; 15(3): 406–408.

14. Shi, T., Siu, K. W. M. and Hopkinson, A. C. Generation of $[La(peptide)]^{3+}$ Complexes in the Gas Phase: Determination of the Number of Binding Sites Provided by Dipeptide, Tripeptide, and Tetrapeptide Ligands. J Phys Chem A. 2007; 111(45): 11562–11571.

15. Kohtani, M., Jarrold, M. F., Wee, S. and O'Hair, R. A. J. Metal Ion Interactions with Polyalanine Peptides. J Phys Chem B. 2004; 108(19): 6093–6097.

16. Prell, J. S., Demireva, M., Oomens, J. and Williams, E. R. Role of Sequence in Salt-Bridge Formation for Alkali Metal Cationized GlyArg and ArgGly Investigated with IRMPD Spectroscopy and Theory. J Am Chem Soc. 2009; 131(3): 1232–1242.

17. Dunbar, R. C., Polfer, N. C., Berden, G. and Oomens, J. (2012). Metal ion binding to peptides: Oxygen or nitrogen sites? Int J Mass Spectrom. 2012; 330–332: 71–77.

18. Dunbar, R. C., Steill, J. D., Polfer, N. C. and Oomens, J. Peptide Length, Steric Effects, and Ion Solvation Govern Zwitterion Stabilization in Barium-Chelated Di- and Tripeptides. J Phys Chem B. 2009; 113(31): 10552–10554.

19. Grese, R. P., Cerny, R. L. and Gross, M. L. Metal ion-peptide interactions in the gas phase: a tandem mass spectrometry study of alkali metal cationized peptides. J Am Chem Soc. 1989; 111(8): 2835–2842.

20. Teesch, L. M. and Adams, J. Fragmentations of gas-phase complexes between alkali metal ions and peptides: metal ion binding to carbonyl oxygens and other neutral functional groups. J Am Chem Soc. 1991; 113(3): 812–820.

21. Morishetti, K. K., Russell, S. C., Zhao, X., Robinson, D. B. and Ren, J. Tandem mass spectrometry studies of protonated and alkali metalated peptoids: Enhanced sequence coverage by metal cation addition. Int J Mass Spectrom. 2011 308(1), 98–108.

22. Bluhm, B. K., Shields, S. J., Bayse, C. A., Hall, M. B. and Russell, D. H. Determination of copper binding sites in peptides containing basic residues: a combined experimental and theoretical study. Int J Mass Spectrom. 2001; 204(1): 31–46.

23. Mallis, L. M. and Russell, D. H. Fast-atom-bombardment-tandem mass spectrometry studies of alkali-metal ions of small peptides. Anal Chem. 1986; 58(6): 1076–1080.

24. Lin, T. and Glish, G. L. C-Terminal Peptide Sequencing via Multistage Mass Spectrometry. Anal Chem. 1998; 70(24): 5162–5165.

25. Lin, T., Payne, A. H. and Glish, G. L. Dissociation pathways of alkali-cationized peptides: Opportunities for C-terminal peptide sequencing. J Am Soc Mass Spectrom. 2001; 12(5): 497–504.

26. Shvartsburg, A. A. Gas-Phase Metal Trications in Protic Solvent Complexes. J Am Chem Soc. 2002; 124(27): 7910–7911.

27. Shvartsburg, A. A. and Siu, K. W. M. Is There a Minimum Size for Aqueous Doubly Charged Metal Cations? J Am Chem Soc. 2001; 123(41): 10071–10075.

28. Li, H., Siu, K. W. M., Guevremont, R. and Blanc, J. C. Y. L. Complexes of silver(I) with peptides and proteins as produced in electrospray mass spectrometry. J Am Soc Mass Spectrom. 1997; 8(8): 781–792.

29. Nemirovskiy, O. and Gross, M. Determination of calcium binding sites in gas-phase small peptides by tandem mass spectrometry. J Am Soc Mass Spectrom. 1998; 9(10): 1020–1028.

30. Glover, M. S., Dilger, J. M., Zhu, F. and Clemmer, D. E. The binding of Ca^{2+}, Co^{2+}, Ni^{2+}, Cu^{2+}, and Zn^{2+} cations to angiotensin I determined by mass spectrometry based techniques. Int J Mass Spectrom. 2013; 354–355: 318–325.

31. Kohtani, M., Kinnear, B. S. and Jarrold, M. F. Metal-Ion Enhanced Helicity in the Gas Phase. J Am Chem Soc. 2000; 122(49): 12377–12378.

32. Shi, T., Siu, K. W. M. and Hopkinson, A. C. Generation of $[La(peptide)]^{3+}$ Complexes in the Gas Phase: Determination of the Number of Binding Sites Provided by Dipeptide, Tripeptide, and Tetrapeptide Ligands. J Phys Chem A. 2007; 111(45): 11562–11571.

33. Commodore, J. J. and Cassady, C. J. The Effects of Trivalent Lanthanide Cationization on the Electron Transfer Dissociation of Acidic Fibrinopeptide B and its Analogs. J Am Soc Mass Spectrom. 2016; 27(9): 1499–1509.

34. Hu, P., Sorensen, C. and Gross, M. L. Influences of peptide side chains on the metal ion binding site in metal ion-cationized peptides: Participation of aromatic rings in metal chelation. J Am Soc Mass Spectrom. 1995; 6(11): 1079–1085.

CHAPTER 5

Aliphatic Peptide Radical Cat

ions and $[a_3+H]^{\bullet+}$ Ions

5.1 Introduction

The most easily formed peptide radical cations have aromatic side chains on an amino acid residue [1-7]. The higher ionization energies of aliphatic amino acids compared to those of aromatic amino acids makes generation of radical cations more of a challenge in the gas phase. Under collision-induced dissociation in electrospray mass spectrometry, fragmentations of metal/peptide complexes $[Cu(II)(peptide)(amine)]^{2+}$ give molecular radical cations of peptides, hydrogen deficient radicals. Formation of protonated peptides and peptide cleavage compete with the generation of peptide radical cations by this method. The auxiliary ligand and metal both affect this process. For aliphatic peptides, there were no molecular radical cations observed by CID of copper/peptide ternary complexes, unless the auxiliary ligand was 12-crown-4 [13] or another sterically encumbered ligand, for example 1,4,7-triazacyclononane (9-aneN_3); the fragmentation of $[Cu(II)(12\text{-crown-}4)(GGX)]^{2+}$ under CID conditions using ESI mass spectrometry produced the molecular radical cations of peptide $[GGX]^{\bullet+}$, where X=G, A, P, I, L and V, although in lower abundance compared to those containing X=W and Y. $[a_3+H]^{\bullet+}$ ions were observed as more abundant products than $[GGX]^{\bullet+}$ for aliphatic peptides when dissociating $[Cu(II)(12\text{-crown-}4)(GGX)]^{2+}$; but an $[a_3+H]^{2+}$ ion was not observed in the CID spectrum of $[Cu(II)(12\text{-crown-}4)(GGW)]^{2+}$. When the auxiliary ligand was terpy, there was no $[GGX]^{\bullet+}$ or $[a_3+H]^{\bullet+}$ present in the CID spectrum of $[Cu(II)(terpy)(GGP)]^{2+}$.

Fragmentations of molecular radical cation of peptides give richer information on peptide sequence compared to that provided by protonated peptides [2,14,15], so this encouraged further in-depth investigation of molecular peptide radical cations in recent years [7,12, 16-35].

Earlier research showed peptides containing lysine, arginine, histidine, tyrosine or tryptophan easily form peptide radical cations under CID condition by fragmentation of the copper-peptide-auxiliary complexes [2,9-13, 21, 26, 30,-34], and methionine-containing small peptides were also reported to give radical cations [12, 22]. Fragmentation of protonated peptides is charge-driven, largely giving b- and y-type ions [36], while fragmentation of peptide radical cations can be charge- or radical-driven, giving richer fragmentation information compared to that of protonated peptides [30, 34]. Dissociations at the N-C_α bond of tryptophan and tyrosine residues and formation of $[z_n\text{-H}]^{\bullet+}$ ions, by proton transfer from C_β of W or Y residue to the amide group carbonyl oxygen before the N-C_α bond cleavage, is the major fragment observed for W- or Y-containing peptides (See Figure 5.1). Either N-terminal fragment elimination as ammonia or amide happens, depending on the position of W on the peptide. For C-terminal tryptophan-containing peptide, cleavage of the C_α-C bond and proton transfer from the carboxylic group to an amide oxygen can lead to the elimination of CO_2 and formation of $[a_3\text{+H}]^{\bullet+}$.

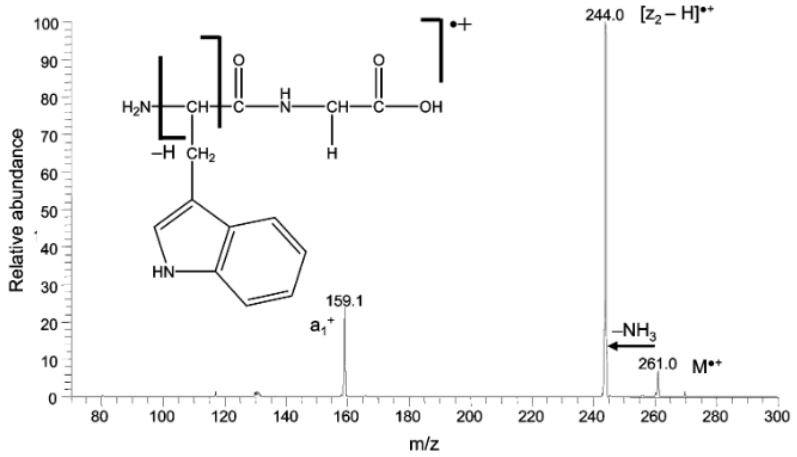

Figure 5.1 (a) CID spectrum of the $M^{\bullet+}$ ions of WG. Relative energy =10% of 5 eV. Experiment was performed on a ThermoFinnigan LCQ ion trap mass spectrometer. Adopted from [34].

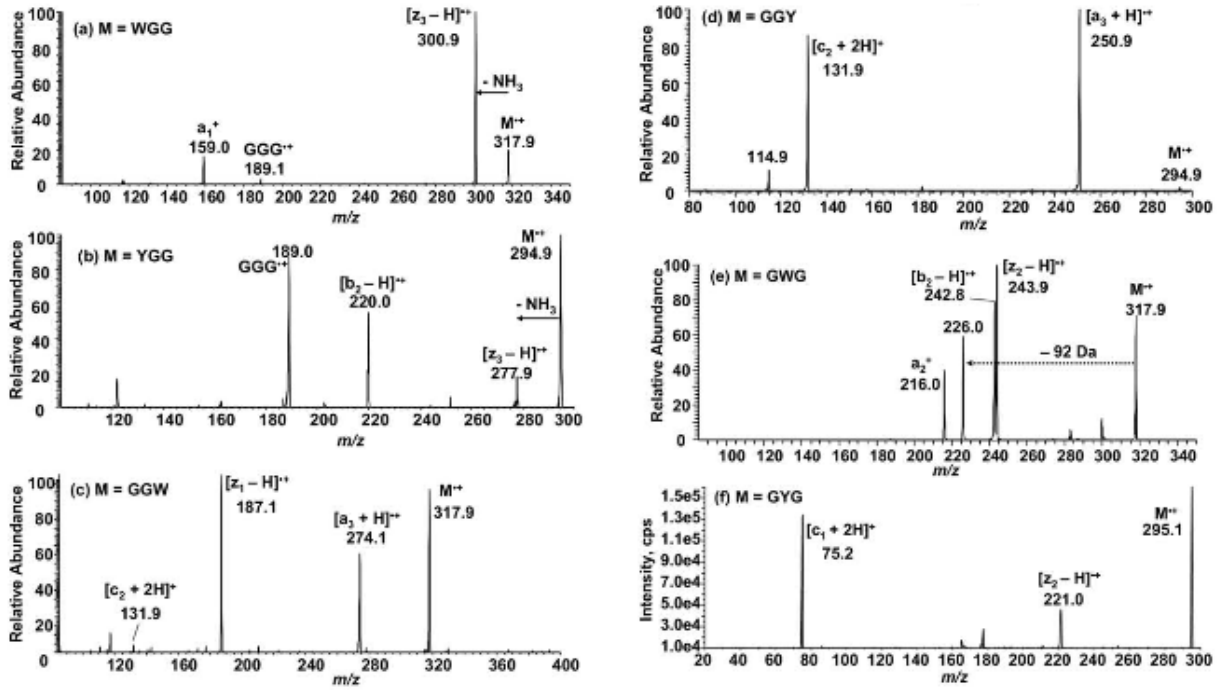

Figure 5.1 (b). CID spectra of (a) $[WGG]^{\bullet+}$ at a relative collision energy =8%, (b) $[YGG]^{\bullet+}$ at 10%, (c) $[GGW]^{\bullet+}$ at 8%, (d) $[GGY]^{\bullet+}$ at 10%, (e) $[GWG]^{\bullet+}$ at 10%, and (f) $[GYG]^{\bullet+}$ at a laboratory collision energy of 10eV. Adopted from [30]

A C_α-centered peptide radical has a captodative structure [37] which is stabilized by the electron-withdrawing carbonyl oxygen and electron-donating nitrogen, and it can be generated and isolated after side chain loss e.g. *p*-quinomethide or 3-methylene-3*H*-indole from Y or W [7,9,34]. In the gas phase, peptide radical cations with well-defined initial C_α-centered radical locations were produced for examining the mobility of the radical center [16]. CID of copper(II)-peptide ternary complexes where peptide = YGG, GYG or GGY, gave triglycine radical cations with different initial radical locations. Dissociation into different products and theoretical calculations (DFT) on $[G^{\bullet}GG]^+$, $[GG^{\bullet}G]^+$, $[GGG^{\bullet}]^+$ established that these three ions have distinct structures that dissociate more readily than interconvert.

Many molecular peptide radical cations are distonic ions, with the charge and radical centers not located in the same place. Frequently the location of the radical will migrate via abstraction of a hydrogen atom before low-energy dissociation occurs [35]. The radical migration, depends on kinetics and thermodynamics. The kinetics is related to the intrinsic barrier to radical migration and is dictated by the structural constraints that favour alignment of radical donor and acceptors. Meanwhile, the thermodynamics is related to the relative stabilities of the two radical species. The stabilities of the radicals can be estimated based on the bond dissociation energy (BDE) [35, 38]. Peptide radical-directed dissociation has backbone dissociation and side-chain loss [35]. The backbone dissociation leads to mainly a/x type fragments or sometimes c/z type fragments initiated by the β position on the side chain. The side chain loss has two generic dissociation mechanisms [15, 35] as shown in Scheme 5.1, a) C_α-initiated partial loss of side chain; b) C_γ-initiated whole side chain loss.

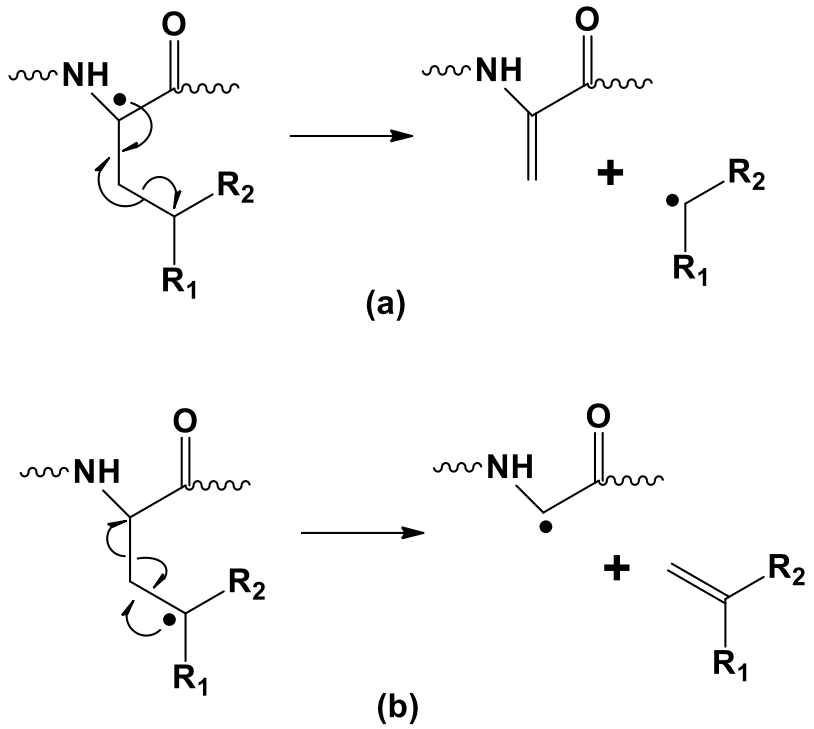

Scheme 5.1 Adopted from references 15 and 25

In contrast to the study on the fragmentation of aromatic residue-containing peptide radical cations, information on the dissociation of aliphatic peptide radical cations is rather scarce.

Proline is known to accumulate in plant tissue during abiotic stresses; it also scavenges free radicals produced under abiotic stress [39-40]. Histidine and proline are important sites of protein attack by radicals, which may cause protein cleavage [41]. Proline residue is well known for its “proline effect” on directing the fragmentation to its N-terminal peptide bond and has been widely investigated with mass spectrometry [42-46]. However, there is no research on the fragmentation of aliphatic proline-containing peptide radical cations under CID-ESI-MS. Here, based on the results in Chapter 3, we report more details of the generation of proline-containing aliphatic peptide radical cations by dissociation of Europium(III)-peptide-acetonitrile complexes. This is the first example of producing hydrogen deficient peptide radical cations by dissociation

of the metal (III)-peptide complexes with a 3+ charge state. The aliphatic peptide radical cations were generated either by CID of the copper ternary system or Europium/peptide complexes. Abundant $[a_3+H]^{\bullet+}$ ions were observed in the CID spectra of Eu/peptide complexes, so $[a_3+H]^{\bullet+}$ ions were also isolated and fragmented under CID to study the mechanism by which they fragment.

5.2 Results and Discussion

5.2.1 Formation of N-terminal proline containing aliphatic peptide radical cations

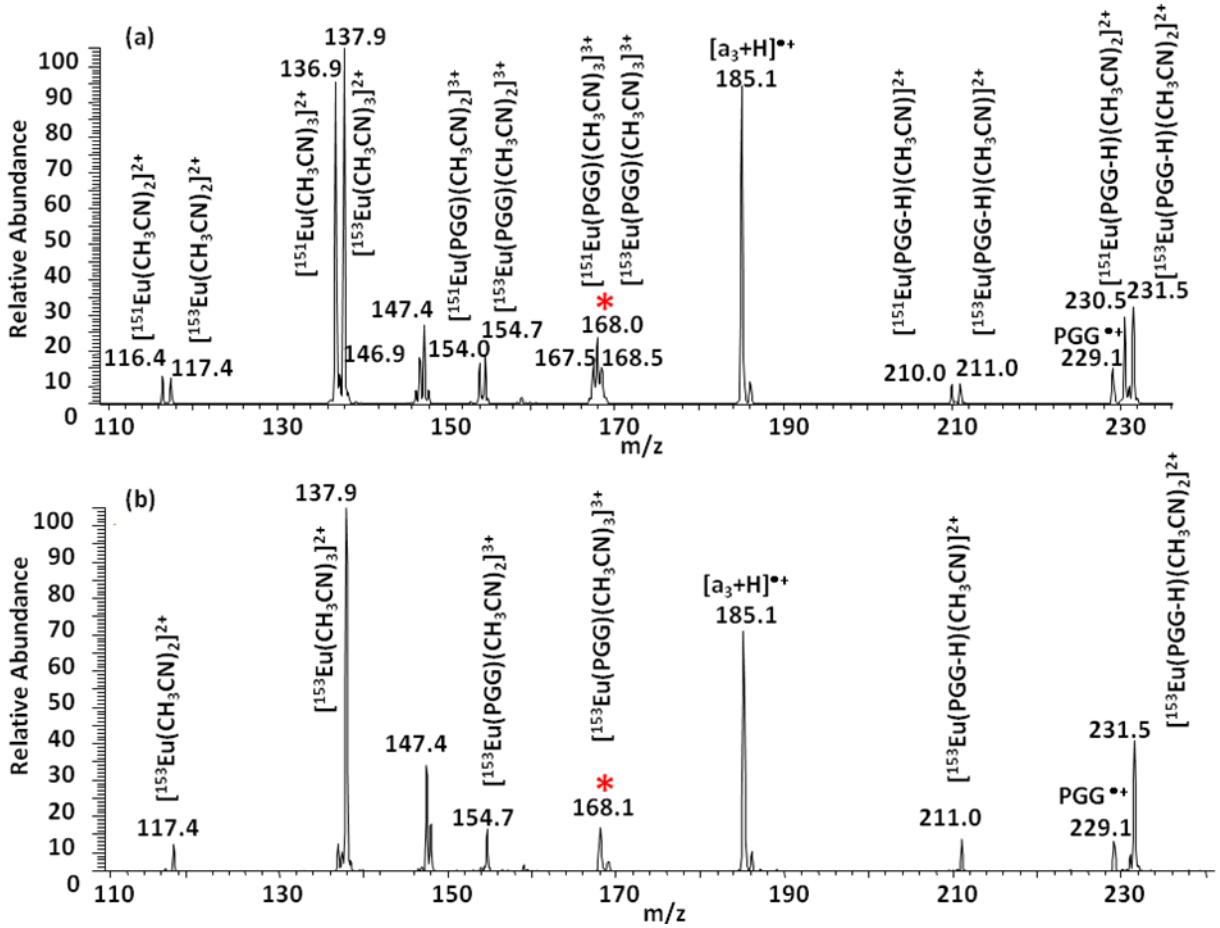

Figure 5.2 (top) CID spectra of $[Eu(PGG)(CH_3CN)_3]^{3+}$ (m/z 168.0) CE=11.0 and (bottom) $[^{153}Eu(PGG)(CH_3CN)_3]^{3+}$ (*m/z* 168.3) CE=15.0. The precursor ions are labelled with asterisks (*).

Figure 5.2(a) shows the CID spectra of $[Eu(PGG)(CH_3CN)_3]^{3+}$, where *m/z* =168.0. Since naturally occurring europium has two isotopes of 47.8% ^{151}Eu and 52.2% ^{153}Eu, the mass to charge ratios of $[^{151}Eu(PGG)(CH_3CN)_3]^{3+}$ and $[^{153}Eu(PGG)(CH_3CN)_3]^{3+}$ are 167.7 and 168.3 respectively. When selecting the precursor at 168.0, with isolation window = 1, the complex $[Eu(PGG)(CH_3CN)_3]^{3+}$ formed from both isotopes were selected. CID of $[Eu(PGG)(CH_3CN)_3]^{3+}$ at m/z 168.0 shows dual peaks when the product contains Eu, and the differences between the dual peaks are 0.667, 1 and 2 for tripositive ions, dipositive ions and monopositive ions, respectively. For example, the product ions 154.0 and 154.7 are the tripositive ions $[Eu(PGG)(CH_3CN)_2]^{3+}$ formed by peeling off one acetonitrile molecule from the precursor, and the product ions 136.9 and 137.9, differing by 1.0 Th, are the dipositive ions $[Eu(CH_3CN)_3]^{2+}$. When there is no Eu in the fragments, single peaks are observed, like $[PGG]^{\bullet+}$ (*m/z* 229.0) and $[a_3+H]^{\bullet+}$ (*m/z*185.1). To confirm the component of the fragments, precursor $[Eu(PGG)(CH_3CN)_3]^{3+}$ at *m/z* 168.3 was fragmented, and CID spectrum is shown in Figure 5.2(b). Since the ion at *m/z* 168.8, the $[^{153}Eu(PGG)(CH_3CN)_3]^{3+}$ ion, is mainly selected instead of a mixture of $[^{153}Eu(PGG)(CH_3CN)_3]^{3+}$ and $[^{153}Eu(PGG)(CH_3CN)_3]^{3+}$ at *m/z* 168.0, the dual peaks we observed in Figure 5.1(a) are now only shown as single peaks at 117.4, 137.9, 154.7, 231.5.

CID of $[Eu(PGG)(CH_3CN)_3]^{3+}$ shows the following major fragments category: 1) radical cations $[PGG]^{\bullet+}$ and $[a_3+H]^{\bullet+}$; 2) $[Eu(CH_3CN)_n]^{2+}$, the counterpart of peptide radical cations after dissociation; 3) complexes $[Eu(PGG\text{-}H)(CH_3CN)_n]^{3+}$ (n=1 and 2); 4) $Eu(PGG)(CH_3CN)_2]^{3+}$ by peeling off one CH_3CN solvent molecule. The dissociation pathways can be summarized in the following equations:

(1) $[Eu(III)(PGG)(CH_3CN)_3]^{3+} \longrightarrow [Eu(II)(CH_3CN)_3]^{2+} + CO_2 + [a_3+H]^{\bullet+}$

(2) $[Eu(III)(PGG)(CH_3CN)_3]^{3+} \longrightarrow [Eu(II)(CH_3CN)_3]^{2+} + [PGG]^{\bullet+}$

(3) $[Eu(III)(PGG)(CH_3CN)_3]^{3+} \longrightarrow [Eu(III)(PGG\text{-}H)(CH_3CN)_2]^{2+} + [CH_3CN+H]^{+}$

(4) $[Eu(III)(PGG)(CH_3CN)_3]^{3+} \longrightarrow [Eu(III)(PGG)(CH_3CN)_2]^{3+} + CH_3CN$

Since the abundances of $[Eu(CH_3CN)_3]^{2+}$, $[a_3+H]^{\bullet+}$ and $[PGG]^{\bullet+}$ are 100%, 91% and 11%, respectively, we can say that the electron transfer between Eu^{3+} and PGG is the predominant dissociation pathway, and the formation of molecular radical cations $[PGG]^{\bullet+}$ is only a minor fragmentation channel. A moderate abundance (28%) of $[Eu(PGG\text{-}H)]^{2+}$ is formed by proton transfer from the peptide to CH_3CN.

5.2.2 Fragmentation of aliphatic [tripeptide]$^{\bullet+}$ ions

Molecular radical cations $[tripeptide]^{\bullet+}$ and $[a_3+H]^{\bullet+}$ ions from various aliphatic tripeptides with a proline residue in different positions have been formed (by the same method, unless stated to be otherwise), isolated and fragmented. The results are discussed in the following sections. The peptides do not contain basic residues or aromatic residues that conventionally facilitate the generation of peptide molecular radical cations and the peptide radical cations are generated directly from the dissociation of metal/peptide/auxiliary ligand complexes.

a) N-terminal proline-containing tripeptides

Figure 5.3 shows the CID spectra of the $[peptide]^{\bullet+}$ for PGG, PAG and PAA, and for comparison, Figure 5.4 shows the CID spectra of $[peptide+H]^{+}$. Protonated peptides predominantly give the $[b_2]^{+}$ ions. Moderate abundance of $[a_1]^{+}$ ions is observed for PGG, and $[a_2]^{+}$ ions observed for PAG and PAA. The major products in the CID of $[peptide]^{\bullet+}$ for PGG, PAG and PAA are radical cations $[b_n\text{-}H]^{\bullet+}$, where n=2, 3; $[a_2+H]^{\bullet+}$ ions are present too, although in very low abundance in

the CID spectrum of $[PAG]^{\bullet+}$. Protonated peptide cleavage is also observed, indicated by the presence of $[a_n]^+$ and $[b_2]^+$ ions.

While the $[a_3+H]^{\bullet+}$ ions is the major product in the CID spectra of $[Eu(PGG)(CH_3CN)_3]^{3+}$ (Figure 5.1), these ions are not observed in any of the CID spectra of $[PGG]^{\bullet+}$, $[PAG]^{\bullet+}$ or $[PAA]^{\bullet+}$ in Figure 5.3.

By comparison, in the fragmentation of $[GGW]^{\bullet+}$ ions [13,34] derived from $[Cu(terpy)(GGW)]^{2+}$, $[Cu(12\text{-crown-}4)(GGW)]^{2+}$ or $[Cu(dien)(GGW)]^{2+}$, the $[a_3+H]^{\bullet+}$ ion is a major product.

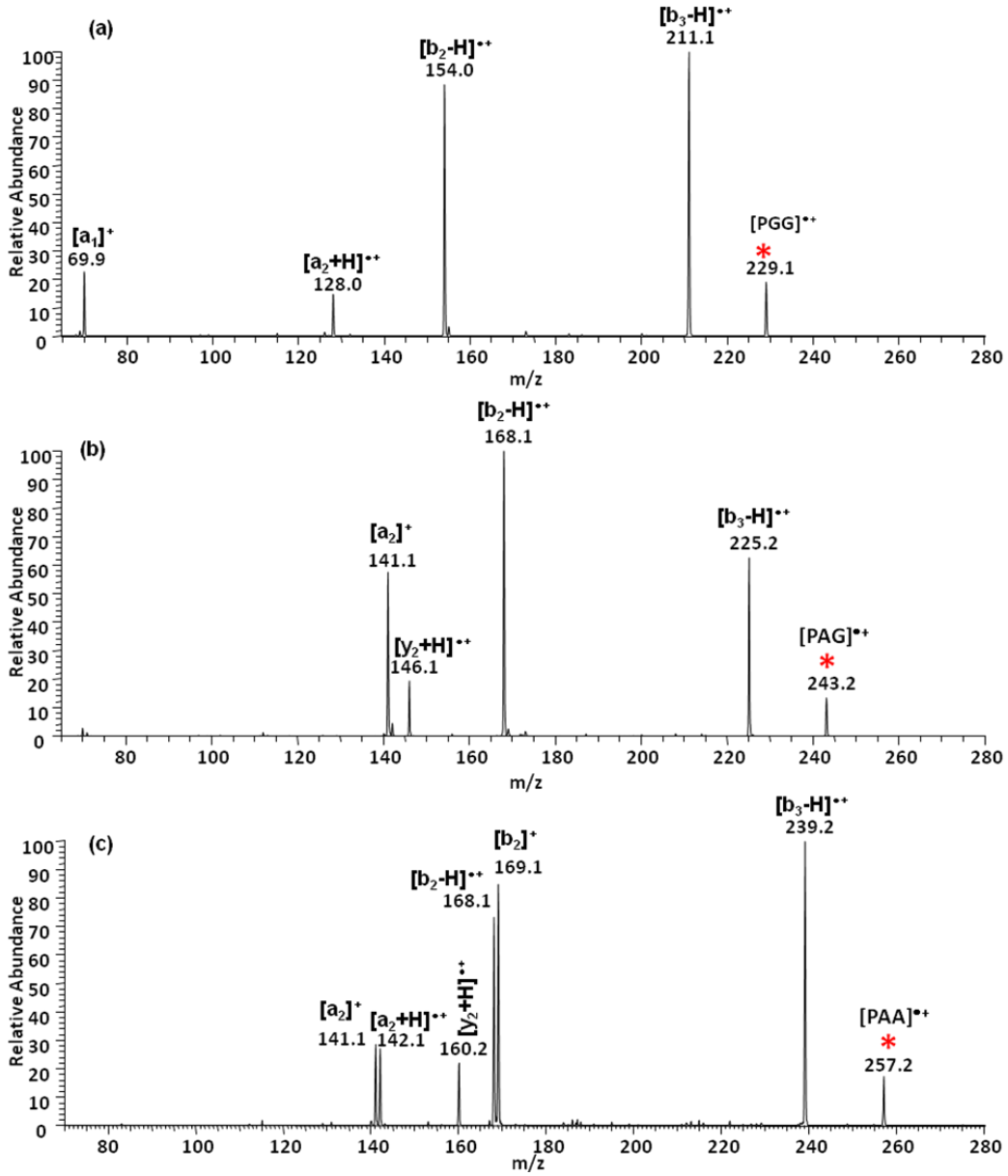

Figure 5.3 (a) CID spectrum of $[PGG]^{\bullet+}$ (*m/z* 229.1), CE=21, obtained from $[Eu^{153}(PGG)(CH_3CN)_3]^{3+}$; (b) CID spectrum of $[PAG]^{\bullet+}$ (*m/z* 243.2), CE=19, obtained from $[Eu^{153}(PAG)(CH_3CN)_3]^{3+}$; (c) CID spectrum of $[PAA]^{\bullet+}$ (*m/z* 257.1), CE=20, obtained from $[Eu^{153}(PAA)(CH_3CN)_3]^{3+}$. The precursor ions are labelled with an asterisk (*)

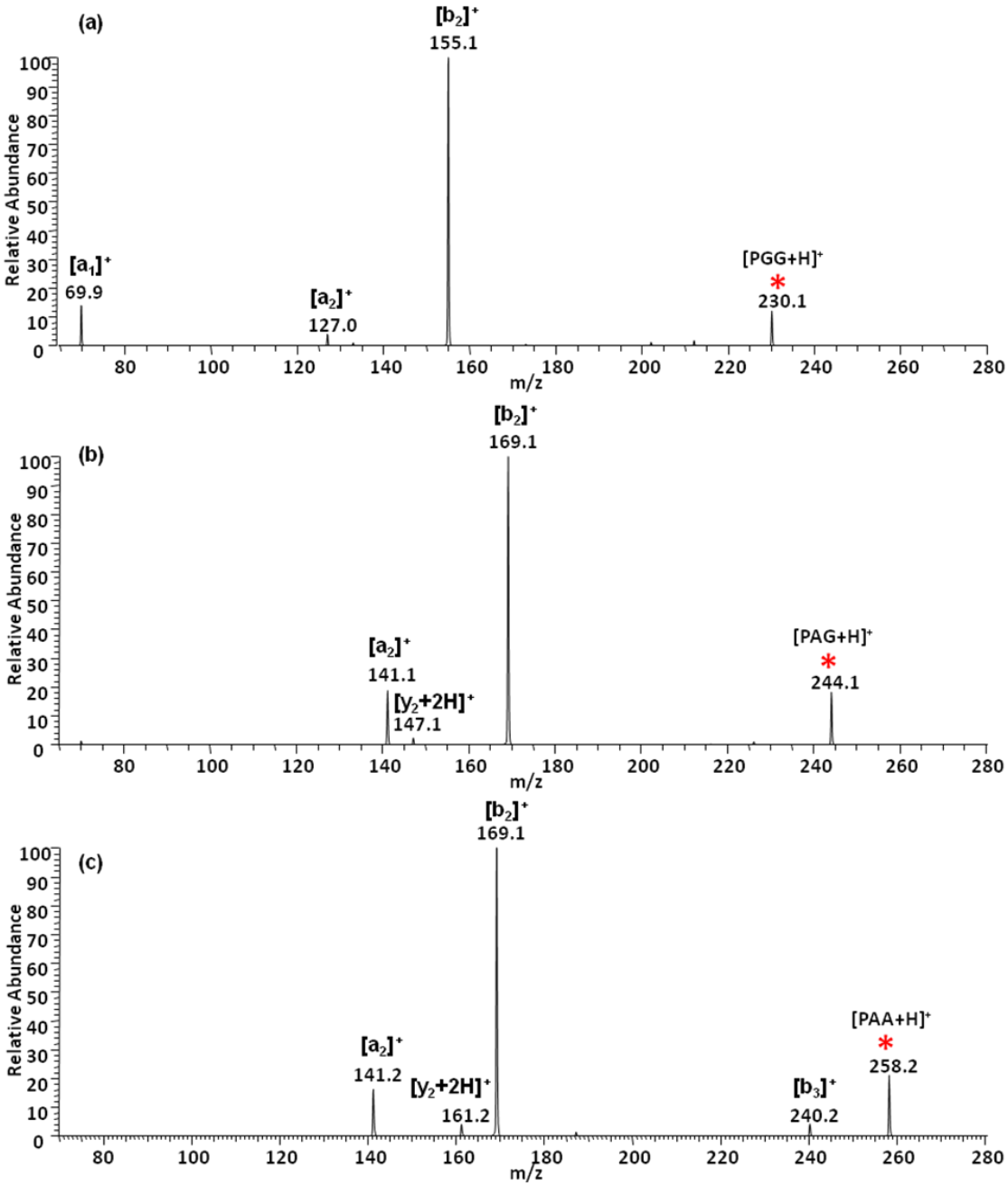

Figure 5.4 (a) CID spectrum of $[PGG+H]^+$ (*m/z* 230.1) CE=22; (b) CID spectrum of $[PAG+H]^+$ (*m/z* 244.1) CE=21; (c) CID spectrum of $[PAA+H]^+$ (*m/z* 258.0) CE=20. The precursor ions are labelled with asterisks (*)

b) Tripeptides with proline in the central position

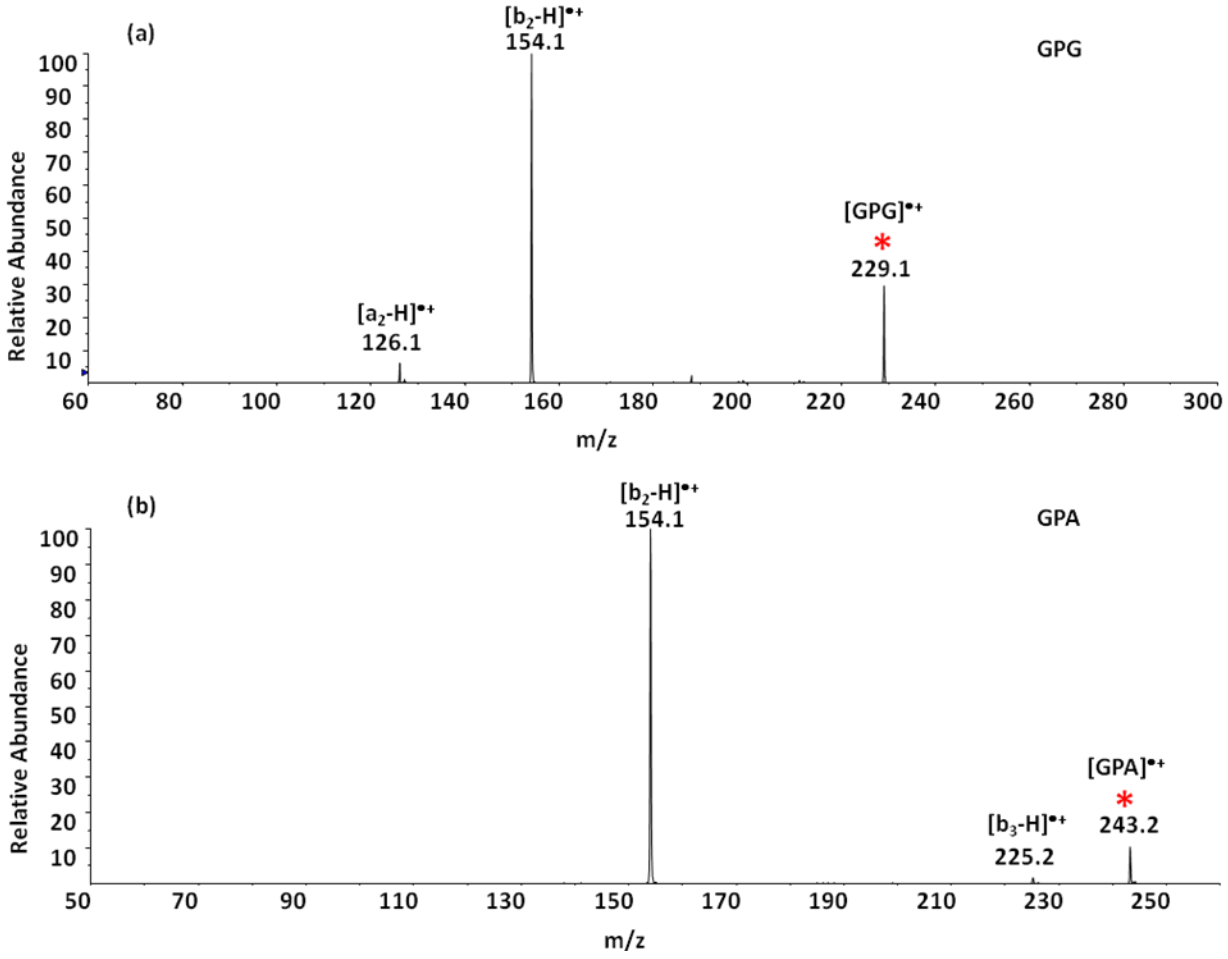

Figure 5.5 (a) CID spectrum of $[GPG]^{\bullet+}$ (*m/z* 228.9), AF_2=70, obtained from $[Cu(GPG)(18\text{-}Crown\text{-}6)]^{2+}$; (b) CID spectrum of $[GPA]^{\bullet+}$ (*m/z* 243.1), AF_2=55, obtained from $[Cu(GPA)(18\text{-}Crown\text{-}6)]^{2+}$, with AB Sciex QTrap 2000. The precursor ions are labelled with an asterisk (*).

$[GPG]^{\bullet+}$ and $[GPA]^{\bullet+}$ were produced from the dissociation of $[Cu(peptide)(18\text{-}Crown\text{-}6)]^{2+}$ in the AB Sciex QTrap 2000. CID spectra of $[GPG]^{\bullet+}$ and $[GPA]^{\bullet+}$ (Figure 5.5) are simple, with the $[b_2\text{-}H]^{\bullet+}$ ions the predominant products. In contrast in the fragmentations of $[PGG]^{\bullet+}$, $[PAG]^{\bullet+}$ and $[PAA]^{\bullet+}$, $[b_3\text{-}H]^{\bullet+}$ and $[b_2\text{-}H]^{\bullet+}$ ions are the major products, and the CID spectra have additional products.

c) Tripeptides with proline at the C-terminus

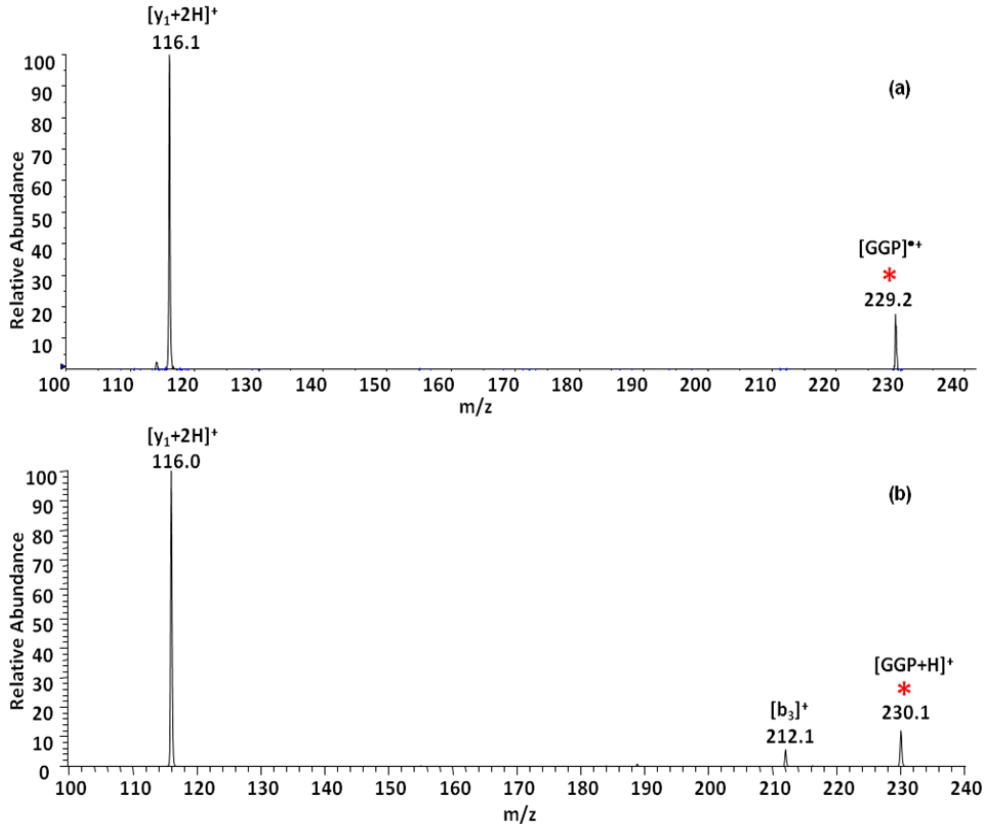

Figure 5.6 (a) CID spectrum of $[GGP]^{\bullet+}$ (*m/z* 228.8), AF_2=85, obtained from $[Cu(GGP)(18\text{-}Crown\text{-}6)]^{2+}$; with AB Sciex QTrap 2000. (b) CID spectrum of $[GGP+H]^+$ (*m/z* 230.0), CE=18, obtained with Thermo LTQ Obitrap Elite mass spectrometer. The precursor ions are labelled with asterisks (*)

Figure 5.6 shows the CID spectra of $[GGP]^{\bullet+}$ and protonated GGP. Unlike in the dissociations of the $[peptide]^{\bullet+}$ containing an N-terminal proline or a proline residue in the second position, the CID spectrum of $[GGP]^{\bullet+}$ is very simple and similar to that of protonated GGP. The proline effect causes cleavage of the peptide bond to the N-terminus of proline, and formation of the closed-shell ion $[y_1+2H]^+$ is dominant, negating the impact of the radical on the fragmentation.

d) Tripeptides GGG and GAG

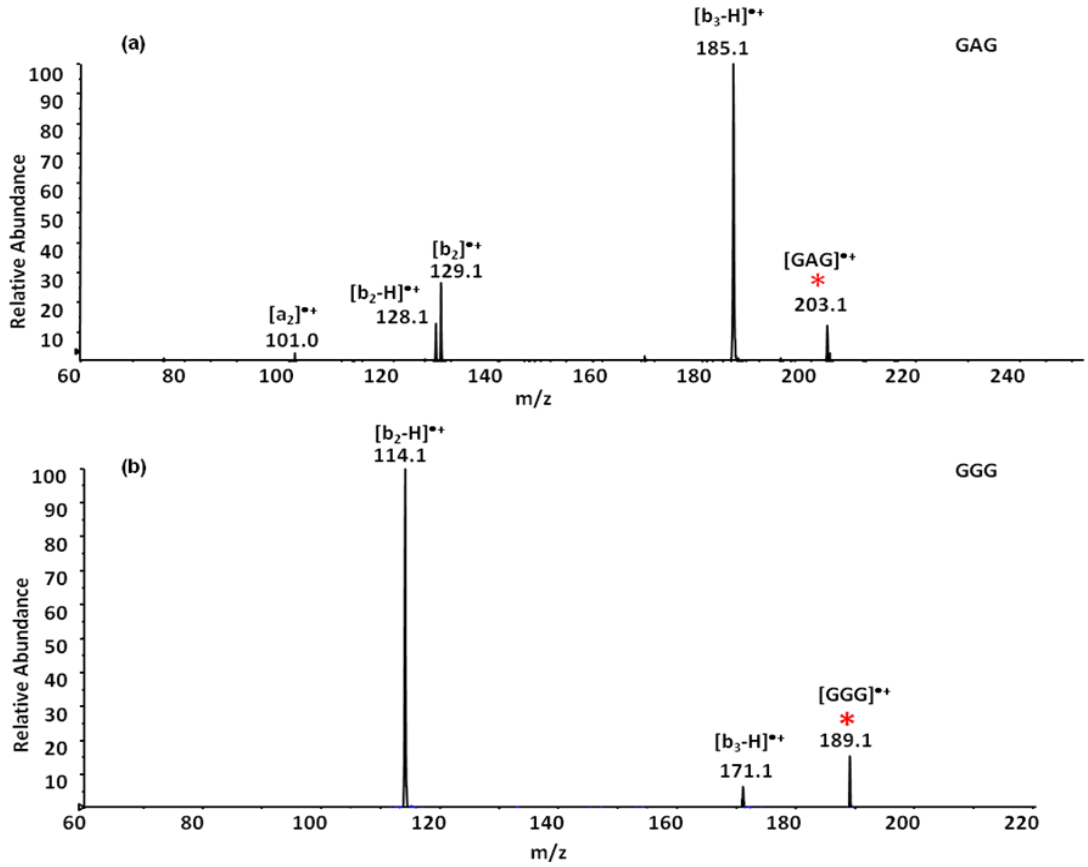

Figure 5.7 (a) CID spectrum of $[GAG]^{\bullet+}$ (*m/z* 202.9), AF_2=85, obtained from $[Eu(GAG)(CD_3CN)_3]^{3+}$; (b) CID spectrum of $[GGG]^{\bullet+}$ (*m/z* 189.0), AF_2=45, obtained from $[Cu(GGG)(18\text{-crown-}6]^{2+}$; obtained with AB Sciex QTrap 2000. The precursor ions are labelled with an asterisk (*)

Figure 5.7 shows the fragmentation of $[GAG]^{\bullet+}$ and $[GGG]^{\bullet+}$, which are formed in the CID of $[Eu(GAG)(CD_3CN)_3]^{3+}$ and $[Cu(GGG)(18\text{-crown-}6]^{2+}$ respectively. $[b_3\text{-H}]^{\bullet+}$ and $[b_2\text{-H}]^{\bullet+}$ are observed in both CID spectra above, although $[b_3\text{-H}]^{\bullet+}$ is the major product in the CID of $[GAG]^{\bullet+}$, while $[b_2\text{-H}]^{\bullet+}$ is the major product in the CID of $[GGG]^{\bullet+}$. This CID spectrum is different from the CID spectra of $[G^{\bullet}GG]^{+}$, $[GG^{\bullet}G]^{+}$ and $[GGG^{\bullet}]^{+}$, which were generated by loss of the side chain from $[YGG]^{+}$, $[GYG]^{+}$ and $[GGY]^{+}$ respectively [16]. The spectra of

$[GGG]^{\bullet+}$generated from metal/peptide complexes here indicates the structure of $[GGG]^{\bullet+}$ is either a mixture of $[G^{\bullet}GG]^{+}$ and $[GG^{\bullet}G]^{+}$, or is only the higher energy $[GG^{\bullet}G]^{+}$ ion [16].

Figure 5.8 shows the CID spectra of $[GPG]^{\bullet+}$ions formed from Cu/peptide ternary complexes and Eu/peptide complexes. The difference between the CID spectra of $[GPG]^{\bullet+}$ions indicates the $[GPG]^{\bullet+}$ ions formed are probably different isomers due to different structures (keto, enol or iminol) peptide may take in the Cu/peptide ternary complexes and Eu/peptide complex. Further study including more experiment with various peptides and theoretical calculation method will be used to confirm this interesting result.

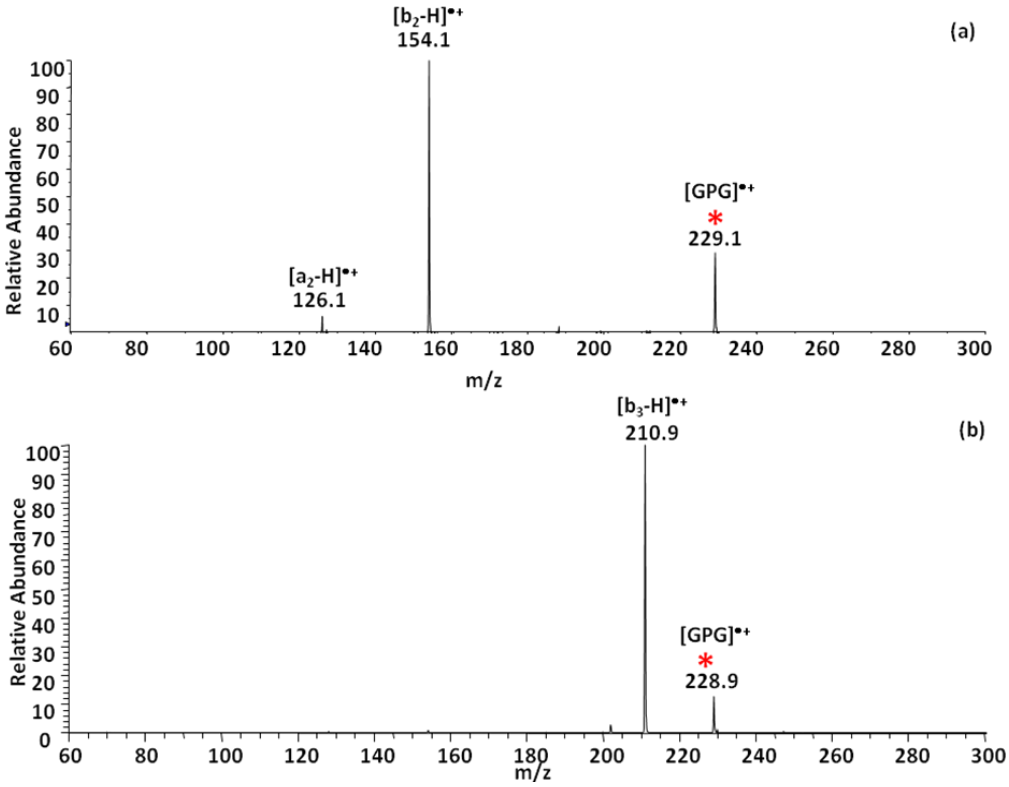

Figure 5.8 (a) CID spectrum of $[GPG]^{\bullet+}$ (*m/z* 228.9) obtained from $[Cu(GPG)(18\text{-Crown-}6)]^{2+}$, with AB Sciex QTrap 2000; (b) CID spectrum $[GPG]^{\bullet+}$ (*m/z* 2291) obtained from $[Eu(GPG)(CH_3CN)_3]^{3+}$, with Thermo Fisher LTQ-Orbitrap Eleite mass spectrometer. The precursor ions are labelled with an asterisk (*)

Table 5.1 Product ions and relative abundance (%) in the fragmentations of aliphatic peptide radical cations

[Peptide]$^{\bullet+}$	**PGG**	**PAG**	**PAA**	**GPG**		**GPA**	**GGP**	**GAG**	**GGG**
Metal ion	**Eu(III)**	**Eu(III)**	**Eu(III)**	**Eu(III)**	**Cu(II)**	**Cu(II)**	**Cu(II)**	**Eu(III)**	**Cu(II)**
$[b_3\text{-H}]^{\bullet+}$	100	58	100	100		2		100	6
$[b_2\text{-H}]^{\bullet+}$	88	100	78		100	100		13	100
$[a_2\text{-H}]^{\bullet+}$	18		30		10				
$[y_2\text{+H}]^{\bullet+}$		18	24						
$[a_2\text{+H}]^{\bullet+}$									
$[y_1\text{+2H}]^{+}$							100		
$[b_2]^{+}$			86					26	
$[a_2]^{+}$		55	38					3	
$[a_1]^{+}$	34	3							

Table 5.1 summarizes the product ions of the fragmentation of $[peptide]^{\bullet+}$, and we can see that $[b_2\text{-}H]^{\bullet+}$ ions are abundant products in almost all CID spectra, except $[GGP]^{\bullet+}$, where the proline effect plays the main role in backbone dissociation. This is consistent with the fragmentation pattern of $[GGI]^{\bullet+}$ obtained from $[Cu(GGI)(12\text{-}Crown\text{-}4)]^{2+}$[13], where the major product is $[b_2\text{-}H]^{\bullet+}$.

$[b_3\text{-}H]^{\bullet+}$ ions are major products in the CID spectra of N-terminal proline-containing $[peptide]^{\bullet+}$, and $[GAG]^{\bullet+}$ ions. The radical cations $[peptide]^{\bullet+}$ are all formed in the dissociation of Europium(III)/peptide complexes. Further study on the dissociation mechanism of copper(II)/peptide ternary system and Europium/peptide complexes are seemingly necessary.

The representative structures of $[b_3\text{-}H]^{\bullet+}$, $[b_2\text{-}H]^{\bullet+}$ and of $[a_2+H]^{\bullet+}$ ions from the dissociation of aliphatic $[peptide]^{\bullet+}$ can be seen in the Scheme 5.2, exemplified by PGG.

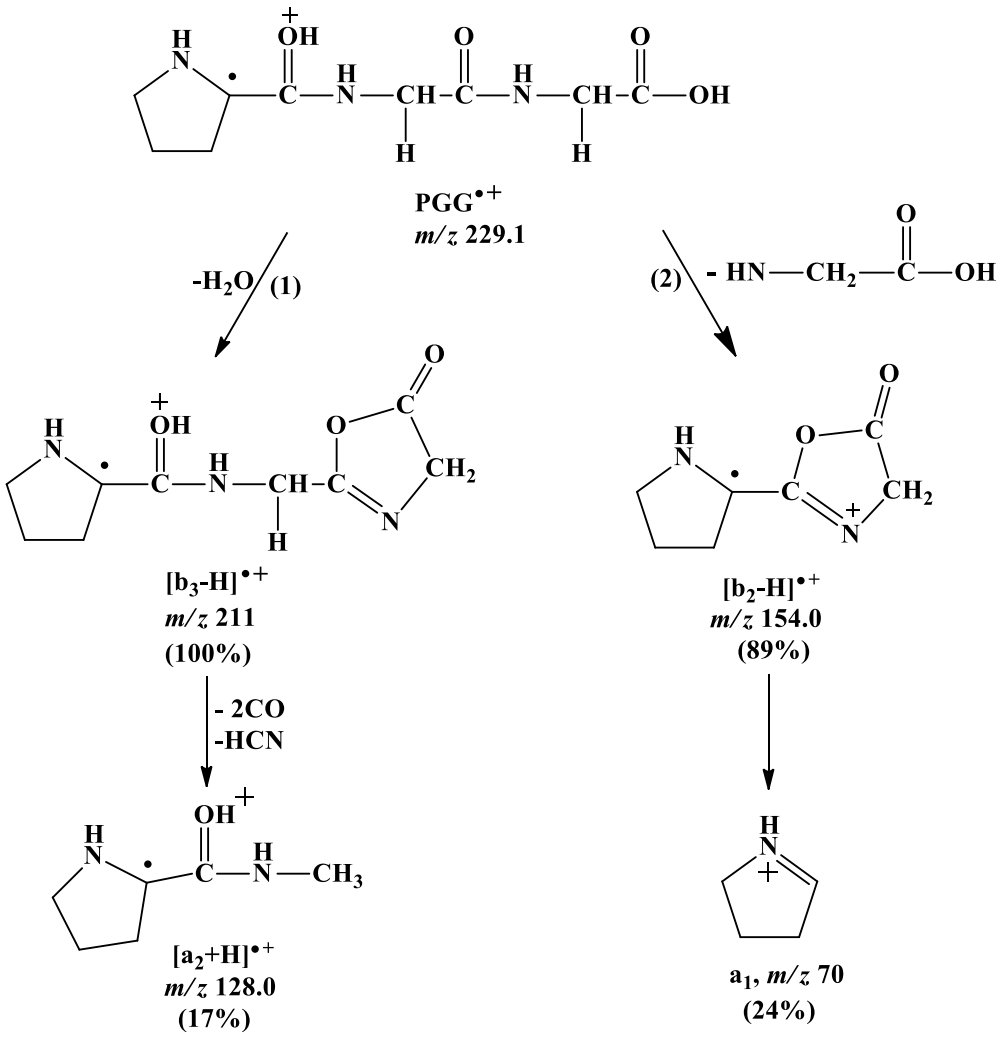

Scheme 5.2 Possible structure of the products of CID of $[PGG]^{\bullet+}$

5.2.3 Fragmentations of $[a_3+H]^{\bullet+}$ ions

As mentioned earlier in this Chapter, $[a_3+H]^{\bullet+}$ ions were not generated in the dissociation of aliphatic $[peptide]^{\bullet+}$ ions. Instead, abundant $[a_3+H]^{\bullet+}$ ions were generated directly when dissociating the $[Eu(Peptide)(CH_3CN)_3]^{3+}$ complexes. In this section, fragmentations of $[a_3+H]^{\bullet+}$ ions are investigated.

a) N-terminal proline-containing tripeptides

Figure 5.9 shows the CID spectra of $[a_3+H]^{\bullet+}$ ions of PGG, PAG, PAA derived from the dissociation of $[Eu(peptide)(CH_3CN)_3]^{3+}$ complexes. Abundant $[b_2-H]^{\bullet+}$ ions exist in each CID spectrum. They are formed by breaking the second peptide bond (see Scheme 5.3). A radical fragment, the product of cleaving the first amide bond and losing CO and 3,4-dihydo-2-*H*-pyrrole, exists in each spectrum in an order of increasing abundance for PGG, PAG, PAA at *m/z* 88, 102 and 116. These internal $[a_2+H]^{\bullet+}$ radical cations are N-alkylated amides of the central residue of the peptide and are complementary ions to the $[a_1]^+$ ions. High abundances of $[a_2]^+$ or $[a_1]^+$ ions are also observed in each CID spectrum.

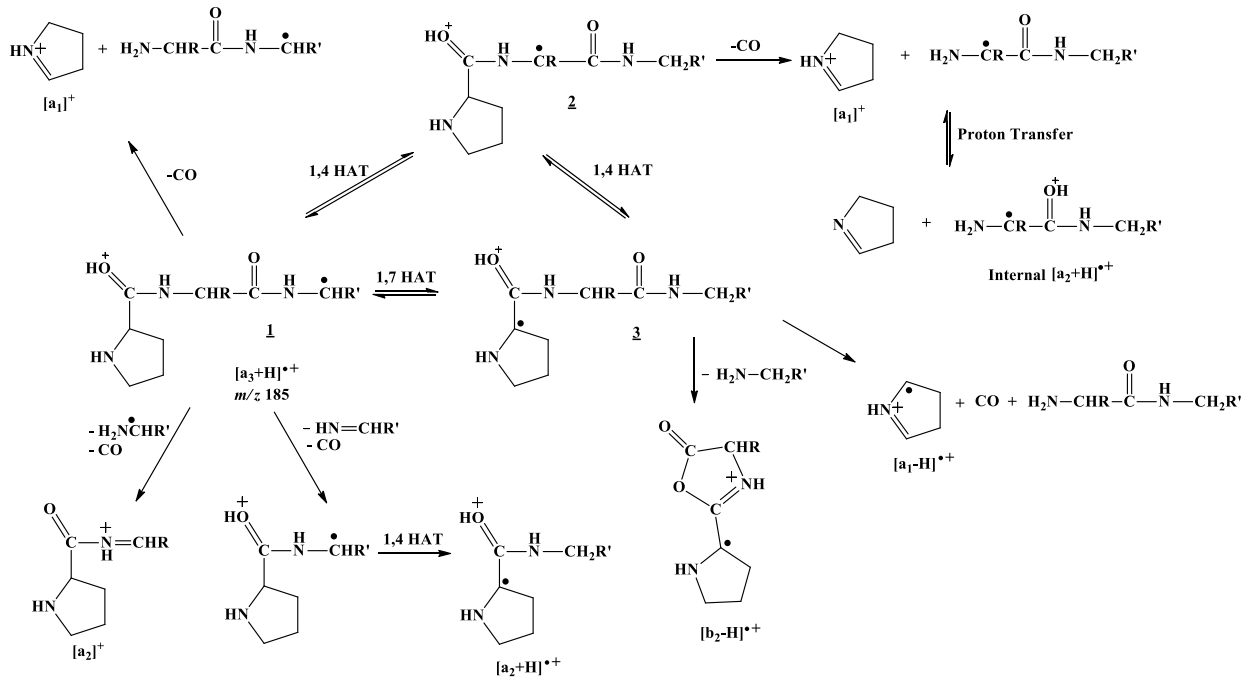

Scheme 5.3 Possible structure of the products of CID of $[a_3+H]^{\bullet+}$ derived from PGG, PAG and PAA.

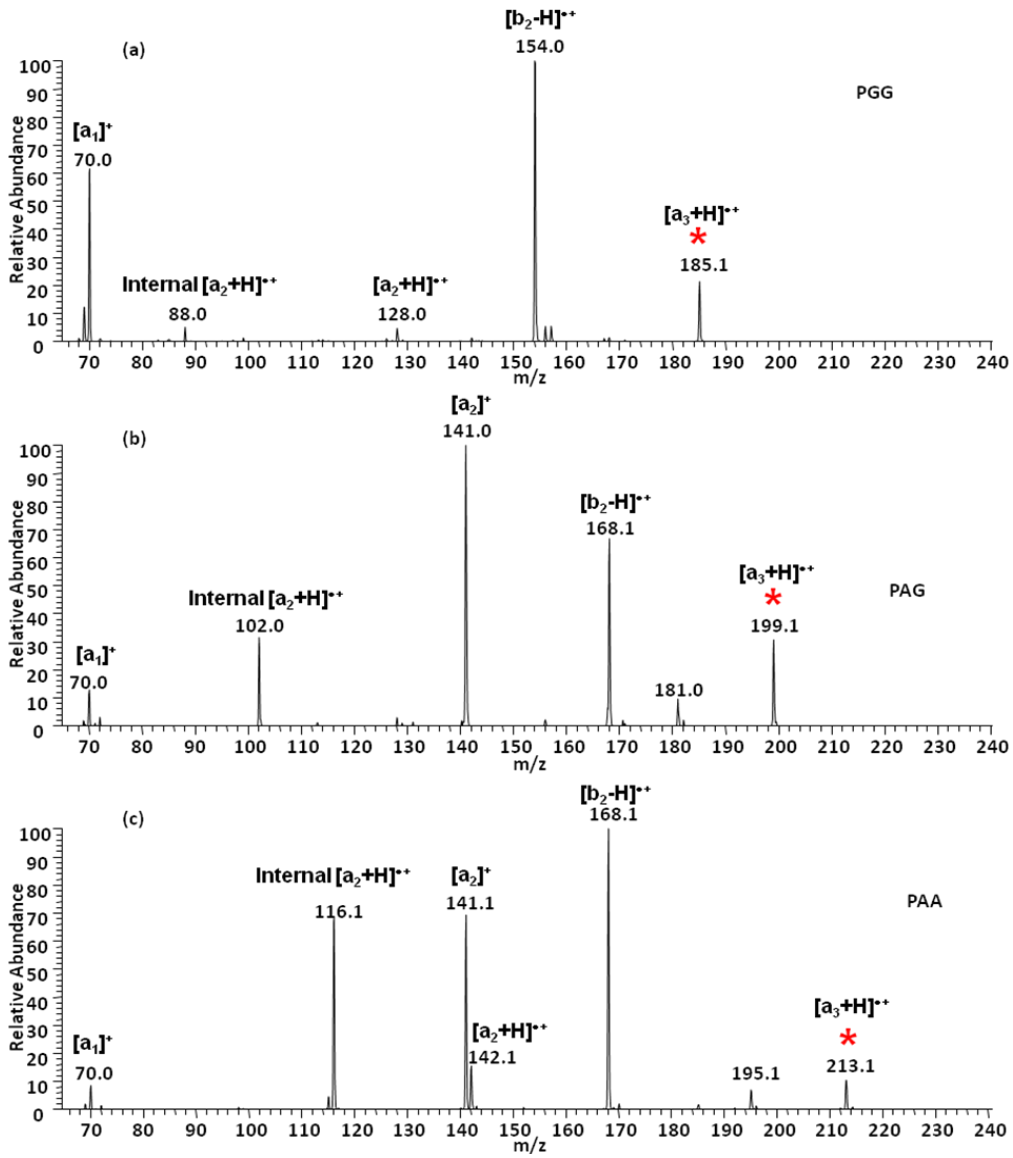

Figure 5.9 CID spectra of $[a_3+H]^{\bullet+}$ of (a) PGG, *m/z* 185.0, CE=18, obtained from $[Eu(PGG)(CH_3CN)_3]^{3+}$; (b) PAG, *m/z* 199.1, CE=17, obtained from $[Eu(PAG)(CH_3CN)_3]^{3+}$; (c) PAA, *m/z* 212.9, CE=19, obtained from $[Eu^{153}(PAA)(CH_3CN)_3]^{3+}$. The precursor ions are labelled with an asterisk (*)

b) Tripeptides with proline in the central position

Unlike in the CID of $[a_3+H]^{\bullet+}$ ions of PGG, PAG, PAA, dissociations of $[a_3+H]^{\bullet+}$ ions of GPG, APG have the closed-shell $[a_2]^+$ ion as the predominant product, although $[b_2\text{-}H]^{\bullet+}$ ions are observed, together with $[b_2]^+$ ions and other small amounts of fragments from H_2O loss/NH_3 loss. Possible structures are shown in Scheme 5.4.

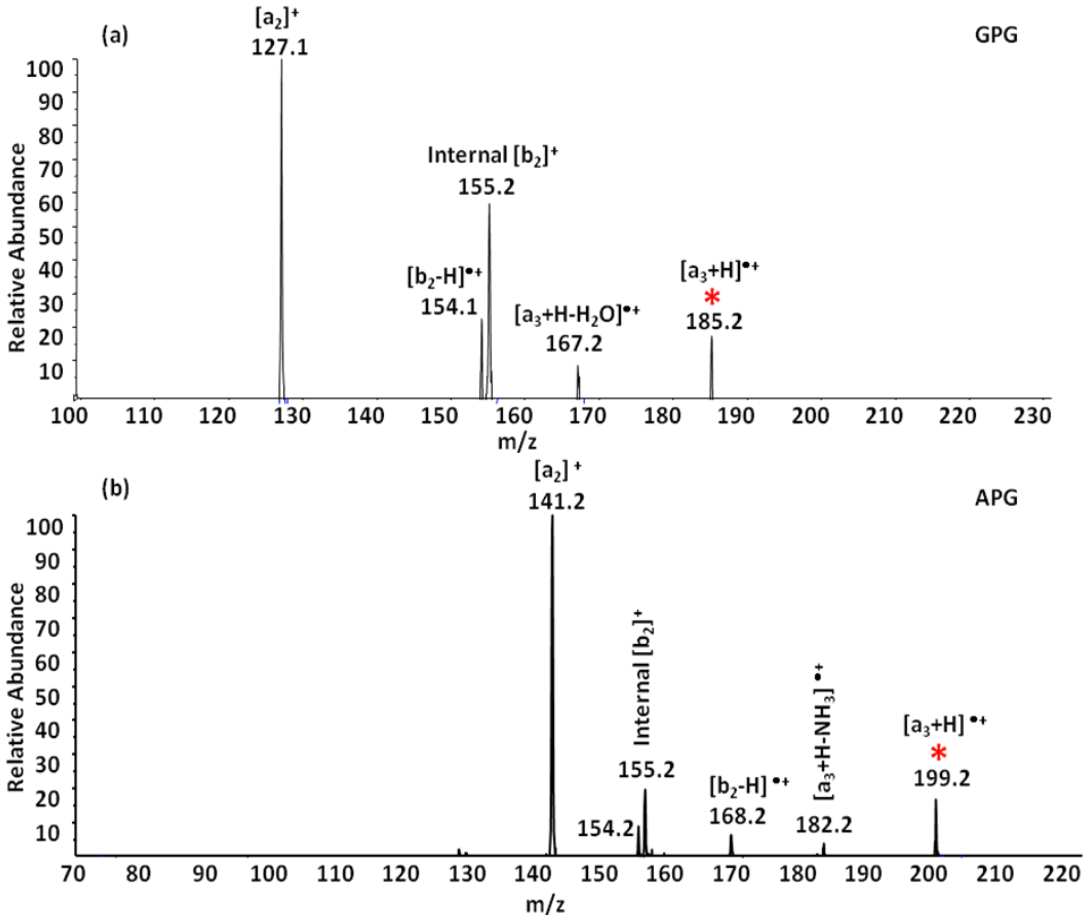

Figure 5.10 CID spectra of (a) $[a_3+H]^{\bullet+}$ of GPG, *m/z* 185.2, (b) $[a_3+H]^{\bullet+}$ of APG, *m/z* 199.2, obtained from $[Cu(GPG)(18\text{-Crown-}6)]^{2+}$ with AB Sciex QTrap 2000. The precursor ions are labelled with an asterisk (*)

Comparisons of the spectra in Figures 5.10a and 5.10b enable us to make the following deductions:

(1) There is an internal $[b_2]^+$ ion in the spectrum of APG but no $[b_2]^+$ ion. This suggests that the ion at m/z 155.2 in Figure 5.9a is probably the internal $[b_2]^+$ ion.

(2) There is no internal $[a_2]^+$ ion in Figure 5.10b but there is an $[a_2]^+$ ion, indicating that the ($H_2NC^{\bullet}H_2$+CO) loss occurs simultaneously from the C-terminus, possibly as $H_2NCH_2CO^{\bullet}$ from the initially formed $[a_3+H]^{\bullet+}$ ion.

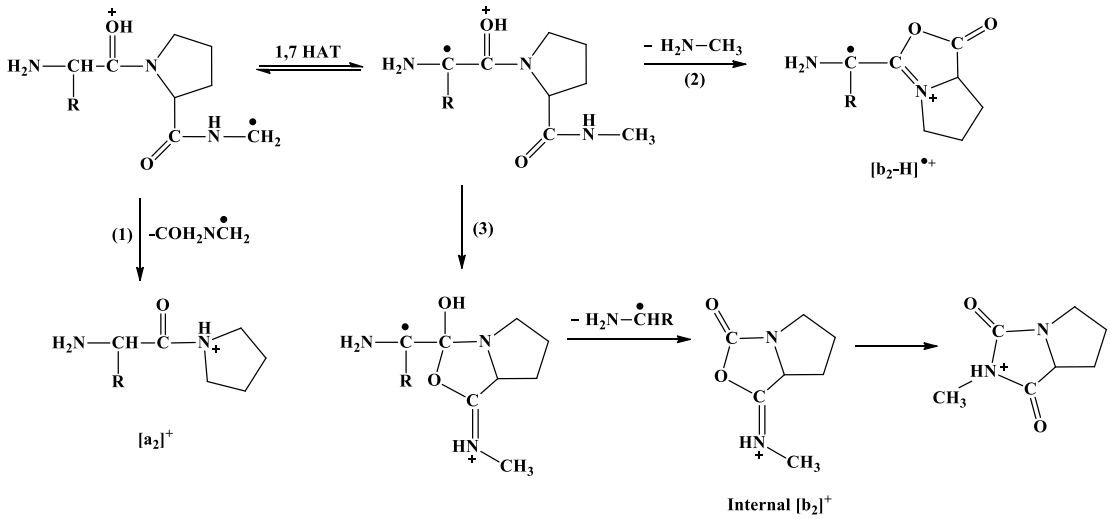

Scheme 5.4 Possible structures of the products of CID of $[a_3+H]^{\bullet+}$ derived from GPG and APG.

c) Tripeptides with proline at the C-terminus

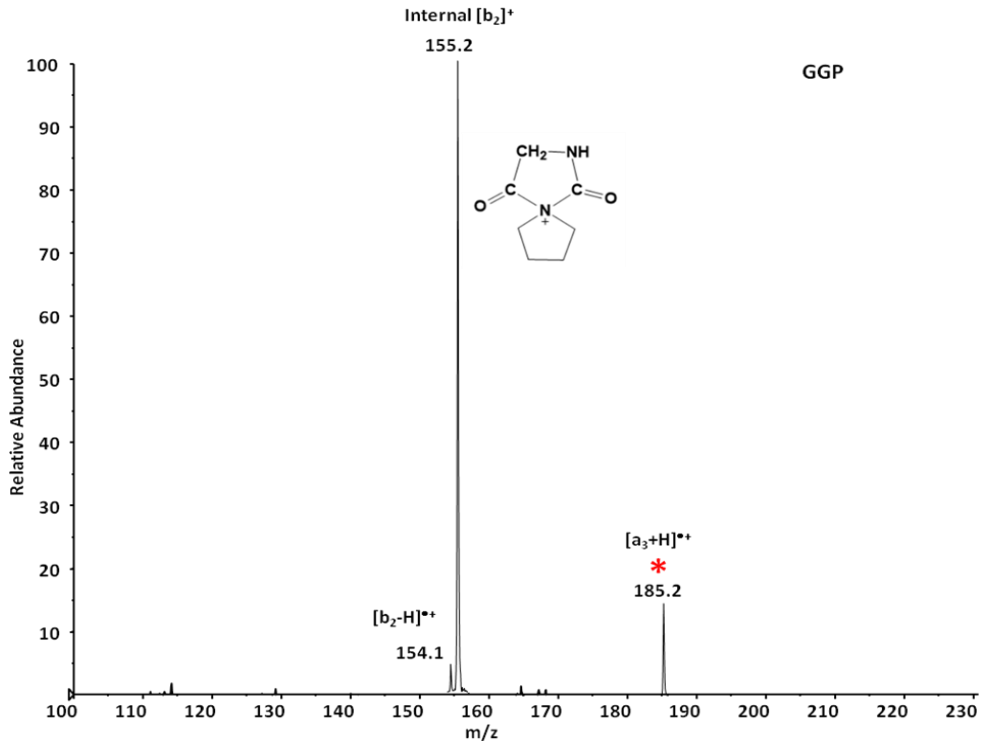

Figure 5.11 CID spectrum of $[a_3+H]^{\bullet+}$ of GGP, *m/z* 184.8, obtained from $[Cu(GGP)(18\text{-Crown-}6)]^{2+}$ with AB Sciex QTrap 2000. The precursor ions are labelled with an asterisk (*)

Formation of internal $[b_2]^+$ ions is the major channel in the dissociation of $[a_3+H]^{\bullet+}$ ions of GGP. Radical migration to the N-terminus results in the formation of internal $[b_2]^+$ ions by losing the radical $H_2NC^{\bullet}H_2$. The mechanism is identical to the third pathway in Scheme 5.4.

d) Tripeptides GGG, AGG and GGA

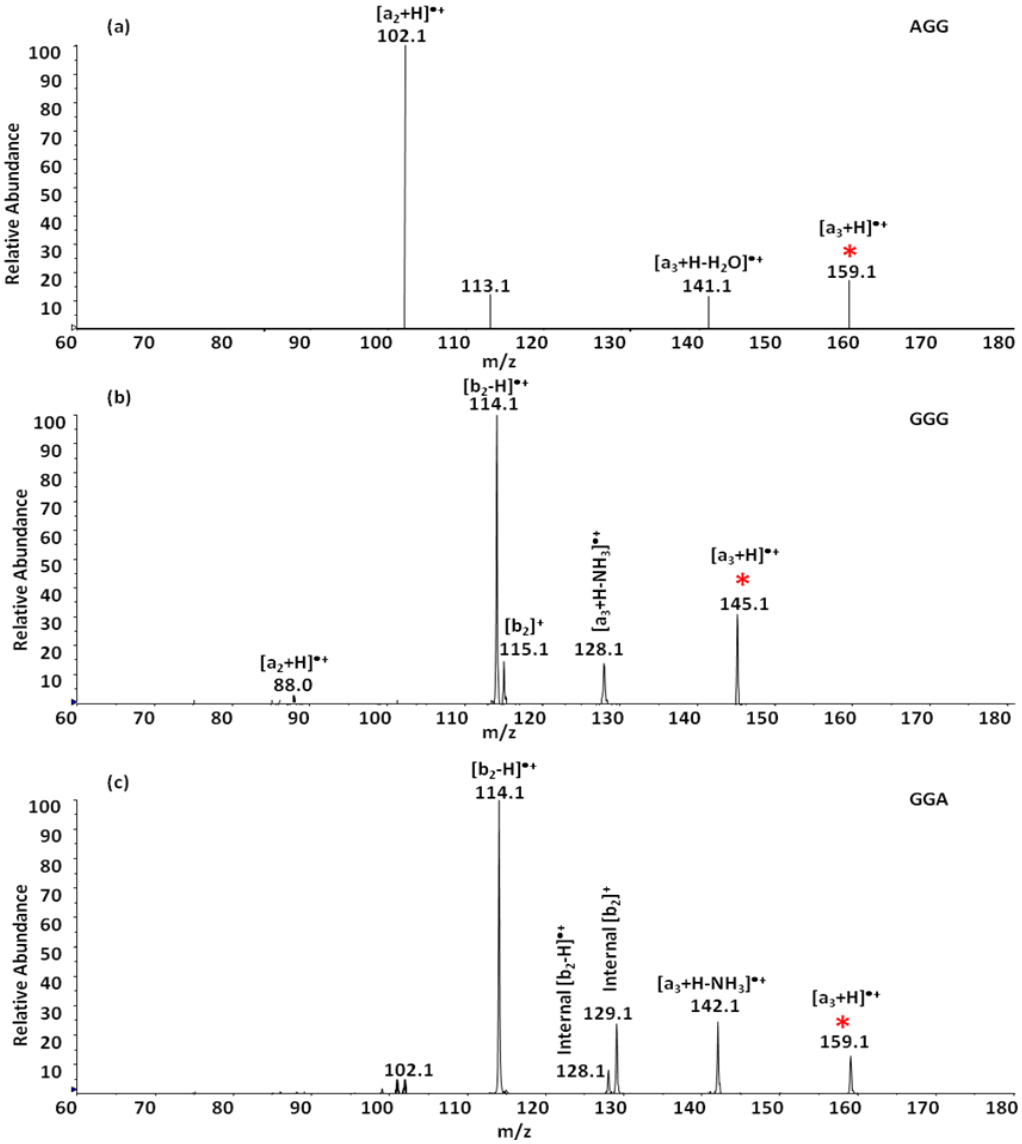

Figure 5.12 CID spectra of $[a_3+H]^{\bullet+}$ of (a) AGG, *m/z* 159.0 obtained from $[Eu(AGG)(18\text{-Crown-}6)]^{3+}$; (b) GGG, *m/z* 145, CE=17, obtained from $[Cu(GGG)(18\text{-Crown-}6)]^{2+}$; (c) GGA, *m/z* 159.0 obtained from $[Eu^{153}(GGA)(18\text{-Crown-}6)]^{3+}$ with AB Sciex QTrap 2000. The precursor ions are labelled with asterisks (*)

$[b_2\text{-H}]^{\bullet+}$ ions at m/z 114 are observed in the dissociation of the $[a_3\text{+H}]^{\bullet+}$ ions of GGG and GGA, and are created by loss of H_2NCH_2R (R=H or CH_3). The product is probably an oxazolone with an α-radical at the N-terminus. The $[a_2\text{+H}]^{\bullet+}$ ion is the predominant product in the dissociation of $[a_3\text{+H}]^{\bullet+}$ of AGG and this is most easily rationalised in terms of loss of $HN{=}CH_2$ and CO from the C-terminus of the initially formed $[a_3\text{+H}]^{2+}$ ion. Neutral losses of NH_3 or H_2O are present in each spectrum.

Table 5.2 summarizes the product ions of $[a_3\text{+H}]^{\bullet+}$ of aliphatic peptides. $[b_2\text{-H}]^{\bullet+}$ ions are formed in the CID spectra of eight out of nine $[a_3\text{+H}]^{\bullet+}$ ions, the exception being AGG, where $[a_2\text{+H}]^{\bullet+}$ is the predominant product.

Proton-driven peptide bond cleavage products are observed in each of spectrum except that of AGG. All proline-containing peptides have abundant a-type or b-type product ions, while eight out of the nine peptides studied show a-type or b-type product ions in the CID spectra of their $[a_3\text{+H}]^{\bullet+}$ ions.

Table 5.2 Product ions and relative abundance (%) in the fragmentation of $[a_3+H]^{\bullet+}$ of aliphatic peptides

[Peptide]$^{\bullet+}$	**PGG**	**PAG**	**PAA**	**GPG**	**APG**	**GGP**	**AGG**	**GGG**	**GGA**
Metal ion	**Eu(III)**	**Eu(III)**	**Eu(III)**	**Cu(II)**	**Cu(II)**	**Cu(II)**	**Eu(III)**	**Cu(II)**	**Eu(III)**
$[-H_2O]^{\bullet+}$		9	7	9			12		
$[b_2-H]^{\bullet+}$	100	65	100	22	6	4 (Internal)		100	100
$[a_2+H]^{\bullet+}$	8		16				100		
$[b_2]^+$				57	20 (Internal)	5; 100 (Internal)		14	25 (Internal)
$[a_2]^+$		100	70	100	100				
$[a_1]^+$	72	13	9						
$[-CO_2$ - ]	6	32	68						
Other							14$[-H_2O-CO_2]$	15$[-NH_3]$	26$[-NH_3]$

5.2.4 Fragmentations of $[b_3\text{-H}]^{\bullet+}$ and $[b_2\text{-H}]^{\bullet+}$ ions

Since $[b_3\text{-H}]^{\bullet+}$ ions are present in high abundance in the CID spectra of PGG, PAG, PAA and GAG radical cations, fragmentation of $[b_3\text{-H}]^{\bullet+}$ ions was studied. For $[b_3\text{-H}]^{\bullet+}$ ions examined here, the dissociation pattern is very simple, with $[a_2\text{+H}]^{\bullet+}$ as the predominant product, and a loss of 83 Da or 97 Da, depending on whether the residue at the C-terminus was G or A. The difference clearly indicates that it is the C-terminal residue that is lost.

A possible mechanism involving a classical oxazolone is given in Scheme 5.5.

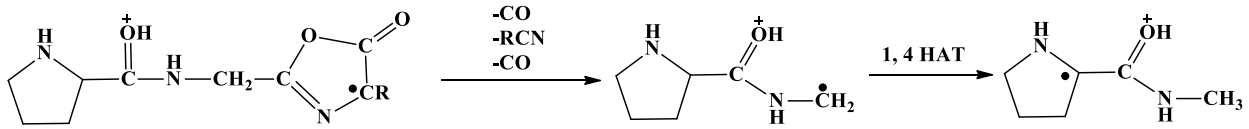

Scheme 5.5 A possible mechanism for loss of 83 Da (when R=H) or 97 Da (R=CH_3)

The end product is a radical cation stabilized by the captodative effect.

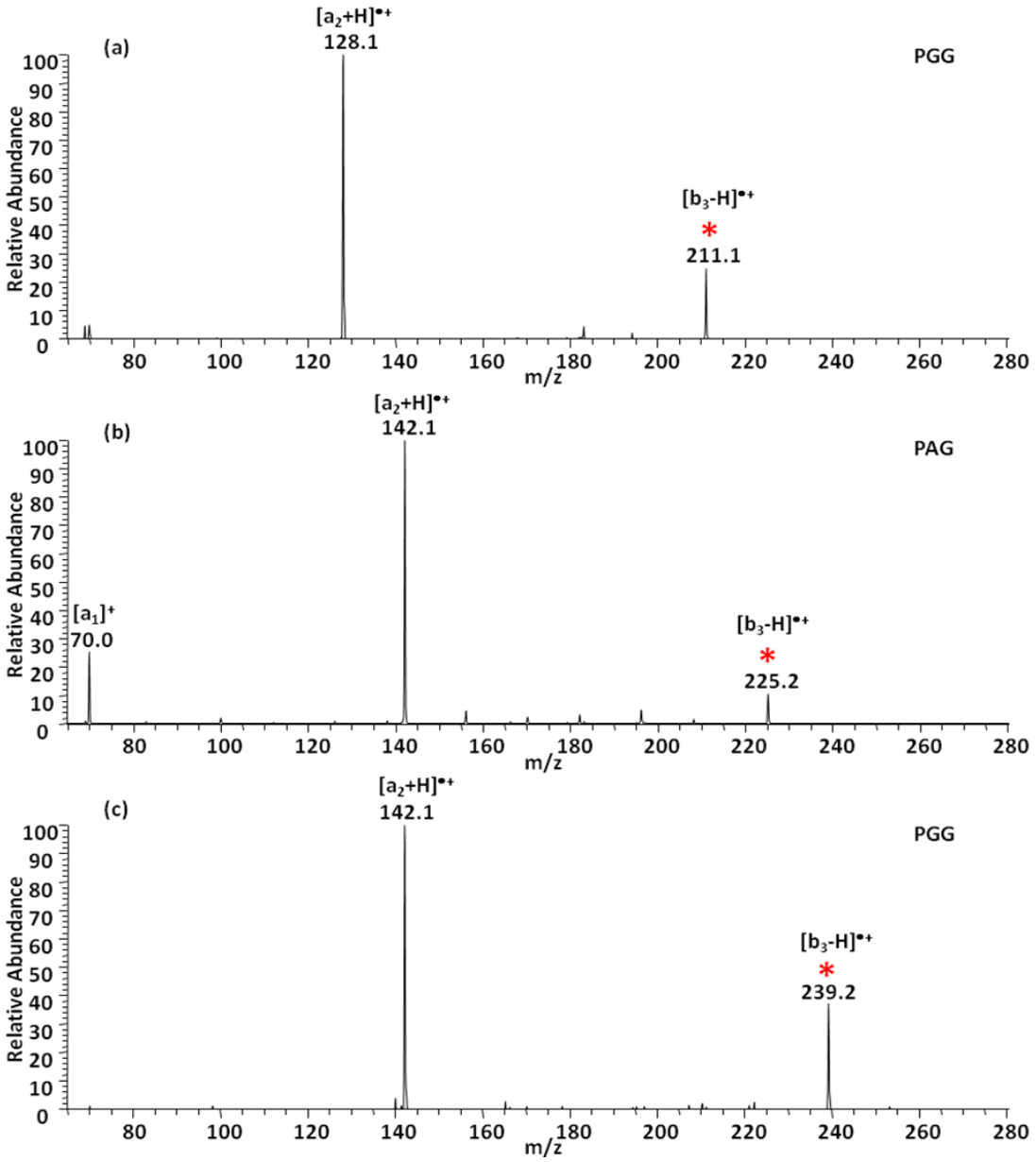

Figure 5.13 CID spectra of $[b_3\text{-H}]^{\bullet+}$ of (a) PGG, *m/z* 211.1 derived from $[PGG]^{\bullet+}$; (b) PAG, *m/z* 225.1 derived from $[PAG]^{\bullet+}$; (c) PAA, *m/z* 239.0 derived from $[PAA]^{\bullet+}$, obtained from $[Eu(Peptide)(CH_3CN)_3]^{3+}$. The precursor ions are labelled with asterisks (*)

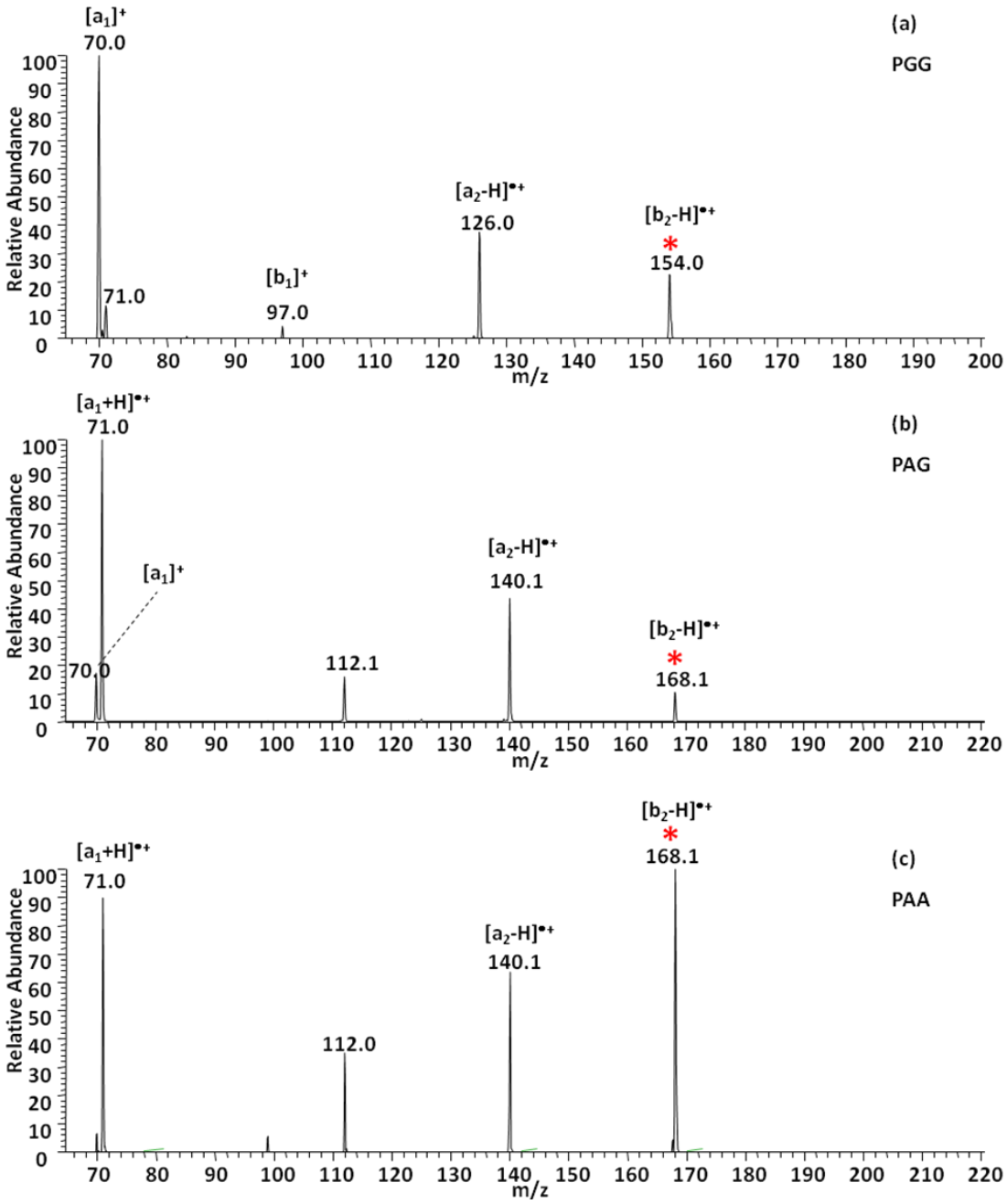

Figure 5.14 CID spectra of $[b_2\text{-H}]^{\bullet+}$ of (a) PGG, *m/z* 154.0 derived from $[PGG]^{\bullet+}$; (b) PAG, *m/z* 168.1 derived from $[PAG]^{\bullet+}$; (c) PAA, *m/z* 168.1 derived from $[PAA]^{\bullet+}$, obtained from $[Eu(Peptide)(CH_3CN)_3]^{3+}$. The precursor ions are labelled with asterisks (*)

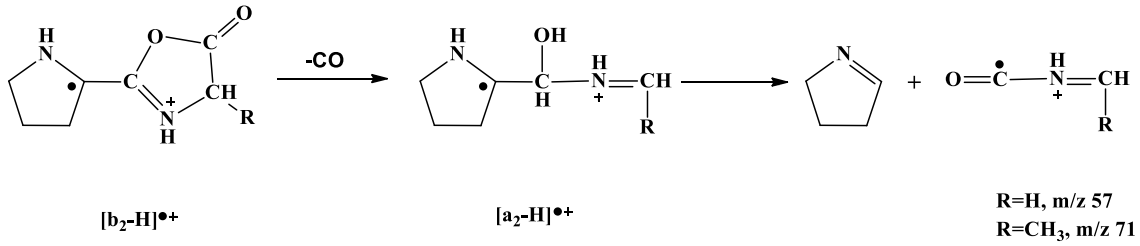

Scheme 5.6 Possible structure of the products of CID of $[b_2\text{-H}]^{\bullet+}$ derived from PGG, PAG and PAA.

Abundant $[a_2\text{-H}]^{\bullet+}$ ions at *m/z* 126 (R=H) and 140 (R=CH_3) are present in each CID spectrum of $[b_2\text{-H}]^{\bullet+}$ ions. Breaking the $C^{\bullet}$-C bond of the $[a_2\text{-H}]^{\bullet+}$ ion gives the ion at *m/z* 71 for ions derived from PAA and PAG (Scheme 5.6). A subsequent proton transfer creates the $[a_1]^+$ ion at m/z 70.

5.3 Conclusion

Aliphatic peptide radical cations generated from the dissociations of Eu(III)/peptide complexes or Cu(II)/peptide complexes have been studied. Although there is no single rule to govern the dissociation of all the $[\text{peptide}]^{\bullet+}$ ions investigated, $[b_3\text{-H}]^{\bullet+}$/ $[b_2\text{-H}]^{\bullet+}$ appear in the spectra of eight out of nine peptides studied, with the only exception of GGP, which gave $[y_1+2H]^+$ due to the proline effect. In addition to the radical cations fragments, proton-driven peptide backbone cleavage products are also formed by losing neutral radical fragments. Coincidently, $[b_3\text{-H}]^{\bullet+}$ ions are the major product (abundance>50%) in the CID spectra of $[\text{peptide}]^{\bullet+}$ derived from Eu/peptide complexes and only minor product (abundance <10%) in the CID spectra of $[\text{peptide}]^{\bullet+}$ derived from Cu/peptide complexes, which suggest that a further comparison between the dissociation of peptide radical cations formed from Eu/peptide and Cu/peptide complexes is

necessary, and DFT calculations will be used to find the preferred structure of the peptide take in Eu/peptide and Cu/peptide complexes.

For $[a_3+H]^{\bullet+}$ ions of aliphatic peptides, the dissociation pattern is harder to generalize, although $[b_2-H]^{\bullet+}$ ions are formed from eight out of the nine peptides studied; the exception is AGG, where the $[a_2+H]^{\bullet+}$ ions are produced. More abundant proton-driven peptide backbone cleavage products are observed for proline-containing peptides.

Dissociations of $[b_3-H]^{\bullet+}$ and $[b_2-H]^{\bullet+}$ ions were also investigated, although limited to peptides with N-terminal prolines. $[b_3-H]^{\bullet+}$ ions have one predominant fragmentation channel giving $[a_2+H]^{\bullet+}$ ions, while $[b_2-H]^{\bullet+}$ ions have several dissociation channels giving $[a_2-H]^{\bullet+}$, $[a_1+H]^{\bullet+}$, or $[a_1]^+$.

The data based on the dissociation of peptide radical cations has grown extensively in the last two decades since the method of CID-ESI-MS of the copper(II)-peptide-ligand ternary system was developed to generate radical cations of peptides containing aromatic and basic residues. Various ligands and peptides have been studied; however, there are fewer examples for aliphatic peptides. In this Chapter, with the newly discovered method (CID of Eu(III)/peptide complexes) to generate peptide radical cations, the radical cations of proline-containing and A/G containing aliphatic peptides have been investigated for first time.

5.4 References

1. Van Berkel, G. J. and Asano, K. G. Chemical Derivatization for Electrospray Ionization Mass Spectrometry. 2. Aromatic and Highly Conjugated Molecules. Anal Chem. 1994; 66(13): 2096–2102.

2. Chu, I. K., Rodriquez, C. F., Lau, T.-C., Hopkinson, A. C., and Siu, K. W. M. Molecular Radical Cations of Oligopeptides. J Phys Chem B. 2000; 104(15): 3393–3397.

3. Cui, W., Hu, Y. and Lifshitz, C. Time resolved photodissociation of small peptide ions. Eur Phys J D - Atomic, Molecular, Optical and Plasma Physics. 2002; 20(3): 565–571.

4. Barlow, C. K., Wee, S., McFadyen, W. D. and O'Hair, R. A. J. Designing copper(II) ternary complexes to generate radical cations of peptides in the gas phase: Role of the auxiliary ligand. Dalton Trans. 2004; 0(20): 3199–3204.

5. Edirisinghe, P. D., Moore, J. F., Calaway, W. F., Veryovkin, I. V., Pellin, M. J. and Hanley, L. Vacuum Ultraviolet Postionization of Aromatic Groups Covalently Bound to Peptides. Anal Chem. 2006; 78(16): 5876–5883.

6. Schäfer, M., Drayß, M., Springer, A., Zacharias, P. and Meerholz, K. Radical Cations in Electrospray Mass Spectrometry: Formation of Open-Shell Species, Examination of the Fragmentation Behaviour in ESI-MSn and Reaction Mechanism Studies by Detection of Transient Radical Cations. Eur J Org Chem. 2007; (31): 5162–5174.

7. Hopkinson, A. C. Radical cations of amino acids and peptides: Structures and stabilities. Mass Spectrom Rev. (2009). 28(4), 655–671.

8. Tureček, F. Copper-biomolecule complexes in the gas phase. The ternary way. Mass Spectrom Rev, 2007; 26(4):563–582.

9. Chu, I. K., Rodriquez, C. F., Hopkinson, A. C. and Siu, K.W.M. Formation of molecular radical cations of enkephalin derivatives via collision-induced dissociation of electrospray-generated copper (II) complex ions of amines and peptides. J Am Soc Mass Spectrom. 2001; 12(10): 1114–1119.

10. Mädler, S., Kai-Chi Lau, J., Williams, D., Wang, Y., Saminathan, I. S., Zhao, J., Siu, K.W.M. and Hopkinson, A. C. (2014). Fragmentation of Peptide Radical Cations Containing a Tyrosine or Tryptophan Residue: Structural Features That Favor Formation of $[x_{(n-1)} + H]^{\bullet+}$ and $[z_{(n-1)} + H]^{\bullet+}$ Ions. J Phys Chem B, 118(23), 6123–6133.

11. Mu, X., Song, T., Xu, M., Lai, C.-K., Siu, C.-K., Laskin, J. and Chu, I. K. Discovery and Mechanistic Studies of Facile N-Terminal Cα–C Bond Cleavages in the Dissociation of Tyrosine-Containing Peptide Radical Cations. J Phys Chem B. 2014; 118(16): 4273–4281.

12. Siu, C.-K., Ke, Y., Guo, Y., Hopkinson, A. C. and Siu, K. W. M. Dissociations of copper(II)-containing complexes of aromatic amino acids: radical cations of tryptophan, tyrosine, and phenylalanine. Phys Chem Chem Phys, 2008; 10(38): 5908–5918.

13. Chu, I. K., Siu, S. O., Lam, C. N. W., Chan, J. C. Y. and Rodriquez, C. F. Formation of molecular radical cations of aliphatic tripeptides from their complexes with Cu^{II}(12-crown-4). Rapid Commun Mass Spectrom. 2004; 18(16): 1798–1802.

14. Karnezis, A., Barlow, C. K., O'Hair, R. A. J. and McFadyen, W. D. Peptide derivatization as a strategy to form fixed-charge peptide radicals. Rapid Commun Mass Spectrom, 2006; 20(19): 2865–2870.

15. Wee, S., O'Hair, R. A. J. and McFadyen, W. D. Comparing the gas-phase fragmentation reactions of protonated and radical cations of the tripeptides GXR. International Journal of Mass Spectrometry. 2004; 234(1–3): 101–122.

16. Chu, I. K., Zhao, J., Xu, M., Siu, S. O., Hopkinson, A. C. and Siu, K. W. M. Are the Radical Centers in Peptide Radical Cations Mobile? The Generation, Tautomerism, and Dissociation of Isomeric α-Carbon-Centered Triglycine Radical Cations in the Gas Phase. J Am Chem Soc. 2008; 130(25): 7862–7872.

17. Chung, T. W., Hui, R., Ledvina, A., Coon, J. J. and Tureček, F. Cascade Dissociations of Peptide Cation-Radicals. Part 1. Scope and Effects of Amino Acid Residues in Penta-, Nona-, and Decapeptides. J Am Soc Mass Spectrom. 2012; 23(8): 1336–1350.

18. Kalli, A.and Hess, S. (2012). Electron Capture Dissociation of Hydrogen-Deficient Peptide Radical Cations. J Am Soc Mass Spectrom. 2012; 23(10): 1729–1740.

19. Kong, R. P. W., Quan, Q., Hao, Q., Lai, C.-K., Siu, C.-K. and Chu, I. K. Formation and Dissociation of Phosphorylated Peptide Radical Cations. J Am Soc Mass Spectrom. 2012; 23(12): 2094–2101.

20. Lam, C. N. W., Ruan, E. D. L., Ma, C. Y. and Chu, I. K. Non-zwitterionic structures of aliphatic-only peptides mediated the formation and dissociation of gas phase radical cations. J Mass Spectrom, 2006; 41(7): 931–938.

21. Laskin, J., Yang, Z., Ng, C. M. D. and Chu, I. K. Fragmentation of α-radical cations of arginine-containing peptides. J Am Soc Mass Spectrom. 2010; 21(4): 511–521.

22. Lau, J. K.-C., Lo, S., Zhao, J., Siu, K. W. M. and Hopkinson, A. C. Fragmentation Chemistry of $[Met\text{-}Gly]^{\bullet+}$, $[Gly\text{-}Met]^{\bullet+}$, and $[Met\text{-}Met]^{\bullet+}$ Radical Cations. J Am Soc Mass Spectrom, 2013; 24(4): 543–553.

23. Ledvina, A. R., Coon, J. J. and Tureček, F. Competitive hydrogen atom migrations accompanying cascade dissociations of peptide cation-radicals of the z+ type. J Am Soc Mass Spectrom. 2015; 377, 44–53.

24. Moss, C. L., Chamot-Rooke, J., Nicol, E., Brown, J., Campuzano, I., Richardson, K., Williams J. P., Bush, M. F., Bythell, B., Paizs, B. and Turecek, F. Assigning Structures to Gas-Phase Peptide Cations and Cation-Radicals. An Infrared Multiphoton Dissociation, Ion Mobility, Electron Transfer, and Computational Study of a Histidine Peptide Ion. J Phys Chem B. 2012; 116(10): 3445–3456.

25. Mu, X., Lau, J. K.-C., Lai, C.-K., Siu, K. W. M., Hopkinson, A. C. and Chu, I. K. Isomerization versus dissociation of phenylalanylglycyltryptophan radical cations. Phys Chem Chem Phys. 2017; 19(25): 16923–16933.

26. Ng, D. C. M., Song, T., Siu, S. O., Siu, C. K., Laskin, J. and Chu, I. K. Formation, Isomerization, and Dissociation of α-Carbon-Centered and π-Centered Glycylglycyltryptophan Radical Cations. J Phys Chem B. 2012; 114(6): 2270–2280.

27. Nguyen, H. T. H., Shaffer, C. J. and Tureček, F. Probing Peptide Cation–Radicals by Near-UV Photodissociation in the Gas Phase. Structure Elucidation of Histidine Radical Chromophores Formed by Electron Transfer Reduction. J Phys Chem B, 2015; 119(10): 3948–3961.

28. Oh, H. B. and Moon, B. Radical-driven peptide backbone dissociation tandem mass spectrometry: Radical-Driven peptide backbone dissociation MS/MS. Mass SpectromRev. 2015; 34(2): 116–132.

29. Piatkivskyi, A., Happ, M., Lau, J. K.-C., Siu, K. W. M., Hopkinson, A. C. and Ryzhov, V. Investigation of Fragmentation of Tryptophan Nitrogen Radical Cation. J Am Soc Mass Spectrom. 2015; 26(8): 1388–1393.

30. Siu, C., Ke, Y., Orlova, G., Hopkinson, A. C. and Michael siu, K. Dissociation of the N–Cα Bond and Competitive Formation of the $[z_n - H]^{\bullet+}$ and $[c_n + 2H]^+$ Product Ions in Radical

Peptide Ions Containing Tyrosine and Tryptophan: The Influence of Proton Affinities on Product Formation. J Am Soc Mass Spectrom. 2008; 19(12): 1799–1807.

31. Chu, I. and Laskin, J. Review: Formation of peptide radical ions through dissociative electron transfer in ternary metal–ligand–peptide complexes. Eur J Mass Spectrom. 2011; 17(6): 543.

32. Lam, C. N. W., Siu, S. O., Orlova, G. and Chu, I. K. Macrocyclic effect of auxiliary ligand on the gas-phase dissociation of ternary copper(II)–GGX complexes. Rapid Commun Mass Spectrom. 2006; 20(5): 790–796.

33. Ke, Y., Zhao, J., Verkerk, U. H., Hopkinson, A. C. and Siu, K. W. M. Histidine, Lysine, and Arginine Radical Cations: Isomer Control via the Choice of Auxiliary Ligand (L) in the Dissociation of [Cu II (L)(amino acid)]$^{\bullet 2+}$ Complexes. J Phys Chem B, 2007; 111(51), 14318–14328.

34. Bagheri-Majdi, E., Ke, Y., Orlova, G., Chu, I. K., Hopkinson, A. C. and Siu, K. W. M. Copper-Mediated Peptide Radical Ions in the Gas Phase. J Phys Chem B, 2004; 108(30): 11170–11181.

35. Tureček, F. and Julian, R. R. Peptide Radicals and Cation Radicals in the Gas Phase. Chem Rev. 2013; 113(8): 6691–6733.

36. Paizs, B. and Suhai, S. Fragmentation pathways of protonated peptides. Mass Spectrom Rev. 2005; 24(4): 508–548.

37. Viehe, H. G., Janousek, Z., Merenyi, R. and Stella, L. The captodative effect. Acc Chem Res. 1985; 18(5): 148–154.

38. Moore, B. N. and Julian, R. R. Dissociation energies of X–H bonds in amino acids. Phys Chem Chemical Phys. 2012; 14(9): 3148–3154.

39. Verbruggen, N. and Hermans, C. Proline accumulation in plants: a review. Amino Acids. 2008; 35(4): 753–759.

40. Kaul, S., Sharma, S. S. and Mehta, I. K. Free radical scavenging potential of L-proline: evidence from in vitro assays. Amino Acids. 2008; 34(2): 315–320.

41. Dean, R. T., Wolff, S. P. and McElligott, M. A. Histidine and Proline are Important Sites of Free Radical Damage to Proteins. Free Radical Res Commun. 1989; 7(2): 97–103.

42. Loo, J. A., Edmonds, C. G., and Smith, R. D. Tandem mass spectrometry of very large molecules. 2. Dissociation of multiply charged proline-containing proteins from electrospray ionization. Anal Chem.1993; 65(4): 425–438.

43. Tabb, D. L., Smith, L. L., Breci, L. A., Wysocki, V. H., Lin, D. and Yates, J. R. Statistical Characterization of Ion Trap Tandem Mass Spectra from Doubly Charged Tryptic Peptides. Anal Chem. 2003; 75(5): 1155–1163.

44. Grewal, R. N., El Aribi, H., Harrison, A. G., Siu, K. W. M. and Hopkinson, A. C. Fragmentation of Protonated Tripeptides: The Proline Effect Revisited. J Phys Chem B. 2004; 108(15): 4899–4908.

45. Bleiholder, C., Suhai, S., Harrison, A. G.and Paizs, B. (2011). Towards Understanding the Tandem Mass Spectra of Protonated Oligopeptides. 2: The Proline Effect in Collision-Induced Dissociation of Protonated Ala-Ala-Xxx-Pro-Ala (Xxx = Ala, Ser, Leu, Val, Phe, and Trp). J Am Soc Mass Spectrom, 22(6), 1032–1039.

46. Vaisar, T.and Urban, J. (1996). Probing Proline Effect in CID of Protonated Peptides. J Mass Spectrom, 31(10), 1185–1187.

CHAPTER 6

Generation and Fragmentations of Small Dipositively Charged $[a_n + H]^{2+}$ and $[b_n + H]^{2+}$ Ions

6.1 Introduction

Peptide fragmentation has been of interest for protein identification, which is the foundation for proteomics [1-4]. a-, b-, and y-type ions are common products in the fragmentations of protonated peptides. Under collision-induced dissociation (CID), a protonated peptide undergoes fragmentations mainly at the peptide bonds to produce either $[b_n]^+$ or $[y_n + 2H]^+$ ions, depending on the proton affinities of the fragments. The $[y_n + 2H]^+$ ion is simply a protonated truncated peptide. By contrast, the $[b_n]^+$ ion is known to feature an oxazolone ring at the C-terminus and it can subsequently lose CO to produce an $[a_n]^+$ ion which possesses an imine structure [5-13]. When the peptide contains a basic residue, the existence of doubly charged protonated peptide fragments are possible [10-12]. Otherwise, observation of small $[a_n + H]^{2+}$ and $[b_n + H]^{2+}$ (n = 2 or 3) ions is difficult in the gas phase due to the large Coulombic repulsion that leads to facile dissociation.

Interestingly, in a study on the CID of $[La(GGG)(CH_3CN)_n]^{3+}$ (n = 2 or 3) complexes, dipositively charged $[a_2 + H]^{2+}$ and $[a_3 + H]^{2+}$ ions of GGG were observed [14]. The $[a_3 + H]^{2+}$ ion, in which one of the protons is located at the N-terminal amine while the other proton is at the C-terminal imine was generated based on the charge disproportionation reaction as shown in Scheme 6.1. When this dipositive ion was subjected to front-end fragmentation, the even smaller $[a_2 + H]^{2+}$ ion was observed in the CID spectrum. [14].

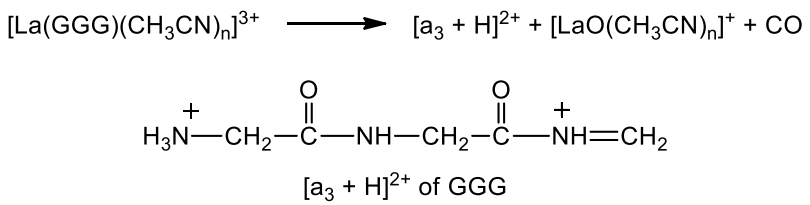

Scheme 6.1

Later, observations of $[a_3 + H]^{2+}$ and $[a_2 + H]^{2+}$ ions of PPP and PP were also reported in the CID of $[La(PPP)(CH_3CN)_n]^{3+}$ and $[La(PP)(CH_3CN)_n]^{3+}$ respectively. The high stabilities of these dipositive ions are attributed to the secondary amine of the proline residue which is able to accommodate the excess positive charges in the molecule (Scheme 6.2) [15].

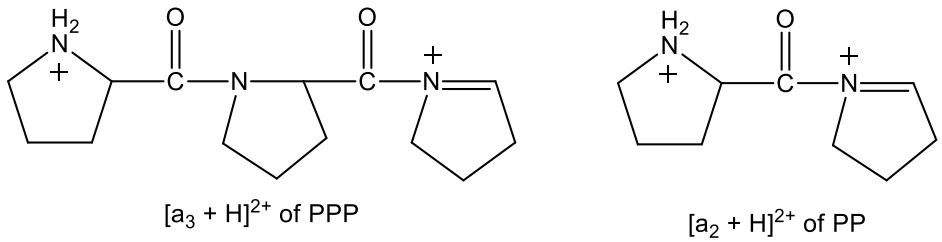

Scheme 6.2 Structures for the $[a_3 + H]^{2+}$ and $[a_2 + H]^{2+}$ ions of PPP and PP.

Since CID of La^{3+}/PPP and La^{3+}/PP complexes gave abundant dipositive $[a_3 + H]^{2+}$ and $[a_2 + H]^{2+}$ ions, a further systematic study aiming for generating high-abundance $[a_n + H]^{2+}$ ions (n = 2 or 3) from small peptides was carried out [16] and it was found that most abundant $[a_n + H]^{2+}$ ions were observed when proline residue was at the N-terminus of the peptides.

The $[a_n + H]^{2+}$ ions (n = 2 or 3) being investigated in this work includes aliphatic, proline-containing, and tryptophan-containing peptides. In addition, the possibility of generating unprecedented dipositive $[b_n + H]^{2+}$ ions and their fragmentations is also discussed.

6.2 Result and Discussion

6.2.1 Chemistry of dipositively charged $[a_3 + H]^{2+}$ and $[a_2 + H]^{2+}$ ions

a) $[a_3+H]^{2+}$ ions of proline-containing peptides

Figure 6.1 shows the CID spectra of $[La(PGG)(CH_3CN)]^{3+}$ (*m/z* 136.3), $[Ce(PGG)(CH_3CN)]^{3+}$ (*m/z* 136.7) and $[Ce(PGG)(CD_3CN)]^{3+}$ (*m/z* 137.7). From Figure 6.1a and 6.1b, it is seen that the fragmentation patterns of La^{3+}/peptide and Ce^{3+}/peptide complexes are very similar. The major product ion is the $[a_3 + H]^{2+}$ ion of PGG (*m/z* 92.5) in both spectra. The complementary ion, $[MO(CH_3CN)]^+$, is also observed (*m/z* 195.9 when M = La and *m/z* 196.9 when M = Ce). The ion at *m/z* 155 corresponds to the $[b_2]^+$ ion, which is a fragmentation product of $[a_3 + H]^{2+}$ (*vide infra*). In addition, the formation of the metal/deprotonated peptide complex $[M(PGG – H)]^{2+}$ (*m/z* 183.5 when M = La and *m/z* 184.0 when M = Ce) as well as its dissociations products are also observed. The comparable CID spectra suggests that $[a_3 + H]^{2+}$ ions can be generated by both La^{3+}- or Ce^{3+}-peptide complexes. The capability of generating dipositive ions from both metal ions allows us to avoid isolation of isobaric ions. In the following context, the $[a_n + H]^{2+}$ ions are produced from either La^{3+} or Ce^{3+} complexes, unless otherwise stated.

Deuterated acetonitrile (CD_3CN) has been used to further identify the fragment ions. Figure 6.1c shows the fragmentations of $[Ce(PGG)(CD_3CN)]^{3+}$. For the tripositive ions containing one CD_3CN, the mass-to-charge ratio (*m/z*) is shifted by 1.0 relative to the CID spectrum of $[Ce(PGG)(CH_3CN)]^{3+}$. For monopositive ions with one CD_3CN, the shift becomes 3.0 *m/z* while the *m/z* is unchanged when the ion does not contain any CD_3CN. Thus, it is clear that the ions at *m/z* 92.5 and 155.1 do not contain metal ion and a solvent molecule.

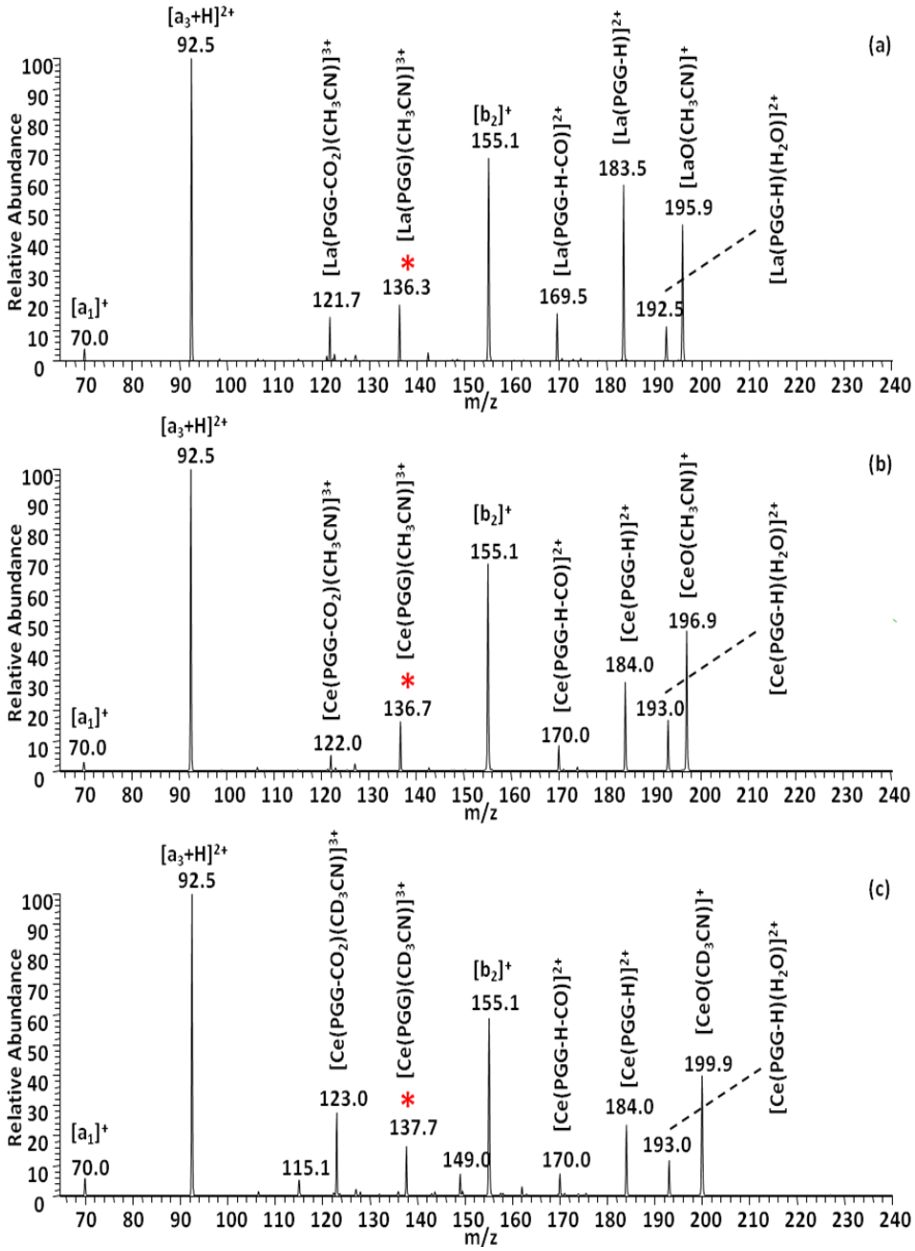

Figure 6.1 CID spectra of (a) $[La(PGG)(CH_3CN)]^{3+}$ (*m/z* 136.3) CE=11.3; (b) $[Ce(PGG)(CH_3CN)]^{3+}$ (*m/z* 136.7) CE=11.5; (c) $[Ce(PGG)(CD_3CN)]^{3+}$ (*m/z* 137.7) CE=11.6. The precursor ion is labelled with an asterisk (*).

In the previous works to study the fragmentation chemistry of the $[a_3 + H]^{2+}$ ions, front-end fragmentation techniques were used (carried out in a API3000 triple-quadrupole mass spectrometer). A drawback to this technique is that the ions are probably hot before being introduced into the collision cell. In order to have a better understanding of the fragmentation patterns of the $[a_3 + H]^{2+}$ ions, the hybrid linear ion trap Orbitrap Elite tandem mass spectrometry was used in this study. Figure 6.2a and 6.2b show the MS/MS spectra of $[a_3 + H]^{2+}$ ions derived from $[Ce(PGG)(CH_3CN)]^{3+}$ and $[Ce(PG(^{18}O)G)(CH_3CN)]^{3+}$ complexes, respectively, where the second amide oxygen is labeled by isotope ^{18}O in the latter complex. Identical fragmentation patterns are found in these spectra. The $[a_3 + H]^{2+}$ ion dissociates to give $[b_2]^+$ (*m/z* 155.0 or *m/z* 157.0) in the labeled peptide in Figure 6.2b by losing $H_2N^+{=}CH_2$ from the C-terminus as the major product ions. Also, the $[a_2]^+$ ion at *m/z* 127.0 is the subsequent fragmentation product by the loss of CO from $[b_2]^+$ (Scheme 6.3).

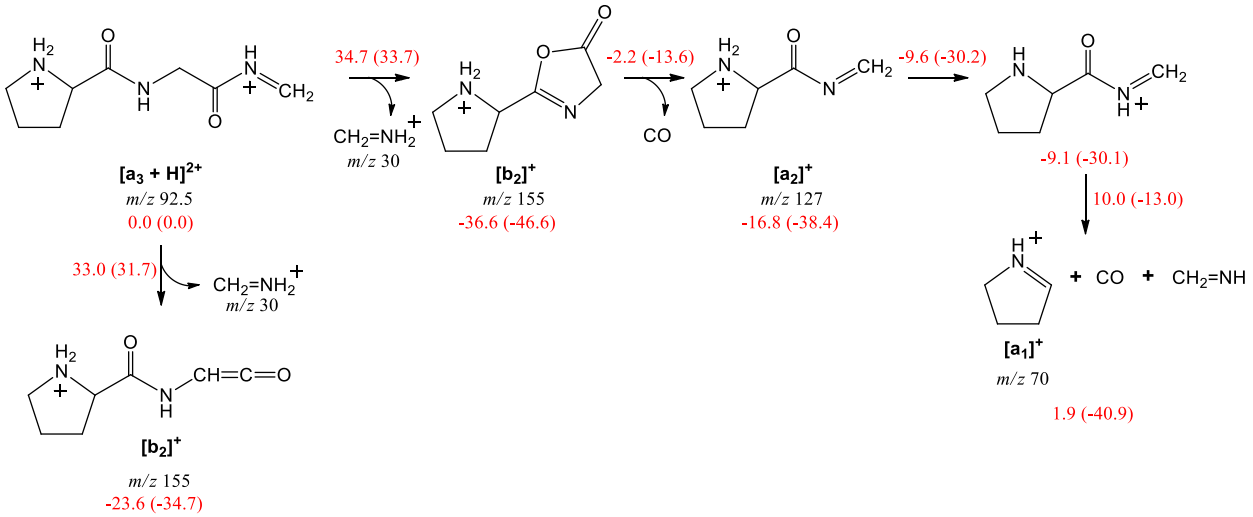

Scheme 6.3 Fragmentation mechanisms of $[a_3 + H]^{2+}$ of PGG. Relative enthalpies (ΔH^o_0) and free energies (ΔG^o_{298}, in parenthesis) are calculated at the B3LYP/6-31++G(d,p) level. All energies are in kcal mol^{-1}.

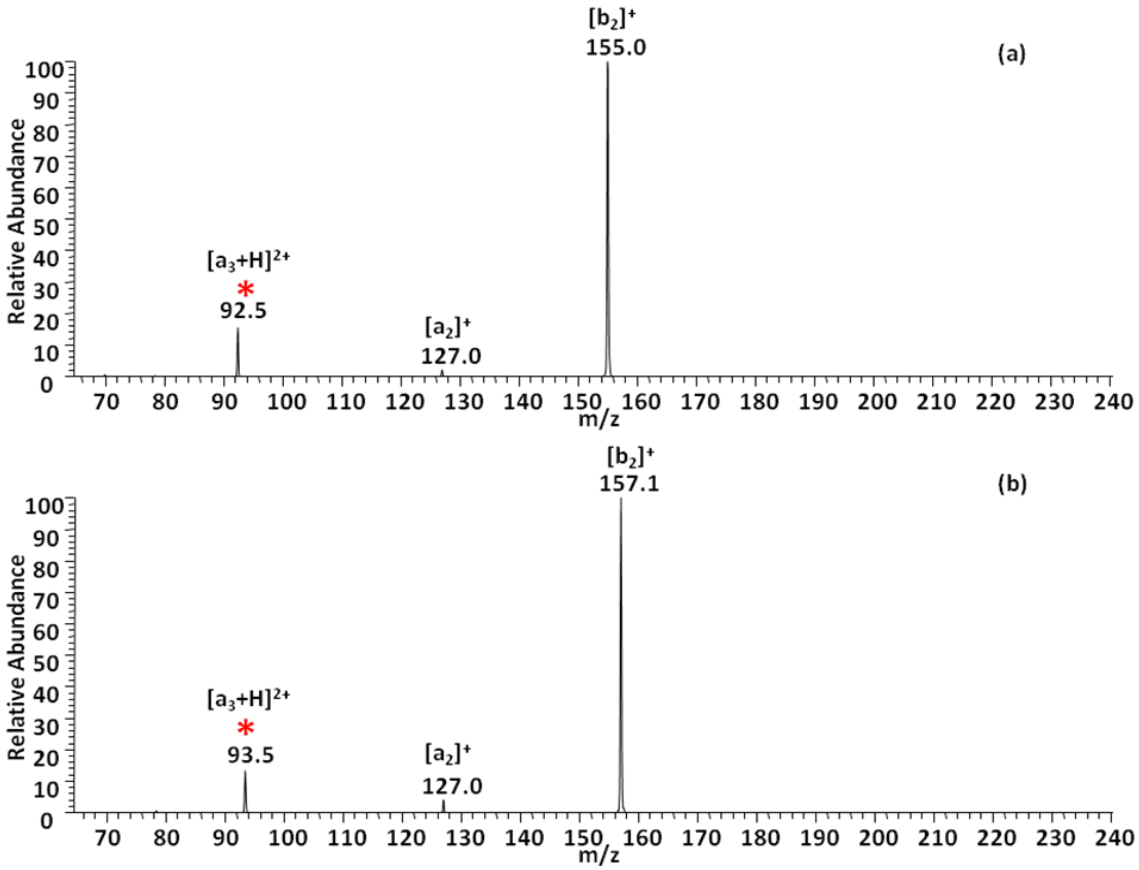

Figure 6.2 CID spectra of (a) $[a_3 + H]^{2+}$ of PGG (*m/z* 92.5, CE=9) and (b) $[a_3 + H]^{2+}$ of PG(^{18}O)G (*m/z* 93.5), where G(^{18}O) denotes the amide oxygen of glycine containing ^{18}O-labelling. The precursor ion is labelled with an asterisk (*).

Figure 6.3a shows the CID spectrum of $[a_3 + H]^{2+}$ ion derived from $[Ce(PAA)(CH_3CN)]^{3+}$, which has very similar fragmentation chemistry to that of PGG. Again, the $[b_2]^+$ ion (*m/z* 169) is the most abundant fragment ion together with a moderate abundance of $[a_2]^+$ ion (*m/z* 141) and small amount of $[a_1]^+$ at *m/z* 70.

DFT calculations have been employed to investigate the energetics for the dissociations of $[a_3 + H]^{2+}$ by using PGG as an example (Scheme 6.3). Loss of $H_2N^+{=}CH_2$ from the $[a_3 + H]^{2+}$ ion is facilitated by nucleophilic attack by the first amide oxygen on the second amide carbon resulting in the cleavage of the second amide bond to lose $HN{=}CH_2$. Proton transfer from the newly formed oxazolone ring to the $HN{=}CH_2$ moiety leads to the formation of monopositive $[b_2]^+$ (*m/z* 155) and $[a_1]^+$ ion (*m/z* 30, not shown in the CID spectrum). The barrier for the dissociation is 34.7 kcal mol^{-1}. The oxazolone $[b_2]^+$ ion can further lose CO to produce an $[a_2]^+$ ion at *m/z* 127 with the barrier of -2.2 kcal mol^{-1}. Further proton transfer to the amide nitrogen weakens the amide bond. Cleavage of the amide bond of the $[a_2]^+$ ion results in the loss of CO and $HN{=}CH_2$ at the same time to produce an $[a_1]^+$ ion at *m/z* 70. Note that loss of $NH_2^+{=}CH_2$ from $[a_3 + H]^{2+}$ can also be facilitated by the formation of a ketene structure. The barrier to this dissociation is 33.0 kcal mol^{-1}, slightly lower than for the formation of an oxazolone structure.

Figure 6.3b shows another example of $[a_3 + H]^{2+}$ ion which is derived from $[Ce(PPP)(CH_3CN)]^{3+}$. The $[a_1]^+$ ion (*m/z* 70) is the base peak in the spectrum along with moderate abundances of $[a_2]^+$ and $[b_2]^+$ ions at *m/z* 167.2 and 195.2, respectively. The ion at *m/z* 126 is the subsequent loss of neutral pyrrolidine ring (69 Da) from the $[b_2]^+$ ion and it can further dissociate by loss of CO to produce the ion at *m/z* 98. The fragmentation mechanisms of $[a_3 + H]^{2+}$ of PPP has been studied previously [15] and those results are reproduced and are summarized in Scheme 6.4.

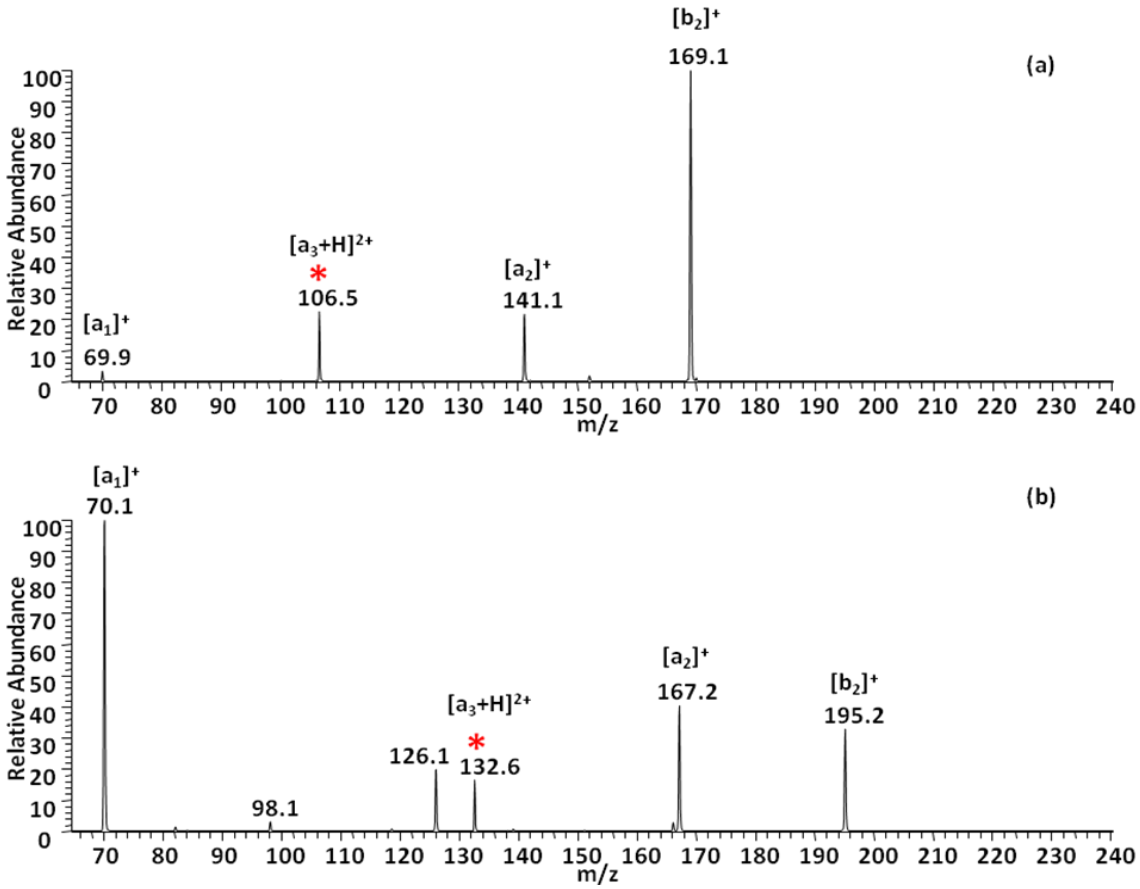

Figure 6.3 CID spectra of (a) $[a_3 + H]^{2+}$ of PAA (*m/z* 106.5, CE=12) and (b) $[a_3 + H]^{2+}$ of PPP (*m/z* 132.6, CE=15). The precursor ion is labelled with an asterisk (*).

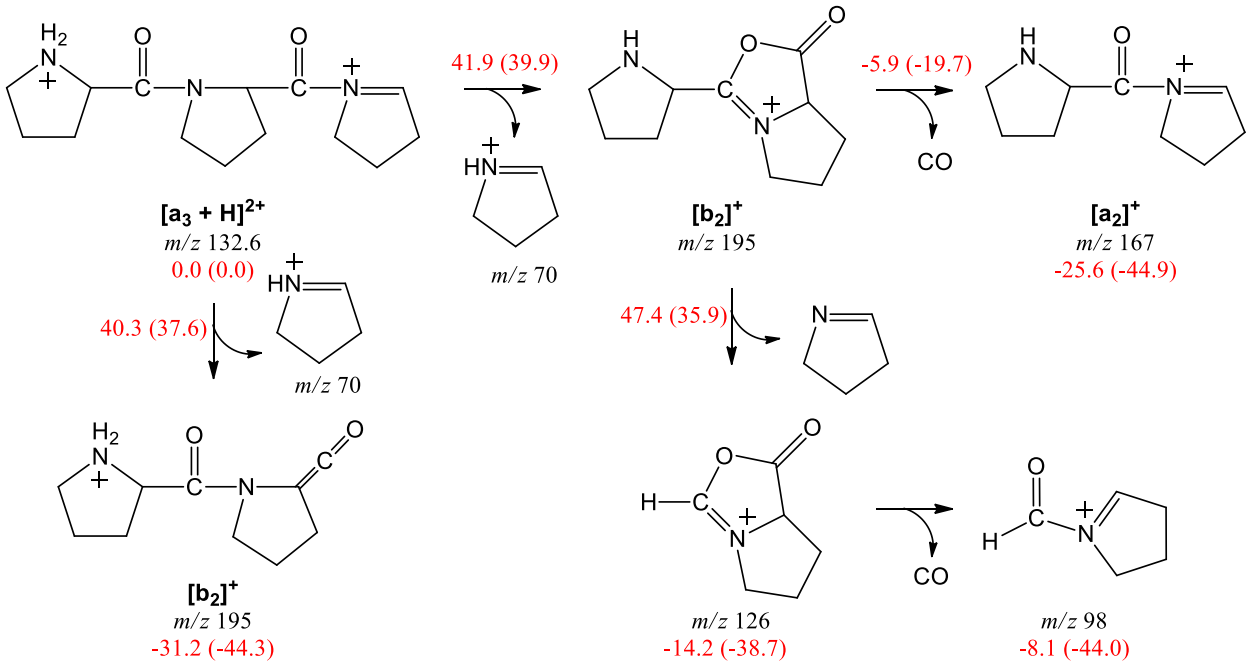

Scheme 6.4 Fragmentation mechanisms of $[a_3 + H]^{2+}$ of PPP adopted from Ref [15]. Relative enthalpies (ΔH^o_0) and free energies (ΔG^o_{298}, in parenthesis) are calculated at the B3LYP/6-311++G(d,p) level. All energies are in kcal mol^{-1}.

b) $[a_3+H]^{2+}$ ions of GGA

As mentioned in the previous section, early study on the dissociation of $[a_3 + H]^{2+}$ of GGG was carried out by front-end fragmentation. To avoid overheating the ion, here, the fragmentation chemistry of the dipositive ions of the aliphatic tripeptide is re-examined by using the ion-trap mass spectrometer. In order to obtain more information from the CID spectrum, the $[a_3 + H]^{2+}$ ion of GGA has been studied (instead of GGG). The CID spectrum of $[a_3 + H]^{2+}$ of GGA is summarized in Figure 6.4. Similar to that of GGG, the major product ions are $[a_2]^+$ and $[b_2]^+$ ions at *m/z* 87 and 115, respectively. In addition, the formation of internal $[a_2]^+$ ion at *m/z* 101.0 is also observed. This internal $[a_2]^+$ ion is produced by the cleavage of the first amide bond (Scheme 6.5).

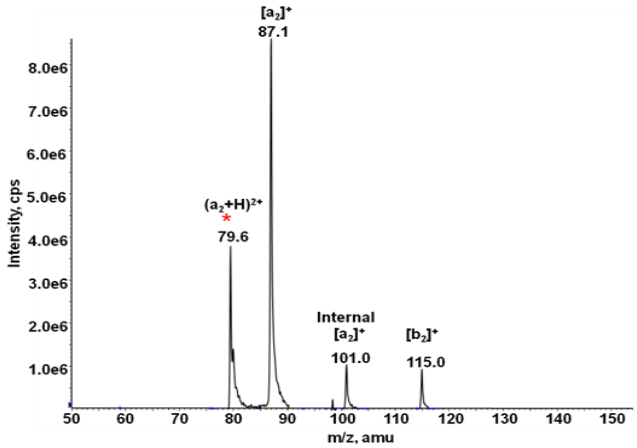

Figure 6.4 CID spectra of $[a_3 + H]^{2+}$ of GGA (*m/z* 79.6). The precursor ion is labelled with an asterisk (*).

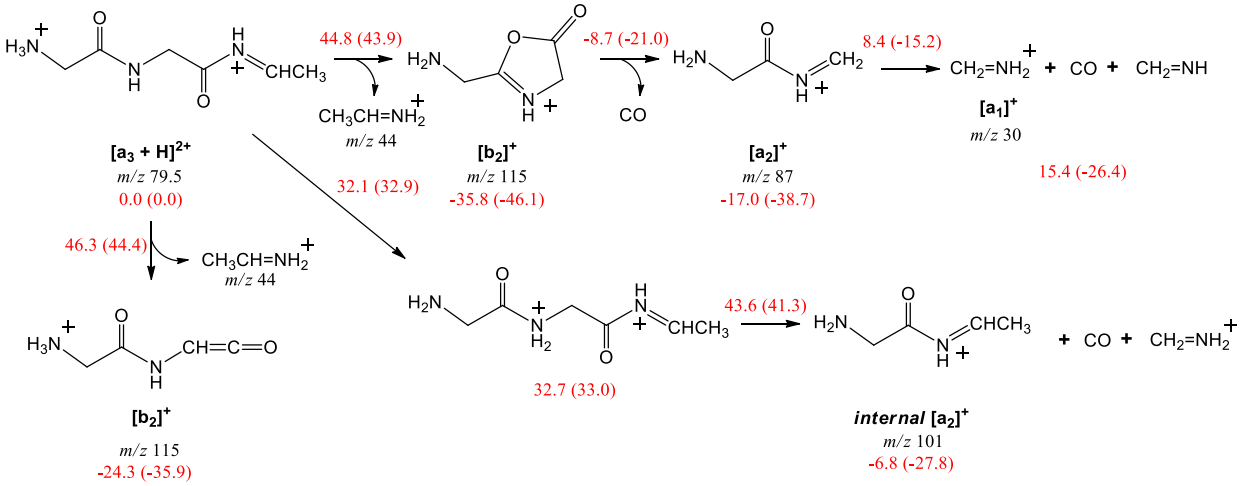

Scheme 6.5 Fragmentation mechanisms of $[a_3 + H]^{2+}$ of GGA. Relative enthalpies (ΔH^o_0) and free energies (ΔG^o_{298}, in parenthesis) are calculated at the B3LYP/6-31++G(d,p) level. All energies are in kcal mol^{-1}.

c) $[a_3+H]^{2+}$ ions of tryptophan-containing peptides

In addition to the $[a_3 + H]^{2+}$ ions derived from aliphatic peptides, $[a_3 + H]^{2+}$ ions containing an aromatic residue have been successfully generated from Ce^{3+} complexes. Figure 6.5a – 6.5c summarizes the CID spectra of $[a_3 + H]^{2+}$ ions of GWG, GWA, and AWG, respectively. The presence of the aromatic side chain makes the fragmentation pathway more complicated. Both monopositive and dipositive product ions are found in the spectra. In Figure 6.5a, the product ions at *m/z* 244.1 and 216.1 correspond to the $[b_2]^+$ ion (loss of $H_2N^+{=}CH_2$) and its dissociation product $[a_2]^+$, respectively with the latter being the base peak in the spectrum. The $[a_3 + H]^{2+}$ ion can also lose neutral $HN{=}CH_2$ (29 Da) to produce dipositive $[b_2 + H]^{2+}$ ion (*m/z* 122.5). Losses of neutral NH_3 and NH_4^+ ion from the $[a_3 + H]^{2+}$ ion lead to the ion pairs at *m/z* 128.5 and 256.0, respectively. Those ions can further lose a CO molecule to produce $[a_3 + H – NH_3 – CO]^{2+}$ (*m/z* 114.5) and $[a_3 + H – NH_4 – CO]^+$ (*m/z* 228.1), respectively. Comparable fragmentation patterns can be found in the CID spectra of $[a_3 + H]^{2+}$ of GWA and AWG (Figure 6.5b and 6.5c). Note that the ion at *m/z* 230 in Figure 6.5b corresponds to the formation of *internal* $[a_2]^+$ ion by the loss of $(H_2N^+{=}CH_2 + CO)$ from the N-terminus. Thus, the ion at *m/z* 216 in Figure 6.5a probably contains a mixture of regular and *internal* $[a_2]^+$ ion as they are isobaric for GWG. The same dissociation channels leading to the losses of NH_3/NH_4^+ and $(NH_3 + CO)/(NH_4^+ + CO)$ from $[a_3 + H]^{2+}$ of GWA and AWG producing ions at *m/z* 135.4, 270.1, 121.5, and 242.1, respectively are observed in Figure 6.5b and 6.5c. The fragmentation pathways of the $[a_3 + H]^{2+}$ ion using GWG as the model system are summarized in Scheme 6.6a.

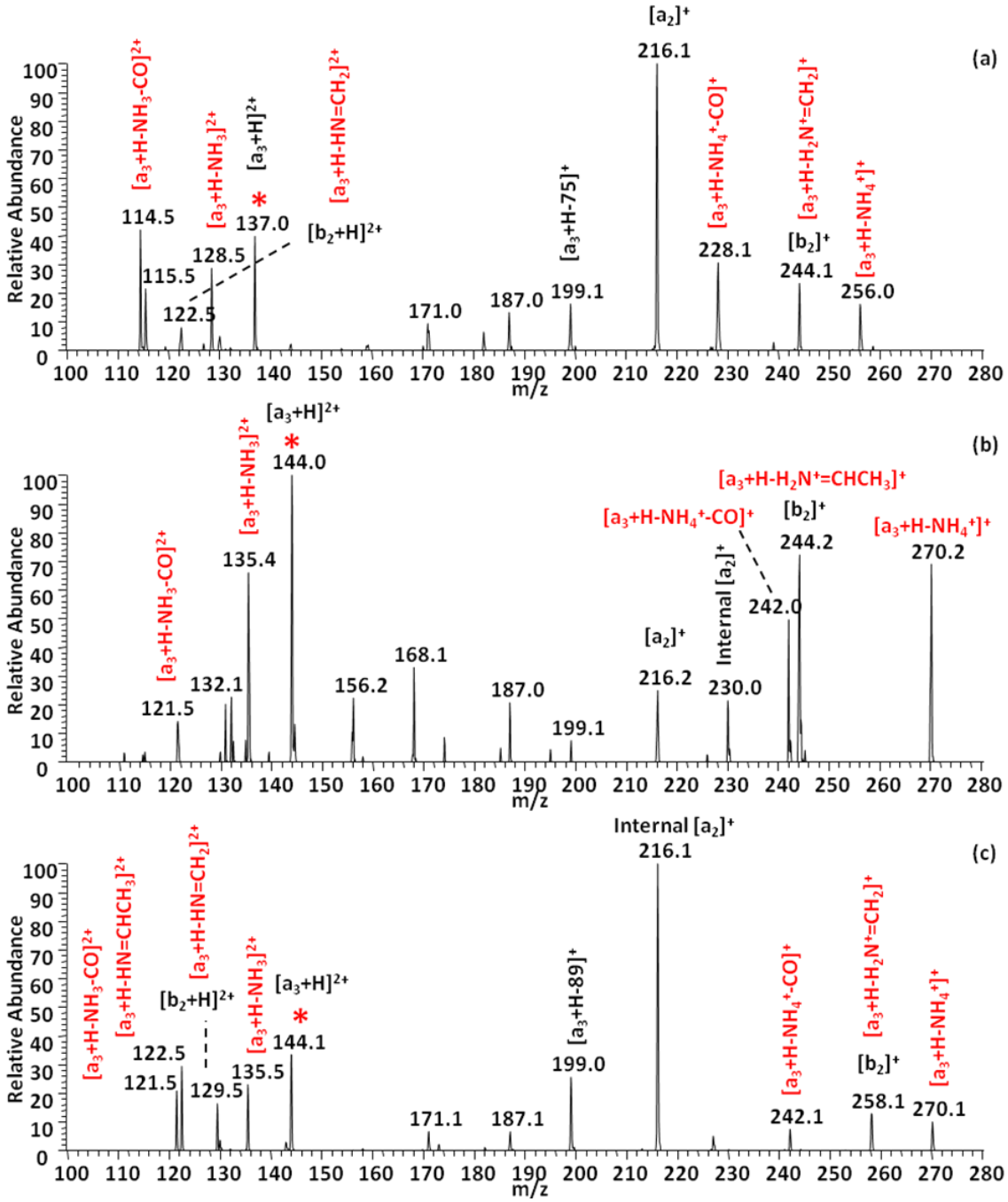

Figure 6.5 CID spectra of (a) $[a_3 + H]^{2+}$ of GWG (*m/z* 137.0, CE=14); (b) $[a_3 + H]^{2+}$ of GWA (*m/z* 144.0, CE=13) and (c) $[a_3 + H]^{2+}$ of AWG (*m/z* 144.0, CE=16). The precursor ion is labelled with an asterisk (*).

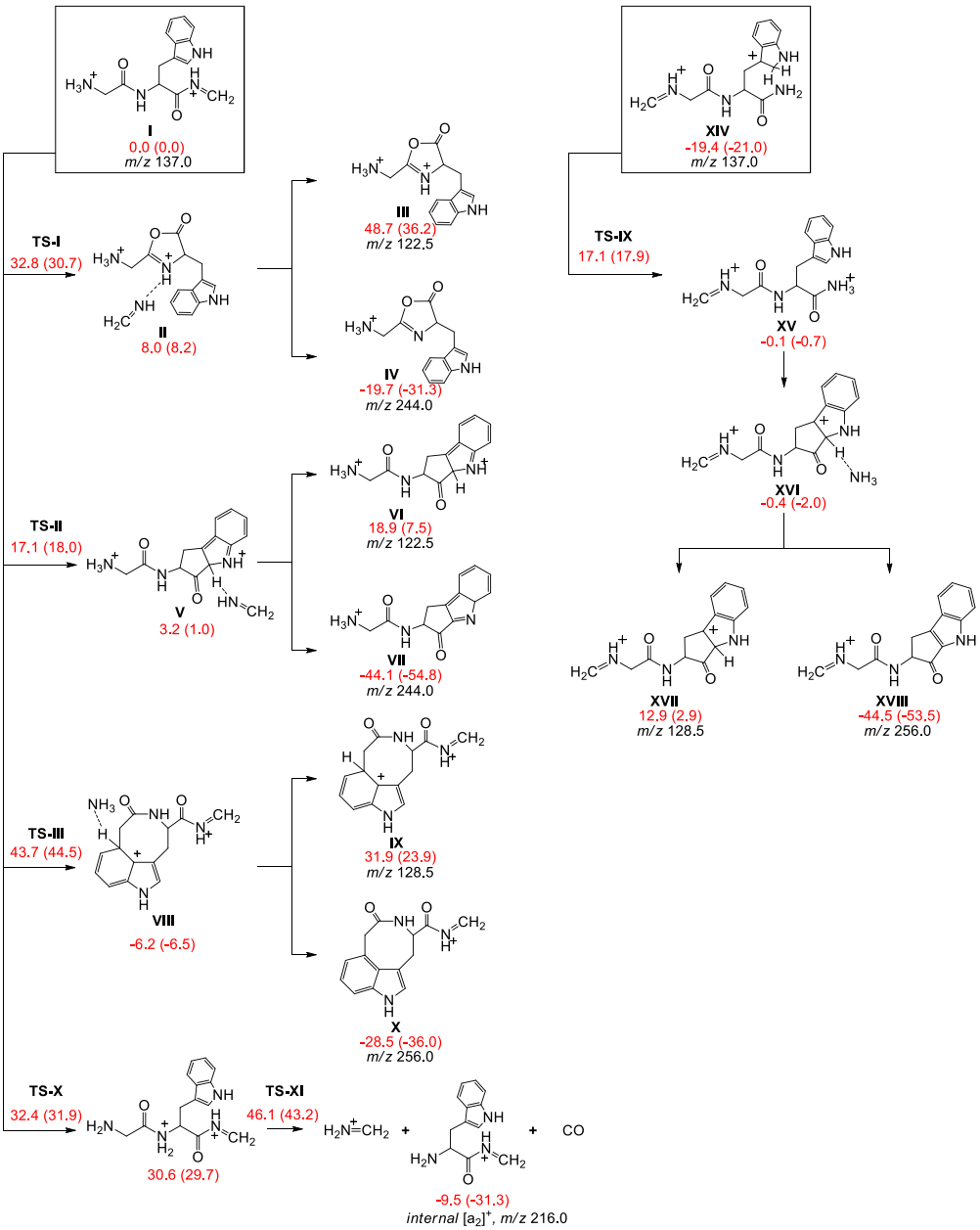

Scheme 6.6 (a) Fragmentation mechanisms of $[a_3 + H]^{2+}$ derived from GWG. Relative enthalpies (ΔH^o_0) and free energies (ΔG^o_{298}, in parenthesis) are calculated at the B3LYP/6-31++G(d,p) level. All energies are in kcal mol^{-1}.

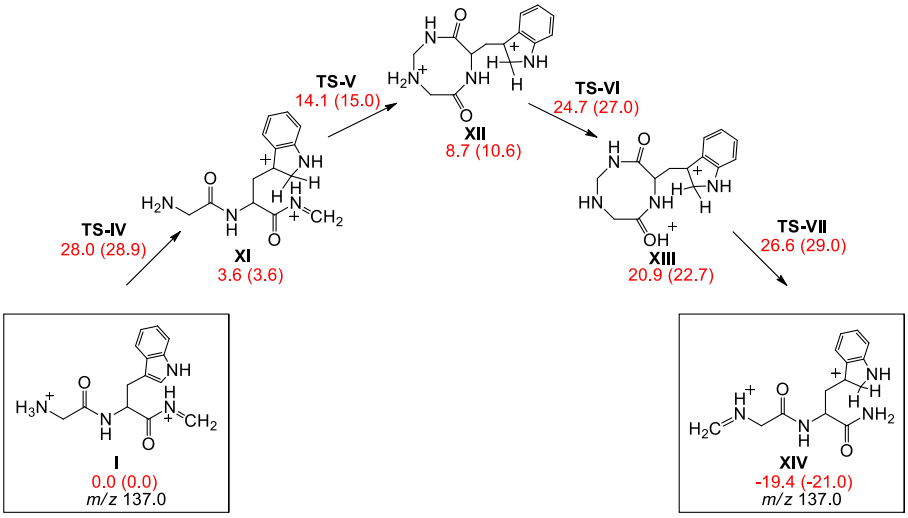

Scheme 6.6 (b) Structural isomerization of $[a_3 + H]^{2+}$ of GWG. Relative enthalpies (ΔH^o_0) and free energies (ΔG^o_{298}, in parenthesis) are calculated at the B3LYP/6-31++G(d,p) level. All energies are in kcal mol^{-1}.

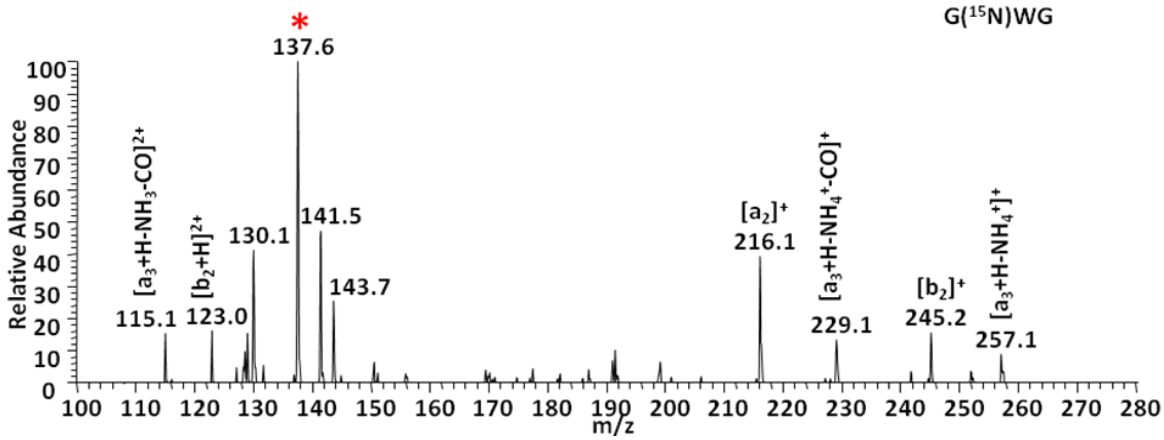

Figure 6.6 CID spectrum of $[a_3 + H]^{2+}$ of G(^{15}N)WG (*m/z* 137.5, CE=14). The precursor ion is labelled with an asterisk (*).

According to the DFT calculations, the energy required to lose $H_2N^+=CH_2$ is 32.8 kcal mol^{-1} (**TS-I**) by using the amide oxygen as an attacking group. Alternatively, by using the indole ring as an attacking group, loss of $H_2N^+=CH_2$ can also occur (**TS-II**) and the energy barrier for the dissociation is smaller, 17.1 kcal mol^{-1}. The $[a_3 + H]^{2+}$ ion can also lose neutral $HN=CH_2$ again from the C-terminus. This results in the formation of the $[b_2 + H]^{2+}$ ion (Structure **VI**) and the energy required for this dissociation is the thermodynamic energies of the products (18.9 kcal mol^{-1}). NH_3 could be lost from the N-terminus of the $[a_3 + H]^{2+}$ ion, facilitated by nucleophilic attack by the indole ring on the α-carbon of the N-terminus (**TS-III**). This will lead to the formation of an 8-membered ring structure (**Structure IX**). If the proton is transferred to the NH_3, loss of NH_4^+ is observed (**Structure X**). The critical barrier for this fragmentation is calculated to be 43.7 kcal mol^{-1}, which is much higher than the barrier to formation of **VI**.

The loss of NH_3 is a common fragmentation pathway in monopositive $[a_n]^+$ ions. Recent research works showed that loss of NH_3 from $[a_n]^+$ ion is mainly from the C-terminus via cyclization [17-19]. It is further supported by ^{15}N labeling experiment and IRMPD spectroscopy. Cyclization of $[a_3 + H]^{2+}$ ions is difficult if both positive charges are on the backbone. However, the presence of the Trp residue in GWG can accommodate one of the positive charges on the aromatic ring *via* proton transfer; the backbone of the peptide then effectively becomes singly charged and cyclization can take place (Scheme 6.6b). Calculations have shown that proton transfer from the N-terminal amine to the C2 position of the indole ring is only 28.0 kcal mol^{-1} (**TS-IV**). It results in one of the positive charges being delocalized onto the aromatic system and the other is on the imine at the C-terminus (Structure **XI**). Nucleophilic attack by the N-terminal amine to the C-terminal imine leads to the cyclic $[a_3 + H]^{2+}$ structure (**XII**). Upon proton transfer and ring opening, another linear structure of $[a_3 + H]^{2+}$ with the imine group at the N-terminus and an

amide in the C-terminus is formed (Structure **XIV**). This imine-amide structure is energetically lower than the initial $[a_3 + H]^{2+}$ structure by 19.4 kcal mol^{-1}.

Proton transfer from the indole ring to the C-terminal amide nitrogen will produce a protonated amide (Structure **XV**) that can easily lose NH_3 via nucleophilic attack by the indole ring (**TS-IX**). If the positive charge is transferred to NH_3, loss of NH_4^+ will be observed. The critical barrier to lose NH_3/NH_4^+ is 17.1 kcal mol^{-1} relative to $[a_3 + H]^{2+}$; thus, loss of NH_3/NH_4^+ from the C-terminus via cyclization is energetically more favourable.

Isotopically labeled peptide, G(^{15}N)WG, where the N-terminal amine is labeled by ^{15}N, has been synthesized to examine the pathway leading to the loss of NH_3 from the $[a_3 + H]^{2+}$ ion. The CID spectrum (Figure 6.6) shows that the ^{15}N-label is retained in the product ions of $[a_3 + H - NH_4]^+$ and $[a_3 + H - NH_4 - CO]^+$ indicating that loss of NH_3 does not involve the amine on the N-terminus. This result is in an excellent agreement with our theoretical predictions. Formation of the *internal* $[a_2]^+$ ion is facilitated by a 1,4-proton transfer from the N-terminus to the first amide nitrogen followed by the cleavage of the first amide bond (**TS-XI**). A similar mechanism has been found in the fragmentation of $[a_2 + H]^{2+}$ of GGA. The energy barrier to this dissociation channel is calculated to be 46.1 kcal mol^{-1}.

d) $[a_3+H]^{2+}$ ions of PWG

The previous sections have shown that the $[a_3 + H]^{2+}$ ions can be generated in significant abundance with the proline residue at the N-terminus. In addition, the presence of the tryptophan residue in the $[a_3 + H]^{2+}$ ion can lead to dissociation giving both monopositive and dipositive product ions. Therefore, it is interesting to study the fragmentation of the $[a_3 + H]^{2+}$ ion which contains both Pro and Trp residues. Figure 6.7 illustrates the CID spectrum of the $[a_3 + H]^{2+}$ ion derived from PWG.

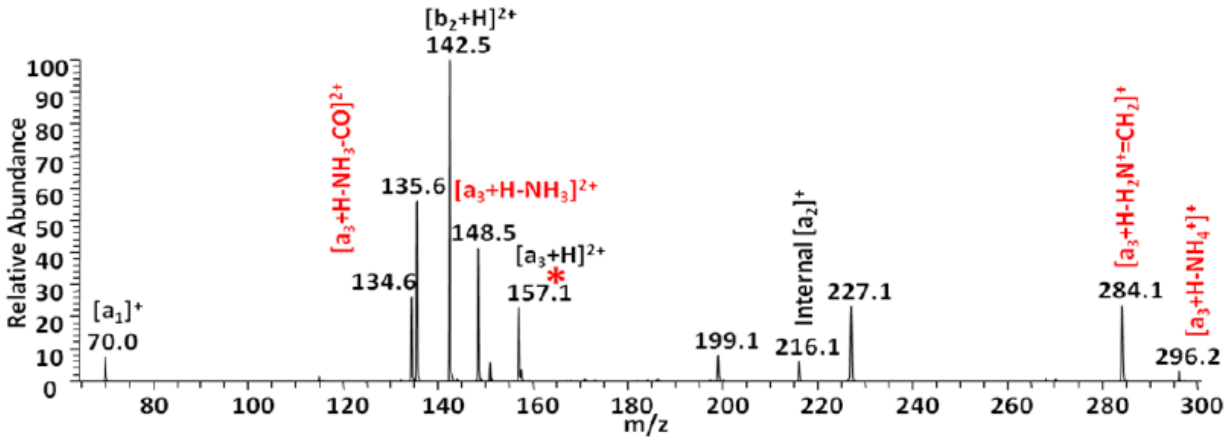

Figure 6.7 CID spectrum of $[a_3 + H]^{2+}$ of PWG, (*m/z* 157.1, CE=16).The precursor ion is labelled with an asterisk (*).

The high abundance of $[b_2 + H]^{2+}$ (*m/z* 142.5) and moderate amount of $[b_2]^+$ (*m/z* 284.1) suggests the cleavage of the second peptide bond leading to the loss of $NH{=}CH_2/NH_2^+{=}CH_2$ from the C-terminus. More interesting are the fragment ions related to the loss of NH_3/NH_4^+ from the $[a_3 + H]^{2+}$ ion, *i.e.*, ions at *m/z* 296.2 (loss of NH_4^+), *m/z* 148.5 (loss of NH_3), *m/z* 134.6 (loss of NH_3 + CO). Obviously, loss of NH_3 cannot occur at the N-terminus from PWG. These losses must be the consequence of the cyclization of the $[a_3 + H]^{2+}$ ion and the formation of an imine-amide structure (Scheme 6.7). Upon protonation on the amide, loss of NH_3/NH_4^+ can be accomplished by a similar mechanism as described in Scheme 6.6.

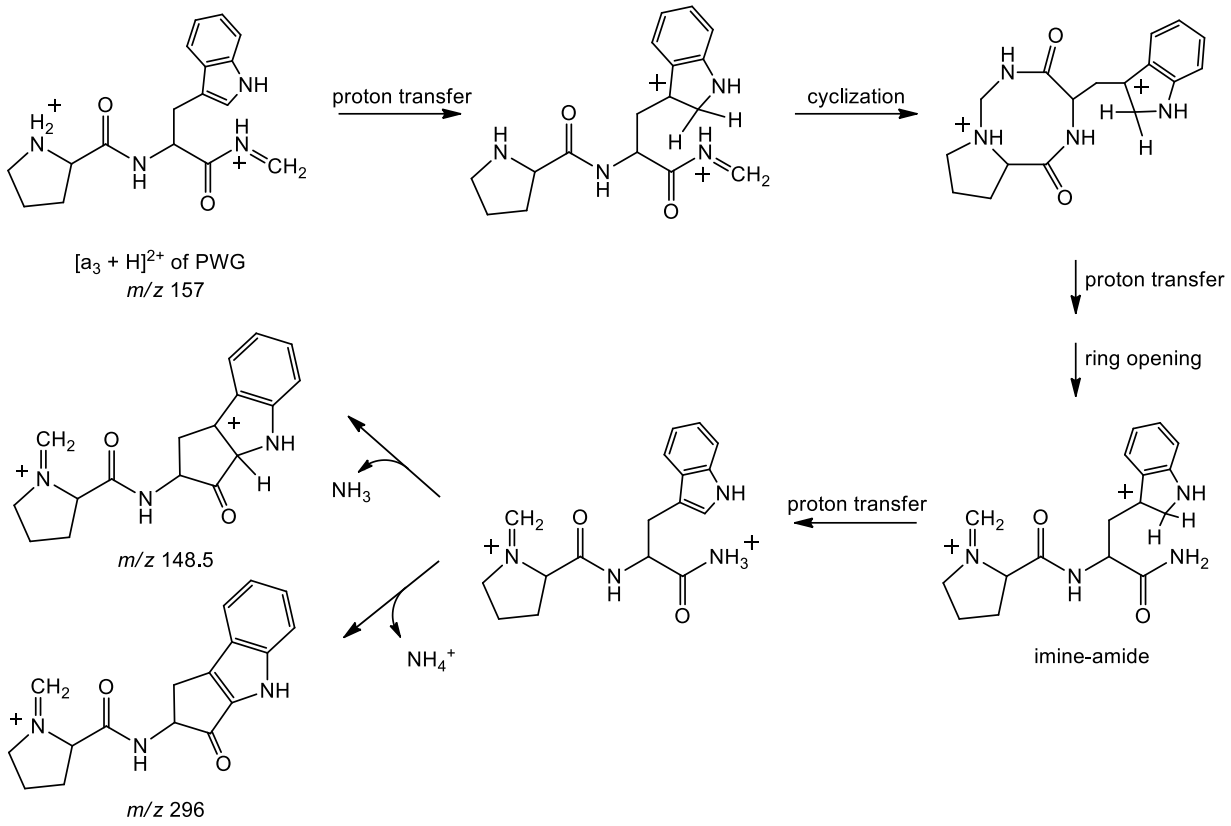

Scheme 6.7 Structural isomerization of $[a_3 + H]^{2+}$ of PWG.

e) $[a_2+H]^{2+}$ ions of PG and PA

The observation of $[a_2 + H]^{2+}$ is more challenging than that of $[a_3 + H]^{2+}$ due to the stronger Coulombic repulsion of the two positive charges in a smaller molecule. In the previously reported example [15], the stability of the $[a_2 + H]^{2+}$ ion derived from PP was attributed to the pyrrolidine rings at both ends of the molecule. Here, we have successfully observed even smaller $[a_2 + H]^{2+}$ ions derived from PG and PA.

These $[a_2 + H]^{2+}$ ions were generated from CID of the $[Ce(PG)(CH_3CN)]^{3+}$ and $[Ce(PA)(CH_3CN)]^{3+}$ complexes. Note that the $[a_2 + H]^{2+}$ of PG was also produced in the CID of the yttrium(III) complex, $[Y(PG)(CH_3CN)]^{3+}$. The fragmentation patterns of these $[a_2 + H]^{2+}$ have also been investigated by tandem mass spectrometry. Figures 6.8a and 6.8b display the CID spectra of $[a_2 + H]^{2+}$ of PG and PA, respectively. The $[a_1]^+$ ion at *m/z* 70 is the major product ion

in the spectra in both cases, due to cleavage of the C_α–C bonds. The low abundance of the monopositive $[a_2 + H]^+$ ion in the spectrum is possibly formed via the loss of a proton to the collision gas.

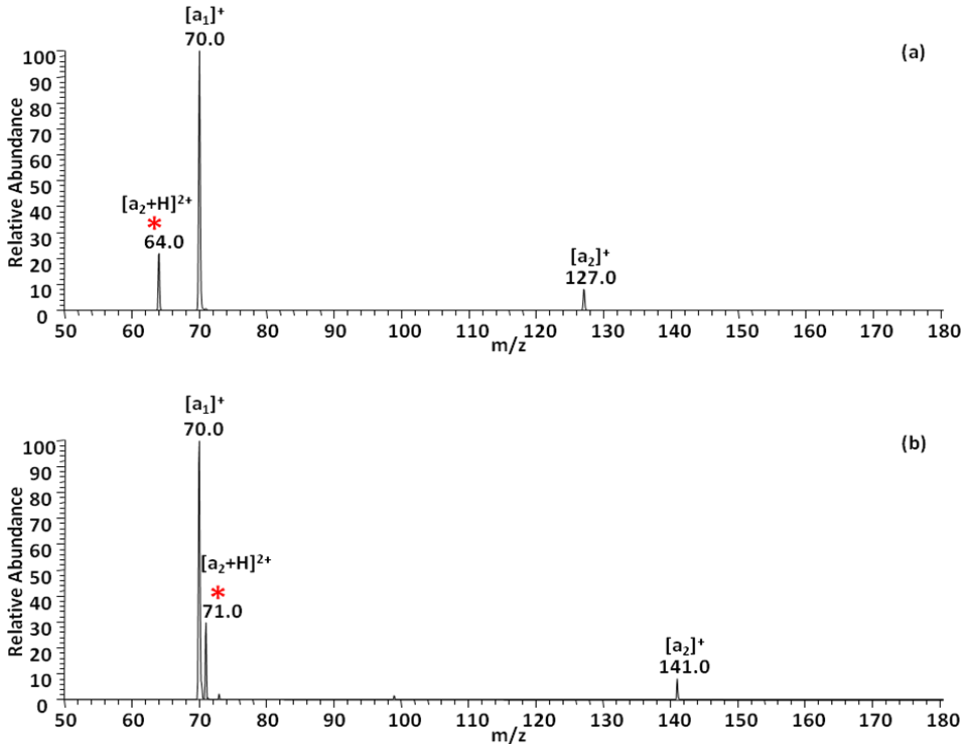

Figure 6.8 CID spectra of (a) $[a_2 + H]^{2+}$ of PG (*m/z* 64.0) and (b) $[a_2 + H]^{2+}$ of PA (*m/z* 71.0). The precursor ion is labelled with an asterisk (*).

f) Summary of dipositively charged $[a_n + H]^{2+}$ ions

Table 6.1 summarizes the dissociation products of the $[a_n + H]^{2+}$ (n = 2 or 3) from dipeptides and tripeptides. In the fragmentations of $[a_3 + H]^{2+}$, bond cleavages usually occurr at the second amide bonds resulting in the formations of monopositive $[b_2]^+$ and $[a_1]^+$ ions. Calculation results show that the $[b_2]^+$ ion is a mixture of oxazolone and ketene structures. Bond cleavage in the first amide bond of $[a_3 + H]^{2+}$ is also possible and it will produce $[a_1]^+$ and *internal* $[a_2]^+$ ions. The presence of Trp in the $[a_3 + H]^{2+}$ produces both monopositive and dipositive fragment ions.

Table 6.1 Relative abundance (%) of fragmentation products of $[a_n+H]^{2+}$

$[a_3+H]^{2+}$ from tripeptide				
Tripeptides	*$[b_2]^+$*	*$[a_2]^+$*	*$[a_1]^+$*	*Other*
PGG	100			
PAA	100	22		
PPP	33	42	100	
GPG	100			
PGA	100	24	12	
GPA	100	27	18	
GGA	12	100		Internal $[a_2]^+$ *m/z* 101 , (14%)
GWG	24	100 [(a)]		$[a_3+H-NH_3]^{2+}$ (30%) and $[a_3+H-NH_4^+]^+$ (18%); $[a_3+H-HN=CH_2]^{2+}$ (8%) and $[a_3+H-H_2N^+=CH_2]^+$ (24%); $[a_3+H-NH_3-CO]^{2+}$ (42%) and $[a_3+H-NH_4^+-CO]^+$ (31%);
GWA	70	24		$[a_3+H-NH_3]^{2+}$ (63%) and $[a_3+H-NH_4^+]^+$ (66%); $[a_3+H-H_2N^+=CHCH_3]^+$ (70%); $[a_3+H-NH_3-CO]^{2+}$ (13%) and $[a_3+H-NH_4^+-CO]^+$ (48%);
AWG	13	100		$[a_3+H-NH_3]^{2+}$ (23%) and $[a_3+H-NH_4^+]^+$ (11%); $[a_3+H-HN=CHCH_3]^+$ (29%); $[a_3+H-H_2N^+=CHCH_3]^+$ ($[b_2]^+$,13%) and $[a_3+H-NH_3-CO]^{2+}$ (21%) and $[a_3+H-NH_4^+-CO]^+$ (8%);
PWG	25		8	(Internal $[a_2]^+$ *m/z* 216)(7%) $[a_3+H-NH_3]^{2+}$ (42%) ; $[a_3+H-HN=CH_2]^{2+}$ (100%) and $[a_3+H-H_2N^+=CH_2]^+$ (24%); $[a_3+H-NH_3-CO]^{2+}$ (26%);
PGW			11	(Internal $[a_2]^+$ *m/z* 216) (100%); (*m/z* 198) (20%)
PHG	100			$[b_2+H]^{2+}$(55%)
GKG		100		
GRG	6	100		
GGH	27			(Internal $[a_1]^+$ *m/z* 110) (27%); (Internal $[a_2]^+$) (*m/z* 167) (100%);
$[a_2+H]^{2+}$ from dipeptide				
Dipeptide		*$[a_2]^+$*	*$[a_1]^+$*	*Other*
PG		9	100	
PA		7	100	
GH				(Internal $[a_1]^+$*m/z* 110.0) (100%)
HG			100	
PP			100	
$[a_2+H]^{2+}$ from tripeptide				
Tripeptide			*$[a_1]^+$*	*Other*
PWG			82	(Internal $[a_1]^+$ *m/z* 159.1) (100%); (*m/z* 187.1) (100%)
PHG			32	(Internal $[a_1]^+$ *m/z* 110.0) (100%);

[(a)] $[a_2]^+$ of GWG is probably a mixture of $[a_2]^+$and internal $[a_2]^+$

Losses of NH_3 and NH_4^+ are common fragmentation pathways and ^{15}N-labeling experiments showed that ammonia loss is not from the N-terminus amine but from the C-terminal residue. This finding is also supported by theoretical calculations.

6.2.2 Chemistry of $[b_3 + H]^{2+}$ and $[b_2 + H]^{2+}$ ions

a) $[b_3+H]^{2+}$ ions of PGG

We have shown that CID of $[Ce(PGG)(CH_3CN)_n]^{3+}$ (n = 1 or 2) can produce the $[a_3 + H]^{2+}$ ion of PGG. Here, we report the results of fragmentation of $[Ce\,(PGG)]^{3+}$. Figure 6.9a shows the CID spectrum of $[Ce(PGG)]^{3+}$. The major product ion at *m/z* 106.5 corresponds to the $[b_3 + H]^{2+}$ ion of PGG, the first example of a dipositive b-type ion without a basic residue. The ion at *m/z* 83.5 is its subsequent product ion, $[b_3 + H - H_2O - CO]^{2+}$ (*vide infra*). Formation of $[a_3 + H]^{2+}$ of PGG at *m/z* 92.5 is also observed, but at relatively lower abundance.

$$[Ce(PGG)]^{3+} \longrightarrow CeO^+ + [b_3 + H]^{2+}$$

m/z 123.0 *m/z* 156 *m/z* 106.5

Figure 6.9 (b) shows the multi-stage mass spectrum of the $[b_3 + H]^{2+}$ ion (*m/z* 106.5). As we have already seen in the CID spectra of $[Ce(PGG)]^{3+}$, $[b_3 + H - CO - H_2O]^{2+}$ at *m/z* 83.5 is the major product ion. The fragments of $[a_1]^+$ (*m/z* 70), and the ions at *m/z* 115, 157 and 98 are also found. The structure of the $[b_3 + H]^{2+}$ is unclear, but as there is little loss of CO, it should be different from the conventional $[b_3]^+$, which is an oxazolone.

In order to deduce the structure and fragmentation mechanisms of this unprecedented $[b_3 + H]^{2+}$ ion of PGG, two isotopically labeled peptides, *i.e.* P(^{18}O)GG and PG(^{18}O)G have been synthesized (the first and second amide oxygen were labeled with ^{18}O, respectively). These labeled tripeptides were then complexed with Ce^{3+} and fragmented to generate the $[b_3 + H]^{2+}$ ions. The CID spectra of these $[b_3 + H]^{2+}$ ions are displayed in Figure 6.10.

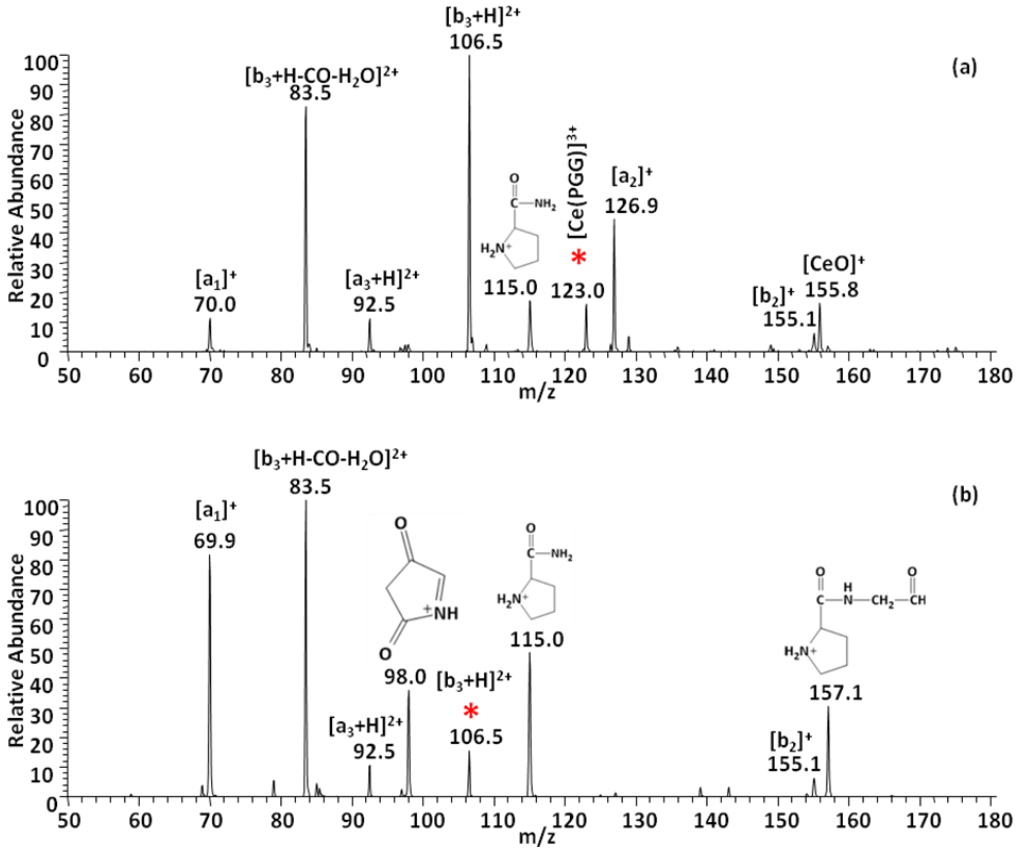

Figure 6.9 CID spectra of (a) $[Ce(PGG)]^{3+}$ (*m/z* 123.0, CE=11.5) and (b) $[b_3 + H]^{2+}$ of PGG (*m/z* 106.5, CE=17). The precursor ion is labelled with an asterisk (*).

Figures 6.10 (a) and 6.10 (b) show the CID spectra of $[b_3 + H]^{2+}$ of P(^{18}O)GG and PG(^{18}O)G, respectively. The precursor ions are at *m/z* 107.5 in both spectra indicating that the isotope labels are retained in the formation of $[b_3 + H]^{2+}$ ions. In other words, the carboxyl oxygen at the C-terminus is lost in the formation of the $[b_3 + H]^{2+}$ ion.

$$[Ce(P(^{18}O)GG)]^{3+} \longrightarrow CeO^{+} + [b_3(^{18}O) + H]^{2+}$$

m/z 123.7 *m/z* 156 *m/z* 107.5

$$[Ce(PG(^{18}O)G)]^{3+} \longrightarrow CeO^{+} + [b_3(^{18}O) + H]^{2+}$$

m/z 123.7 *m/z* 156 *m/z* 107.5

In addition, the $[b_3 + H - CO - H_2O]^{2+}$ ion of P(^{18}O)GG has *m/z* 84.5 (Figure 6.10a) while that of PG(^{18}O)G is shifted to *m/z* 83.5 (Figure 6.10b). It implies that the losses of H_2O and CO in the CID of $[b_3 + H]^{2+}$ originated from the two glycine residues, *i.e.*, the amide oxygen in proline is intact. Obviously, the $[b_3 + H]^{2+}$ ion does not have an oxazolone structure as it does not lose *only* CO. Also the corresponding $[a_3 + H]^{2+}$ ion of PGG does not lose a water molecule (Figure 6.2). A possible structure of the $[b_3 + H]^{2+}$ ion is suggested below (structure **XIX**); this features a pyrrolidine-2,4-dione at the C-terminus. This $[b_3 + H]^{2+}$ ion is possibly generated by the enol form of PGG complexing with the Ce^{3+} ion.

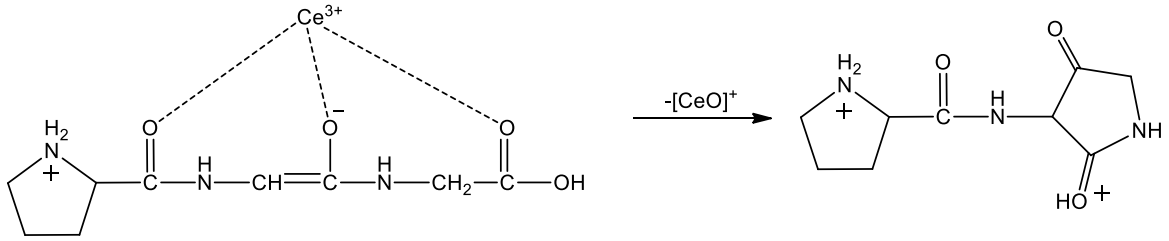

(enol form of PGG in complex with Ce^{3+}) $[b_3 + H]^{2+}$ of PGG, **XIX**

Possible fragmentation mechanisms of the $[b_3 + H]^{2+}$ ion of PGG have been studied by DFT calculations and are summarized in Scheme 6.8. In order to lose CO and H_2O from structure **XIX**, the proton at the proline residue migrates to the first amide oxygen (*pathway A*). This is then followed by nucleophilic attack by the N-terminal amine on the protonated amide carbon at the C-terminus resulting in the formation of a tricyclic structure (**XXI**) and loss of a H_2O molecule concurrently. The energy barrier to loss of water molecule is 75.8 kcal mol^{-1}. Structure **XXI** can further lose CO to produce an imine structure **XXII** with the energy barrier of 70.0 kcal mol^{-1}. Note that the amide oxygen of proline is not lost in the dissociation mechanism which is consistent with the labeling experiment. As the barrier for the loss of H_2O is higher than that for loss of CO, only the ion $[b_3 + H - CO - H_2O]^{2+}$ (*m/z* 83.5) would be observed with significant amounts in the CID spectrum (Figure 6.9b).

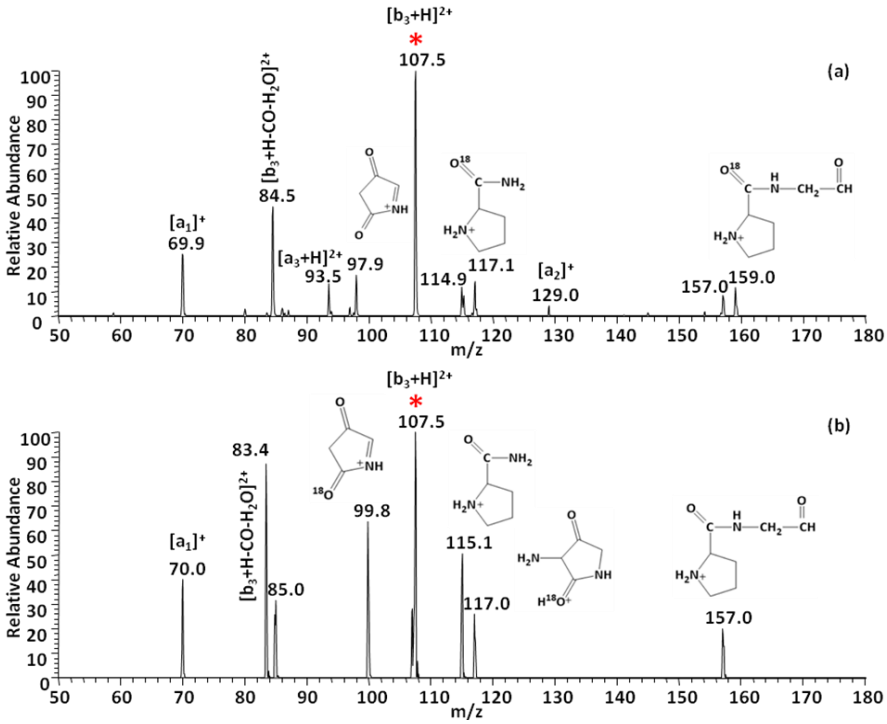

Figure 6.10 CID spectra of (a) $[b_3 + H]^{2+}$ of P(^{18}O)GG (*m/z* 107.5 CE=14) and (b) $[b_3 + H]^{2+}$ of PG(^{18}O)G (*m/z* 107.5, CE=14). The precursor ion is labelled with an asterisk (*).

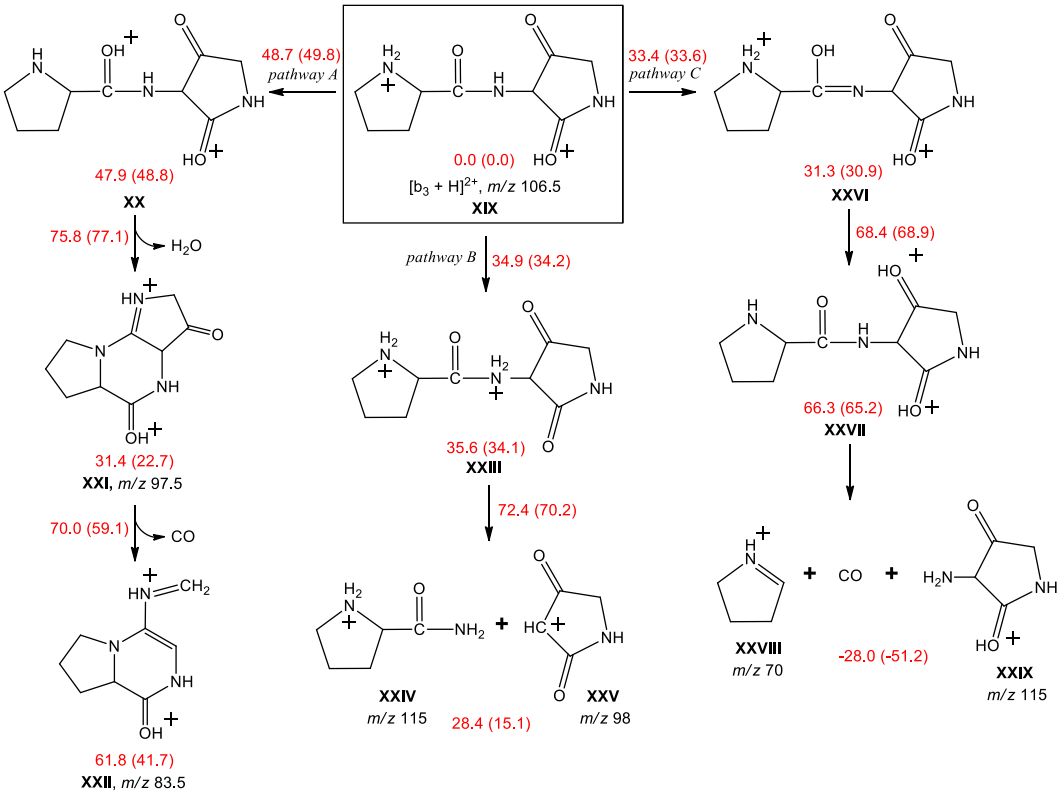

Scheme 6.8 Fragmentation mechanisms of $[b_3 + H]^{2+}$ of PGG. Relative enthalpies (ΔH^o_0) and free energies (ΔG^o_{298}, in parenthesis) are calculated at the B3LYP/6-31++G(d,p) level. All energies are in kcal mol^{-1}.

Structure **XIX** can also undergo 1,4-proton transfer from the amide oxygen to the first amide nitrogen (Structure **XXIII**, *pathway B*). Cleavage of the N–C_α bond (energy barrier of 72.4 kcal mol^{-1}) will produce monopositive proline amide (**XXIV**) and a five-membered ring structure (**XXV**) at *m/z* 115 and 98, respectively.

By undergoing several steps of proton migration (*pathway C*), structure **XXVII** can be formed where both protons are located on the C-terminal pyrrolidine-2,4-dione. Finally, 1,4-proton transfer from the carbonyl oxygen to the first amide nitrogen will break the C_α–C and C–N bonds at the same time to generate ions at *m/z* 70 and 115 (structures **XXVIII** and **XXIX**).

b) $[b_3+H]^{2+}$ ions of PWG and PGW

Apart from the $[b_3 + H]^{2+}$ ion of PGG, $[b_3 + H]^{2+}$ ions of PWG can also be observed in the CID of $[Ce(PWG)]^{3+}$. Isolation and CID of the $[b_3 + H]^{2+}$ ion of PWG (Figure 6.11a) shows similar fragmentation patterns to that of $[b_3 + H]^{2+}$ of PGG. The ion at *m/z* 148.1, the major fragmentation product, corresponds to the loss of (H_2O + CO) while no $[a_3 + H]^{2+}$ ion is observed in the spectrum. It reveals the $[b_3 + H]^{2+}$ ion of PWG has similar structural feature (pyrrolidine-2,4-dione) as that of PGG. The energy-resolved diagram of $[b_3 + H]^{2+}$ of PWG (Figure 6.12) shows the ion at *m/z* 148 has the earliest onset. It again implies the loss of water and CO occurs simultaneously. This result can be explained by our mechanism proposed in Scheme 6.8 (*pathway A*) that the energy barrier in the dissociation of H_2O is higher than the subsequent fragmentation barrier (loss of CO). Thus, water and CO are lost concurrently from the $[b_3 + H]^{2+}$ ion.

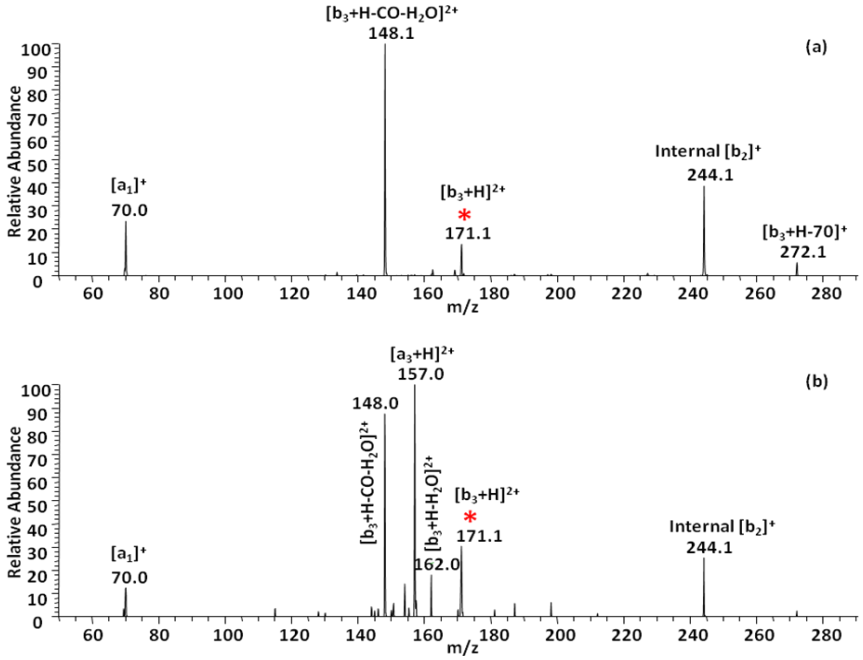

Figure 6.11 CID spectra of (a) $[b_3 + H]^{2+}$ of PWG (*m/z* 171.1, CE=19) and $[b_3 + H]^{2+}$ of PGW (*m/z* 171.1, CE=23). The precursor ion is labelled with an asterisk (*).

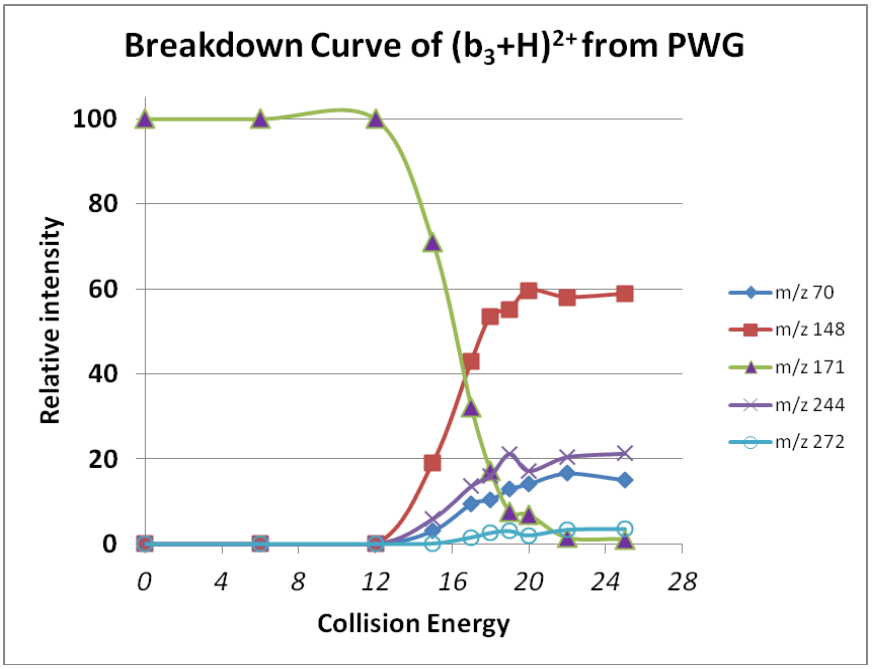

Figure 6.12 Breakdown curve for the $[b_3 + H]^{2+}$ ion of PWG (*m/z* 171) derived from $[Ce(PWG)]^{3+}$.

Interestingly, when the Trp residue is at the C-terminus in the $[b_3 + H]^{2+}$ ion, loss of CO (*m/z* 157) is the most abundant product ion, although the losses of ($CO + H_2O$) are still in high abundance (Figure 6.11b). One possible explanation is that the $[b_3 + H]^{2+}$ ion isolated in the CID spectrum of PGW is a mixture.

In addition to structure **A** (Scheme 6.9) featuring a pyrrolidine-2,4-dione in the C-terminus, the $[b_3 + H]^{2+}$ ion of PGW may contain an oxazolone structure, structure **B** or a tricyclic structure, structure **C**. The latter two structures can lose CO very easily. Thus, abundant $[a_3 + H]^{2+}$ ion is observed.

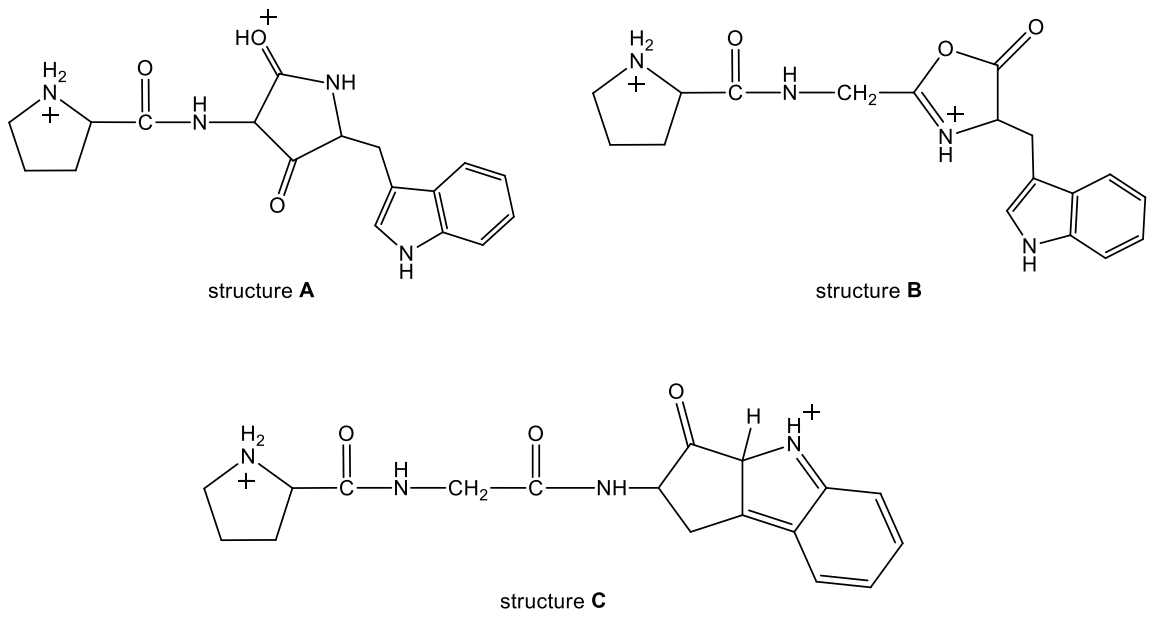

Scheme 6.9 Possible structures for the $[b_3 + H]^{2+}$ ion of PGW.

c) $[b_3+H]^{2+}$ ions of PPP

Unlike the $[b_3 + H]^{2+}$ ions from PGG and PWG, the dipositive b_3 ion of PPP (derived from $[Ce(PPP)]^{3+}$ does not lose H_2O and CO easily. Instead, the $[a_1]^+$ ion at *m/z* 70 is the most abundant product ion (Figure 6.13). Also the $[a_2]^+$ (*m/z* 167) and $[b_2]^+$ ions (*m/z* 195) are in moderate amounts. A plausible fragmentation mechanism is summarized in Scheme 6.10.

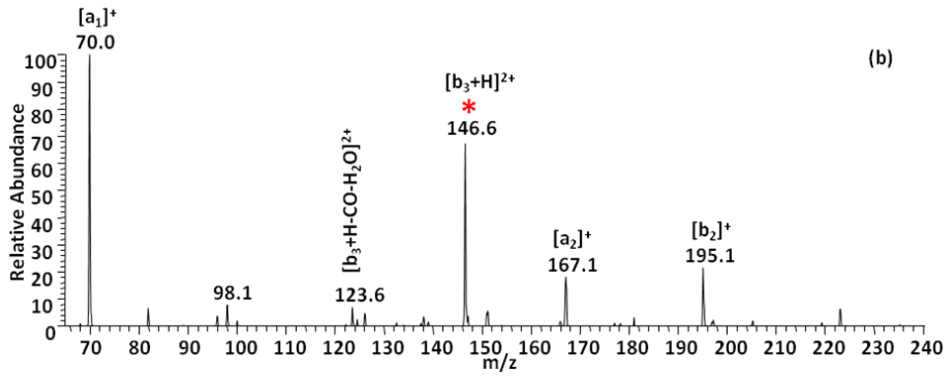

Figure 6.13 CID spectrum of $[b_3 + H]^{2+}$ of PPP (*m/z* 146.6, CE=17). The precursor ion is labelled with an asterisk (*).

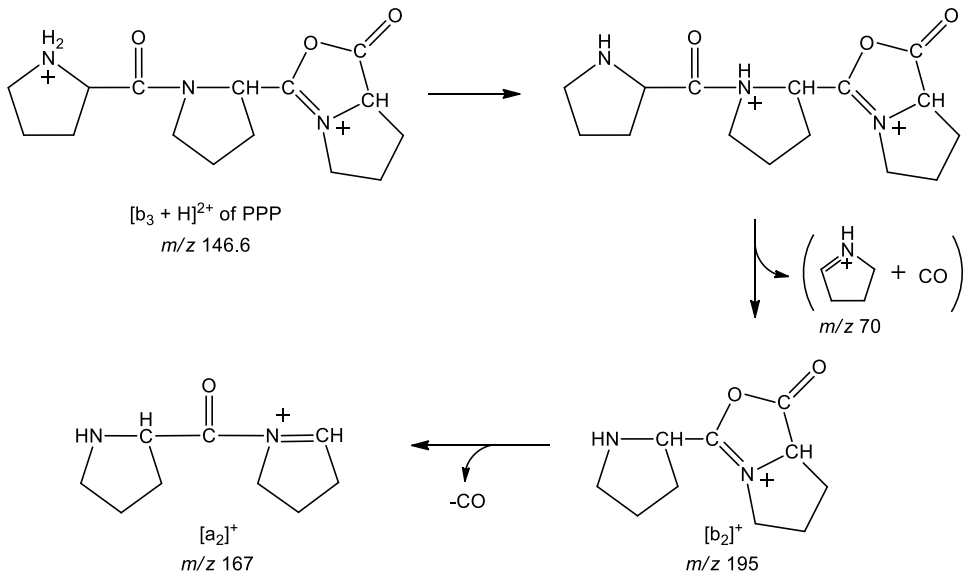

Scheme 6.10 Proposed fragmentation mechanism for the $[b_3 + H]^{2+}$ ion of PPP.

The low abundance of $[b_3 + H - CO - H_2O]^{2+}$ in the CID spectrum suggests the $[b_3 + H]^{2+}$ ion does not have the pyrrolidine-2,4-dione structure at the C-terminus. It is probably due to the bulky backbone of proline residue which prohibits the formation of pyrrolidine-2,4-dione. In contrast, the oxazolone structure can explain the fragmentation channels easily (Scheme 6.10). Proton migration from the N-terminal amine to the first amide nitrogen weakens the first amide bond. The protonated amide can lose CO and the N-terminal imine ($[a_1]^+$ ion at *m/z* 70) resulting in the formation of monopositive internal $[b_2]^+$ ion at *m/z* 195. Further loss of CO from the oxazolone ring leads to the $[a_2]^+$ ion at *m/z* 167.

d) $[b_3+H]^{2+}$ ions of PHG and GGH

The $[b_3 + H]^{2+}$ ion of PHG can also be observed in the CID of $[Ce(PHG)]^{3+}$. The presence of the basic His residue in the peptide can stabilize the dipositive ion better as the imidazole side chain can carry one of the positive charges. CID of the $[b_3 + H]^{2+}$ ion of PHG gives only one fragment ion at *m/z* 123.6 which corresponds to the loss of H_2O and CO (Figure 6.14a). This result indicates the dipositive ion probably has the pyrrolidine-2,4-dione structure (Scheme 6.11).

The $[b_3 + H]^{2+}$ ion of PHG can also be generated from dipositive $[PHGG + 2H]^{2+}$ ion under CID conditions. The loss of Gly residue from the C-terminus can produce the isomeric $[b_3 + H]^{2+}$ ion of PHG at *m/z* 146.5. Tandem MS experiments show that this new $[b_3 + H]^{2+}$ ion loses CO to produce $[a_3 + H]^{2+}$ ion as the major pathway (Figure 6.14b) and no H_2O loss is observed. The result indicates that the $[b_3 + H]^{2+}$ ion derived from $[PHGG + 2H]^{2+}$ possesses the conventional oxazolone structure (Scheme 6.11). Thus, it is not surprising that it shows different fragmentation patterns from the $[b_3 + H]^{2+}$ ion derived from $[Ce(PHG)]^{3+}$ as the latter has a pyrrolidine structure.

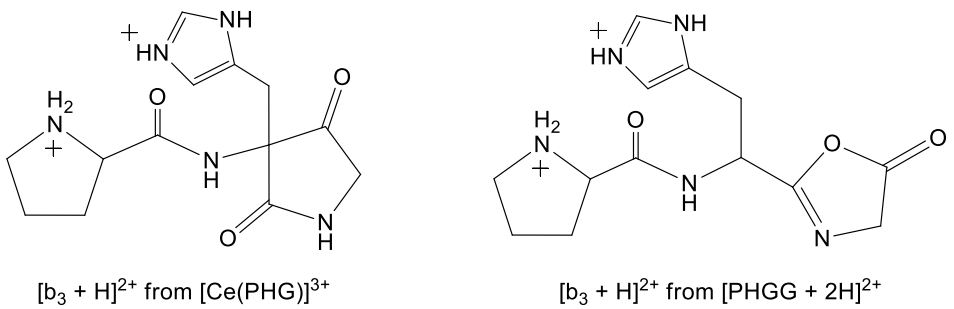

Scheme 6.11 structures of $[b_3 + H]^{2+}$ of PHG.

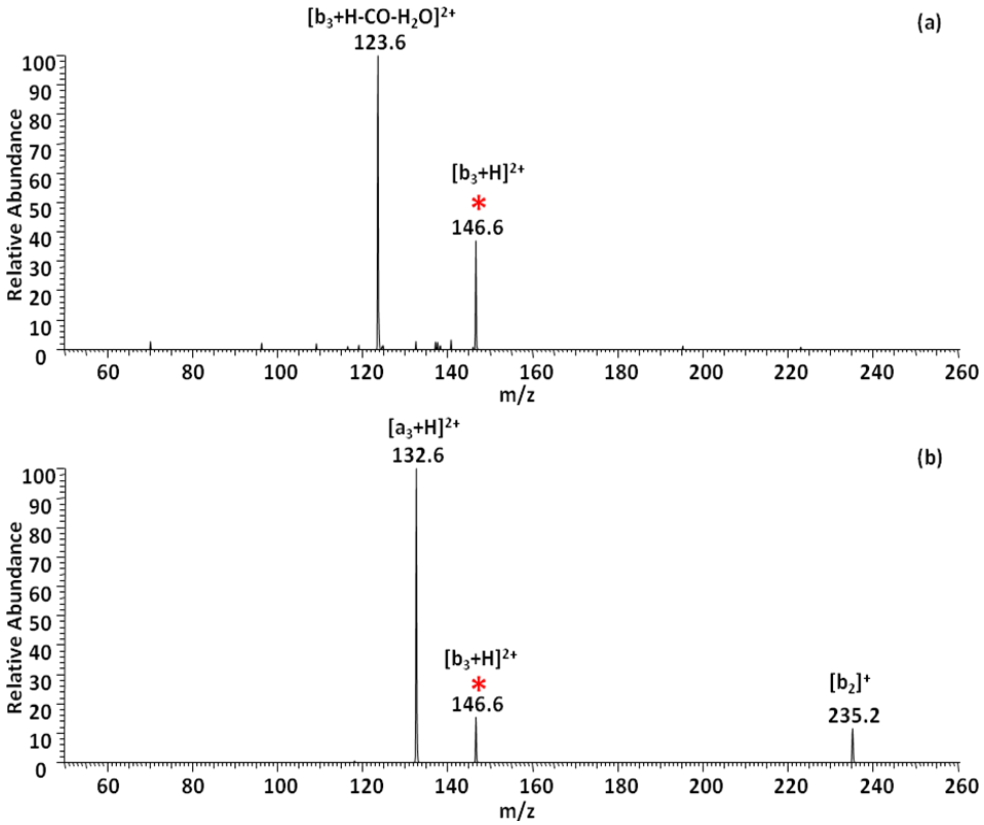

Figure 6.14 CID spectra of (a) $[b_3 + H]^{2+}$ (*m/z* 146.5) derived from $[Ce(PHG)]^{3+}$, CE=13.5 and (b) $[b_3 + H]^{2+}$ (*m/z* 146.5) derived from $[PHGG + 2H]^{2+}$, CE=12. The precursor ion is labelled with an asterisk (*).

Thus far, all the $[b_3 + H]^{2+}$ ions generated have a proline residue at the N-terminus. Here we report the CID spectrum of the dipositive $[b_3 + H]^{2+}$ without a Pro residue, *i.e.* $[b_3 + H]^{2+}$ of GGH. The high proton affinity of the His residue is capable of stabilizing the dipositive ion by delocalizing one of the positive charges onto the imidazole ring. The CID spectrum of the $[b_3 + H]^{2+}$ of GGH is displayed in Figure 6.15. Unlike most of the dipositive $[b_3 + H]^{2+}$ ions, loss of $(CO + H_2O)$ is not observed in the spectrum. In fact, the fragmentation chemistry of this $[b_3 + H]^{2+}$ ion resembles the conventional b-type ion chemistry by loss of CO to form the $[a_3 + H]^{2+}$ as the major product ion. The imidazole can facilitate nucleophilic attack on the carbon of the protonated amide to induce peptide bond cleavage to generate non-oxazolone $[b]^+$ ion. Thus, the $[b_3 + H]^{2+}$ of GGH should have similar structural features. The details of the fragmentation mechanism are summarized in Scheme 6.12.

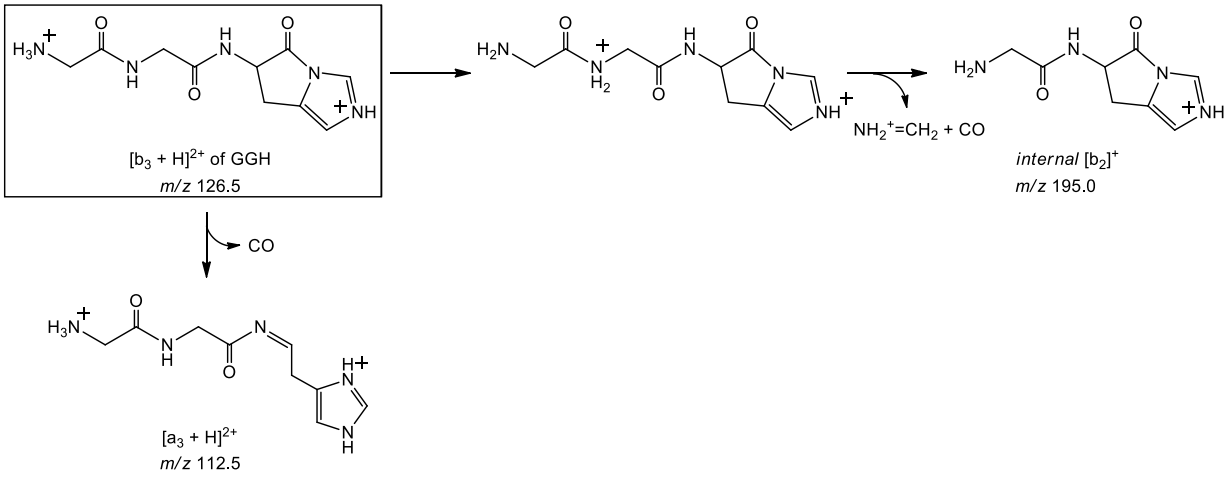

Scheme 6.12 Proposed fragmentation mechanisms for the $[b_3 + H]^{2+}$ of GGH.

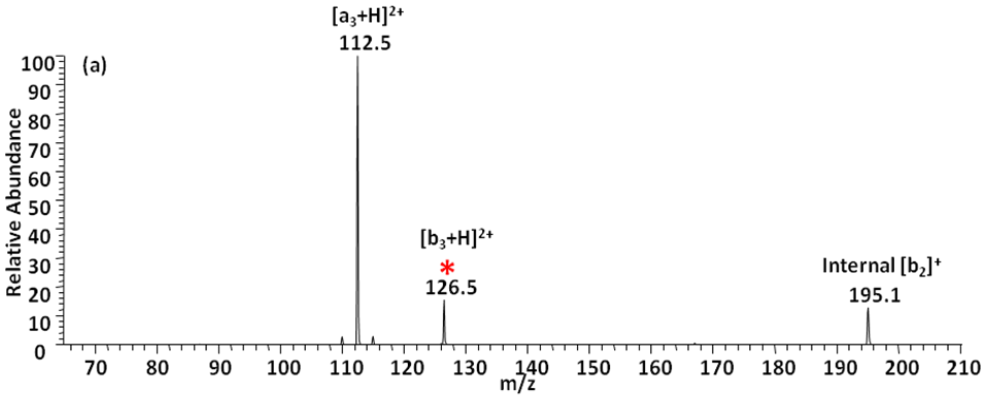

Figure 6.15 CID spectrum of $[b_3 + H]^{2+}$ of GGH (*m/z* 126.5, CE=12). The precursor ion is labelled with an asterisk.

Table 6.2 Relative abundance (%) of fragmentation products of $[b_n + H]^{2+}$

$[b_3+H]^{2+}$ from tripeptide			
Tripeptides	*$[a_3+H]^{2+}$*	*$[b_3+H\text{-}CO\text{-}H_2O]^{2+}$*	*Other*
PGG	10	100	$[a_1]^+$ (81%); *m/z* 115(49%); m/z *98* (36%); m/z *157* (30%); m/z *155* (6%)
PWG		100	$[a_1]^+$ (26%); Internal $[b_2]^+$ (*m/z* 244 32%); *m/z* 272 (5%)
PGW	100	87	$[b_3+H\text{-}H_2O]^{2+}$ (18%); Internal $[b_2]^+$, *m/z* 244, (25%); $[a_1]^+$ (12%)
PPP	5	10	$[a_1]^+$ (100%); $[b_2]^+$ (23%); $[a_2]^+$ (18%); *m/z* 98, (8%);
PHG		100	
GGH	100		Internal $[b_2]^+$, *m/z* 195, (15%);
$[b_2+H]^{2+}$ from dipeptide			
Dipeptide	*$[a_2+H]^{2+}$*	*$[b_2+H\text{-}CO\text{-}H_2O]^{2+}$*	
PA	29		*m/z* 55, (21%); *m/z* 115, (12%);
PP	100	23	$[a_1]^+$ (23%); $[a_2]^+$ (9%)
KG		100	
GH	100		Internal $[a_1]^+$(*m/z* 110.0, 23%);
$[b_2+H]^{2+}$ from tripeptide			
Tripeptide	*$[a_2+H]^{2+}$*	*$[b_2+H\text{-}CO\text{-}H_2O]^{2+}$*	
PWG	100		$[a_1]^+$ (37%); Internal $[b_1]^+$ (*m/z* 187.1, 9%); Internal $[a_1]^+$ (*m/z* 159.1, 9%); *m/z* 170.0 (12%); *m/z* 115.1 (7%)
PHG	100		

6.3 Conclusion

$[Ln(III)(tripeptide)(CH_3CN)_n]^{3+}$, where n is 1 or 2 and Ln is La, Ce or Y, dissociate by loss of CH_3CN, CO and MO^+, creating $[a_3 + H]^{2+}$ ions. $[a_3 + H]^{2+}$ ions usually cleave at one of the amide bonds creating two singly charged ions, a $[b_2]^+$ ion and an iminium ion derived from the C-terminal residue. In the presence of tryptophan residue, the $[a_3 + H]^{2+}$ ion also lose NH_3 via cyclization.

Higher abundance of $[b_3 + H]^{2+}$ ion was created by CID of $[Ln(tripeptide)]^{3+}$ for tripeptides PGG, PWG, PPP, PGA and PAA without solvent, while a tiny amount of $[b_3 + H]^{2+}$ was generated by CID of the metal/peptide complexes with solvent. The relative amounts of $[b_3 + H]^{2+}$ to $[a_3 + H]^{2+}$ ions created by CID of $[Ln(tripeptide)]^{3+}$ depends on the composition of the peptide. Composition of peptides will decide the preferred mode of the fragmentation, either loss of CO to form $[a_3+H]^{2+}$, or loss of (CO + H_2O) (shown in Table 6.2). When the C-terminal amino acid residue is more basic, formation of $[a_n+H]^{2+}$ is the preferred channel, while loss of (CO + H_2O) is the dominant dissociation pathway if the N-terminal amino acid residue is more basic. $[a_3+H]^{2+}$ ions do not lose water and therefore are not intermediates in the loss of (CO + H_2O). Experiments with ^{18}O labeled peptides P(^{18}O)GG and PG(^{18}O)G indicate that the oxygens in the (CO and H_2O) combination lost from $[b_3 + H]^{2+}$ ions are *both* from glycine residues.

6.4 References

1 Wysocki, V. H., Resing, K. A., Zhang, Q., Cheng, G. Mass spectrometry of peptides and proteins. Methods. 2005; 35(3): 211–222.

2. Medzihradszky, K. F., Chalkley, R. J. Lessons in de novo peptide sequencing by tandem mass spectrometry: Lessons in de novo peptide sequencing. Mass Spectrom Rev. 2015; 34(1):43–63.

3. Resing, K. A., Ahn, N. G. Proteomics strategies for protein identification. FEBS Letters. 2005; 579(4): 885–889

4. Kinter, M., Sherman, N.E. Protein sequencing and identification using tandem mass spectrometry. Wiley-Interscience. 2000

5. Tabb, D. L., Smith, L. L., Breci, L. A., Wysocki, V. H., Lin, D., Yates, J. R. Statistical characterization of ion trap tandem mass spectra from doubly charged tryptic peptides. Anal Chem. 2003; 75(5): 1155–1163.

6. Roepstorff, P., Fohlman, J. Proposal for a common nomenclature for sequence ions in mass-spectra of peptides. Biomed Mass Spectrom. 1984; 11(11): 601–601.

7. Johnson, R. S., Martin, S. A., Biemann, K., Stults, J. T., Watson, J. T. Novel fragmentation process of peptides by collision-induced decomposition in a tandem mass spectrometer: differentiation of leucine and isoleucine. Anal Chem. 1987; 59(21): 2621–2625.

8. Chu, I. K., Siu, C.-K., Lau, J. K.-C., Tang, W. K., Mu, X., Lai, C. K., Guo, X., Wang, X., Li, N., Xia, Y., Kong, X., Oh, H. B., Ryzhov, V., Turecek, F., Hopkinson, A. C., Siu, K. W. M. Proposed nomenclature for peptide ion fragmentation. Int J Mass Spectrom. 2015; 390: 24–27.

9. Paizs, B. and Suhai, S. Fragmentation pathways of protonated peptides. Mass Spectrom Rev. 2005; 24(4), 508–548.

10. Xue, G., Liu, Z., Wang, L. and Zu, L. The role of basic residues in the fragmentation process of the lysine rich cell-penetrating peptide TP10: Fragmentation of lysine rich peptide TP10. J Mass Spectrom. 2015; 50(1), 220–227.

11. Harrison, A. G. The gas-phase basicities and proton affinities of amino acids and peptides. Mass Spectrom Rev. 1997; 16(4), 201–217.

12. Huang, Y., Wysocki, V. H., Tabb, D. L., Yates, J. R. The influence of histidine on cleavage C-terminal to acidic residues in doubly protonated tryptic peptides. Int J Mass Spectrom. 2002; 219(1), 233–244.

13. Shvartsburg, A. A., Jones, R. C. Attachment of metal trications to peptides. J Am Soc Mass Spectrom. 2004; 15(3), 406–408.

14. Shi, T., Siu, C.-K., Siu, K. W. M., Hopkinson, A. C. Dipositively charged protonated a_3 and a_2 ions: generation by fragmentation of $[La(GGG)(CH_3CN)_2]^{3+}$. Angew Chem Int Ed. 2008; 47(43): 8288–8291.

15. Zhao, J., Siu, C.-K., Shi, T., Hopkinson, A. C., Siu, K. W. M. Abundant dipositively charged protonated a_2 and a_3 ions from diproline and triproline. J Phys Chem B. 2009; 113(14): 4963–4969.

16. Saminathan, I. S., Zhao, J., Siu, K. W. M., Hopkinson, A. C. Doubly charged protonated a ions derived from small peptides. Phys Chem Chem Phys. 2011; 13(41): 18307.

17. Verkerk, U. H., Siu, C.-K., Steill, J. D., El Aribi, H., Zhao, J., Rodriquez, C. F., Oomens, J, Hopkinson, A.C. and Siu, K. W. M. a_2 Ion Derived from Triglycine: An N 1 -Protonated 4-Imidazolidinone. J Phys Chem Lett, (2010); 1(5): 868–872.

18. Bythell, B. J., Maître, P. and Paizs, B. Cyclization and Rearrangement Reactions of a n Fragment Ions of Protonated Peptides. J Am Chem Soc, 2010; 132(42): 14766–14779.

19. Zhao, J., Lau, J. K.-C., Grzetic, J., Verkerk, U. H., Oomens, J., Siu, K. W. M., and Hopkinson, A. C. Structures of a_n* Ions Derived from Protonated Pentaglycine and Pentaalanine: Results from IRMPD Spectroscopy and DFT Calculations. J Am Soc Mass Spectrom, 2013; 24(12): 1957–1968.

CHAPTER 7

Dipositive Lanthanide (III)/Deprotonated Peptide Complexes

7.1 Introduction

Electrospray mass spectrometry is used for peptide sequencing, and research on how metal ions interact with peptides and affect their fragmentation can provide information potentially useful in peptide sequencing and also provide information on how metal ions work in biological systems. When the metal ion/peptide complex has no solvent, direct indication on the intrinsic interacting property of metal ion and peptide can be obtained.

Divalent copper-peptide binding has been investigated more thoroughly. Copper (II) prefers to bind to the terminal amino group and to the C-terminal carboxylate group. It prefers a square-planar geometry. When ternary copper (II) complexes containing a deprotonated amino acid and 2,2′-bipyridine ligand was fragmented by CID, reductive decarboxylation occurred, and fragmentation also happened at the amino acid side chain due to the formation of a α-carbon radical [1-5]. When a neutral amino acid or a peptide replaced the ligand, the reaction mechanism was similar [6]. CO_2 was lost from deprotonated amino acid or peptide during the reductive decarboxylation, and Cu(II) was reduced to Cu(I) and C_α position radical was formed from the deprotonated amino acid or peptide. Studies on the direct interaction of trivalent metal/peptide are rather rare due to the challenge in forming the tripositive/peptide complexes in the gas phase. The low 3rd ionization energy of rare earth metals will help to stabilize the metal/peptide complex in aprotic ligands [7-9], for example, acetonitrile, acetone, DMSO; consequently, tripositive complexes of trivalent metal ion and peptide can be formed by electrospray ionization [10-13]. The deprotonated doubly-charged ion $[Ln(III)(peptide\text{-}H)]^{2+}$ can be formed in the fragmentation of $[Ln(III)(Peptide)(CH_3CN)_n]^{3+}$, or from the full scan of the

mixture of Ln(III) with peptide in acetonitrile/water, and then peeling off all the solvent molecules in ESI mass spectrometry. For the complexes of the alkali metal-cationized small peptides $[M(I)(peptide)]^+$, metal ions will coordinate with amide carbonyl oxygens, side chain aromatic rings and C-terminal carbonyl oxygens, or the N-terminal amino nitrogen, with C-terminal carbonyl oxygen preferred; the calculated metal–ion affinities of five dipeptide binding sites (kJ/mol) based on simplified model system using DFT MPW1PW91/6-311+G(d,p) is shown below (Chart 7.1) [14].

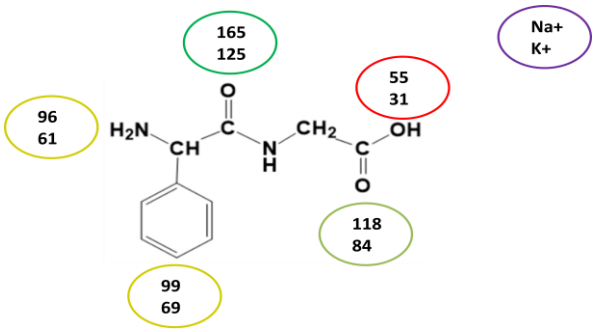

Chart 7. 1 Calculated metal-ion affinities of dipeptide binding site (kJ/mol) based on simplified model system using DFT MPW1PW91/6-311+G(d,p) for Na^+ and K^+. Adopted from [14]

The metal-ion affinities for Na^+ and K^+ are in the order of amide C=O >acid C=O > ring ≥ terminal N > acid OH. The experimental result is consistent with the calculated result.

IRMPD study on the alkali and alkaline earth metal cations show that the complexes of metal/peptide (di or tri) coodination can be switched between charge-solvated and salt-bridged zwitterions depending on the length of the peptide chain, metal ion size, metal ion charge, and sterically available Lewis-basic side chain interaction with metal ion [15]. The trivalent metal ion/(peptide-H) complex is a compact salt-bridge structure, where the metal ion displaced a proton at an acidic site, and coordinates with all the carbonyl oxygen atoms of the peptide backbone [12]. IRMPD experiments and theoretical calculation showed [12] that N-terminal

amine nitrogen and all carbonyl group coordinate with metal ions, and when there is an aromatic ring, at least one of the carbonyl groups will be displaced by the aromatic group to coordinate with metal ion.

Due to the challenge of the high charge-density of trivalent ions in the gas phase, trivalent metal-peptide binding has drawn more attention. Investigation of the dipositive complexes of Ln(III)/(peptide-H) have been carried out by electron capture dissociation with electrospray ionization, where Ln=La, Tm, Lu, Sm, Ho, Yb, Pm, Tb or Eu. It was found that the salt-bridge structure is favoured with the metal coordinating with a carboxylate group [16]. ECD fragmentation showed predominantly *c/z* fragmentation except when the metal was Eu; the latter is reduced and the complex loses small neutral molecules and the fragments *b/y* type ions are predominant.

Praseodymium, Pr(III), is used to form the dipositive metal/deprotonated peptide complex too with ETD [17]. For larger peptides, this ion gives informative sequence coverage.

When one neutral peptide was attached to the metal/deprotonated peptide complex, its fragmentation is also investigated [18] for metal M=Mn^{2+}, Co^{2+}, Ni^{2+}, Cu^{2+}, Zn^{2+}, for the peptide with or without aromatic amino acid residue. For the longer peptides GGGG and FGGF, fragmentation shows the loss of the whole neutral peptide as shown in equation 1.

$$[M(II)(peptide)(peptide\text{-}H)]^+ \longrightarrow [M(II)(peptide\text{-}H)]^+ + peptide \qquad \text{(Equation 1)}$$

For the shorter peptides GG and GF, $[M(II)(GF)(GF\text{-}H)]^+$ and $[M(II)(GG)(GG\text{-}H)]^+$ complexes show the loss of CO_2 as the major fragmentation pathway, with exceptions of 1) $[Co(II)(GF)(GF\text{-}H)]^+$, the cinnamic acid loss is the dominant channel; 2) $[Mn(II)(GG)(GG\text{-}H)]^+$,

where loss of $2CO_2$ is the dominant channel. Neutral peptide loss is only observed as the major channel from $[Cu(II)(GG)(GG\text{-}H)]^+$.

When the peptide is replaced by an amino acid (AA)[19], the neutral amino acid does not participate in the fragmentation of $[Cu(II)/(AA)(AA\text{-}H)]^+$ by comparing with the CID spectrum with that of $[Cu(II)/(AA\text{-}H+Na)(AA\text{-}H)]^+$. The $[Cu(II)/(AA)(AA\text{-}H)]^+$ complex is decarboxylated while Copper(II) is reduced to Copper(I). A radical site is generated at the C_α of the decarboxylated moiety.

In this work, we investigate the fragmentation of Cerium(III)/deprotonated tripeptide under collision-induced dissociation. Ce^{3+} is an open-shell ion and has very close chemical and physical properties to La^{3+}. In the acetonitrile/water solution, it easily forms $[Ce(peptide\text{-}H)(CH_3CN)_n]^{2+}$ under electrospray conditions. Acetonitrile molecules can be peeled off one by one by increasing the collision energy or by using multi-stage mass spectrometry. The $[Ce(peptide)(peptide\text{-}H)]^{2+}$ complex is finally generated and can be fragmented by CID. From the experimental results of Chapter 3, we know Europium (III) can be reduced to Europium (II) during fragmentation, which is different from most of other trivalent rare earth metal ions; here we compare its behaviour to that of Cerium.

7.2 Result and Discussion

7.2.1 Fragmentation of $[Ce(peptide\text{-}H)]^{2+}$ ions

The CID spectra of M(III)/peptide complexes show that $[Ce(peptide\text{-}H)]^{2+}$ is frequently the more abundant product ion than $[Ce(peptide)]^{3+}$. These $[Ce(peptide\text{-}H)]^{2+}$ ions were isolated and subjected to collision-induced fragmentation. Figure 7.1 shows the CID spectra of $[Ce(AWG)(CH_3CN)]^{3+}$ and $[Ce(AWG\text{-}H)]^{2+}$ as examples. The results are shown in Table 7.1;

Table 7.1a CID spectra of $[Ce(peptide\text{-}H)]^{2+}$ Ions

Peptide	*m/z*	Abundance (%) of Doubly Charged Fragments					Abundance (%) of Singly Charged Ion (*m/z*)
		-CO	$-CO_2$	$-H_2O$	$-CO-H_2O$	Other	
GWG	228.5	100		33			{10(326.9), 20(130)}
AWG	235.5	100		60			{11(341), 23(130)}
GWA	235.5	100			15		
GYG	217	100		22			
GYA	224	100					
GGW	228.5	100	50				
GGM	201	15	24	100			
GGY	217		100	37	42		
AAY	231		100	20			
YGG	217	100	15	15	20	60(208.4)	
YAA	231	70		41	39	100 (222.5)	{20(136), 14(326)}
MGG	201	100		22			{15(104),17(298)}, 17(341)
WGG	228.5	100	57	53	32	15 (197.5)	{30(159) , 15(297.8)}, {31(169), 22(288)}
FGA	216	100		20	40	18(180)	{26(120), 16(312)}, {24(130), 17(302)},
GMG	201	19		38		100 (192.5), 30(177), 27(170)	
GFG	209	100		21			15(388)
GFA	216	100					
GGF	209	48	100				
GGG	164	100		34			18(297.9)
GAG	171	100		34			45(311.9)
GGA	171	100		36			29(311.9)
AAA	185	99		100			55(325.9)
MMM	275	18	100	43		26(239), 15(229), 58(251)	
WWW	357.5		100			40 (327)	{40(130), 28(585)}, 32 (541),
PAA	198	77		100			{75(70), 45(326)}, 39(298)
AAP	198			100			17(352)
PAG	191	38		100			{95(70), 47(311.9)}, 16(141), 38(283.9), 16(255.9)
PGA	191	94		100			{98(70), 28(311.9)}, 30(269.9), 27(-b_1)
GGP	184			100			73(338)
APG	191	100					28(337.9)
GPG	184	100					
GPA	191	100					29(155)

Peptide	***m/z***	**Abundance (%) of Doubly Charged Fragments**					**Abundance (%) of Singly Charged Ion (*m/z*)**
		-CO	**-CO_2**	**-H_2O**	**-CO-H_2O**	**Other**	
PGG	184	90		81			{100(70), 23(297.9)}, 15(269.9), 28(255.9), 20(253.9)
PGW	248.5	100	30				
PWG	248.5	70		100			{22(130), 14(367)}, 24(427), 22(383.9),
PGGG	212.5	66		100	15		{43(70),18(355)},43(327)
PLGG	240.5	50		100	28		24(383)
PPPP	272.5			75		100(238), 26(216)	

Table 7.1b Interpretation of the CID spectra of $[Ce(peptide\text{-}H)]^{2+}$

Peptide	*m/z*	Abundance (%) of Doubly Charged Fragments					Abundance (%) of Singly Charged Ion (*m/z*)
		-CO	$-CO_2$	$-H_2O$	$-CO-H_2O$	Other	
GWG	228.5	100		33			{10($[Ce(GGG\text{-}2H)]^+$), 20(3-methylene-3H-indolium ion)}
AWG	235.5	100		60			{11($[Ce(AGG\text{-}2H)]^+$), 23(3-methylene-3H-indolium ion) }
GWA	235.5	100			15		
GYG	217	100		22			
GYA	224	100					
GGW	228.5	100	50	10			
GGM	201	15	24	100			
GGY	217		100	37	42		
AAY	231		100	20			
YGG	217	100	15	15	20	60($-NH_3$)	
YAA	231	70		41	39	100 ($-NH_3$)	{20($[[a_1]^+$), 14($-[a_1]^+$)}
MGG	201	100		22			{15($[a_1]^+$),17($-[a_1]^+$)}, 17($-CH_2=S^+CH_3$)
WGG	228.5	100	57	53	32	15 ($-CO_2-H_2O$)	{30($[a_1]^+$) , 15($-[a_1]^+$)}, {tryptophan-$2H_2O+H^+$), 22(288)}
FGA	216	100		20	40	18(-36?)	{26($[a_1]^+$), 16($-[a_1]^+$)}, {24(Phenyalanine-$2H_2O+H^+$), 17(302)},
GMG	201	19		38		100 ($-NH_3$), 30($-CH_3SH$), 27($-CO_2-H_2O$)	
GFG	209	100		21			15($-[a_1]^+$)
GFA	216	100					
GGF	209	48	100				
GGG	164	100		34			18($-[a_1]^+$)
GAG	171	100		34			45($-[a_1]^+$)
GGA	171	100		36			29($-[a_1]^+$)
AAA	185	99		100			55($-[a_1]^+$)
MMM	275	18	100	43		26(-36), 15($-CO_2$ - CH_3SH), 58($-CH_3SH$)	
WWW	357.5		100			40 ($-NH_3-CO_2$)	{40(3-methylene-3H-indolium ion), 28($[Ce(WGW\text{-}2H)]^+$)}, 32 ($-CO_2$ -3-methylene-3H-indolium ion),
PAA	198	77		100			{75($[a_1]^+$), 45($-[a_1]^+$)}, 39($-b_1$)
AAP	198			100			17($-[a_1]^+$)
PAG	191	38		100			{95($[a_1]^+$), 47($-[a_1]^+$)}, {16($[a_2]^+$), 12($-[a_2]^+$)}, 38($-b_1$), 16($-[b_1]^+$ -CO)

Peptide	***m/z***	**Abundance (%) of Doubly Charged Fragments**					**Abundance (%) of Singly Charged Ion (*m/z*)**
		-CO	**-CO_2**	**-H_2O**	**-CO-H_2O**	**Other**	
PGA	191	94		100			{98($[a_1]^+$), 27(-$[a_1]^+$)}, 30(-dehydroproline amide), 27([Ce(GA-2H)]$^+$)
GGP	184			100			73(-$[a_1]^+$)
APG	191	100					28(-$[a_1]^+$)
GPG	184	100					
GPA	191	100					29($[b_2]^+$)
PGG	184	90		81			{100($[a_1]^+$), 23(-$[a_1]^+$)}, 15 [Ce(GG-2H)]$^+$, 28(-dehydroproline amide), 20(-$[a_1]^+$ -CO_2)
PGW	248.5	100	30				
PWG	248.5	70		100			{22(3-methylene-3H-indolium ion), 14[Ce(PGG-2H]$^+$ }, 24(-$[a_1]^+$), 22(-protonated dehydroproline amide),
PGGG	212.5	66		100	15		{43($[a_1]^+$),18(-$[a_1]^+$)},43([Ce(GGG-2H)]$^+$)
PLGG	240.5	50		100	28		24([Ce(LGG-2H)]$^+$))
PPPP	272.5			75		100(- ) 26 (-  -CO_2)	

In the column for singly charged product ions the curly parentheses, {....}, indicate complementary pairs of ions. In this situation ions with abundances lower than 15% are retained.

only ions with an abundance ≥15% are reported. In Table 7.1a the m/z values are reported along with their relative abundances and in Table 7.1b possible structures of the product ions are given.

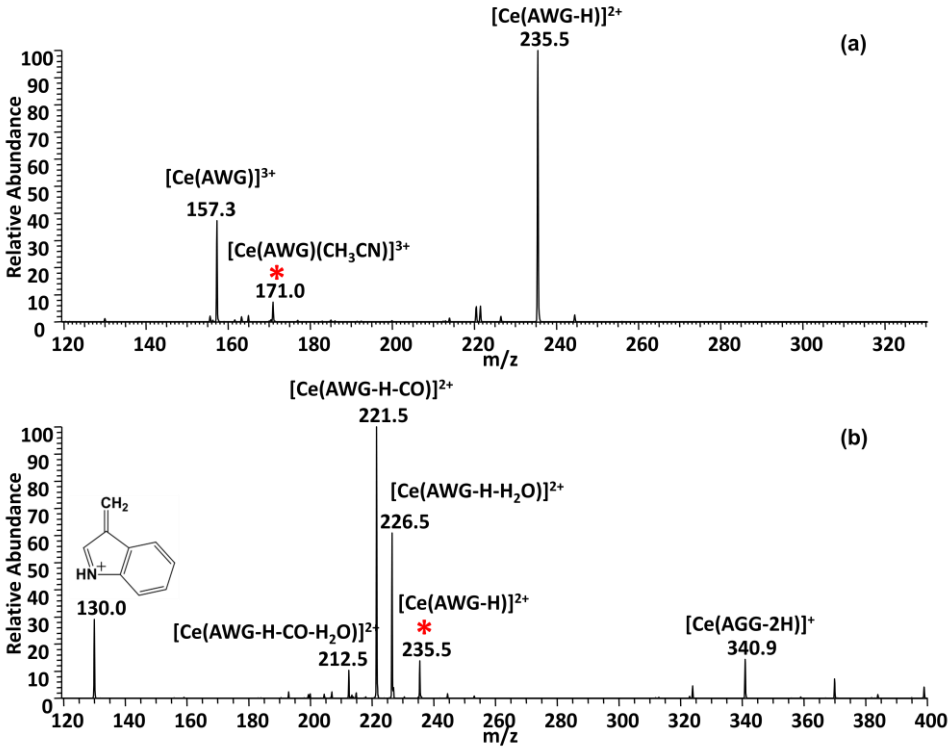

Figure 7.1 CID spectra of (a) $[Ce(AWG)(CH_3CN)]^{3+}$ (*m/z* 171.0) (CE=12); (b) $[Ce(AWG\text{-}H)]^{2+}$ (*m/z* 235.5) (CE=13.5). The precursor ions are labelled with an asterisk (*)

The $[Ce(peptide\text{-}H)]^{2+}$ ions mainly dissociate by losses of small neutral molecules, losing CO, H_2O, CO_2, ($CO+H_2O$) or NH_3, depending on the composition of the peptide. The only exception is in the dissociation of $[Ce(PGG\text{-}H)]^{2+}$, where cleavage of the first amide bond gives the $[a_1]^+$ ion, but even for this ion dissociation channels resulting in losses of CO and H_2O are major contributors.

1) <u>CO loss</u> is the major common fragmentation pathway for most peptides investigated. For 19 out of 37 complexes listed in Table 7.1, the dominant pathway is CO loss, and for another 10 it is

a very significant pathway. For peptides with Y, W, F, or M at the C-terminus abundant CO_2 loss is observed and some of these peptides also lose CO. For the two peptides with a proline residue at the C-terminus, CO loss or CO_2 loss is not observed; instead, H_2O loss is the major fragmentation channel. By contrast, when the proline residue is in the second position loss of CO is the *only* major channel. When proline is at the N-terminus loss of water is dominant but most complexes also lose CO. The one exception is $[Ce(PGW-H)]^+$, where loss of CO is dominant, but there is also some loss of CO_2 and no loss of H_2O.

2) <u>H_2O loss</u>: 27 out of 37 complexes lose water. For GGM, AAA, PAA, AAP, PAG, PGA, GGP, PWG, PGGG and PLGG, water loss is the major pathway and for AWG and PGG, water loss is very significant (≥60%).

3) <u>Loss of CO_2</u> occurs from 11 of the 37 complexes. It happens only when F, W, Y or M is at the N- or C-terminus of the peptide. CO_2 loss is 100% only when F, W, Y or M is at the C-terminus (for example: GGY, AAY, GGF, MMM, WWW). CO_2 losses from other peptides are GGW (50%), GGM (24%) and PGW (30%).

4) <u>$(CO+H_2O)$ loss</u> is observed in 10 out of 37 cases; however, its abundance is ≤40%.

5) <u>NH_3 loss</u> happens for YGG (60%), YAA (100%), GMG (100%), WGG (10%); It also happens for WWW by losing (CO_2 + NH_3) at 40% abundance, and GYG by losing (NH_3+H_2O) at 12% abundance.

6) <u>Losses from the side chain.</u> For peptides where M is in the second residue position, CH_3SH loss is observed, for example GMG (30%), MMM (58%). Tripeptides with a tryptophan residue in the central location (GWG, AWG, WWW, and PWG) all lose the side chain as 3-methylene-3H-indolium ion (*m/z* 130).

7) In addition to small neutral molecule losses, the complexes can also cleave into two singly-charged small ions. Cleavage at the first amide bond to form an $[a_1]^+$ ion is observed in 20 out of 37 cases with abundance ≥10%. Frequently it is only the complementary ion that is observed as the $[a_1]^+$ ion has too small an *m/v* value to be observable. Most singly charged ions have abundances ≤30%, except those derived from GAG (45% $[a_1]^+$ loss), AAA (55% $[a_1]^+$ loss), PAA (75% $[a_1]^+$), PAG (95% $[a_1]^+$), PGA (98% $[a_1]^+$), GGP (73% $[a_1]^+$ loss), PGG (100% $[a_1]^+$), and PGGG (43% $[a_1]^+$).

7.2.2 Fragmentation of [Ce(Peptide)(Peptide-H)]$^{2+}$ Ions

$[Ce(pept)(peptide\text{-}H)]^{2+}$ ions can be observed in the full scan of the mixture of Ce(III)/ peptide solutions. Tables 7.2a and 7.2b show the fragmentation pattern of these complexes, where a neutral peptide is solvating the $[Ce(pept\text{-}H)]^{2+}$ ion.

Table 7.2a CID spectra of [Ce(peptide)(peptide-H)]$^{2+}$ ions

Peptide	*m/z* of [Ce(Peptide) (Peptide-H)]$^{2+}$	Abundance (%) of Doubly Charged Fragments			Abundance (%) of Singly Charged Ion (*m/z*)
		-H_2O	-CO -H_2O	Other	
AWG	401.5	31		78(384),28(366), 98 (373), 17 (355.5)	{100(545), 19 (258)}, {85(673), 58(130)}, 16(230), 15(655), 28 (684), 20 (731), 16(714)
GWA	401.5	82	54	78(357), 50(384), 30(373), 23 (343), 16 (348.5)	{100 (130), 42(673)}, {55(244), 88(559)}, 30 (684), 22 (655), 24(216), 96(731)
GYG	364.5	22		100(336), 34 (347)	44(193), 66(508), 28 (671), 16 (384)
GYA	378.5	100	27	30(350), 12(334)	24(193), 42(685), 25(536),
GGW	387.5	20		98(294)	{100 (130), 67(645)}
GGM	332.5			100 (308.5)	
GGY	364.5	82	70	45(307.5), 34(282.5)	50(136), 100(565), 24(597), 20(614)
AAY	392.5	24	23		36(136), 100(621), 38(713), 54(642), 29(625)
YGG	364.5			100(356)	{18(296), 15(433)}, 15(432.9)
YAA	392.5			100(384)	{20(235), 27(550)}, {14(324), 14(461)}, 16(207)
MGG	332.5			30(324), 38(308.5), 38(304)	100(533)
WGG	387.5			100(379)	
GMG	332.5			17(304), 16(308.5)	{100(476), 10(189)}, 19(161), 22(113)
GFG	348.5	15	15	44 (331), 100(320), 15(302.5)	35(177), 16(120), 48(639), 68(492)
GFA	362.5		40	12 (260.5), 20 (334), 17 (318)	100(653), 21 (606), 35(520), 18(177)
GGF	348.5	73	91	32(320), 76 (291.5)	{18 (582), 10 (115)}, 92 (549), 100(120),
GGG	258.5	58	54	100(201.5), 43(250), 28(241),34(230)	{22(115),22(402)}, 82(459)
GAG	272.5	42	30	36(255), 42(208.5),50(244)	{96(416), 20(129)}, 100(487), 28(101)
GGA	272.5	18	100	58(215.5)	68(473)
AAA	300.5		57		100(529), 28(458)
MMM	480.5			100(456.5)	20(698)
WWW	645.5			100(637), 25(552), 24(441)	49(1104), 19(1161), 37(918)
PAA	326.5	100	76		{11(169), 48(484)}, 42(186), 78(555), 59(581)
AAP	326.5	19			100(555), 16(581), 38(510)
PAG	312.5	100	20	42(284),10(240.5), 27(290.5)	{12(98),28(527)}, {17(169), 22(456)},

Peptide	***m/z* of [Ce(peptide) (peptide-H)]$^{2+}$**	**Abundance (%) of Doubly Charged Fragments**			**Abundance (%) of Singly Charged Ion (*m/z*)**
		-H_2O	**-CO -H_2O**	**Other**	
GGP	298.5	46		100(270), 52(241.5), 18(281)	93(499), 16(482)
APG	312.5	52		100(277), 72(284),	{46(456), 15(169)}, 67(553),)
GPG	298.5	22	16	100(270),	15(539), 19(442)
GPA	312.5		100	20 (267.5)	95 (553)
PGG	298.5	94	25	46 (270), 33(276.5)	{22(98), 100(499)}, {22(155), 38(442)}, 17(70)

Table 7.2b Interpretation of the CID spectra of [Ce(peptide)(peptide-H)]$^{2+}$

Peptide	*m/z* of [Ce(Peptide) (Peptide-H)]$^{2+}$	Abundance (%) of Doubly Charged Fragments			Abundance (%) of Singly Charged Ion (*m/z*)
		-H_2O	-CO -H_2O	Other	
AWG	401.5	31		78(-H_2O-NH_3),28(-A_{res}), 98 (-G_{res}), 17 (-G_{res}-H_2O-NH_3)	{100(-[b_2]$^+$), 19 ([b_2]$^+$)}, {85(-130), 58(3-methylene-3H-indolium ion)}, 16([a_2]$^+$), 15(-130 -H_2O), 28 (684), 20 (-[a_1]$^+$-CO), 16(-protonated alanine amide)
GWA	401.5	82	54	78(-A), 50(-H_2O-NH_3), 30(-G_{res}), 23 (-58.5), 16 (-alanine, -ammonia)	{100 (3-methylene-3H-indolium ion), 42(-130)}, {55([b_2]$^+$,), 88(-[b_2]$^+$)}, 30 (684), 22 ((-130-H_2O), 24([a_2]$^+$), 96(-[a_1]$^+$ of A - CO)
GYG	364.5	22		100(-G_{res}), 34 (-H_2O-NH_3)	44([a_2]$^+$), 66(-[b_2]$^+$), 28 (-CO -$H_2CNH_2^+$), 16 (384)
GYA	378.5	100	27	30(-G_{res})	24([a_2]$^+$), 42(-[a_1]$^+$-CO), 25(-[b_2]$^+$),
GGW	387.5	20		98(-W_{res} +H)	{100 (3-methylene-3H-indolium ion), 67(-130)}
GGM	332.5			100 (-HSCH3)	
GGY	364.5	82	70	45(-GG_{res}), 34(-Y_{res})	50([a_1]$^+$of Y), 100(-[a_1]$^+$of Y -CO), 24(-132) 20(-[b_2]$^+$)
AAY	392.5	24	23		36([a_1]$^+$of Y), 100(-[a_1]$^+$ of Y-CO), 38(-[a_1]$^+$-CO), 54(-[b_2]$^+$), 29(-160)
YGG	364.5			100(-NH_3)	{18(YGG+H)$^+$, 15(-(YGG+H)$^+$)}
YAA	392.5			100(-NH_3)	{20([b_2]$^+$), 27(-[b_2]$^+$)}, {14(YAA+H)$^+$, 14(-(YAA+H)$^+$,)}, 16([a_2]$^+$)
MGG	332.5			30(-NH_3), 38(-$HSCH_3$), 38(-G_{res})	100(-2Gres-H_2O)
WGG	387.5			100(-NH_3)	
GMG	332.5			17(-G_{res}), 16(-$HSCH_3$)	{100(-[b_2]$^+$), 19([a_2]$^+$), 22(113)
GFG	348.5	15	15	44 (-H_2O-NH_3), 100(-G_{res}), 15(-H_2O-NH_3-G_{res})	35([a_2]$^+$), 16([a_1]$^+$of F), 48(-[a_1]$^+$-CO), 68(-[b_2]$^+$)
GFA	362.5		40	20 (-G_{res}), 17 (-A)	100(-[a_1]$^+$ of A -CO), 21 (-119), 35(-[b_2]$^+$), 18([a_2]$^+$)
GGF	348.5	73	91	32(-G_{res}), 76 (-GG_{res})	{18 (-[b_2]$^+$), 10 ([b_2]$^+$)}, 92 (-[a_1]$^+$of F-CO), 100([a_1]$^+$ of F),
GGG	258.5	58	54	100(-GG_{res}), 43(-NH_3), 28(-H_2O-NH_3),34(-G_{res})	{22([b_2]$^+$),22(-[b_2]$^+$)}, 82(-[a_1]$^+$-CO)
GAG	272.5	42	30	36(-H_2O-NH_3), 42(-GA_{res}),50(-G_{res})	{96(-[b_2]$^+$), 20([b_2]$^+$)}, 100(-[a_1]$^+$-CO), 28([a_2]$^+$)
GGA	272.5	18	100	58(-GG_{res})	68(- [a_1]$^+$ of A -CO)
AAA	300.5		57		100(-[a_1]$^+$-CO), 28(-[b_2]$^+$)
MMM	480.5			100(-$HSCH_3$)	20(-[b_2]$^+$)
WWW	645.5			100(-NH_3), 25(-W+ NH_3), 24(-204.5)	49(-[a_1]$^+$-CO), 19(-3-methylene-3H-indolium ion), 37(-[b_2]$^+$)

Peptide	***m/z* of [Ce(peptide)(peptide-H)]$^{2+}$**	**Abundance (%) of Doubly Charged Fragments**			**Abundance (%) of Singly Charged Ion (*m/z*)**
		-H_2O	**-CO -H_2O**	**Other**	
PAA	326.5	100	76		{11($[b_2]^+$), 48(-$[b_2]^+$)}, 42([$PANH_2$ +H^+]), 78(-$[a_1]^+$ -CO), 59(- $[a_1]^+$ of A -CO)
AAP	326.5	19			100(-$[a_1]^+$ -CO), 16(-$[a_1]^+$-CO), 38(-$[a_2]^+$-CO)
PAG	312.5	100	20	42(-G_{res}), 27(-CO_2)	{12($[b_1]^+$),28(-$[b_1]^+$)}, {17($[b_2]^+$), 22(-$[b_2]^+$)}
GGP	298.5	46		100(-G_{res}), 52(-GG_{res}), 18(-H_2O-NH_3)	93(-$[a_1]^+$ -CO), 16(-$[b_2]^+$)
APG	312.5	52		100(-A_{res}), 72(-G_{res})	{46(-$[b_2]^+$), 15($[b_2]^+$)}, 12($[a_2]^+$), 67(-$[a_1]^+$-CO)
GPG	298.5	22	16	100(-G_{res})	15(-$[a_1]^+$-CO), 19(-$[b_2]^+$)
GPA	312.5		100	20 (-CO-H_2O-CO_2)	95 (- $[a_1]^+$ of A -CO)
PGG	298.5	94	25	46 (-G_{res}), 33(-CO_2)	{22($[b_1]^+$), 100(-$[b_1]^+$)}, {22($[b_2]^+$), 38(-$[b_2]^+$)}, 17($[a_1]^+$)

When an extra peptide molecule is present in a complex it essentially acts as a solvent molecule but, unlike in the fragmentation of $[Ce(peptide\text{-}H)(CH_3CN)]^{2+}$, where the solvent is easily removed (see Table 7.2), the additional peptide is probably the component that fragments. Only complexes containing YGG and YAA lose the intact peptide and here they are detected as $[YGG + H]^+$ and $[YAA + H]^+$ in relatively low abundances (15 and 10% respectively). As in the fragmentation of the $[Ce(peptide\text{-}H)]^{2+}$ ions, doubly charged fragments are formed after neutral losses of H_2O, (H_2O+CO), (H_2O+NH_3), NH_3 or H_3CSH), while neutral loss is the most abundant channel for only 16 of the 30 peptides reported in Table 7.2. By comparison, in the dissociations of the smaller $[Ce(peptide\text{-}H)]^{2+}$ ions neutral loss is the dominant channel for 34 out of the 35 complexes given in Table 7.1. Singly charged fragments are mainly formed by cleavage of the *second* peptide bond, generating $[a_2]^+$ or $[b_2]^+$ ions. Again, this is in contrast with the fragmentation of the $[Ce(peptide\text{-}H)]^{2+}$ ions, where dissociation into two singly-charged ions, mainly involves breaking the *first* peptide bond.

Individual characteristic losses are as follows:

1. Twenty four out of the 30 complexes listed in Table 7.2 have neutral losses in ≥ 50% abundance.
2. For twenty one out of the 30 complexes have water loss, and it is at >50% abundance for GYA, GGY, GGF, GGG, PAA, PAG, APG and PGG.
3. Seventeen out of the 30 complexes have losses of (H_2O +CO), with ≥40% abundance observed for GWA, GGY, GFA, GGF, GGG, GGA, PAA and GPA.
4. Nine out of the 30 complexes have (H_2O+NH_3) loss, with ≥30% abundance observed for AWG (78%), GWA (50%), GFG (44%), GAG (36%) and GYG (34%).

5. NH_3 loss is observed for YGG (100%), YAA (100%), WGG (100%), WWW (100%), GGG (43%), MGG (30%)
6. For M containing peptides MMM, MGG, GMG, and GGM, there is no water loss or (H_2O+CO) loss. They all lose CH_3SH, which is dominant when the methionine is at C-terminus.
7. For N-terminus proline-containing peptides PGG, PAA and PAG, water loss is the major pathway. Losses of the residue from the C-terminus as (HN=CHR+CO) or (H_2N^+=CHR+CO) are observed.
8. For GGG, there is NH_3 loss and (H_2O+NH_3) loss. For GAG, there is no NH_3 loss; instead, (H_2O+ NH_3) loss is observed. For GGA, no NH_3 loss or (H_2O+ NH_3) loss is observed; instead, (CO+H_2O) loss is dominant. By contrast for AAA, (CO+H_2O) loss is large (57%) and no NH_3 or (NH_3+H_2O) losses are observed. Abundant side chain loss fragments are observed for AWG, GWA, GGW.

Cleavage at the first or second amide bonds produced most of the singly-charged fragments (for 27 out of the 30 complexes), with cleavage at the *second* amide bond preferred, as indicated earlier. Fragmentation of 12 out of 30 complexes resulted in products formed by cleavage at the second amide bond in ≥50% abundance; the peptides in this category are AWG, GWA, GYG, GGY, AAY, GMG, GFA, GGF, GAG, GGA, PAA and GPA. Only 4 out of the 30 complexes have fragmentation products formed by cleavage at the first amide bond that are in ≥50% abundance: these are AAP, GGP, APG and PGG. For AAA and GGG, although the counterpart of (a_1+CO) loss is >80%, it is difficult to assign the position of the amide bond cleavage.

7.2.3 Fragmentation of $[Eu(peptide\text{-}H)(CH_3CN)_n]^{2+}$ Ions

While the fragmentations of $[Ce(peptide\text{-}H)]^{2+}$ complexes have some common patterns including CO loss, water loss, and some CO_2 loss depending on the peptide, the fragmentations of $[Eu(peptide\text{-}H)]^{2+}$ complexes are of interest because they are very different. $[Eu(peptide\text{-}H)]^{2+}$ complexes were difficult to isolate and for this reason most of the data in Table 7.3 are for the more stable $[Eu(peptide\text{-}H)(CH_3CN)]^{2+}$ complexes. Table 7.3 then has mainly fragmentation data for $[Eu(peptide\text{-}H)(CH_3CN)_n]^{2+}$, where n=1; for larger peptides, for example GWG, PPPP or PGGG, then it was possible to examine complexes with n=0.

From Table 7.3 the only products from complexes containing tripeptides are dipositive ions, i.e., neutral loss is the only pathway, except for $[Eu(GGF\text{-}H)]^{2+}$ Very minor products are included to emphasize how clean these spectra are. CO_2 loss is the only *major* fragmentation pathway for all the $[Eu(tripeptide\text{-}H)(CH_3CN)]^{2+}$ complexes. There are very minor losses of CH_3CN (6 to 30%) accompanied by loss of CO_2 for complexes containing peptides GGF, PAG and PGG. The two $[Eu(tetrapeptide\text{-}H)(CH_3CN)]^{2+}$ complexes exhibit a different behaviour, loss of CH_3CN. The product $[Eu(tetrapeptide\text{-}H)]^{2+}$ ions then dissociate by only one channel, the loss of CO_2.

For $[Eu(GGF\text{-}H)]^{2+}$, there is also CO_2 loss at *m/z* 193.5 (29%) observed; however, loss of a neutral with mass 30 Da is the dominant product. The four CID spectra of $[Eu^{151}(GGF\text{-}H)]^{2+}$ and $[Eu^{153}(GGF\text{-}H)]^{2+}$ obtained from $[Eu(GGF\text{-}H)(CH_3CN)]]^{2+}$ and $[Eu(GGF\text{-}H)(CD_3CN)]]^{2+}$ show the same dissociation, so we can conclude that $[H_2NC^{\bullet}H_2]$ radical is lost, presumably from the N-terminal G residue. *m/z* 131 ion, counterpart to *m/z* 299.9, is probably from the phenylalanine residue. The ion at m/z 357 corresponds to a loss of 74 Da, a combined loss of (30 + 44) but this time taking the charge $[H_2NCH_2]^+$ and CO_2.

Table 7.3 Fragmentation of dipositive $[Eu(peptide\text{-}H)(CH_3CN)_n]^{2+}$, where n = 0 or 1

Peptide	Number of (CH_3CN)	*m/z* [with Eu^{151} or Eu^{153}]	Relevant Abundance of Charged Prodcuts	
			$-CO_2$	Other
GWG	0	235 (^{153}Eu)	100	24(204.5)
GGA	1	198 (^{153}Eu)	100	
GGF	1	236 (^{153}Eu)	100	30(193.5)
GGF	0	215.5 (^{153}Eu)	29	100(200.5), {40 (131), 16(299.9)}, 42(357)
GGG	1	191 (^{153}Eu)	100	7(160.5)
PAA	1	225 (^{153}Eu)	100	7(182.5)
PAG	1	218 (^{153}Eu)	100	14(190.5), 12(175.5)
PGG	1	211 (^{153}Eu)	100	6(168.5), 7(183.5)
PPPP	1	298.5 (^{153}Eu)	100	9(276.5), 6(256)
PPPP	0	278 (^{153}Eu)	100	
PGGG	1	238.5 (^{151}Eu)	100	
PGGG	0	218 (^{151}Eu)	100	

Table 7.4 Fragmentation of dipositive complex $[Ce(peptide\text{-}H)(CH_3CN)]^{2+}$

Peptide	Number of (CH_3CN)	*m/z*	Relevant Abundance of Charged Products		
			$-CH_3CN$	$-CH_3CN+H_2O$	Other
WGG	1	249	100		
AWG	1	256	100		
YGG	1	237.5	100		
GYG	1	237.5	100		18(228.5)
GGF	1	229.5	100		
GGG	1	184.5	100	14	
GGA	1	191.5	100		
PAG	1	211.5	100		
PPP	1	244.5	100	15	
GMG	1	221.5	100	15	12(213)
GPG	1	204.5	100	13	
GGP	1	204.5	100	12	
AAA	1	205.5	100	15	
PAP	1	231.5	100	12	
PYG	1	257.5	100	13	
PGGG	1	233	100		

By contrast in the fragmentations of $[Ce(peptide\text{-}H)(CH_3CN)]^{2+}$ complexes as shown in the Figure 7.2 and Table 7.4, loss of CH_3CN is the only major pathway. This suggests that Eu(III) requires more coordination than Ce(III) in the gas phase.

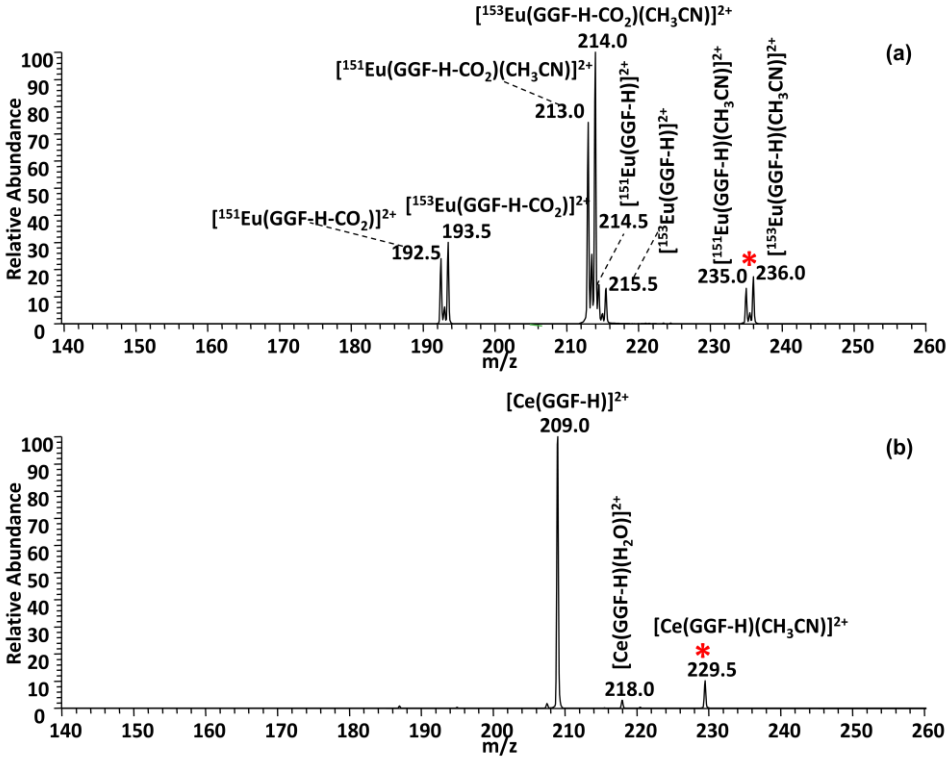

Figure 7.2 CID spectra of (a) $[Eu(III)(GGF\text{-}H)(CH_3CN)]^{2+}$ *m/z* 235.5 (CE=11); (b) $[Ce(III)(GGF\text{-}H)(CH_3CN)]^{2+}$ *m/z* 229.5 (CE=11.8). The precursor ions are labelled with an asterisk (*)

7.3 Conclusion

$[Ce(peptide\text{-}H)]^{2+}$ ions probably have carboxylate anions attached to Ce^{3+} with coordination also from the carbonyl oxygen of the two peptide bonds (Structure **1**). In the absence of additional side chain interactions these complexes dissociate predominantly by the loss of CO and a plausible intermediate structure that eliminates CO would be a metal oxide cation, MO^+, ligated

by a CO and an $[a_3]^+$ ion, structure **II**. Much of the dissociation chemistry can be rationalized in terms of these two structures.

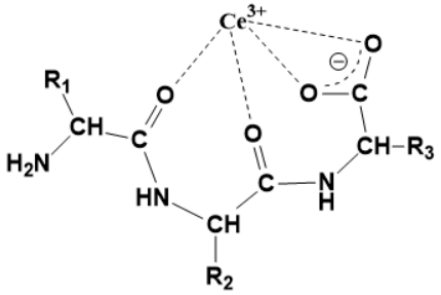

I

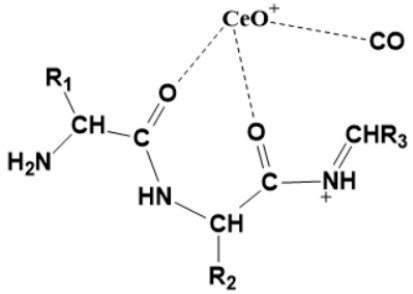

II

Peptides that contain an aromatic side chain or a methionine residue at the C-terminus (or to a lesser extent at the N-terminus) have an additional functional group that can coordinate with the metal ion in structure **I** and this can weaken the coordination with the carboxylate anion facilitating the loss of CO_2. Loss of ammonia from complexes containing YAA and YGG is more easily rationalized in terms of structure **II,** where there is a mobile proton. Similarly, the structure with a mobile proton makes it easier to explain the water loss that occurs predominantly from peptides containing a proline residue at the N-terminus.

Fragmentations to give two singly charged ions are relatively minor pathways for most $[Ce(peptide\text{-}H)]^{2+}$ ions. Cleavage of the first peptide bond is the major pathway by which singly charged ions are formed and this could occur from either structure **I** or **II**. Formation from **I** would involve forming a complex with a $NH^- \rightarrow Ce^{3+}$ interaction and forming an $[a_1]^+$ ion plus CO. Cleavage of these same products from **II** is essentially by the same mechanism by which a protonated peptide fragments. Another pathway leading to two singly charged ions is by breaking the C_α-C_β bond of a tryptophan residue located in the central position in the peptide

chain (R3), giving a 3-methylene-3H-indolium ion; this could occur from either **I** or **II**, in each case formally creating a negative charge on the oxygen of the second residue.

In the fragmentations of $[Ce(peptide\text{-}H)(peptide)]^{2+}$ complexes, neutral losses are also observed but there is more tendency to form two singly charged ions. If the 'neutral' peptide is complexed to structure **I** as a zwitterion **(**structure **III**) then there is a mobile proton available in the 'neutral' peptide and consequently formation of $[b_2]^+$ ions by cleavage of the second peptide bond becomes the dominant pathway, as in the dissociations of the corresponding protonated peptides. For several of the complexes, the $[b_2]^+$ ion consists of small amino acid residues and proton transfer to the complementary ion occurs, resulting in a dipositive ion being observed.

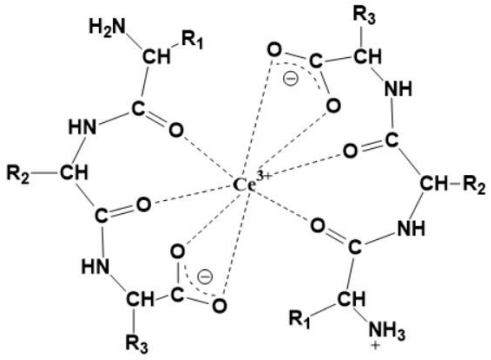

III

In contrast with the dissociations of $[Ce(peptide\text{-}H)]^{2+}$complexes, losses of *only* CO or CO_2 are not observed from $[Ce(peptide\text{-}H)(peptide)]^{2+}$, but for some complexes loss of water is a major channel, again particularly for complexes in which the N-terminal peptide is proline.

The dissociation behaviour of $[Ce(peptide\text{-}H)(CH_3CN)]^{2+}$ and $[Eu(peptide\text{-}H)(CH_3CN)]^{2+}$ complexes are quite different. The former loses only CH_3CN whereas the latter loses only CO_2, which is another example of how these two lanthanide metals show very different behaviour.

7.4 References

1. Hu, P. and Loo, J. A. Gas-Phase Coordination Properties of Zn^{2+}, Cu^{2+}, Ni^{2+}, and Co^{2+} with Histidine-Containing Peptides. J Am Chem Soc. 1995; 117(45): 11314–11319.

2. Gatlin, C. L., Tureček, F. and Vaisar, T. Gas-phase complexes of amino acids with Cu(II) and diimine ligands. Part I. Aliphatic and aromatic amino acids. J Mass Spectrom. 1995; 30(11): 1605–1616.

3. Gatlin, C. L., Tureček, F. and Vaisar, T. Gas-phase complexes of amino acids with Cu(II) and diimine ligands. Part II. Amino acids with O, N and S functional groups in the side-chain. J Mass Spectrom. 1995; 30(11): 1617–1627.

4. Seymour, J. L., and Tureček, F. Structure, energetic and reactivity of ternary complexes of amino acids with Cu(II) and 2,2′-bipyridine by density functional theory. A combination of radical-induced and spin-remote fragmentations. J Mass Spectrom. 2002; 37(5): 533–540.

5. Tureček, F. Copper-biomolecule complexes in the gas phase. The ternary way. Mass Spectrom Rev. 2007; 26(4): 563–582.

6. Wang, P., Ohanessian, G. and Wesdemiotis, C. Cu(II)-Catalyzed Reactions in Ternary [Cu(AA)(AA – H)]+ Complexes (AA = Gly, Ala, Val, Leu, Ile, t-Leu, Phe). Eur J Mass Spectrom. 2009; 15(2): 325–335.

7. Shvartsburg, A. A. and Jones, R. C. Attachment of metal trica tions to peptides. J Am Soc Mass Spectrom. 2004; 15(3): 406–408.

8. Shvartsburg, A. A. Acetonitrile complexes of triply charged metal ions: are ligated trications intrinsically more prone to charge reduction than dications? Chem Phys Lett. 2002; 360(5): 479–486.

9. Shvartsburg, A. A. DMSO Complexes of Trivalent Metal Ions: First Microsolvated Trications Outside of Group 3. J Am Chem Soc. 2002; 124(41): 12343–12351.

10. Shi, T., Hopkinson, A. C. and Siu, K. W. M. Coordination of Triply Charged Lanthanum in the Gas Phase: Theory and Experiment. Chem Eur J. 2007; 13(4): 1142–1151.

11. Shi, T., Siu, K. W. M. and Hopkinson, A. C. Generation of $[La(peptide)]^{3+}$ Complexes in the Gas Phase: Determination of the Number of Binding Sites Provided by Dipeptide, Tripeptide, and Tetrapeptide Ligands. J Phys Chem A. 2007; 111(45), 11562–11571.

12. Prell, J. S., Flick, T. G., Oomens, J., Berden, G. and Williams, E. R. Coordination of Trivalent Metal Cations to Peptides: Results from IRMPD Spectroscopy and Theory. The J Phys Chem A. 2010; 114(2): 854–860.

13. Pu, D., Vincent, J. B. and Cassady, C. J. The effects of chromium (III) coordination on the dissociation of acidic peptides. J Mass Spectrom. 2008; 43(6): 773–781.

14. Polfer, N. C., Oomens, J. and Dunbar, R. C. Alkali Metal Complexes of the Dipeptides PheAla and AlaPhe: IRMPD Spectroscopy. ChemPhysChem. 2008; 9(4): 579–589.

15. Dunbar, R. C., Steill, J. D., Polfer, N. C. and Oomens, J. Peptide Length, Steric Effects, and Ion Solvation Govern Zwitterion Stabilization in Barium-Chelated Di- and Tripeptides. J Phys Chem B. 2009; 113(31): 10552–10554.

16. Flick, T. G., Donald, W. A. and Williams, E. R. Electron Capture Dissociation of Trivalent Metal Ion-Peptide Complexes. J Am Soc Mass Spectrom. 2013; 24(2): 193–201.

17. Commodore, J. J. and Cassady, C. J. Effects of acidic peptide size and sequence on trivalent praseodymium adduction and electron transfer dissociation mass spectrometry. J Mass Spectrom. 2017; 52(4): 218–229.

18. Utley, B. and Angel, L. A. Effects of Transition Metal Ion Identity and π-Cation Interactions in Metal—Bis(Peptide) Complexes Containing Phenylalanine. Eur J Mass Spectrom. 2010; 16(6): 631–643.

19. Wang, P., Ohanessian, G. and Wesdemiotis, C. Cu(II)-Catalyzed Reactions in Ternary $[Cu(AA)(AA – H)]^+$ Complexes (AA = Gly, Ala, Val, Leu, Ile, t-Leu, Phe). Eur J Mass Spectrom. 2009; 15(2): 325–335.

Summary and Future Work

Summary

Investigation on the interaction of metal ions with peptides in the gas phase provides useful information for peptide sequencing and examining conformation of proteins. The interaction of lanthanide (III) ions with peptides in the gas phase draws more interest since it is challenging due to the high charge-density. In this dissertation, the fragmentation chemistry of the tripositive complexes of lanthanide ions and small peptides is examined, and a new route to generate peptide radical cations has been discovered. Several other new findings are also reported, and the results of the following five areas of research are described here:

1) Fragmentation of tripositive complexes of Eu(III)/peptide can generate radical cations for tryptophan-; tyrosine-; phenylalanine- and methionine- containing small peptides and even aliphatic peptides, by reducing Eu(III) to Eu(II) via accepting an electron from the neutral peptide to form radical cations or $[a_3+H]^{\bullet+}$ ions. CID of the tripositive complexes of Ln(III)/peptide, where Ln = yttrium, lanthanum, cerium, samarium, gadolinium and terbium, show similar fragmentation behaviour to each other, but do not form radical cations. A possible reason for this is that europium has a larger 3rd ionization energy compared to those of the other lanthanide elements examined. More important is that Eu^{2+} has a particulary stable electronic configuration attributed to its half-filled electronic shell $4f^7$ which stabilizes the complexes containing Eu^{2+}. Fragmentation of Yb(III)/peptide coplexes also generates peptide radical cations, but it only works for aliphatic peptide like PGG, instead of aromatic peptides, for example GYG. Ytterbium has the largest 3rd ionization energy among lanthanide(III), and Yb^{2+} also has extra stability due to its fully-filled electronic shell $4f^{14}$; however, Eu(III) is easier to be reduced to Eu(II) than that of Yb(III) to Yb(II) due to its higher E^0 in aqueous complexes.

2) The dissociation behavior of tripositive Ce(III)/peptide and Eu(III)/peptide complexes are different. Abundant CO loss is only observed in the dissociation of Ce(III)/peptide complexes, and in contrast, CO_2 loss is the predominant dissociation pathway for Eu(III)/peptide complexes. Similary, the dissociations of $[Ce(peptide\text{-}H)]^{2+}$ and $[Eu(peptide\text{-}H)]^{2+}$ have CO loss and CO_2 loss as the predominant channels, respectively. The other two major differences are that peptide radical cation are only generated in the fragmentation of Eu(III)/peptide complexes, and $[a_n+H]^{2+}$ and $[b_n+H]^{2+}$ ions are only observed when Ce(III)/peptide complexes dissociate.

3) Dissociation of $[Eu(peptide)(CH_3CN)_n]^{3+}$ ions give both peptide radical cations and $[a_3+H]^{\bullet+}$. The dissociation of aliphatic $[peptide]^{\bullet+}$ investigated show that $[b_3\text{-}H]^{\bullet+}$/ $[b_2\text{-}H]^{\bullet+}$ ions appear in the spectra of most peptides studied. For the $[a_3+H]^{\bullet+}$ ions of aliphatic peptides, the dissociation pattern is harder to generalize, although $[b_2\text{-}H]^{\bullet+}$ ions are again observed for most peptides studied. Dissociations of $[b_3\text{-}H]^{\bullet+}$ and $[b_2\text{-}H]^{\bullet+}$ ions for peptides with N-terminal prolines show that $[b_3\text{-}H]^{\bullet+}$ ions have one predominant fragmentation channel giving $[a_2+H]^{\bullet+}$ ions, while $[b_2\text{-}H]^{\bullet+}$ ions have several dissociation channels giving $[a_2\text{-}H]^{\bullet+}$, $[a_1+H]^{\bullet+}$, or $[a_1]^+$.

4) $[a_3+H]^{2+}$ ions usually cleave at the second amide bond creating two singly-charged ions, a $[b_2]^+$ ion and an iminium ion derived from the C-terminal residue. Some $[a_3+H]^{2+}$ ions also lose small neutral molecules (ammonia, carbon monoxide or an imine). The composition of the peptide will dictate the preferred mode of the fragmentation of the $[b_3+H]^{2+}$ ions, either loss of CO to form $[a_3+H]^{2+}$, or loss of CO plus H_2O. When the C-terminal amino acid residue is basic, formation of $[a_n+H]^{2+}$ is the preferred channel, while loss of (CO + H_2O) is the dominant dissociation pathway if N-terminal amino acid residue is basic. $[a_3+H]^{2+}$ ions do not lose water and therefore are not intermediates in the loss of (CO + H_2O).

5) In the absence of additional side chain interactions, $[Ce(peptide\text{-}H)]^{2+}$ complexes dissociate predominantly by the loss of CO. In the fragmentations of $[Ce(peptide\text{-}H)(peptide)]^{2+}$ complexes losses of H_2O and /or ($CO+H_2O$) are frequently observed, and losses of NH_3 and/or amino acid residues are also observed depending on the peptide sequence and composition. In addition, it is more likely to form two singly charged ions. In contrast with the dissociations of $[Ce(peptide\text{-}H)]^{2+}$complexes, losses of *only* CO or CO_2 are not observed from $[Ce(peptide\text{-}H)(peptide)]^{2+}$ but for some complexes loss of water is a major channel, again particularly for complexes in which the N-terminal peptide is proline. The dissociation behaviour of $[Ce(peptide\text{-}H)(CH_3CN)]^{2+}$ and $[Eu(peptide\text{-}H)(CH_3CN)]^{2+}$ complexes are quite different, losing CH_3CN or CO_2 respectively.

Suggested Future Work

1) Investigate the fragmentation chemistry of tripositive Ytterbium/peptide complexes. A preliminary study shows that CID of $[Yb(III)(PGG)(CH_3CN)_6]^{3+}$ complexes generate $PGG^{\bullet+}$. Ytterbium has the second largest 3rd ionization energy relative to other lanthanide elements. The Yb^{2+} ion has a particularly stable electronic configuration because it has a fully-filled electronic shell, $4f^{14}$. Further investigation of the Yb(III)/peptide complexes will give more comprehensive understanding of the dissociation chemistry of Ln(III)/peptide complexes. Various tripeptides with different ionization energies should be studied by CID of $[Yb(III)(peptide)(CH_3CN)_m]^{3+}$ to define the range of ionization energies of peptides that will give radical cations.

2) Different ligands should be studied by fragmentation of $[Eu(III)(peptide)(ligand)_m]^{3+}$ and $[Yb(III)(peptide)(CH_3CN)_m]^{3+}$ complexes to improve the yield of $[peptide]^{\bullet+}$, especially the sterically encumbered ligands, for example, 12-crown-4, 1,4,7-triazacyclononane and other

auxiliary ligands that suppress the competitive channels of formation of peptide radical cations by CID of Cu/peptide ternary complexes.

3) Tripositive complexes of Ln(III)/peptide in the absence of solvent provide intrinsic interaction between the trivalent ions and peptides. Extending the investigation of the dependence of dissociation behavior on the composition of the peptide will be necessary. In addition to W-containing tripeptides, Y-, M- and F- containing tripeptides can be good candidates to study the direct interaction between trivalent ions with peptides by CID of $[Ln(peptide)]^{3+}$ ions.

4) A further comparison between the dissociation of peptide radical cations formed from Eu/peptide and Cu/peptide complexes is necessary. $[b_3\text{-}H]^{\bullet+}$ ions are the major products (abundance>50%) in the CID spectra of $[peptide]^{\bullet+}$ derived from Eu/peptide complexes and only a minor product (abundance <10%) in the CID spectra of $[peptide]^{\bullet+}$ derived from Cu/peptide complexes, which suggests that the peptide radical cations initially formed by Cu^{2+} or Eu^{3+} might be different. DFT calculation will disclose the structures of the $[peptide]^{\bullet+}$ ions, their precursors and metal/peptide complexes, where metal = Eu(III) or Cu(II), and give their geometries, which may help to explain the different fragmentation patterns observed in this work.

5) When the peptides are longer, the $[a_n+H]^{2+}$ ions are more unstable as the distance between the two positive charges is bigger; hence the structure of the $[a_n+H]^{2+}$ ion is less rigid and permits proton mobility leading to dissociation. Preliminary experiments show the $[a_4+H]^{2+}$ ion is observed for PGGG, although the abundance is very low. Further experiments are suggested to improve the abundance, and to examine the possible structure of $[a_4+H]^{2+}$.

6) Compared to Cerium(III), Yttrium(III) has a smaller ionic radius (88 pm versus 103.4 pm), but it has similar ionization energy to Ce(III). In this work, it has been found that CID of

Yttrium(III)/PGG conplexes give abundant dipositive b ions, so further study on the fragmentation pattern of Yttrium(III)/peptide complexes may provide more interesting information on the dipositive a and b ions.

7) Investigate the fragmentation chemistries of $[Eu(peptide\text{-}H)]^{2+}$ and $[Yb(peptide\text{-}H)]^{2+}$ ions, to compare with those of $[Ce(peptide\text{-}H)]^{2+}$ ions. The information will help to disclose the intrinsic interaction between lanthanide(III) ions and deprotonated peptides. There are only a few examples for the dissociation of $[Eu(peptide\text{-}H)]^{2+}$ complexes for tripeptides. The research can be extended to peptides containing basic amino acid residues, methionine-containing peptides or tetrapeptides to increase the possibility of observing $[Eu(peptide\text{-}H)]^{2+}$ for further investigation.

Appendix

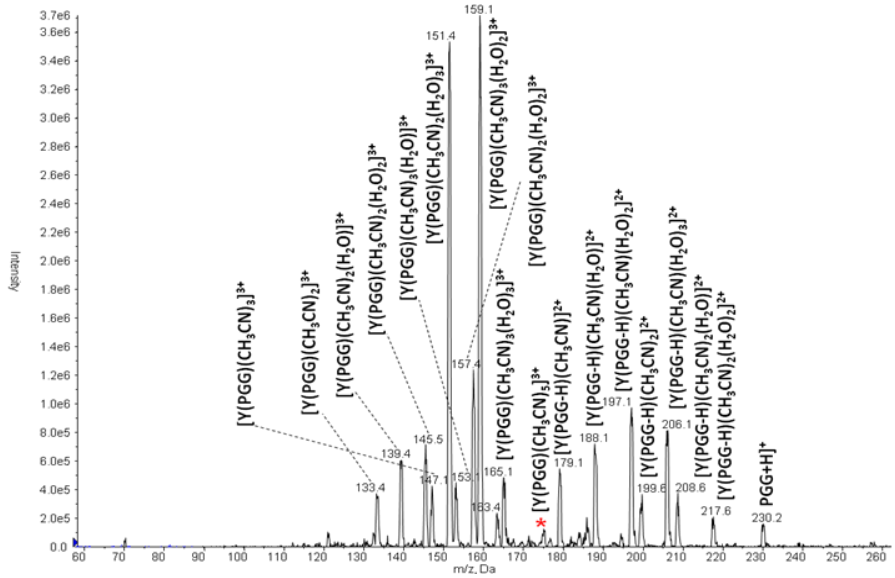

Figure A 1 CID spectrum of $[Y(PGG)(CH_3CN)_5]^{3+}$ at *m/z* 174.6 , E_{lab}=30 eV. The precursor ion is labelled with an asterisk (*)

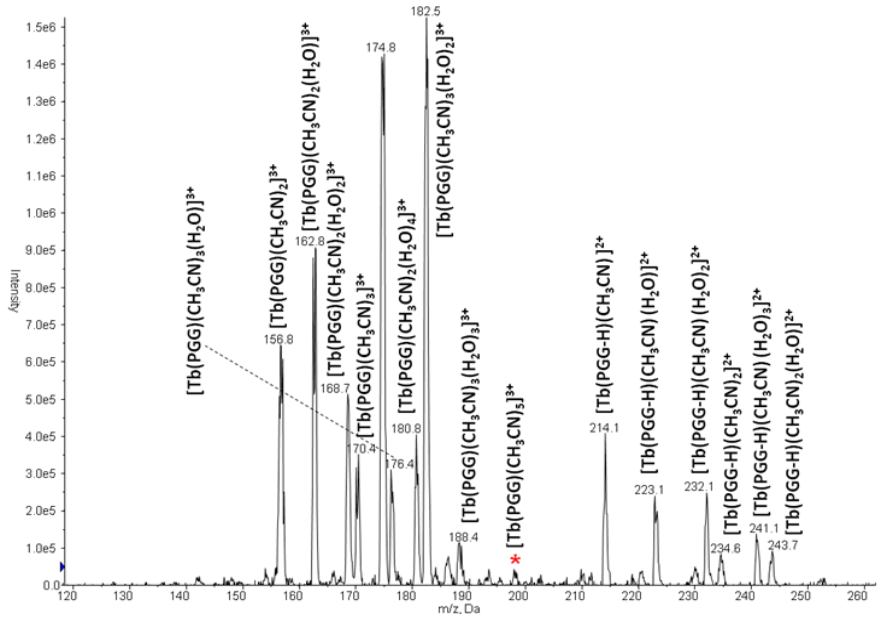

Figure A 2 CID spectrum of $[Tb(PGG)(CH_3CN)_5]^{3+}$ at *m/z* 174.6 , E_{lab}=30 eV. The precursor ion is labelled with an asterisk (*)

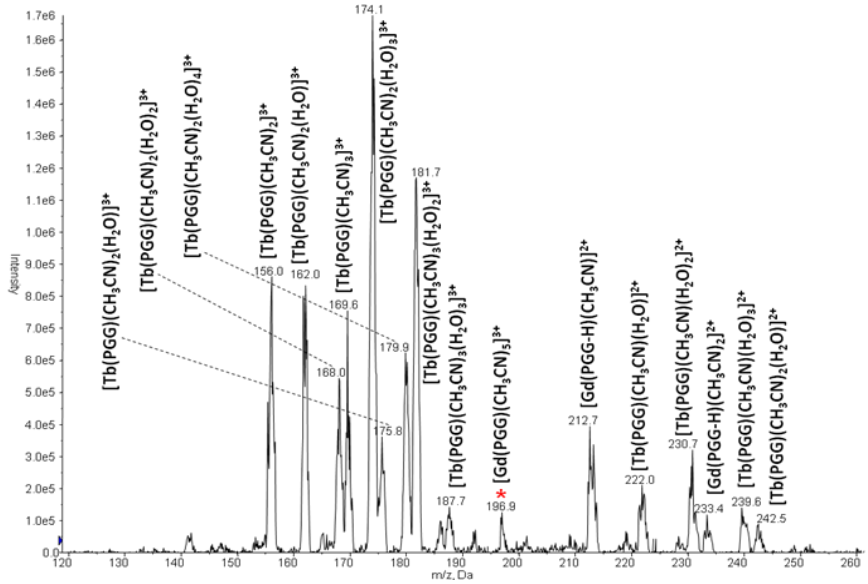

Figure A 3 CID spectrum of $[Gd(PGG)(CH_3CN)_5]^{3+}$ at *m/z* 197.0 , E_{lab}=30 eV. The precursor ion is labelled with an asterisk (*)

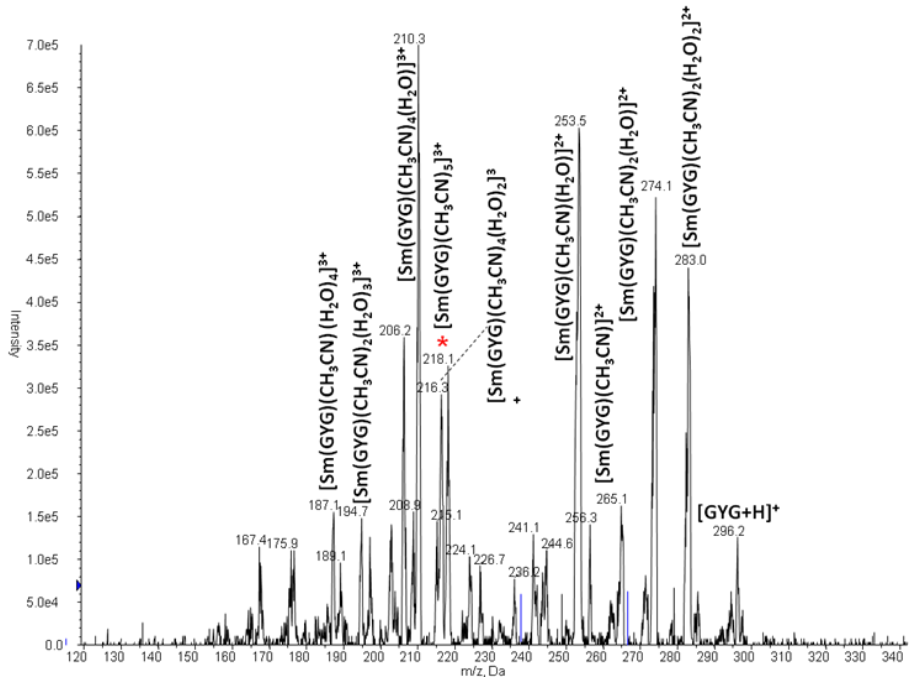

Figure A 4 CID spectrum of $[Sm(GYG)(CH_3CN)_5]^{3+}$ at *m/z* 217.8 , E_{lab}=15 eV. The precursor ion is labelled with an asterisk (*)

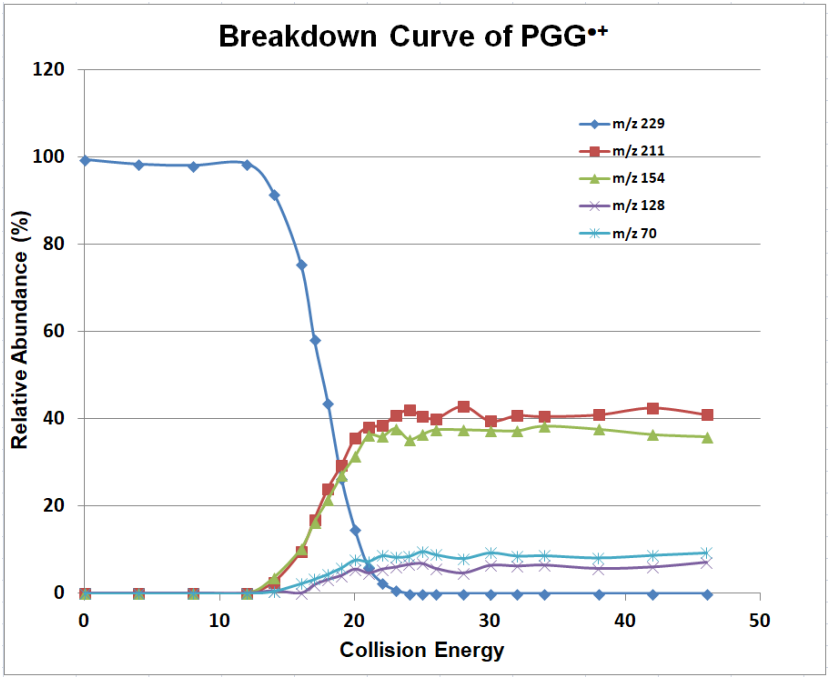

Figure A 5 Breakdown curve of $[PGG]^{\bullet+}$ (*m/z* 229) derived from $[Eu^{153}(PGG)(CH_3CN)_3]^{3+}$